…science sans conscience n'est que ruine de l'âme…

François Rabelais

Pantagruel (1542)

UNIVERSITE LILLE 2 DROIT ET SANTE

ECOLE DOCTORALE BIOLOGIE ET SANTE

ANNEE UNIVERSITAIRE 2013 – 2014

THESE POUR LE DIPLOME D'ETAT DE DOCTEUR EN SCIENCES

DISCIPLINE : PHYSIOLOGIE ET BIOLOGIE DES ORGANISMES
SPECIALITE : PHYSIOLOGIE

MECANISMES DE REGULATION DE L'INFLAMMATION INTESTINALE: FACTEURS ENVIRONNEMENTAUX, MOLECULAIRES ET MICROBIENS

PRESENTEE ET SOUTENUE PUBLIQUEMENT LE 23 SEPTEMBRE 2014
PAR
GUILLAUME PINETON DE CHAMBRUN

DIRIGEE PAR LE PROFESSEUR **PIERRE DESREUMAUX**

MEMBRES DU JURY :

Monsieur le Professeur **Pierre Blanc** (Université Montpellier 1)	Rapporteur
Monsieur le Professeur **Guillaume Savoye** (Université de Rouen)	Rapporteur
Madame le Docteur **Christel Neut** (Université Lille 2 droit et santé)	Examinateur
Monsieur le Docteur **Nicolas Barnich** (Université Clermont 1)	Examinateur
Monsieur le Professeur **Pierre Desreumaux** (Université Lille 2 droit et santé)	Directeur de thèse

RESUME DE THESE

Titre : Mécanismes de régulation de l'inflammation intestinale: Facteurs environnementaux, moléculaires et microbiens.

Résumé : La maladie de Crohn (MC) et la rectocolite hémorragique (RCH) sont les deux principales formes cliniques des maladies inflammatoires chroniques de l'intestin (MICI) responsables d'une atteinte inflammatoire de la paroi du tube digestif avec des ulcérations. Ce sont des maladies fréquentes en Europe et en Amérique du Nord avec plus de 2,5 millions de malades. Du fait de l'augmentation importante de leur prévalence, de leur morbidité, du retentissement sur la qualité de vie des malades et du coût de leur prise en charge médicale, les MICI sont devenues un problème majeur de santé publique. Au cours de ces maladies, l'inflammation intestinale peut être contrôlée par les traitements médicamenteux ou la chirurgie sans pour autant obtenir de guérison complète et définitive. Bien que leur origine reste mal connue, l'hypothèse actuelle présente les MICI comme des maladies multifactorielles, secondaires à une réponse immunitaire muqueuse anormale dirigée contre la flore intestinale, survenant chez des individus génétiquement prédisposés et entrainant une inflammation intestinale. Le but du travail était d'explorer les mécanismes à l'origine de cette inflammation intestinale associée au développement des MICI en étudiant plus particulièrement certains facteurs environnementaux, moléculaires et microbiens. Nous avons étudié tout d'abord l'aluminium comme facteur environnemental en démontrant qu'il pouvait participer au développement et à l'aggravation de l'inflammation intestinale sur des modèles de colite chez la souris. Nous avons ensuite étudié un facteur moléculaire important pour l'apoptose des cellules, la caspase-8. Nous avons montré que cette caspase-8 maintenait l'homéostasie intestinale des

cellules épithéliales intestinales et que son absence entrainait une inflammation intestinale ressemblant à la maladie de Crohn. Finalement nous nous sommes intéressés à un facteur microbien, *Saccharomyces cerevisiae* CNCM I-3856 qui est une levure. Nous avons démontré que cette levure était capable d'induire un effet anti-inflammatoire et analgésique chez l'animal en activant PPARα dans le colon. Chez l'homme nous avons montré dans une étude randomisée que *Saccharomyces cerevisiae* CNCM I-3856 réduisait les douleurs abdominales chez les patients atteints du syndrome de l'intestin irritable. En conclusion, l'exploration de ces trois facteurs environnementaux, moléculaires et microbiens permet de mieux comprendre le développement de l'inflammation intestinale. La perspective de ce travail est le développement dans un futur proche des nouvelles thérapeutiques ciblées permettant de lutter contre l'inflammation intestinale.

ABSTRACT OF THE THESIS

Title: Regulatory mechanisms of intestinal inflammation: Environmental, molecular and microbial factors.

Abstract: Crohn's disease (CD) and ulcerative colitis (UC) are the two main clinical forms of chronic inflammatory bowel disease (IBD) responsible for intestinal inflammation with ulceration of the mucosa. These are common diseases in Europe and North America with over 2.5 million patients. Due to the significant increase in their prevalence, their morbidity, the impact on quality of life of patients and the cost of their medical care, IBD has become a major public health problem. In these diseases, intestinal inflammation may be controlled by drug treatment or surgery without obtaining a complete and final cure. Although their origin remains unclear, the current hypothesis presents IBD as multifactorial diseases secondary to an abnormal mucosal immune response directed against the intestinal flora, occurring in genetically predisposed individuals and causing intestinal inflammation. The aim of this work was to explore the mechanisms behind this intestinal inflammation associated with the development of IBD studying some particular environmental, molecular and microbial factors. We studied first the aluminum as an environmental factor and demonstrated that he could participate in the development and exacerbation of intestinal inflammation in models of colitis in mice. We then studied an important factor in molecular cell apoptosis, caspase-8. We have shown that caspase-8 was maintaining intestinal homeostasis in intestinal epithelial cells and that absence of caspase-8 leads to intestinal inflammation mimicking Crohn's disease. Finally we studied a microbial factor, *Saccharomyces cerevisiae* CNCM I-3856 which is yeast. We demonstrated that this yeast was capable of inducing an anti-inflammatory and analgesic effect in animals by activating PPARα in

the colon. In humans we have shown in a randomized study that *Saccharomyces cerevisiae* CNCM I-3856 reduced abdominal pain in patients with irritable bowel syndrome. In conclusion, the exploration of these three environmental molecular and microbial factors helps to better understand the development of intestinal inflammation. The perspective of this work is the development in the near future of new targeted therapies directed against intestinal inflammation.

Mots clés: inflammation, aluminium, caspase-8, *Saccharomyces cerevisiae*, maladies inflammatoires chroniques de l'intestin

Key words: inflammation, aluminum, caspase-8, *Saccharomyces cerevisiae,* inflammatory bowel diseases

Laboratoires:

1. Unité Inserm U995 « Inflammation : Mécanismes de Régulation et Interactions avec la Nutrition et les Candidoses » :

Le laboratoire Inserm U995 dirigé par le Pr Pierre Desreumaux a été le laboratoire d'accueil du doctorant pendant la durée de sa thèse d'Université (septembre 2010 à septembre 2014).

Coordonnées :

Unité Inserm U995 « Inflammation : Mécanismes de Régulation et Interactions avec la Nutrition et les Candidoses »
Université Lille 2 – Faculté de Médecine – Université Lille Nord de France
Pôle Recherche – Amphis J & K
Boulevard du Pr. Jules Leclerc
59045 Lille cedex
FRANCE

2. Laboratoire du Professeur Lars Eckmann, Université de San Diego, Californie:

Le laboratoire du Professeur Lars Eckmann dans le département de Médecine à L'université de Californie San Diego a été de laboratoire d'accueil du doctorant dans le cadre d'une mobilité internationale de janvier 2011 à novembre 2012. L'ensemble des expériences concernant l'étude de la caspase-8 dans l'inflammation intestinale ont été réalisé dans ce laboratoire.

Coordonnées :

Eckmann laboratory
Division of Gastroenterology
Department of Medicine
University of California San Diego
9500 Gilman Drive
La Jolla, CA 92093-0956
USA

RESUMES DES ARTICLES

1. Premier article:

Titre: Aluminum enhances inflammation and decreases mucosal healing in experimental colitis in mice.

Pineton de Chambrun et al. Mucosal immunol. 2014.

The increasing incidence of inflammatory bowel diseases (IBD) in developing countries has highlighted the critical role of environmental pollutants as causative factors in their pathophysiology. Despite its ubiquity and immune toxicity, the impact of aluminum in the gut is not known. This study aimed to evaluate the effects of environmentally relevant intoxication with aluminum in murine models of colitis and to explore the underlying mechanisms. Oral administration of aluminum worsened intestinal inflammation in mice with 2,4,6-trinitrobenzene sulfonic acid- and dextran sodium sulfate -induced colitis and in chronic colitis in $IL10^{-/-}$ mice. Aluminum increased the intensity and duration of macroscopic and histologic inflammation, colonic myeloperoxidase activity, inflammatory cytokines expression, and decreased epithelial cell renewal compared with control animals. Under basal conditions, aluminum impaired intestinal barrier function. *In vitro*, aluminum induced granuloma formation and synergized with lipopolysaccharide to stimulate inflammatory cytokines expression by epithelial cells. Deleterious effects of aluminum in intestinal inflammation and mucosal repair strongly suggest that aluminum might be an environmental IBD risk factor.

2. Deuxième article:

Titre: Caspase-8 controls attachment and integrity of the intestinal epithelium upon microbial challenge.

Pineton de Chambrun et al. Nat Cell Biol. *Manuscript ready for submission.*

Caspase-8 is a key mediator of ligand-activated apoptosis, but has other functions, including regulation of endocytosis in epithelial cells. The physiological importance of these different activities for intestinal homeostasis is poorly understood. The aim of this study was to study the physiological functions of caspase-8 in intestinal epithelial cells (IECs). We generated mice specifically lacking *Casp8* in IECs ($Casp8^{\Delta IEC}$) by crossing $Casp8^{fl/fl}$ mice to Tg(Vil-cre) mice. Six weeks old $Casp8^{\Delta IEC}$ mice do not present any macroscopic or microscopic intestinal abnormalities compared with $Casp8^{fl/fl}$ mice. However, after bacterial stimulation $Casp8^{\Delta IEC}$ mice present a rapid detachment of IECs leading to villus destruction and mucosal inflammation. This IECs detachment required TNF signaling and occurred in living cells with no involvement of apoptosis or necroptosis. Immunofluorescence analysis reveals disappearance of basal β1-integrin in IECs of $Casp8^{\Delta IEC}$ mice after LPS stimulation, suggesting active endocytosis and degradation of adhesion molecules. Consistent with this, IECs from $Casp8^{\Delta IEC}$ mice lack normal constitutive degradation of proteins important for clathrin-dependent endocytosis and LPS-induced IEC detachment is prevented in $Casp8^{\Delta IEC}$ mice treated with the endocytosis inhibitor chlorpromazine. Furthermore, $Casp8^{\Delta IEC}$ mice treated with LPS show abnormal autophagic activation in IECs compared to $Casp8^{fl/fl}$ mice, and IEC detachment is abolished in $Casp8^{\Delta IEC}$ mice lacking autophagy. Thus, caspase-8 controls IECs adhesion and maintains intestinal barrier integrity in response to infectious stimuli by regulating clathrin-dependent endocytosis and autophagy.

3. Troisième article:

Titre: TLR3, TRIF, and caspase 8 determine double-stranded RNA-induced epithelial cell death and survival in vivo.

McAllister, Lakhdari, Pineton de Chambrun et al. J Immunol. 2013.

TLR3 signaling is activated by dsRNA, a virus-associated molecular pattern. Injection of dsRNA into mice induced a rapid, dramatic, and reversible remodeling of the small intestinal mucosa with significant villus shortening. Villus shortening was preceded by increased caspase 3 and 8 activation and apoptosis of intestinal epithelial cells (IECs) located in the mid to upper villus with ensuing luminal fluid accumulation and diarrhea because of an increased secretory state. Mice lacking TLR3 or the adaptor molecule TRIF mice were completely protected from dsRNA-induced IEC apoptosis, villus shortening, and diarrhea. dsRNA-induced apoptosis was independent of TNF signaling. Notably, NF-κB signaling through IκB kinase β protected crypt IECs but did not protect villus IECs from dsRNA-induced or TNF-induced apoptosis. dsRNA did not induce early caspase 3 activation with subsequent villus shortening in mice lacking caspase 8 in IECs but instead caused villus destruction with a loss of small intestinal surface epithelium and death. Consistent with direct activation of the TLR3-TRIF-caspase 8 signaling pathway by dsRNA in IECs, dsRNA-induced signaling of apoptosis was independent of non-TLR3 dsRNA signaling pathways, IL-15, TNF, IL-1, IL-6, IFN regulatory factor 3, type I IFN receptor, adaptive immunity, as well as dendritic cells, NK cells, and other hematopoietic cells. We conclude that dsRNA activation of the TLR3-TRIF-caspase 8 signaling pathway in IECs has a significant impact on the structure and function of the small intestinal mucosa and suggest signaling through this pathway has a host protective role during infection with viral pathogens.

4. Quatrième article:

Titre: *Saccharomyces cerevisiae* CNCM I-3856 strain decreases intestinal pain and induces PPARα activation in the gut.

Rousseaux, Pineton de Chambrun et al. *Manuscript in preparation*.

There is growing evidence suggesting a potential role of intestinal microbiota in numerous pathologies and more precisely in IBS pathophysiology and symptom generation. Experimental and clinical data suggest that specific probiotics belonging to the *Lactobacillus* and *Bifidobacterium* species may attenuate abdominal pain in IBS. Roles of yeasts and more precisely of *Saccharomyces cerevisiae* strain on the modulation of intestinal pain remain unknown. The aim of this study was to evaluate the functional role of *Saccharomyces cerevisiae* CNCM I-3856 strain on intestinal pain in rats and their mechanisms of actions. Firstly, we showed that *S. cerevisiae* CNCM I-3856 at 10^7CFU/day induces the expression and activation of PPARα *in vitro* and *in vivo*. Then, we demonstrated that oral administration of *S. cerevisiae* CNCM I-3856 reduced significantly the inflammation in TNBS colitis in mice. Also, oral administration of the *S. cerevisiae* CNCM I-3856 (10^6 CFU/day) during 15 days decreased normal visceral perception, allowing a 20% increase in the pain threshold (p=0.013). Moreover, this analgesic effect was induced rapidly within 10 days, maintained for the duration of the treatment and disappeared 3 days after the last *S. cerevisiae* CNCM I-3856 administration. In a model of chronic colonic hypersensitivity, elicited by butyrate enemas and mimicking irritable bowel syndrome, we showed that the hypersensitivity of rats was improved by the CNCM I-3856 strain. Finally, using PPARα agonist and antagonist, we demonstrated that PPARα is involved in the regulation of pain perception induced by *S. cerevisiae* CNCM I-3856. In conclusion, *S. cerevisiae* CNCM I-3856 is

able to decrease intestinal inflammation and visceral pain in animal models trough the activation of nuclear receptor PPARα.

5. Cinquième article :

Titre: *Saccharomyces cerevisiae* CNCM I-3856 reduces digestive discomfort and abdominal pain in subjects with irritable bowel syndrome: a randomized double-blinded placebo-controlled clinical trial.

Pineton de Chambrun et al. Dig Liv Dis. *Submitted*.

Background/aim: *Saccharomyces cerevisiae* CNCM I-3856 is a well-tolerated yeast inducing in mice a visceral analgesic effect mediated through colonic PPARα expression and activation. The aim of this randomized double-blinded placebo-controlled clinical trial was to evaluate the response of symptoms in subjects with irritable bowel syndrome (IBS) receiving CNCM I-3856. **Patients/Methods**: 179 adults with IBS (Rome III criteria) were randomized to receive once a day $8x10^9$ CFU (500mg) of *Saccharomyces cerevisiae* CNCM I-3856 (n=86, F: 84%, age: 42.5±12.5) or a placebo (n=93, F: 88%, age: 45.4±14) during 8 weeks followed by a 3-week washout period. After a 2-week run-in period, IBS cardinal symptoms (abdominal pain/discomfort, bloating/distension, bowel movement difficulty) were recorded daily and assessed each week according to a 7-point Lickert scale. The subjective global assessment of relief was recorded at weekly intervals during the course of the study. A safety assessment was carried out, and changes in stool frequency and consistency (Bristol Stool Scale), faecal calprotectin levels and the intestinal microbiota were also recorded. **Results**: The proportion of responders defined by an improvement of abdominal pain/discomfort of at least 1 point on the 7-point Lickert scale was significantly higher (p=0.04) in the CNCM I-3856 treated group versus the placebo group (63% vs 47%, OR = 1.88, 95%, CI: 0.99-3.57) in the last 4 weeks of treatment. A non-significant trend of improvement was observed with CNCM I-3856 for the other IBS cardinal symptoms and for the subjective global relief assessment during the same period of

Saccharomyces cerevisiae administration. CNCM I-3856 was well tolerated and did not significantly affect stool frequency and consistency, or faecal calprotectin levels. **Conclusion**: *Saccharomyces cerevisiae* CNCM I-3856 at $4x10^9$ CFU/day conveniently delivered once daily by one capsule is well tolerated and reduces abdominal pain/discomfort without altering stool frequency and consistency. These results suggest that *Saccharomyces cerevisiae* may be a new strategy to improve abdominal pain/digestive discomfort in subjects with irritable bowel syndrome.

TABLE DES MATIERES

Mécanismes de régulation de l'inflammation intestinale: facteurs environnementaux, moléculaires et microbiens

I. INTRODUCTION :

L'inflammation intestinale est caractérisée par la présence d'une infiltration de la muqueuse de l'intestin par des cellules immunitaires activées secrétant des cytokines pro-inflammatoires et pouvant entrainer des lésions de l'épithélium intestinal et une altération des fonctions absorptive, motrice et sensitive du tube digestif [1]. Cette inflammation intestinale peut être observée en réponse à une infection bactérienne digestive aigüe ou dans un contexte de maladie intestinale chronique telles que les maladies inflammatoires chroniques de l'intestin (MICI) ou le syndrome de l'intestin irritable (SII) [1, 2].

Les MICI, dont les deux formes cliniques sont la maladie de Crohn (MC) et la rectocolite hémorragique (RCH), sont des maladies fréquentes en Europe et Amérique du Nord avec plus de 2,5 millions de sujets atteints [3]. Elles sont caractérisées par la présence d'une inflammation intestinale chronique dont l'étiologie est inconnue entrainant des lésions sévères à type d'ulcérations extensives de la muqueuse intestinale [1, 2, 4]. Les patients atteints de MC et de RCH présentent des symptômes invalidants à type de diarrhée, d'émissions glairosanglantes impérieuses et fréquentes, de douleurs abdominales chroniques, de saignement digestif et d'amaigrissement. Ces symptômes sont souvent à l'origine d'une altération de l'état général avec un fort retentissement social et professionnel [5]. Ces maladies touchent principalement des sujets jeunes avec un pic de fréquence entre 20 et 35 ans pour la MC, et entre 30-40 ans pour la RCH.

En France, l'incidence des MICI est d'environ 10/100 000 habitants (6/100 000 pour la MC et 4/100 000 pour la RCH) correspondant à environ 300 nouveaux cas par an et 120 000 patients atteints de MICI en France [6]. La fréquence non négligeable de ces maladies, leur présentation clinique parfois sévère, l'importance de leur retentissement socio-économique et l'absence de traitement médical curatif en font à l'heure actuelle un problème majeur de santé publique.

La MC est responsable d'une inflammation chronique pouvant toucher tout le tube digestif de la bouche à l'anus avec une atteinte préférentielle de l'iléon terminal et du côlon [5, 7]. Elle est aussi caractérisée par une atteinte inflammatoire périnéale responsable de fissures, de fistules et d'abcès de la marge anale. Les patients atteints de MC présentent le plus souvent une diarrhée non glairo-sanglante associée à des douleurs abdominales. Les examens endoscopiques mettent en évidence des lésions muqueuses discontinues avec des ulcérations parfois creusantes et des intervalles de muqueuse saine. Au niveau microscopique, l'inflammation de la MC au niveau de la paroi digestive est chronique, transmurale avec dans 30 à 60% des cas la présence de granulomes épithélioïdes et gigantocellulaires sans nécrose caséeuse [5]. Sans traitement, la MC évolue progressivement vers des séquelles fibreuses entrainant une altération du fonctionnement du tube digestif. L'atteinte inflammatoire muqueuse transmurale peut aussi évoluer soit vers une perforation de la paroi de l'intestin avec abcès intra-abdominal soit vers la constitution d'une sténose digestive fibreuse responsable d'un syndrome occlusif. Ces complications nécessitent fréquemment la réalisation d'une intervention chirurgicale avec résection intestinale pouvant à terme conduire à un syndrome du grêle court ou à une iléostomie terminale.

La RCH est caractérisée par une inflammation chronique strictement localisée au niveau du rectum et du côlon [5, 8]. Les patients atteints de RCH présentent le plus souvent des émissions glairosanglantes fréquentes associées à des douleurs abdominales invalidantes. La

coloscopie met en évidence des lésions muqueuses continues, homogènes du rectum vers les segments d'amont à type d'érythème, de saignement muqueux, d'ulcérations et de pseudopolypes. Au niveau microscopique l'inflammation est localisée à la muqueuse avec la présence de cryptes irrégulières, d'une infiltration lymphoplasmocytaire et d'abcès cryptiques sans granulomes. Sans traitement, la RCH peut évoluer vers une tubulisation progressive du côlon et une microrectie entrainant une perte des fonctions coliques. L'inflammation chronique muqueuse est aussi responsable d'une augmentation du risque de développer un cancer du côlon et certains patients atteints de RCH vont développer une forme gravissime aigue de la maladie, la colite aigue grave pouvant nécessiter en cas d'échec du traitement médical une colectomie totale [5, 8].

L'étiologie des MICI est encore à ce jour méconnue et il n'existe pas de traitement médical curatif de la MC et de la RCH [1, 2, 4]. La RCH peut être guérie au prix d'une intervention chirurgicale lourde, la colectomie totale avec anastomose iléoanale avec des conséquences fonctionnelles invalidantes. Les traitements médicaux classiques utilisés dans les MICI sont les 5-aminosalycilés administrés par voie locale ou par voie orale (principalement pour la RCH), les corticoïdes locaux et systémique, les thiopurines (azathioprine et 6-mercaptopurine), le methotrexate et la ciclosporine (pour les formes graves) [5, 8, 9]. Les avancées récentes dans la compréhension des mécanismes physiopathologiques à l'origine de l'inflammation intestinale chronique au cours des MICI ont permis le développement de nouvelles classes thérapeutiques (FIGURE 1) [2]. Tout d'abord, la mise en évidence d'une infiltration de cellules immunitaires activées au niveau de la muqueuse intestinale des patients atteints de MICI entrainant la sécrétion de cytokine pro-inflammatoire et en particulier du TNFα a permis le développement et l'utilisation des anticorps monoclonaux dirigés contre le TNFα [10-12]. Ces anticorps anti-TNFα

ont été démontrés comme efficace pour le traitement des patients atteints de MC et de RCH dans de larges essais thérapeutiques randomisés et contrôlés [11-16]. L'identification de l'afflux des cellules immunitaires activées au niveau de la muqueuse intestinale et la meilleure compréhension des mécanismes de migration de ces leucocytes ont permis le développement d'anticorps monoclonaux dirigés contre les protéines transmembranaires jouant un rôle dans la migration leucocytaire à travers les vaisseaux du tube digestif soit sur le versant leucocytaire soit sur le versant endothélial [17-21]. Le vedolizumab, un anticorps monoclonal anti-intégrine α4β7, protéine permettant au leucocyte d'adhérer à l'endothélium au niveau du tube digestif, a été récemment montré comme efficace dans le traitement de la RCH et de la MC [18, 20]. Finalement, la reconnaissance de l'importance des voies de signalisation impliquant IL23 et les lymphocytes Th17 a permis le développement de l'ustekinumab, anticorps monoclonal dirigé contre la sous-unité p40 présente dans l'IL-12 et l'IL-23 qui devrait très prochainement obtenir l'AMM pour le traitement de la MC [22].

Malgré ces avancées thérapeutiques, le traitement des MICI reste difficile. Le nombre de classes thérapeutiques reste limité avec une bonne efficacité des traitements chez moins de la moitié des malades et l'apparition d'une perte de réponse secondaire aux différents médicaments. La poursuite de l'exploration des mécanismes physiopathologiques à l'origine des MICI reste fondamentale [2]. Bien que leur origine reste mal connue, l'hypothèse actuelle présente les MICI comme des maladies multifactorielles, secondaires à une réponse immunitaire muqueuse anormale dirigée contre la flore intestinale, survenant chez des individus génétiquement prédisposés (FIGURE 2) [1, 23]. La muqueuse digestive est constituée d'une barrière, l'épithélium intestinal, à l'interface du système immunitaire de l'hôte et de la flore intestinale commensale. Ces éléments ont évolué ensemble au cours du temps afin de communiquer et d'interagir dans un

équilibre assurant le maintien de l'homéostasie intestinale [24]. La rupture de cet équilibre est à l'origine du développement de l'inflammation intestinale chronique observée au cours des MICI. Cette rupture d'équilibre peut être due à plusieurs facteurs tels que des altérations génétiques responsables d'une réponse immunitaire intestinale anormale envers la flore commensale, une altération de la composition de la flore luminale et adhérente à la muqueuse digestive ou une anomalie de la barrière intestinale [1, 24, 25]. L'ensemble de ces anomalies pourrait être favorisé et amplifié par des facteurs environnementaux [6].

Le but de ce travail de thèse était d'étudier les mécanismes régulant l'inflammation intestinale à l'origine des MICI et impliqués dans le SII en explorant les différents facteurs environnementaux, moléculaires et microbiens pouvant participer au déclenchement de cette inflammation intestinale. Pour chacune de ces catégories de facteurs, une approche bibliographique initiale nous a permis d'identifier des pistes de recherche novatrices et prometteuses sur lesquelles nous nous sommes ensuite concentrés pour élaborer des protocoles de recherche expérimentaux :

1) Concernant l'environnement, nous avons identifié la pollution comme étant un nouveau facteur environnemental potentiellement impliqué dans les MICI et nous avons étudié l'effet de l'aluminium sur l'inflammation intestinale.
2) Concernant les altérations génétiques et les facteurs moléculaires, nous avons étudié les anomalies potentielles des voies de mort cellulaire en nous concentrant sur l'exploration des fonctions d'une des protéines régulatrices majeures de ces voies, la caspase-8.
3) Finalement concernant les facteurs microbiens, nous avons étudié l'effet de *Saccharomyces cerevisiae* dans la régulation de l'inflammation et la sensibilité viscérale au cours du SII.

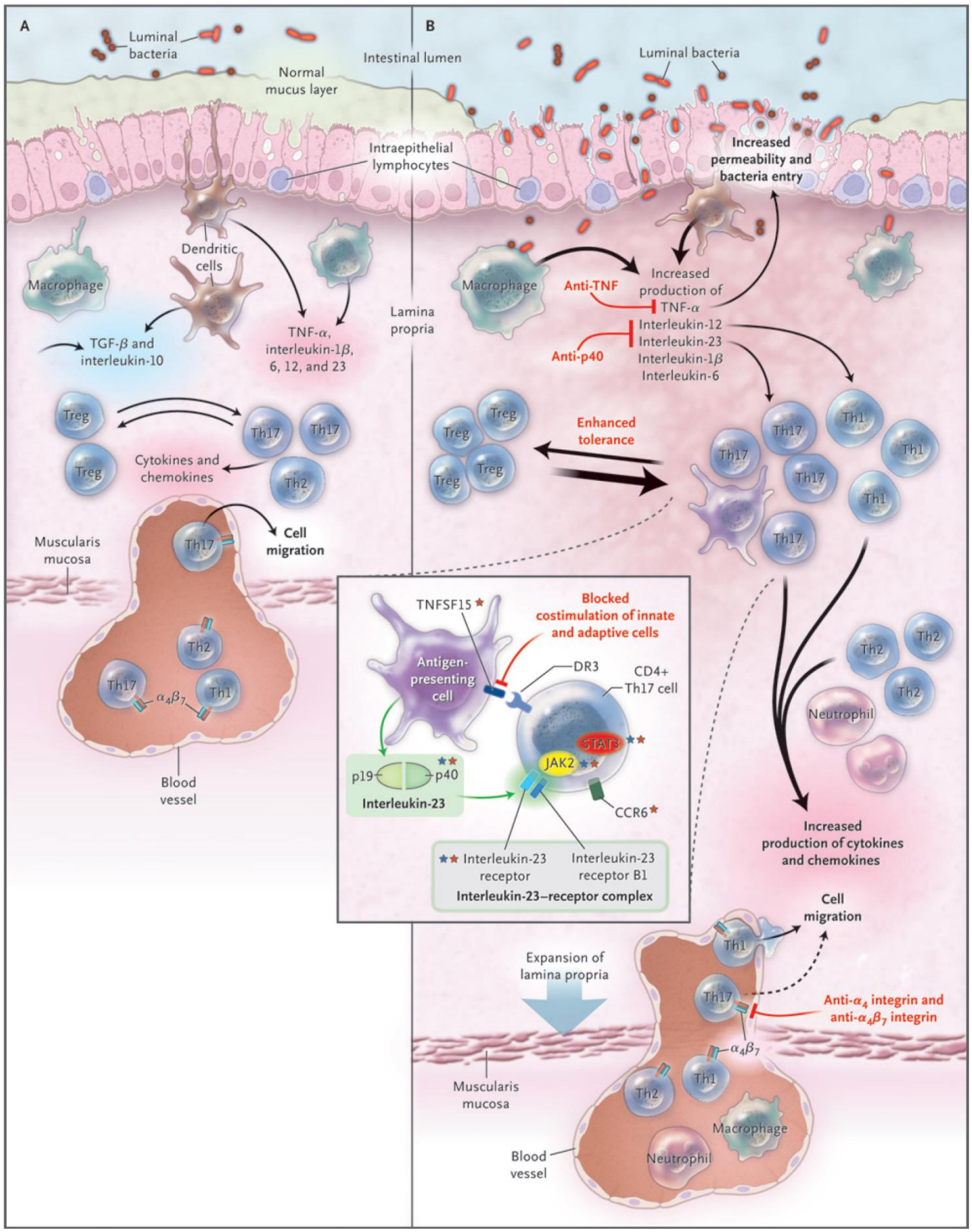

FIGURE 1 : homéostasie et inflammation intestinale [2].

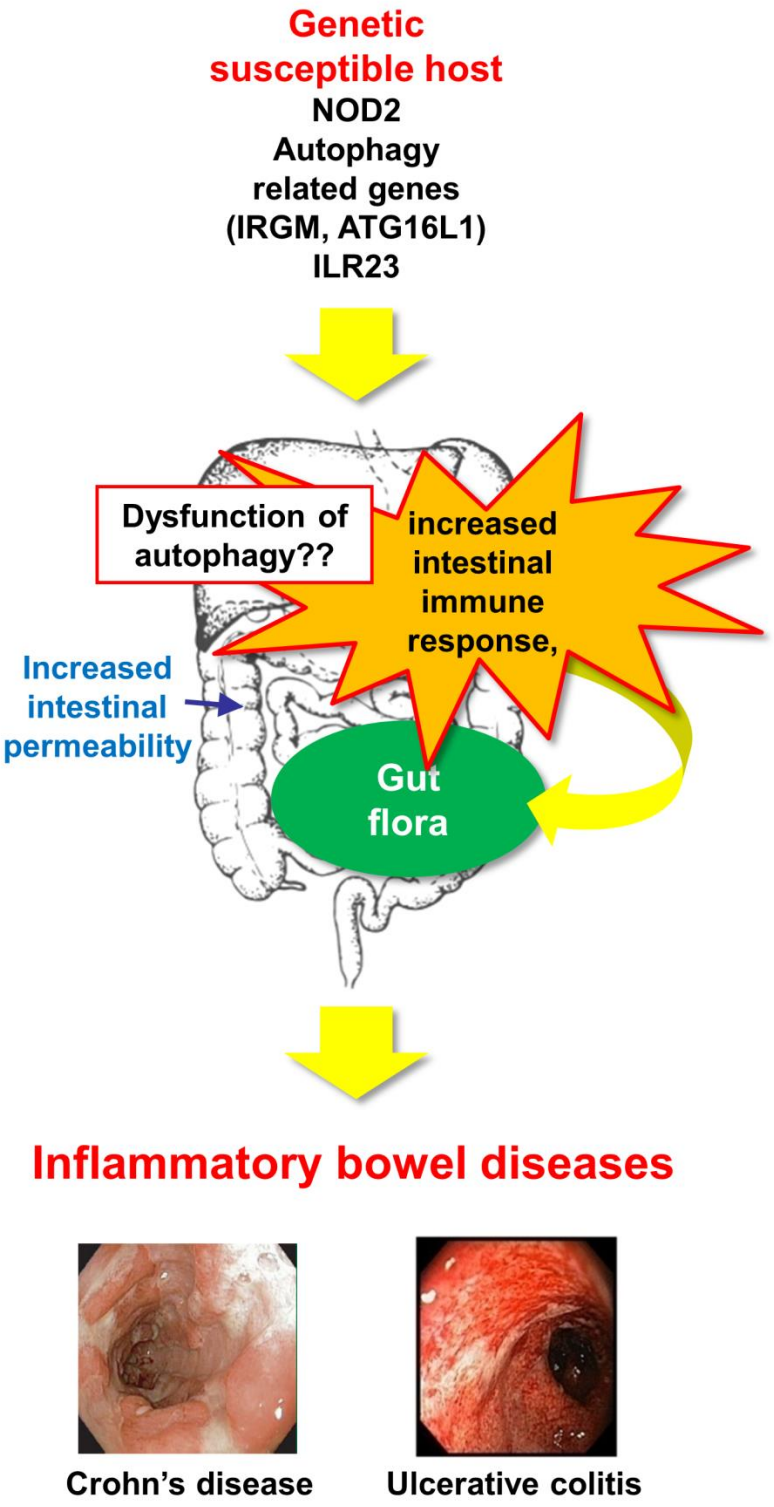

FIGURE 2 : hypothèse physiopathologique des MICI.

II. L'HYPOTHESE ENVIRONNEMENTALE :

A. Facteurs environnementaux et MICI :

Les MICI sont donc des maladies pluri géniques complexes où l'influence des gènes reste cependant faible et ne permet pas d'expliquer à elle seule l'apparition de la maladie (FIGURE 3A et 3B). La faible concordance des MICI chez les jumeaux monozygotes [26], leur forte hétérogénéité spatiale, l'augmentation rapide de leur incidence dans les pays développés et en voie d'émergence [27] et l'augmentation du risque de ces maladies chez les migrants asiatiques ou africains en Europe [28] sont autant d'arguments en faveur de l'implication de facteurs environnementaux [6].

1. Caractéristiques épidémiologiques des MICI et poids de l'environnement

La MC et la RCH sont des maladies fréquentes dans l'hémisphère nord [3] avec une répartition géographique hétérogène au sein d'un même pays [27]. Un des premiers arguments en faveur de l'influence de facteurs externes est le faible taux de concordance chez les jumeaux monozygotes atteints de MICI, respectivement de 33 à 50% et de 13,4 à 18,8% pour la MC et la RCH [26]. La grande majorité des MICI se présentent sous la forme de maladies sporadiques, les formes familiales ne représentant que 5 à 35% des cas en fonction des régions [27]. L'augmentation de la fréquence des MICI dans la plupart des pays durant les 50 dernières années, période trop courte pour voir apparaitre des modifications génétiques significatives, est un deuxième élément en faveur de l'implication de facteurs environnementaux [3].

a. *Données épidémiologiques : hétérogénéité spatiale*

La distribution des MICI dans le monde est hétérogène avec une incidence plus élevée dans les zones développées tels que l'Amérique et l'Europe du Nord ou le Royaume Uni.

L'incidence dans les pays sous-développés ou en voie de développement (Asie, Inde, Afrique) est beaucoup plus faible [27]. Dans les pays à fort revenus et industrialisés comme la France, l'incidence des MICI est comparable à celle du diabète de type 1, de la sclérose en plaques ou de la polyarthrite rhumatoïde [29]. On estime à 14 le nombre de nouveaux cas de MICI par jour en France. L'hétérogénéité spatiale est aussi présente à l'échelle nationale avec par exemple un gradient Nord-Sud en France pour la MC, la plus grande fréquence de MC étant décrite dans la région Nord-Pas-de-Calais. Il existe aussi en Europe un gradient Nord-Sud avec une incidence plus forte des MICI dans les pays du Nord comme le Royaume Uni ou la Norvège [27]. L'hétérogénéité spatiale des MICI, pourrait être expliquée par l'industrialisation des pays riches, l'apparition d'une pollution atmosphérique,

b. Données épidémiologiques : hétérogénéité temporelle

Apparues dans les années 1950 en Europe et en Amérique du Nord avec un taux plus important de RCH que de MC, les MICI ont vu leur fréquence augmenter durant une période de 20 ans pour ensuite se stabiliser [3]. Une caractéristique de la France et de la Belgique est la prédominance de la MC par rapport à la RCH avec une diminution de l'incidence de la RCH dans les cohortes pédiatriques [27]. Ces constatations pourraient être expliquées par la persistance dans l'environnement de facteurs favorisant le développement de la MC. La cinétique de l'incidence des MICI dans les pays en voie de développement suit celle des pays développés avec un retard de quelques décennies. Au Japon, Corée, Singapour, Inde, Afrique et Amérique du sud, l'incidence des MICI initialement faible a commencé à augmenter depuis une vingtaine d'années et n'a pas encore atteint le plateau constaté dans les pays à forte incidence. Que ce soit pour les pays développés ou émergents, l'incidence des MICI a augmenté parallèlement au développement économique, à l'industrialisation et à « l'occidentalisation » des sociétés [3].

L'incidence des MICI évolue parallèlement à celle d'autres maladies polygéniques comme le diabète de type 1 ou la sclérose en plaques dans lesquelles les facteurs environnementaux jouent un rôle primordial [29].

c. Etude des familles et des populations migrantes

Deux autres éléments sont en faveur de l'implication de facteurs environnementaux au cours des MICI. Tout d'abord, 48 formes conjugales de MICI ont été décrites dans la littérature [30]. La prévalence des formes conjugales, bien que faible, est supérieure à la prévalence attendue normalement dans la population générale. Ceci témoigne de facteurs extérieurs partagés par une même famille pouvant participer à l'apparition d'une MICI. Il n'existait pas de regroupement géographique de ces couples et aucun n'était consanguin. Pour la majorité des couples, les symptômes débutaient après le mariage chez les deux conjoints (22 cas) et pour 6 couples, un des conjoints présentait des symptômes avant le mariage et l'autre développait la maladie après le mariage. Dans 66% des cas les conjoints présentaient le même type de MICI avec 17 couples atteints de MC et 3 de RCH [30]. Un autre élément important observé chez les conjoints de patients atteints de MICI est une augmentation anormale de la perméabilité intestinale [31]. Celle-ci a été décrite comme étant un des facteurs responsables du développement de la MC [32]. Elle est augmentée chez les patients atteints de MC, mais aussi dans plus de 23% des cas chez leurs conjoints versus 3% des cas chez les sujets contrôles [31]. L'étude des populations migrantes d'un pays de faible incidence vers un pays de forte incidence de MICI apporte des éléments supplémentaires en faveur des facteurs environnementaux. Plusieurs études ont montré une incidence anormalement élevée de MICI chez des patients originaires de pays à faible incidence comme l'Inde, le Bengladesh et l'Asie du sud-est, vivant en Angleterre et au Canada. Cette modification de l'incidence dans ces populations migrantes

n’apparaissait que chez les sujets migrants durant l’enfance et ceci oriente donc les recherches vers des événements / facteurs intervenant durant les premières années de vie [28].

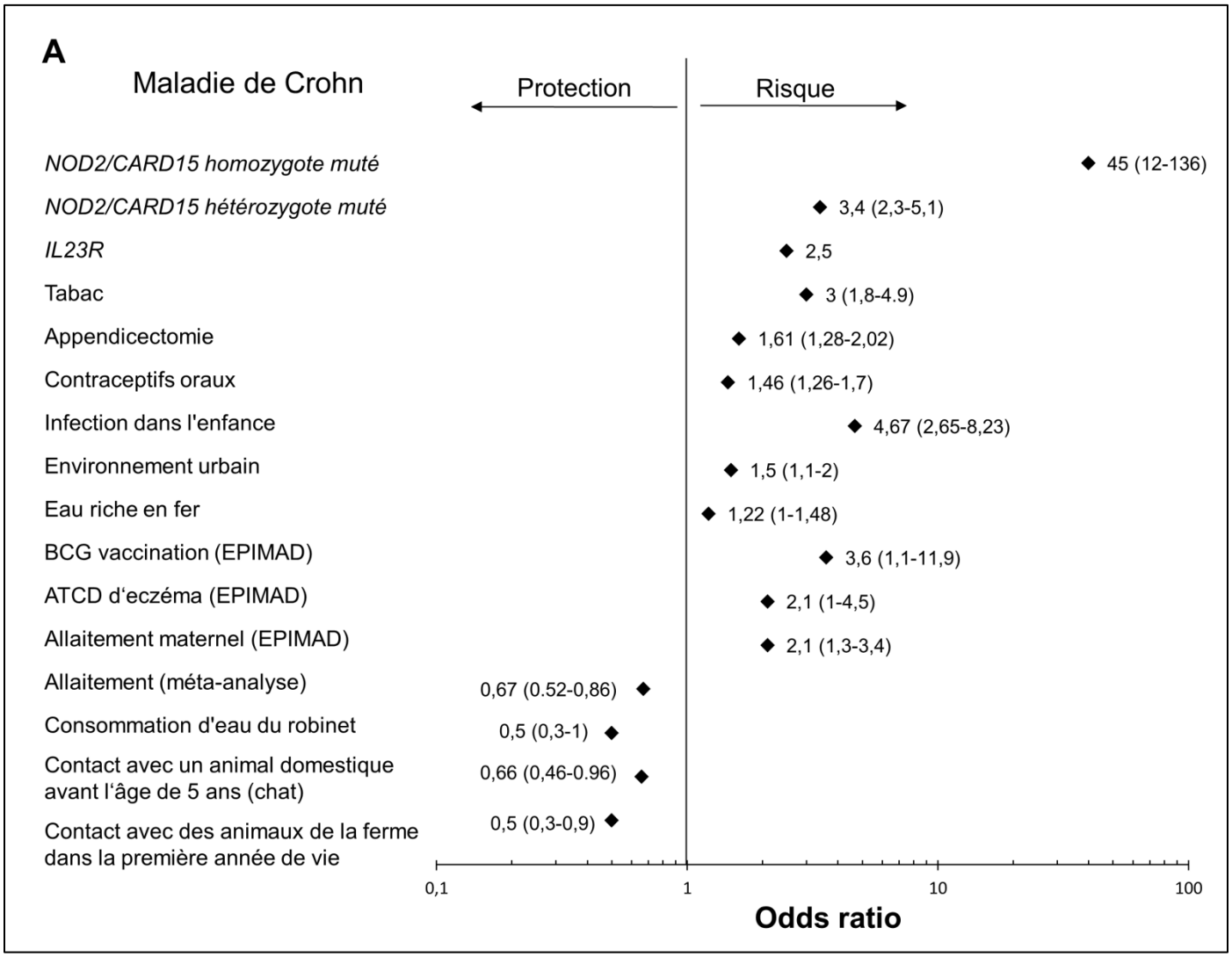

FIGURE 3A : Comparaison du poids des facteurs génétiques et des facteurs environnementaux dans l'apparition d'une MICI [6]. Représentation du risque relatif de développer une maladie de Crohn en fonction des mutations génétiques et des facteurs de risques environnementaux, exprimé à l'aide des Odds ratio. IL23R, interleukine-23; BCG, bacille de Calmette et Guérin; ATCD, antécédents; EPIMAD, registre prospectif des maladies inflammatoires intestinales du Nord de la France.

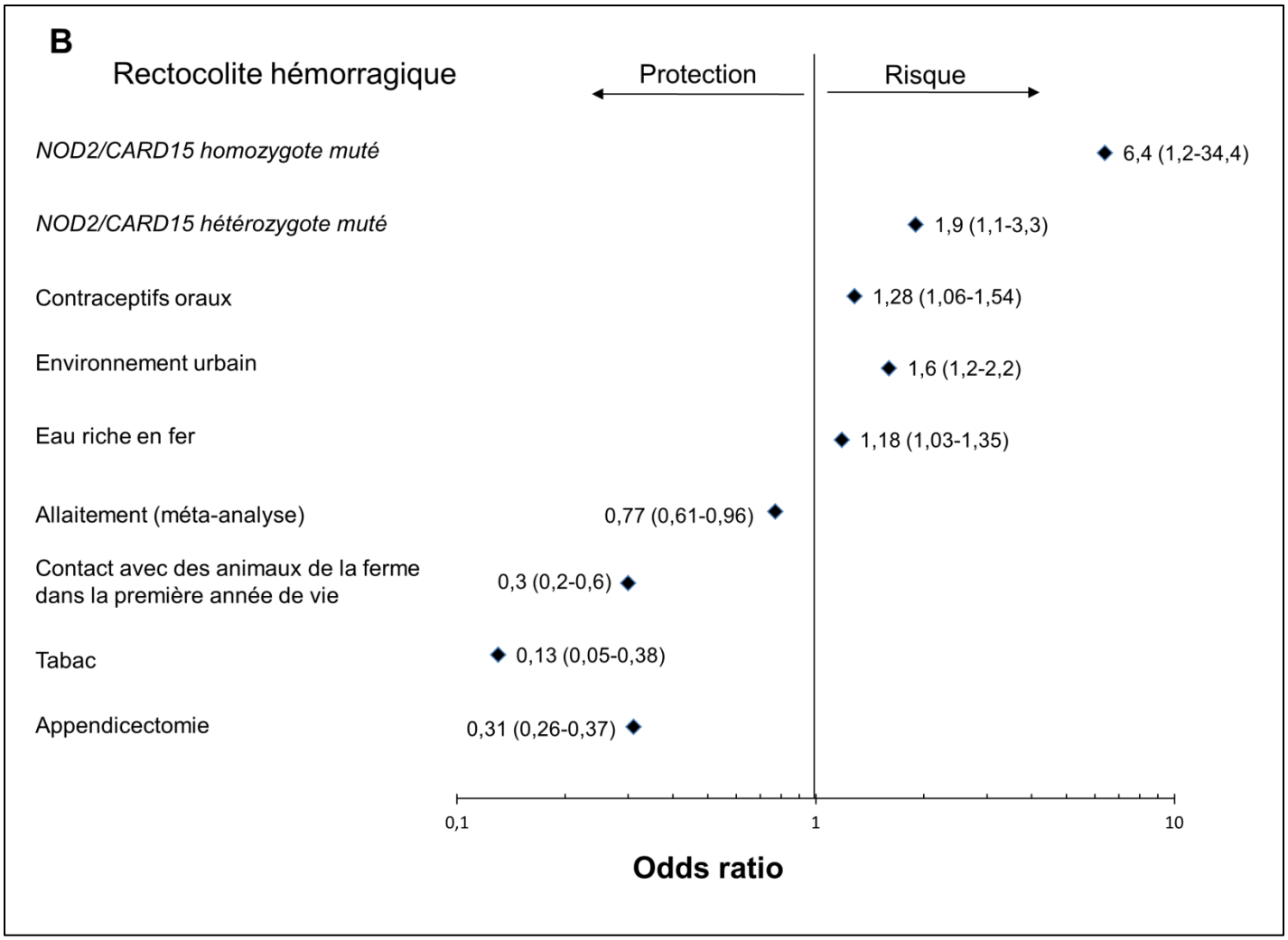

FIGURE 3b : Comparaison du poids des facteurs génétiques et des facteurs environnementaux dans l'apparition d'une MICI [6]. Représentation du risque relatif de développer une rectocolite hémorragique en fonction des mutations génétiques et des facteurs de risques environnementaux, exprimé à l'aide des Odds ratio.

2. Facteurs environnementaux identifiés et suspectés :

De nombreux facteurs environnementaux sont suspectés pouvoir jouer un rôle dans le développement de l'inflammation intestinale au cours des MICI. A ce jour, le tabagisme et l'appendicectomie sont les deux seuls facteurs environnementaux clairement associés aux MICI. Leur particularité est de présenter une influence opposée au cours de la MC et de la RCH (Tableau I) [33]. Leurs mécanismes d'action physiopathologique sont encore méconnus.

Les autres facteurs environnementaux suspectés sont des facteurs alimentaires (sucres, alimentation riche en graisse et pauvre en fibres…), l'allaitement maternel, les traitements contraceptifs oraux, les agents pathogènes microbiens, l'augmentation de l'hygiène et le stress (Tableau I) [6]. Actuellement, le rôle de ces facteurs environnementaux au cours des MICI reste très discuté et aucun n'a pu être identifié avec certitude au cours des nombreuses études épidémiologiques réalisées [34].

Tableau I : Facteurs environnementaux et MICI[6]				
Facteurs environnementaux	Reconnu	Fortement suspecté	Suspecté, controversé	Abandonné
Tabac	x			
Appendicectomie	x			
Médicaments				
Contraceptifs oraux			x	
Allaitement maternel			x	
Facteurs alimentaires		**x**		
Sucre			x	
Alimentation réduite en fibre et en fruit			x	
Eau du robinet			x	
Fastfood			x	
Régime riche en protéines animales			x	
Régime riche en graisses animales		**x**		
Produits de glycation avancés (AGE)		**x**		
Agents pathogènes		**x**		
Virus de la rougeole				x
Mycobacterium paratuberculosis			x	
Yersinia			x	
Listeria			x	
Escherichia coli type AIEC		**x**		
Candida albicans		**x**		
Infections dans l'enfance			x	
Stress			x	
Pollution		**x**		
Microparticules			x	
Hypothèse de l'hygiène		**x**		
Diminution des infections			x	
Vaccinations			x	
Antibiotiques			x	
Eau			x	

Abréviations : MICI, maladie inflammatoire chronique de l'intestin ; AIEC, adherent/invasive *Escherichia coli*

B. Pollution et MICI :

La physiopathologie des MICI s'articule autour de trois groupes de facteurs interagissant entre eux : la susceptibilité génétique, les facteurs environnementaux et la réponse immunitaire dérégulée conduisant à l'inflammation intestinale et aux lésions muqueuses [23]. Depuis la découverte du gène de susceptibilité NOD2/CARD15, plus d'une centaine de loci de susceptibilité aux MICI ont été identifiés. Ces gènes sont impliqués dans le maintien de la barrière intestinale, la réponse immunitaire innée et l'élimination des bactéries [35]. S'appuyant sur l'hypothèse physiopathologique actuelle des MICI et sur les données épidémiologiques, trois axes de recherche concernant les facteurs environnementaux ont émergé, s'articulant autour de la flore intestinale : l'hypothèse de l'hygiène; les nouveaux agents pathogènes; la modification de l'alimentation associée à la pollution industrielle (FIGURE 4). La grande majorité de ces nouveaux facteurs environnementaux est liée à une modification du mode de vie qui caractérise les sociétés modernes des pays industrialisés (Tableau II).

L'alimentation est un facteur qui influence fortement la composition et l'activité métabolique de la flore intestinale. L'alimentation « moderne » peut être définie par une consommation accrue de produits industriels, de graisses saturées, de protéines animales et par la présence de microparticules inorganiques provenant de la pollution ou de la production alimentaire industrielle. Les différents composés alimentaires présents pourraient agir soit directement sur la barrière épithéliale soit sur la composition et le métabolisme de la flore intestinale [23].

Peu de données sont disponibles concernant l'implication de microparticules agissant comme polluants atmosphériques ou terrestres dans l'inflammation intestinale. Par contre,

plusieurs données épidémiologiques et physiopathologiques plaident en faveur de leur rôle. La différence d'incidence entre les pays industrialisés et les pays en voie de développement et l'hétérogénéité spatiale des MICI dans certaines régions de France sont en faveur d'un rôle de facteurs liés à l'activité industrielle [3]. De nombreuses études ont établi les corrélations entre les taux de particules présentes dans l'air et certaines maladies cardiovasculaires et respiratoires [36]. Les polluants majeurs de l'air, produits par l'activité humaine, incluent le dioxyde de soufre (SO_2), les oxydes nitriques, le monoxyde de carbone, les composés organiques volatiles et les métaux toxiques tels que le plomb, le cadmium, l'aluminium ou le cuivre. Le phénomène de déposition atmosphérique conduit au dépôt de ces polluants sur le sol et dans l'eau entrainant une contamination de la nourriture et de l'eau potable et leur permettant donc d'entrer en contact avec le tube digestif [37]. Plusieurs polluants de l'air et de l'eau sont déjà reconnus comme ayant des propriétés pro ou anti-inflammatoires [38].

Plusieurs travaux épidémiologiques récents ont démontrés l'association de ces microparticules avec le développement et l'aggravation des MICI et des travaux expérimentaux ont démontré la présence de microparticules dans la muqueuse intestinale et leur toxicité potentielle sur l'épithélium intestinal [39-45]. Une première étude Canadienne cas-contrôles en population générale publiée en 2010 démontrait que la pollution au NO_2 et au SO_2 était associée à une augmentation de l'apparition de MICI chez les sujets de moins de 25 ans [41]. Une deuxième étude publiée en 2011 a démontré que la pollution atmosphérique était significativement associée avec une augmentation des hospitalisations pour MICI [39]. Auparavant, des travaux expérimentaux avaient identifié la présence de microparticules dans les plaques de Peyer au niveau de l'intestin grêle chez des sujets sains mais aussi au niveau de zones inflammatoires chez des sujets atteints de maladie de Crohn [44, 46]. Plus récemment, des travaux expérimentaux

chez la souris ont montré que les microparticules issues de la pollution atmosphérique pouvaient entrainer une augmentation de la perméabilité intestinale due à une toxicité sur les cellules épithéliales et aggraver l'inflammation intestinale dans un modèle de colite chez des souris mutées pour le gène de l'IL-10 [43, 45]. Deux études cliniques ont étudié l'effet d'un régime pauvre en microparticule sur l'activité de la maladie de Crohn avec des résultats contradictoires [42, 47].

L'interaction entre ces polluants et l'épithélium digestif pourrait donc conduire à leur toxicité directe ou indirecte en intervenant sur la flore intestinale [37, 48]. Parmi ces polluants, les microparticules présentes dans notre alimentation par contamination ou au cours des procédés alimentaires industriels sont susceptibles de participer au déclenchement de l'inflammation intestinale.

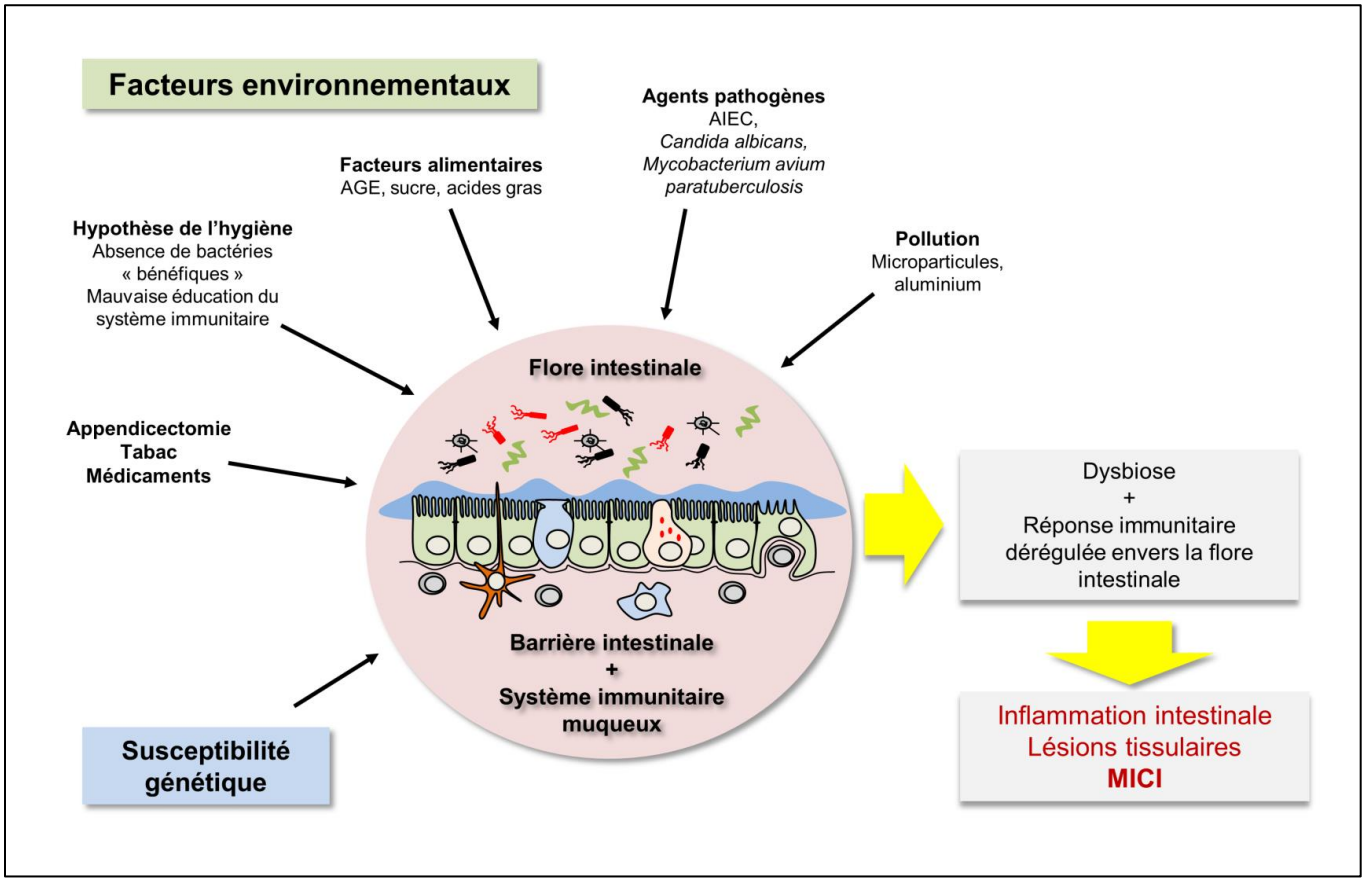

FIGURE 4 : Facteurs environnementaux et physiopathologie des MICI [6]. Dans le cadre d'une susceptibilité génétique entrainant une altération de la barrière intestinale, de la réponse immunitaire innée et de l'élimination des bactéries, les différents facteurs environnementaux vont perturber l'homéostasie intestinale. Ils vont agir soit sur la flore intestinale et entrainer une dysbiose favorisant l'invasion d'espèces pathogènes, soit directement sur la barrière intestinale et le système immunitaire muqueux. Il en résulte une hyperactivation du système immunitaire avec réponse dérégulée envers la flore intestinale provoquant l'inflammation et les lésions tissulaires. AGE, produits de glycation avancés ; AIEC, souche invasive d'*Escherichia coli* ; MICI, maladie inflammatoire chronique intestinale.

Tableau II : Éléments du mode de vie moderne susceptibles d'agir sur la flore microbienne muqueuse intestinale[6]
Amélioration de l'état sanitaire
Diminution des maladies parasitaires endémiques
Sols durs des habitations (moins de contact avec les bactéries de la terre)
Diminution de l'infection à *H. pylori*
Augmentation de l'utilisation des antibiotiques
Vaccinations
Diminution de la taille des familles
Moins de promiscuité dans les conditions de vie
Chaîne du froid
Exposition retardée dans la vie aux infections
Vie sédentaire et obésité
Moins de consommation de nourritures fermentées
Plus de consommation de sucres raffinés, graisses saturées et conservateurs alimentaires
Pollution industrielle : métaux lourds, aluminium, microparticules

C. Aluminium : un nouveau facteur environnemental ?

Parmi les microparticules issues de la pollution, l'aluminium (Al^{3+}) est l'un des meilleurs candidats pouvant participer à la physiopathologie des MICI. Il présente, tout d'abord, une grande biodisponibilité dans l'environnement lui permettant d'interagir facilement avec l'homme et son tube digestif. Il est aussi le métal le plus fréquemment retrouvé dans notre environnement et représente 8% de la croûte terrestre [49-51]. On le trouve de manière ubiquitaire dans les sols et par des phénomènes d'érosions et de solubilisations dans l'atmosphère et dans l'eau [50, 52]. L'activité humaine a augmenté sa biodisponibilité en l'utilisant massivement dans l'industrie métallurgique. Les pluies acides et les engrais utilisés pour l'agriculture qui acidifient les sols augmentent la solubilisation de l'aluminium et sa biodisponibilité pour les végétaux [50, 52]. L'aluminium est utilisé couramment comme additif alimentaire dans la production industrielle des aliments [50, 51]. Il est aussi présent dans de nombreux médicaments, des ustensiles de cuisine et dans certains produits servant à décontaminer l'eau potable [50]. Il a récemment été démontré que l'aluminium, qui est connu pour être un constituant du tabac, passe dans la fumée de cigarette et pourrait contaminer le liquide alvéolaire [53]. L'aluminium, élément non essentiel à l'organisme humain, embrasse donc les caractéristiques à la fois d'un polluant industriel, d'un facteur alimentaire et d'un composant du tabac : tous suspectés de participer au développement des MICI. L'ingestion quotidienne d'aluminium par l'homme est évaluée à 15 mg/j en moyenne pour une dose tolérée déterminée à 1mg/kg/j [50, 52]. Cette consommation assez faible d'aluminium est probablement sous-évaluée et certains rapports récents font état d'une consommation quotidienne beaucoup plus importante dans des pays industrialisés comme les Etats Unis d'Amérique. Cette consommation pourrait atteindre plus de 24mg/j pour la moitié de la population et plus de 95mg/j pour 5% de la population [54, 55].

Deux autres arguments importants en faveur de l'implication de l'aluminium sont sa toxicité humaine établie et son immunogénicité reconnue depuis de nombreuses années [56]. L'aluminium est responsable de troubles neurologiques, d'ostéomalacies et d'anémies microcytaires survenus chez des patients dialysés et traités par chélateur de phosphate à base d'aluminium. Des encéphalopathies néonatales ont aussi été décrites chez des nouveaux nés bénéficiant de nutrition parentérale riche en aluminium. Enfin, l'aluminium est aussi à l'origine de maladies professionnelles avec le développement par exemple de fibrose pulmonaire chez les sujets exposés aux poussières d'aluminium [50, 57]. Grace à son pouvoir immunogène, l'aluminium est utilisé depuis de nombreuses années comme adjuvant des vaccins. L'aluminium hydroxide permet d'augmenter la réponse immunitaire humorale et cellulaire T spécifique à un antigène. Il est capable de stimuler soit une réponse immunitaire Th2 soit une réponse Th1, en fonction des signaux de costimulation associés (antigène de vaccins pour la réponse Th2 ; LPS, inuline Il-12 pour la réponse Th1) [56]. Les mécanismes à l'échelle cellulaire de l'action adjuvante de l'aluminium ont été récemment précisés. L'aluminium entraine l'activation d'un complexe cytosolique appartenant à la famille des NLRs appelé NALP3-inflammasome [58-61]. A travers l'activation de NALP3, l'aluminium entraine la secrétion de cytokines inflammatoires telles que IL-1β et IL-18 ainsi que l'initiation d'une réponse immunitaire humorale adaptative [58, 61]. Ces constations immunitaires récentes relancent la responsabilité de l'aluminium en tant que facteur étiologique des maladies inflammatoires intestinales. Celui-ci serait capable d'exacerber une réponse immunitaire de type Th1 dirigée notamment contre des bactéries ou des antigènes bactériens [62].

Finalement, certaines similitudes entre la MC et les pathologies induites par l'aluminium nous incitent fortement à considérer l'aluminium comme acteur potentiel de la physiopathologie des MICI (Tableaux III) [56]. La description d'une épidémie d'entérite granulomateuse chez des

chevaux élevés à proximité d'une usine utilisant de l'aluminium et intoxiqués par celui-ci supporte l'hypothèse d'une responsabilité de l'aluminium dans les phénomènes inflammatoires granulomateux digestifs [63]. La formation de granulomes induits par l'aluminium a déjà été décrite au niveau de la peau lors des vaccinations et au niveau des poumons après inhalation de poussières d'aluminium [64, 65]. Chez l'homme, dès 1987, des microparticules constituées en partie de silicate d'aluminium étaient mises en évidence au sein des plaques de Peyer [44, 46]. Ces microparticules inorganiques issues de l'environnement pourraient déclencher chez un sujet prédisposé une inflammation granulomateuse [56]. Très récemment, une étude montrant une association entre des mutations activatrices du gène codant pour NALP3 et une susceptibilité accrue à la MC est venue renforcer cette hypothèse [66].

La recherche de facteurs environnementaux responsables de l'apparition et de l'entretien des MICI est un enjeu majeur puisque contrairement aux facteurs génétiques, ils peuvent être contrôlés afin de réduire la fréquence et la morbidité de ces pathologies. Notre hypothèse est que l'aluminium présent dans l'eau de boisson et les aliments contaminés et ingérés par l'homme pourrait participer, chez un sujet génétiquement prédisposé, au déclenchement et à l'entretien d'une inflammation intestinale chronique identique à celle observée au cours des MICI. L'action de l'aluminium au niveau intestinal pourrait soit être dû à une toxicité directe au niveau de la muqueuse intestinale avec modulation de la réponse immunitaire innée des macrophages et des cellules épithéliales, soit passer par une modification et un déséquilibre de l'homéostasie entre la flore intestinale et son hôte.

Le but de notre travail est d'étudier l'effet de l'aluminium sur la réponse immunitaire et inflammatoire intestinale *in vitro,* en particulier au niveau des cellules épithéliales intestinales, d'étudier la modulation d'une inflammation intestinale par l'aluminium, *in vivo* dans des modèles

de colites expérimentales chez la souris et d'étudier les modifications de composition de la flore intestinale adhérente chez l'animal après exposition à l'aluminium.

Tableau III : Propriétés de l'aluminium et physiopathologie de la maladie de Crohn [56]	
Aluminium	**Maladie de Crohn**
Epidémiologie	
Exposition augmentée dans les sociétés industrialisées	Augmentation de la prévalence dans les zones industrialisées
Influence génétique	
Influence génétique de la perméabilité intestinale à l'aluminium	Augmentation de la perméabilité intestinale génétiquement déterminée
Prédisposition génétique aux pathologies dues à l'aluminium	Prédisposition génétique pour les MICI
L'aluminium induit des dommages de l'ADN hélicoïdal	Augmentation des dommages au niveau de l'ADN
Aspects immunologiques	
IL-12 modifie la polarisation Th2 due à l'aluminium	L'IL-12 induit une différenciation Th1
L'aluminium associé à l'IL-12 induit une réponse Th1	La MC est associée avec une réponse Th1 prédominante
L'aluminium associé aux cytokines augmente la réponse Th1	Augmentation des cytokines de type Th1
Induit la différenciation des macrophages	Augmentation des cellules dendritiques matures
Promotion d'une réponse humorale	Expansion des populations cellulaires B
Profil inflammatoire	
Expression de gènes pro inflammatoires	Etat inflammatoire classique
Activité pro-oxydante	Augmentation du stress oxydatif et des facteurs pro-oxydants
Elément pro-apoptotique	Dérégulation de l'apoptose
Induction des gènes de stress	Augmentation de HSP70
Induction de la sécrétion de cytokines pro inflammatoires, TNFα, IL-6	Inflammation médiée par le TNFα et augmentation des cytokines IL-6, IL-2r, MIP1-α
Activation de NF-KB et HIF-1	Dérégulation de NF-KB et activation de HIF-1
Métabolisme du fer	
L'aluminium rentre en compétition avec le fer au niveau des récepteurs de la transferrine	Diminution de l'absorption du fer et du stockage
Augmentation de l'absorption d'aluminium dans les cellules riches en récepteurs de la transferrine	Augmentation des récepteurs libres de la transferrine

Abréviations : MC, maladie de Crohn ; MICI, maladie inflammatoire chronique de l'intestin ; ADN, acide désoxyribonucléique ; IL, interleukine ; Th, lymphocyte T helper ; TNFα, tumor necrosis factor alpha ; HSP, heat shock protein ; NF-KB, nuclear factor kappa beta ; HIF, hypoxia-inductible factor.

D. *Aluminum enhances inflammation and decreases mucosal healing in experimental colitis in mice [67].*

G Pineton de Chambrun[1,2,3,4], M Body-Malapel[1,2,3], I Frey-Wagner[5], M Djouina[1,2,3], F Deknuydt[6,7,8], K Atrott[5], N Esquerre[1,2,3], F Altare[6,7,8], C Neut[1,2,3,9], MC Arrieta[10], T-D Kanneganti[11], G Rogler[5], J-F Colombel[1,2,3,4], A Cortot[1,2,3,4], P Desreumaux[1,2,3,4], and C Vignal[1,2,3]

[1]Univ Lille Nord de France, Lille, France

[2]Inserm U995, Lille, France

[3]UDSL, Lille, France

[4]Hepato-Gastroenterology Department, CHU Lille, Lille, France

[5]University hospital Zurich, division of gastroenterology and hepatology, Zurich, Switzerland

[6]INSERM, UMR892, Nantes, France

[7]CNRS, UMR6299, Nantes, France

[8]Université de Nantes, Nantes, France

[9]Clinical Bacteriology, College of Pharmacy, Lille, France

[10]Finlay Lab, Michael Smith Laboratories, University of British Columbia, Vancouver, BC, Canada

[11]Department of Immunology, St. Jude Children's Research Hospital, Memphis, TN, 38105, USA

Référence de l'article :

Aluminum enhances inflammation and decreases mucosal healing in experimental colitis in mice. Pineton de Chambrun G, Body-Malapel M, Frey-Wagner I, Djouina M, Deknuydt F, Atrott K, Esquerre N, Altare F, Neut C, Arrieta MC, Kanneganti TD, Rogler G, Colombel JF, Cortot A, Desreumaux P, Vignal C. ***Mucosal Immunol.*** 2014 May;7(3):589-601. doi: 10.1038/mi.2013.78. Epub 2013 Oct 16.

1. Introduction:

Inflammatory bowel diseases (IBD), which include Crohn's disease (CD) and ulcerative colitis (UC), are chronic diseases characterized by an excessive uncontrolled intestinal inflammation resulting from an abnormal immune response to commensal microbiota in a susceptible host[24] In the past 10 years, genetic research in IBD has been particularly fruitful. However, among the many susceptibility genes identified (more than 100 to date) none were demonstrated to be necessary or sufficient for disease onset[68, 69] The spatial heterogeneity of CD and UC, their increasing incidence and prevalence with time and in different regions around the world, the low concordance rate in monozygotic twins and the increased risk among migrants from low-incidence to high-incidence areas are strong arguments implying an important role for environmental factors in the pathogenesis of IBD[28, 70] However, besides smoking and appendectomy and, more recently, exposure to antibiotics in childhood, no strong environmental factors have been identified to date[33, 71-73]

The increase of IBD in developing countries has focused attention on the potential role of industrialization and environmental pollutants as causative environmental factors in their pathophysiology[39, 41] Twentieth century industrialization has led to an increased accumulation of heavy metals, and in particular aluminum, in our surrounding ecosystems. Aluminum is ubiquitous and is the most abundant metal element in our environment[49, 51] In the past 50 years, worldwide production of aluminum has regularly increased, from less than 5 million tons in 1960 to more than 25 million tons in 2002, and developed countries have raised their current domestic consumption by 350%[50, 52] A main route of exposure to aluminum for the general population is through food and water. The decline in the use of unprocessed foods and the increased consumption of cakes, pastries and sugar-rich foods characterizing "food

westernization" has resulted in an increased ingestion of aluminum, which exceeds the tolerable weekly intake of 7 mg/kg/week in a significant proportion of the European and North American populations[74] For many years, exposure to aluminum was suggested to favor an abnormal immune response in different diseases, including autoimmune conditions[56] However, despite this known toxicity and a potential gut interaction, aluminum and its effect on intestinal homeostasis and inflammation have not been investigated so far, particularly in the physiopathology of IBD.

The aim of our study was to explore the pro-inflammatory role of aluminum in different models of chemically induced and chronic colitis in mice. Particular attention was paid to the interaction between aluminum and epithelial cells and its role in the immune response against bacteria.

2. Results:

Aluminum worsens colitis induced by TNBS and DSS in mice

In a first set of experiments, C57BL6 mice were fed for four weeks with aluminum citrate (AluCi) or aluminum phosphate (AluP) at a concentration of 1.5 mg of Al element/kg/day. These four weeks' oral administration of aluminum did not induce any macroscopic, histological or molecular colonic inflammation (Supplementary Figure 1). In another set of experiments, C57BL6 mice were treated with AluCi or AluP for 4 weeks before rectal administration of 2,4,6-trinitrobenzene sulfonic acid (TNBS, Figure 1A). Four days after colitis induction, the severity of intestinal inflammation was assessed by macroscopic, histological and molecular parameters. Macroscopic Wallace score of colonic inflammation was significantly increased in both forms of aluminum-treated mice compared to PBS-treated mice (Figure 1B). Aluminum-treated mice presented more severe and extended macroscopic inflammation of the colon with large areas of ulceration (data not shown). Consistently, at the microscopic level, the histological Ameho score of colonic inflammation was more severe in both forms of aluminum-treated mice compared with PBS-treated mice, leading to more extensive ulceration and necrosis involving 80% of the whole colon (Figure 1C-D). MPO activity reflecting neutrophil infiltration was also significantly higher in aluminum-treated mice compared to PBS-treated mice (Figure 1E).

To complete our understanding of the detrimental effect of aluminum observed in TNBS-induced colitis, BALB/C mice were concomitantly treated by aluminum gavage and oral administration of dextran sodium sulfate (DSS) 2.5% in drinking water for 7 days (Figures 2A and 3A). A 2-fold increased mortality was observed in AluCi-treated mice with DSS-induced colitis compared to control animals (Figure 2B). Moreover, mice treated with DSS and AluCi or AluP had more than a 3- and 2-fold body weight loss, respectively, compared to DSS and PBS-treated mice (Figures 2C and 3B). The body weight loss occurred at the lowest aluminum

concentration of 0.15 mg/kg/day and was more pronounced with higher doses such as 1.5 and 15 mg/kg/day (Figure 3B). The disease activity index (DAI), combining weight loss, stool consistency and presence of rectal bleeding, was also increased in both forms of aluminum-treated mice compared to PBS-treated mice with colitis (Figures 2D and 3C). Consistently, colonic myeloperoxydase (MPO) activity was increased in aluminum-treated mice compared to control animals, with colitis together with a more intense inflammatory infiltrate mainly located in the mucosal and submucosal layers (Figure 2E and F). To demonstrate that our results were specific to aluminum, mice were fed with another metal, namely zinc phosphate (ZnP) together with colitis induction (Figure 3A). Mice treated with ZnP experienced the same body weight loss as DSS- and PBS-treated mice and no difference in DAI was observed (Figure 3B and C). As a whole, these results demonstrated that two different forms of aluminum worsened lesion severity in two distinct models of colitis in mice.

Aluminum worsens chronic colitis in IL10$^{-/-}$ mice

We then investigated the effects of aluminum in a chronic colitis model. IL10$^{-/-}$ mice received AluCi in their drinking water for seven weeks with a daily dose of 1.5mg of Al element per kg body weight (Figure 4A). Macroscopic mucosal damage was assessed by mini-endoscopy score (Figure 4B-C). Mucosa from IL10$^{-/-}$ mice receiving water showed overt signs of inflammation. IL10$^{-/-}$ mice treated with AluCi had a mucosa less transparent, a vascular pattern more altered, more fibrin and a significant increase of mucosa granularity compared with IL10$^{-/-}$ mice receiving water. The histological score for IL10$^{-/-}$ mice treated with AluCi was significantly increased compared with the water treated IL10$^{-/-}$ mice (Figure 4D,E). MPO activity was significantly more elevated in AluCi treated IL10$^{-/-}$ mice than in control IL10$^{-/-}$ mice (Figure 4F). Taken together,

these data argued in favor of a worsening effect of oral Aluminum in the development of chronic colitis in IL10$^{-/-}$ mice.

Aluminum increases inflammatory cytokine expression in different models of colitis

AluCi significantly increased the expression of *Il1β* and *Il17a* mRNA in the colon of animals 4 days after TNBS administration (Figure 5A). The modification of this colonic cytokine profile induced by aluminum gavage and TNBS administration was associated with an increased expression of *Nlrp3* mRNA (Figure 5A), a known intracellular innate immune marker of inflammasome response regulated by aluminum[75] Similar data were obtained in animals with DSS-induced colitis, where AluCi administration also significantly up-regulated the colonic expression of inflammatory cytokines and *Nlrp3* mRNA compared to untreated mice with colitis (Figure 5B). Similar results were observed with AluP (data not shown).

In the chronic model of colitis, mucosal levels of *Il1β, Il17a* and *Nlrp3* tended to be higher in the IL10$^{-/-}$ mice intoxicated with AluCi compared to IL10$^{-/-}$ mice receiving water (Figure 5C).

Enhanced inflammatory cytokine expression in aluminum-treated epithelial cells and potentiation by bacterial components

To investigate the potential inflammatory effect of luminal aluminum on the first intestinal layer in contact with luminal antigens and particles, we incubated HT-29 and Caco-2 epithelial cells for 3 hours with increased concentrations of aluminum from 10 to 100 µg of Al element/ml. A dose-response effect of aluminum was observed in Caco-2 cells, leading to an increased expression of the inflammatory cytokines IL8 and IL1β mRNA (Figure 6A). Similar data were obtained with HT-29 epithelial cells (data not shown). Co-incubation of Caco-2 cells with a low concentration

of bacterial lipopolysaccharide (LPS, 1 µg/ml) and increased concentrations of aluminum led to a synergistic and dose-dependent pro-inflammatory effect with an increased expression of IL8 and IL1β mRNA (Figure 6B). Similar data were obtained in HT-29 cells (data not shown).

Aluminum extends colitis duration and decreases mucosal healing

Besides its effects on colitis severity, we investigated the influence of oral administration of AluCi at 1.5 mg Al element/kg on colitis duration in C57BL6 mice submitted to one cycle of 2% DSS for 7 days (Figure 7A). Colonic lesions were evaluated during the 19-day experiment to investigate the persistence of lesions during the recovery period. At the end of DSS administration, mice treated with aluminum continued to lose weight and presented a slow recovery compared to mice with colitis receiving the vehicle (Figure 7B). In contrast, body weight changes were paralleled after day 7 in control mice with or without DSS-induced colitis receiving the vehicle and control animals treated with aluminum (Figure 7B). At day 19, animals with DSS-induced colitis receiving aluminum presented persistent intestinal inflammation, as demonstrated by an increase in DAI, colonic MPO activity and histological lesions (Figure 7C-E). To confirm the deleterious effect of aluminum on colitis healing, we designed a subsequent experiment where aluminum was started just after DSS-induced colitis (Figure 8A). In contrast to control animals, which completely recovered their initial body weight 10 days after DSS-induced colitis, administration of AluCi significantly delayed weight gain and led to a sustained increase of colonic weight/size ratio compared to control animals (Figure 8B and C).

To better evaluate the effects of aluminum on colonic wound healing, we quantified *ex vivo* epithelial cell proliferation and apoptosis in the colon of C57BL6 mice receiving or not receiving aluminum 10 days after DSS-induced colitis (Figure 9A). AluCi administration was

associated with an inhibition of epithelial cell proliferation, as assessed by proliferating cell nuclear antigen (PCNA) immunostaining, compared to control animals (Figure 9A and B). The mean fluorescence of terminal transferase dUTP nick end labeling (TUNEL)-stained colon sections was similar in animals with colitis receiving or not receiving aluminum (Figure 9C and D).

To confirm the direct influence of aluminum on epithelial cell proliferation, we performed an explanatory experiment on HT-29 cells. We showed that aluminum inhibited epithelial cell proliferation by more than 40% without modification of cell death assessed by lactate deshydrogenase (LDH) release (Figure 9E and F).

Aluminum alters the intestinal barrier and induces granuloma formation

We next assessed the intestinal effects of aluminum given once a day (1.5 mg/kg) for 4 weeks on epithelial barrier integrity. The rate of bacterial translocation, reflecting the intestinal barrier, was very low in the mesenteric lymph nodes (MLN) of control C57BL6 mice receiving PBS (Figure 10A). In contrast, more than a 100-fold increased colonization of MLN was observed in animals receiving AluP (Figure 10A). Tight junctions of epithelial cells involving occludins, claudins and zonula occludens are critical to maintain intestinal barrier function. A significant decrease of occludin (*ocln*) mRNA expression was observed in the colon of mice treated with aluminum compared to PBS-treated control animals (Figure 10B). We then evaluated the effect of aluminum on colonic flora bulk and composition. Both remained similar in the colon of mice receiving aluminum or PBS (Figure 10C). Altogether, these data suggest that aluminum enhanced intestinal permeability leading to an increased load of bacteria through the intestinal wall without a concomitant increase of bacterial pressure in the colon.

The number and size of granulomas developed *in vitro* was evaluated after a 4-day incubation of human peripheral blood mononuclear cells (PBMCs) from healthy donors with increasing concentrations of AluP alone and/or together with *Mycobacterium bovis* strain BCG (BCG), adherent/invasive *Escherichia coli* strain LF82 (AIEC) and a non pathogenic *Escherichia coli* K-12 strain DH5α[76, 77] As expected, no granulomas were observed in control wells without aluminum and bacteria. The granuloma count increased proportionally until 700 granuloma counts per well with the increased dose of aluminum, with a positive effect beginning at a very low concentration of aluminum (5 ng Al element/ml) (Figure 10D and E). Same experiments were performed with Zn and no granuloma formation was observed, showing a specific effect of aluminum (date not shown). We then evaluated the effect of a suboptimal concentration of aluminum (5 ng/ml) on bacterial-induced granuloma. As previously described, non-pathogenic *E. coli*, AIEC and mycobacteria induced granuloma formation, with a mean number per well of 101.5±24.5, 224.5±72.3 and 278.8±47.3, respectively[77] Aluminum at the dosage of 5 ng/ml potentiated the effect of bacterial infection on granuloma formation, resulting in an increased number and a bigger size of granuloma (Figure 10F).

Altogether, these data suggest that aluminum administration leads to a leaky gut, enhancing intestinal bacterial translocation and favoring development of granulomas.

3. Discussion:

Our study provides strong evidence that aluminum modulates intestinal inflammation *in vivo* in mice. A daily intake of aluminum at a concentration observed in the environment increased the severity as well as the duration of intestinal inflammation with impaired mucosal repair in different models of colitis in mice. Aluminum mediated intestinal inflammation through several mechanisms, including inflammatory response against bacteria, epithelial cell renewal and occludin expression, which affected the intestinal barrier and favored granuloma formation.

In humans, the principal route of entry of aluminum is the ingestion of food or water containing aluminum[49, 51] Oral bioavailability of aluminum is estimated to be less than 1%[78] Aluminum accumulates in the skeletal system and the brain, and a link with diseases such as osteomalacia, encephalopathy, Alzheimer and Parkinson's diseases have been reported[74, 79, 80] The low percentage of oral bioavailability of aluminum is actually misleading. In fact, after oral administration, 40% of the ingested dose accumulates within the intestinal mucosa, which makes the gut the main storage organ for aluminum in the body[81, 82] Intestinal accumulation of aluminum may be particularly relevant to CD since it has been identified within macrophages of Peyer's patches but also around dilated submucosal lymphatics and in mesenteric lymph nodes[44, 46, 83] In spite of this, the potential toxic role of aluminum in the gut has been poorly studied. Interestingly, a fatal outbreak of granulomatous enteritis with many histological similarities with CD was reported in a group of horses sharing a common environment. In the evaluation of the cluster, an unexpected finding was the presence of aluminum excess in affected tissues[63] Our results are in agreement with a study reported only in abstract form, in which oral aluminum increased histological scores in IL-10 knockout mice[84] Moreover, using two different experimental models of chemically induced colitis developed in mice with different genetic backgrounds, we here demonstrated that small amounts of two different forms of

aluminum enhanced the intensity and duration of intestinal inflammation, leading to an increased mortality, increased body weight loss, more intense macroscopic and histological lesions and enhancement of colonic MPO activities.

Importantly, the dose (1.5 mg/kg) and the route of aluminum administration used in this study are relevant to human exposure. Indeed, it was estimated by a US food additives survey that most Americans ingest from 0.01 to 1.4 mg total aluminum/kg body weight/day. In the same study, it was estimated that approximately 5% of Americans ingested more than 95 mg aluminum/day (>1.36 mg/kg body weight) as additives in commercially-processed foods and beverages[74] In Europe, it was also estimated that the tolerable intake of aluminum is exceeded in a significant proportion of the population, especially in children, who are more vulnerable to toxic effects of pollutants than adults[85, 86] Moreover, these estimations did not take into account aluminum ingestion through pharmaceuticals, which is estimated to account for 99% of the aluminum ingested by individuals consuming aluminum-containing medications[87] Aluminum can be found naturally in different forms, we thus choose to study an organic soluble form (citrate) and a particular form (phosphate). Our results demonstrated that both forms of aluminum worsened colitis and delayed mucosal healing, excluding a form-based effect.

The precise mechanisms involved in the detrimental effects of aluminum on intestinal inflammation are unknown. Aluminum has potential direct cytotoxic effects at high concentrations but most of its biological mechanisms of action have been described when looking at its adjuvant effect in vaccines[88] In the latter case, aluminum-induced inflammation involves the Nlrp3 inflammasome but also Nlrp3-independent effects mediated through macrophages, B and T cells, resulting in an enhanced antigen-specific T-cell response and an increased production of inflammatory cytokines[89] In the present study, no direct intestinal cytotoxic effect of aluminum was detected in control animals fed for 1 month with small amounts of aluminum, nor

when epithelial cells were cultured with high concentrations of aluminum reaching 0.1 mg/ml. Consistent with previous studies analyzing in the skin or the lung the immunobiology of intradermal or inhaled aluminum, oral exposure to aluminum activated Nlrp3 and potentiated the expression of several inflammatory cytokines[64, 65] Furthermore, evidence supporting a key role of epithelial cells in aluminum-sustained intestinal inflammation was obtained both *in vitro* and *in vivo* and was in line with a previous study showing that aluminum decreased the transepithelial electrical resistance of Caco-2 cells[88] Using two different HT-29 and Caco-2 epithelial cell lines, aluminum, in a dose dependent-manner and synergistically with bacterial LPS, enhanced the production of inflammatory cytokines and decreased by more than 40% their ability to proliferate. The relevance of our *in vitro* data was further highlighted by the demonstration that animals treated with aluminum presented an impaired epithelial wound-healing, with sustained inflammation and an increased bacterial translocation to mesenteric lymph nodes. Another mechanism of action of aluminum may be through its direct interaction with bacterial flora. In our experiments, aluminum did not modify the bacterial composition of the colonic flora of mice. It has been hypothesized that aluminum, through metal chelating systems, could gain access to microorganisms and then alter their pathogenicity and ability to induce an exuberant granulomatous response[90] We here demonstrated that aluminum was indeed capable of stimulating granuloma formation, either alone or when associated with bacteria.

Translation of experimental evidence to human diseases remains hazardous. Aluminum exposure has already been implicated in a variety of chronic undetermined inflammatory diseases, such as multiple sclerosis, myofasciitis, pulmonary granulomatosis and rheumatoid arthritis[53, 91-93] Since most people living in industrialized and emerging countries are routinely and inevitably exposed to aluminum, future descriptive, genetic and epidemiological

studies will be necessary to clarify the mechanisms leading to aluminum susceptibility in patients. An emerging concept suggests that dysfunction of xenobiotic processing enzymes expression or activity in the intestinal mucosa may be an important event in the initiation and progression of IBD[94, 95] Indeed, several studies have identified an association between SNP in genes involved in xenobiotics' detoxification and susceptibility to IBD[96, 97] New research activities should now develop standard protocols for measuring aluminum in intestinal tissues of patients with IBD and controls, and analyze these data according to the genetic profile of their detoxification enzymes.

4. Material and Methods:

Animals:

Five- to eight-week-old C57BL6 and BALB/C male mice were purchased from Janvier Laboratory (Le Genest-St-Isle, France). Animals were maintained in specific pathogen free conditions in the animal facility at the Institut Pasteur de Lille. B6-IL10tm1Cgn (interleukine 10-negative ($IL10^{-/-}$)) mice were bred in the animal facility of the University Hospital of Zurich. Animals had access to standard tap water and chow diet *ad libitum*. All animal experiments were approved by the local animal care program and were in accordance with the European convention on research animal protection.

Aluminum treatment:

Aluminum phosphate ($AlH_6O_{12}P_3$, Sigma-Aldrich, Saint-Quentin Fallavier, France) or aluminum citrate ($AlC_6O_7H_5$) were diluted in PBS (Lifetechnologies, Saint Aubin, France) and administered once a day with a gavage needle at a concentration of 1.5 mg of Al element/kg body weight, an amount equivalent to the high end of the total aluminum range ingested daily by humans living in contemporary urban society[74] The duration of aluminum treatment was dependent on the setting of each experiment and was detailed in each figure. A dose-response experiment was performed and aluminum phosphate was given to mice at a concentration of 0.15, 1.5 and 15 mg of Al element/kg body weight/day. Zinc phosphate ($Zn_3(PO_4)_2$) diluted in PBS was used as a control and was orally administered to mice at a concentration of 1.5 mg Zn element/kg body weight/day. Stock solutions of aluminum salts or zinc phosphate, adjusted to mice weight, were prepared weekly. In all experiments, control mice received PBS by gavage.

For experiments performed with $IL10^{-/-}$ mice, AluCi was diluted in their drinking water at a concentration of 0,015mg of Al element/ml to reach a daily exposure of 1.5mg of Al element /kg body weight.

Induction of TNBS and DSS colitis:

TNBS colitis was induced in anesthetized C57BL6 mice by intrarectal administration of TNBS (150 mg/kg, Sigma-Aldrich) diluted in a 1:1 (v/v) mix of 0.9% NaCl and 100% ethanol, as described previously[98] Control animals received an NaCl/ethanol mix using the same technique. Mice were euthanized 4 days after TNBS/ethanol administration.

Acute colitis was induced with 2.5% (w/v) DSS (45 kDa, TdB Consultancy, Uppsala, Sweden) dissolved in water for 7 to 9 days. For recovery experiments, colitis was induced by feeding mice with 2% (w/v) DSS for 7 days, followed by normal water until the end of the experiments, 10 or 12 days after DSS discontinuation. At the end of each experiment, mice were assessed for clinical score and euthanized.

Determination of clinical scores*:*

For TNBS-induced colitis, animals were euthanized and the colon of each mouse was dissected and cut longitudinally to reveal the colonic mucosa. The intensity of colonic lesions was first evaluated macroscopically according to the Wallace score[99] The Wallace score rates macroscopic lesions on a scale from 0 to 10 based on features reflecting inflammation, such as hyperemia, thickening of the bowel and the extent of ulceration. A colon specimen located within the ulceration was used for histological evaluation. The other parts of the colon were frozen for subsequent analysis of mRNA expression and MPO activity quantification.

For DSS-induced colitis, body weight was determined regularly during DSS and the water administration phase until the end of each experiment. At the end of each experiment animals were assessed for clinical score by recording body weight variation, stool consistency and occult blood before being euthanized. A DAI was determined as previously described and is summarized in Supplementary Table 1 [100] Rectal bleeding was assessed with the ColoScreen III Lab Pack (Elitech, Salon-de-Provence, France). The DAI score ranged from 0 (healthy) to 12 (greatest level of colitis). After euthanasia, the colon was carefully dissected and its weight and size were measured. Circular sections of the colon were prepared for histological analysis. The other parts of the colon were frozen for subsequent analysis of mRNA expression and MPO activity quantification.

In the model of chronic colitis, $IL10^{-/-}$ animals were anaesthetized intraperitoneally with a mixture of 100mg ketamine (Vétoquinol, Bern, Swizerland) and 8mg of Xylazine (Bayer, Lyssach, Switzerland) per kg body weight and examined as described previously with the Tele Pack Pal 20043020 (Karl Storz Endoskope, Tuttloingen, Germany)[101] Colonoscopy was scored using the murine endoscopic index of colitis severity (MEICS) scoring system as described previously[102] After euthanasia, circular sections of the colon were prepared for histological analysis. The other parts of the colon were frozen for subsequent analysis of mRNA expression and MPO activity quantification.

Histology:

Colons were fixed in 4% paraformaldehyde, and embedded in paraffin (Labonord, Templemars, France). Tissue sections were stained with May-Grünwald and Giemsa (MGG) and evaluated blindly by 2 investigators. Histological lesions of mice with TNBS-induced colitis were quantified using the modification by Ameho of the histopathological grading system of

Macpherson and Pfeiffer (ranging from 0 to 6)[99] Briefly, histological findings identical to those of normal mice were scored as 0, mild mucosal and/or submucosal inflammatory infiltrate and edema, punctate mucosal erosions, and intact muscularis mucosae were scored as 1, the same histological findings involving 50% of the specimen were scored as 2, prominent inflammatory infiltrate and edema, deeper areas of ulceration extending through the muscularis mucosae into the submucosa, and rare inflammatory cells invading the muscularis propriae but without muscle necrosis were scored as 3, the same histological findings involving 50% of the specimen were scored as 4, extensive ulceration with coagulative necrosis with deep extension of the necrosis into the muscularis propria were scored as 5, and the same histological findings involving 50% of the specimen were scored as 6.

For DSS-induced colitis and chronic colitis, histological lesions were assessed using a score quantifying the intensity of the inflammatory cell infiltrate (score 0–3) and the tissue damage (score 0–3) as previously described[100] Briefly, the presence of occasional inflammatory cells in the lamina propria was scored as 0, increased numbers of inflammatory cells in the lamina propria as 1, confluence of inflammatory cells extending into the submucosa as 2, and transmural extension of the infiltrate as 3. For tissue damage, scores were: 0, no mucosal damage; 1, lymphoepithelial lesions; 2, surface mucosal erosion or focal ulceration; 3, extensive mucosal damage and extension into deeper structures of the bowel wall. The combined histological score ranged from 0 (no changes) to 6 (extensive infiltration and tissue damage).

***MPO activity measurement**:*

MPO activity was measured to monitor the degree of neutrophil infiltration in the colonic lesions during chemically-induced and chronic colitis[103] Colon specimens were homogenized with an Ultra Turrax T8 (Ika-Werke, Staufen, Germany) in a phosphate buffer (pH 6.0)

containing 0.5% hexadecyltrimethyl ammonium and subjected to two sonication and freeze-thaw cycles. The suspensions were centrifuged at 14,000 × g for 15 min at 4°C and the supernatants were reacted with 1 mg/ml o-dianisidine hydrochloride and 0.0005% hydrogen peroxide. The optical density of each sample was read at 450 nm with a Versamax microplate reader (MDS Analytical Technologies). One unit of MPO activity was defined as the amount that degraded 1 µmol peroxidase per minute at 25°C. The results were expressed as absorbance per total quantity of proteins determined by the Bradford method.

***PCNA staining and TUNEL labeling**:*

Ex vivo cell proliferation was assessed by staining for PCNA. Colonic sections were boiled in 0.1 M sodium citrate buffer pH 6.0 for 6 min for antigen unmasking. After washing, sections were blocked for 30 min with 5% BSA in PBS, stained overnight at 4°C with anti-PCNA antibody (1/50) (Santa Cruz Biotechnology, USA), and incubated with Alexa 488 conjugated secondary antibody (1/100) (Invitrogen, France) for 1 hour. Sections were counterstained with DAPI (Molecular Probes, Eugene, Oregon, USA). To ensure specificity of immunostaining, control sections underwent simultaneous staining with isotype control antibody.

Detection of apoptosis was performed by TUNEL assay using the *in situ* cell death detection kit (Roche, France). Sections were permeabilized with 1% Triton X-100, 0.1% sodium citrate, washed and stained for TUNEL according to the manufacturer's instructions. Sections were counterstained with DAPI.

The quantification of positive TUNEL- or PCNA-stained cells was performed randomly using ImageJ processing and analysis software. Images were acquired with a DM5500B microscope equipped with a DFC 310 FX camera (Leica Microsystems, Nanterre, France) and

mucosal layers were photographed at a magnification of x 10 to measure specific fluorescence intensity.

***Cell line stimulation assay**:*

Caco-2 and HT-29 epithelial cells were cultured in 12-well plates (density of 5×10^5 cells/well) with Dulbecco's modified eagle's medium supplemented with 10% fetal bovine serum (Eurobio, France) and 1% penicillin-streptomycin (Invitrogen, France), at 37°C in 5% CO_2 /95% humidified air. Cells were treated with aluminum phosphate at different concentrations (10 to 100 µg Al element/mL) with or without LPS (1 µg/mL, Sigma-Aldrich, France) for 3 to 6 hours. After the incubation period, cells were washed twice with sterile PBS, and then lysed with RA1 buffer containing 1% β-mercaptoethanol (Macherey-Nagel, Germany).

For the determining of cytotoxicity and proliferation, cells were incubated with aluminum for 5 days. Supernatants were collected for LDH (lactate deshydrogenase) measurement (Cytotoxicity detection kit, Roche, France) and cell proliferation was assessed using a colorimetric MTT cell proliferation assay (Interchim, France). Optical density was read at 500 and 570 nm, respectively, with a Versamax microplate reader (MDS Analytical Technologies).

***RNA extraction and Real-Time qPCR**:*

Total RNA was extracted from colonic samples with the NucleoSpin RNAII commercial kit (Macherey-Nagel, Germany), as described by the manufacturer. cDNA was prepared with the High Capacity cDNA Archive kit and RT–qPCR was performed with SyBrGreen (Applied Biosystems). Beta-Actin was used as a reference gene and primer sequences are listed in Supplementary Table 2.

Microbiologic analysis:

Colon samples and mesenteric lymph nodes were introduced into pre-weighed vials containing 1.5 mL of cysteinated Ringer's solution. After physical disruption of the colon specimens, 10-fold dilutions were performed in the same diluent (decimal dilutions from 10^{-2} to 10^{-5}). Each dilution was spread onto plates of nonselective blood agar (modified Columbia agar) incubated at 37°C for 1 week under anaerobic conditions, McConkey plates (BioMerieux, Marcy l'Etoile, France) incubated at 37°C for 48 hours under aerobic conditions, and Man, Rogosa, Sharpe plates incubated at 37°C for 48 hours under CO_2-enriched conditions. Total counts were performed, and different types of colonies were subcultured and identified following established morphological and biochemical criteria. Quantitative results are expressed in log colony forming unit (CFU)/g. The threshold of detection is 10^4 CFU/g.

After disruption of mesenteric lymph nodes in the Ringer's solution, 1 mL was grown in brain-heart enrichment broth (BH) and 0.1 mL was spread onto plates of nonselective blood agar and incubated at 37°C for 1 week under anaerobic conditions. If the BH broth became turbid, 0.1 mL was spread onto plate of nonselective blood agar and incubated at 37°C for 1 week under anaerobic conditions. Subcultured bacteria were identified as above. The threshold of detection was 10^2 CFU/g. All samples were analyzed in a blind manner.

In vitro granulomas formation:

Fresh human blood from healthy volunteers was obtained from the Etablissement Français du Sang and was diluted 1/1 (v/v) with RPMI (Invitrogen, France), layered gently onto a ficoll-paque solution (Amersham, France) and then centrifuged for 40 min at 1800 rpm. PBMCs were collected and washed three times in RPMI medium by 10 min centrifugation at 1800 r.p.m. Cells were counted with a Malassez cell and diluted to a concentration of 1×10^6 cells ml^{-1} in RPMI

media supplemented with 7.5% heat-inactivated human AB serum (Sigma-Aldrich, France). PBMCs were then incubated in 24-well plates with increasing concentrations of aluminum phosphate or alone for 4 to 7 days, at 37°C in a 5% CO_2 atmosphere. In each well, the number of granulomas was counted. Granuloma enumeration was performed using an inverted microscope and a x4 objective (Olympus CK40). Pictures were taken using an inverted microscope with a x4, x10 or x40 objective (Nikon TE300 Eclipse). For experiments with bacterial stimulation, PBMCs were incubated with either $1x10^3$ non-pathogenic *E. coli* K-12 strain DH5α, AIEC strain LF82 or $1x10^4$ BCG, alone or with aluminum phosphate (5 ng Al element/mL) for 4 days at 37°C in a 5% CO_2 atmosphere. Granuloma enumeration was performed as previously described. Results are represented as the total number of granulomas per well and the percentage of small size (index 1) and big size granulomas (index 2 to 4).

Statistical analysis:

Data are presented as the mean ± SEM. Comparison between different treatment groups for quantitative variables was performed using the Wilcoxon-Mann-Whitney test. Two-tailed significance tests were used. Kaplan-Meier analysis with log-rank statistics was performed in survival during DSS-induced colitis. A p value of less than 0.05 was considered statistically significant.

5. Figures:

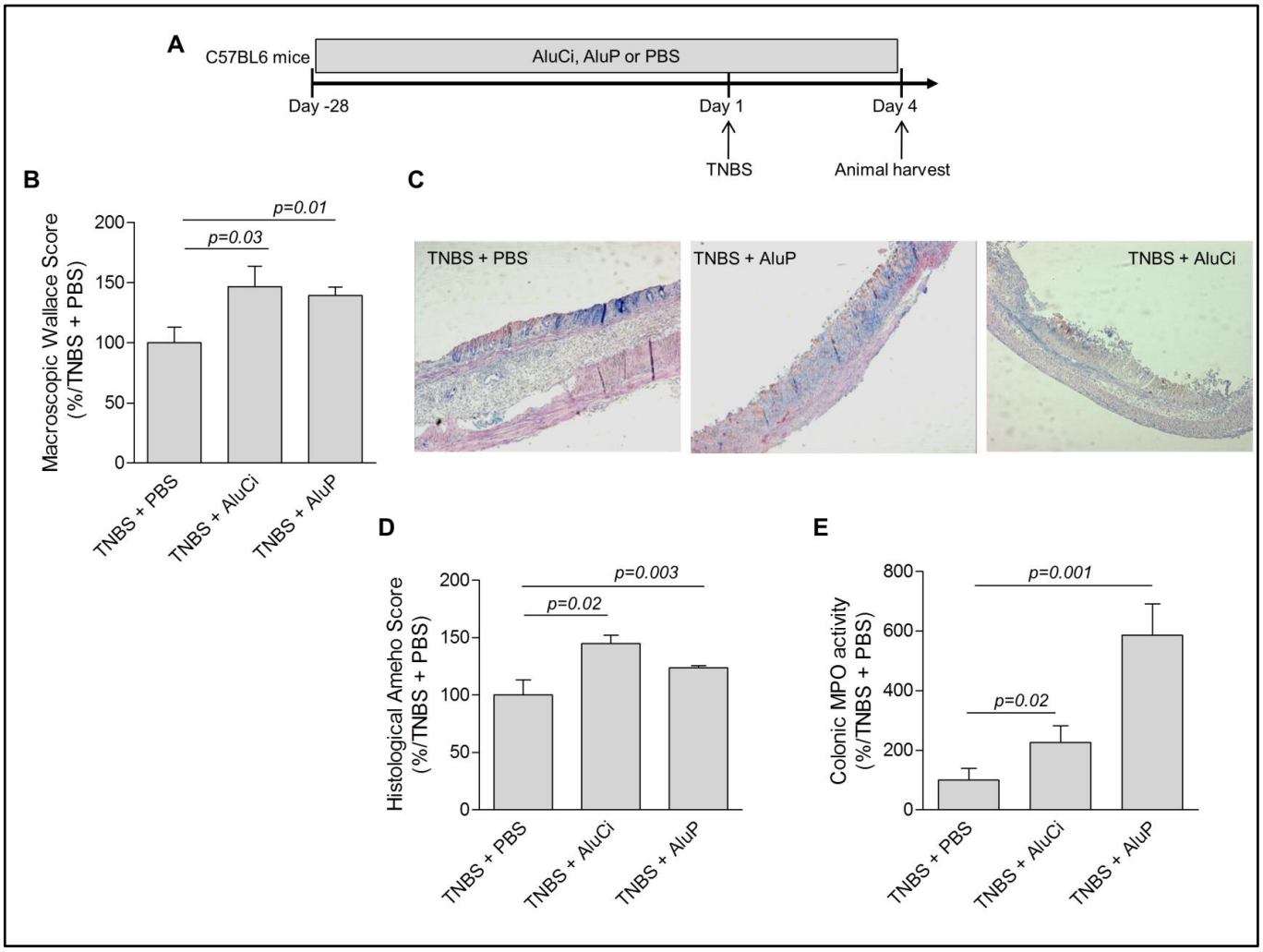

Figure 1: aluminum worsens TNBS-induced colitis. (**A**) C57BL6 mice (n=14/group) were fed with aluminum citrate (AluCi) or aluminum phosphate (AluP) (1.5 mg of Al element/kg/day) or with PBS for 31 days. At day 28, colitis was induced by intra-rectal administration of TNBS. Four days after colitis induction mice were euthanized and colitis parameters were assessed. (**B**) The macroscopic Wallace score was determined as described in Methods. (**C**,**D**) Histopathological changes in colon tissues were examined by MGG staining and scoring was performed as described in Methods. (**E**) MPO activity was measured in colonic lesions. Results are expressed as the percentage of variation compared to TNBS-treated mice.

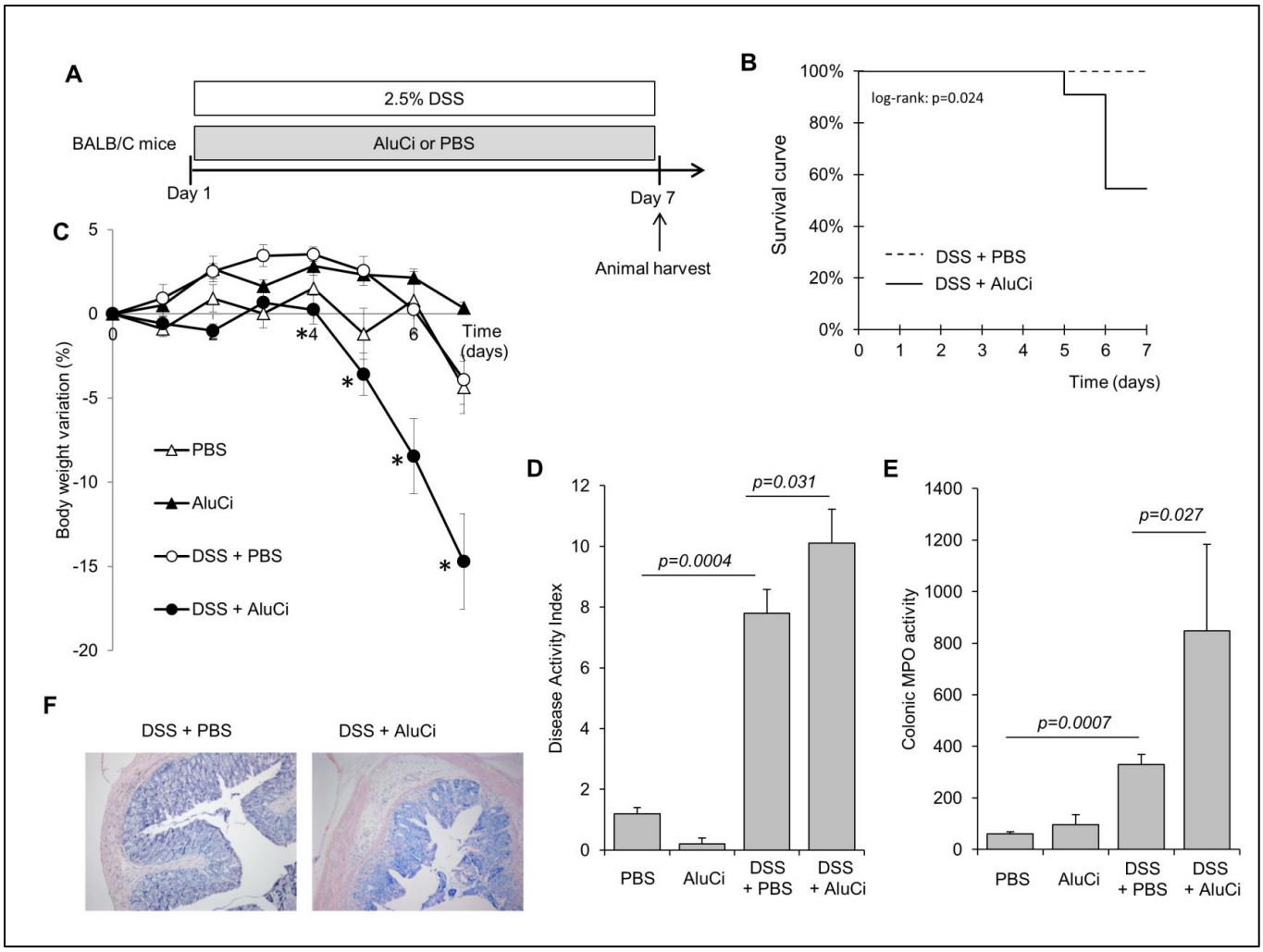

Figure 2: AluCi worsens DSS-induced colitis. (**A**) BALB/C mice (n=10/group) were treated with 2.5% DSS and AluCi (1.5 mg of Al element/kg/day) or PBS for 7 days. Control mice treated with AluCi or PBS without DSS were followed for the same period (n=5/group). (**B**) Survival of mice was monitored until day 7 after the start of DSS. (**C**) Body weight was scored daily. * means p <0.05 between DSS + PBS and DSS + AluCi. (**D**) A disease activity index that included body weight variation, presence of blood in stools and stool consistency was calculated at day 7. (**E**) MPO activity was measured on colons harvested at day 7. (**F**) Histopathological changes of colonic tissues were examined by MGG staining.

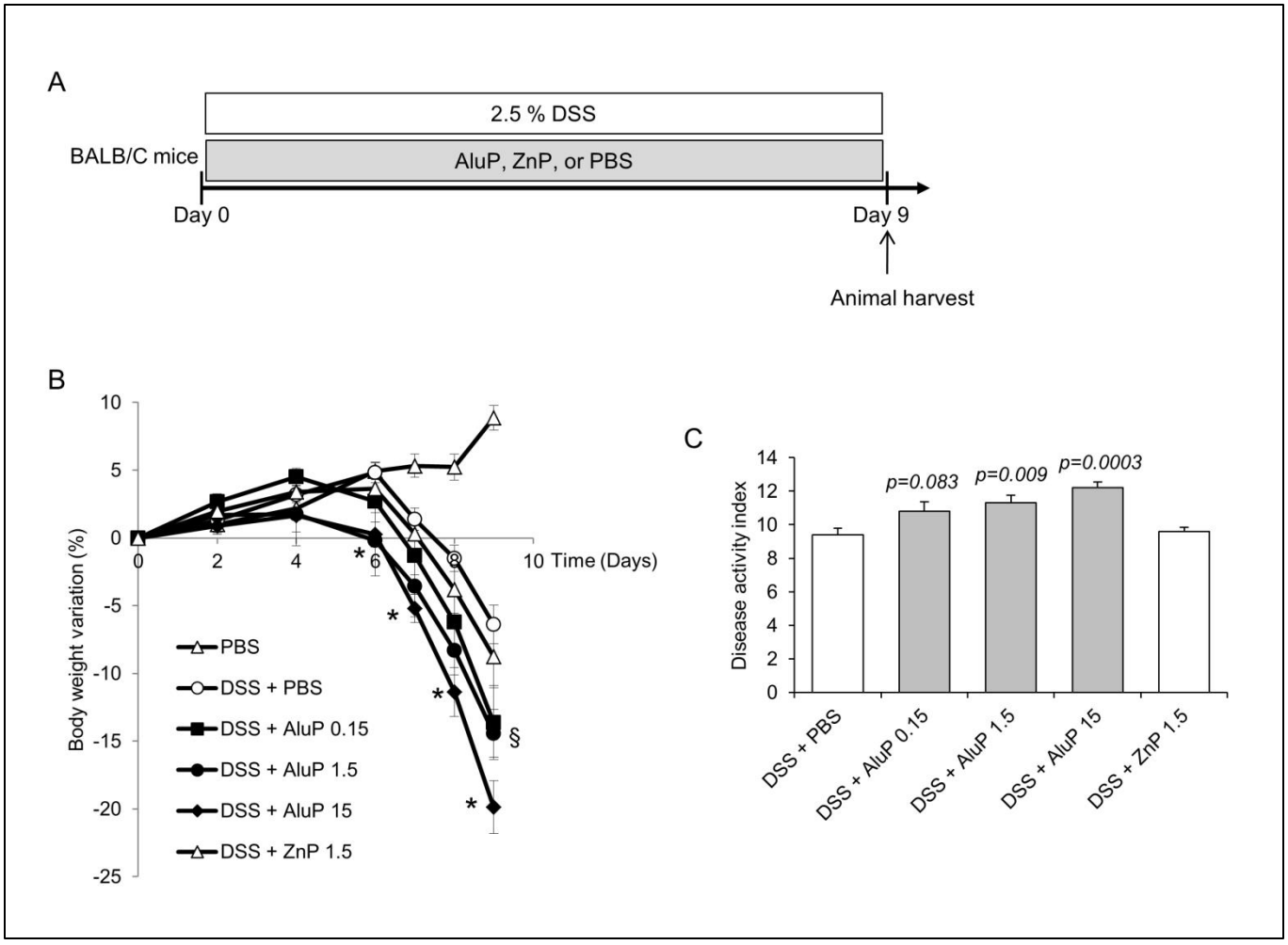

Figure 3: AluP but not ZnP worsens DSS-induced colitis. (**A**) BALB/C mice (n=10/group) were treated with 2.5% DSS and with increasing doses of AluP (0.15, 1.5 and 15 mg of Al element/kg/day) or ZnP (1.5 mg of Zn element/kg/day) or PBS for 9 days. (**B**) Body weight was scored daily. * means $p < 0.05$ between DSS + PBS and DSS + AluP 1.5 and 15, § means $p < 0.05$ between DSS + PBS and DSS + AluP 0.15. (**C**) A disease activity index that included body weight variation, presence of blood in stools and stool consistency was calculated at day 9.

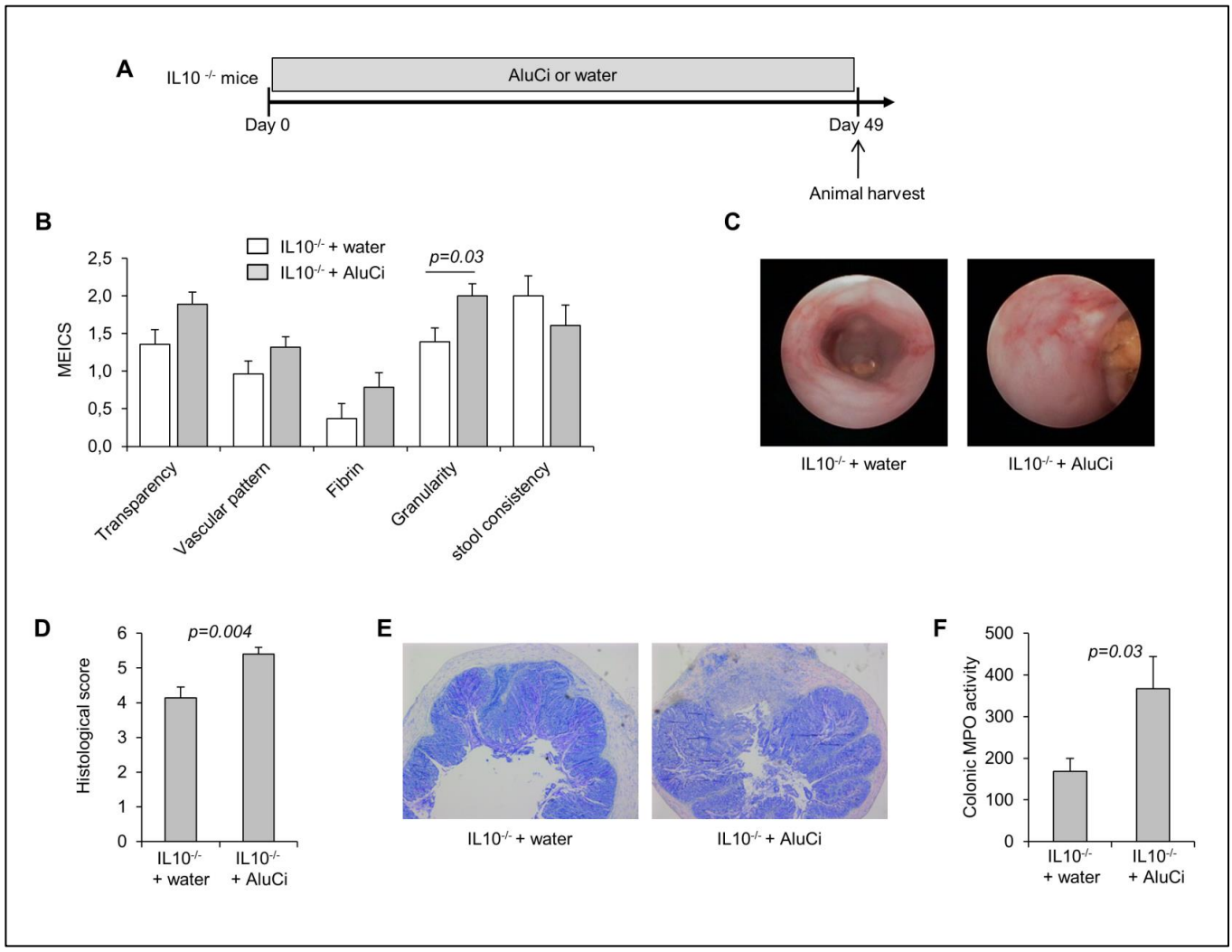

Figure 4: AluCi aggravates chronic colitis in IL10$^{-/-}$ mice. (**A**) Eight-week-old IL10$^{-/-}$ mice were treated with AluCi (1.5 mg of Al element/kg/day) in their drinking water (n=15) or with water only (n=14) for 49 days. (**B**) Mini-endoscopic images were done as described in methods. (**C**) The five parameters of the murine endoscopic index of colitis severity (MEICS) were determined. (**D,E**) Histopathological changes in colon tissues were examined by MGG staining and scoring was performed as described in methods. (**F**) MPO activity was measured in colonic lesions.

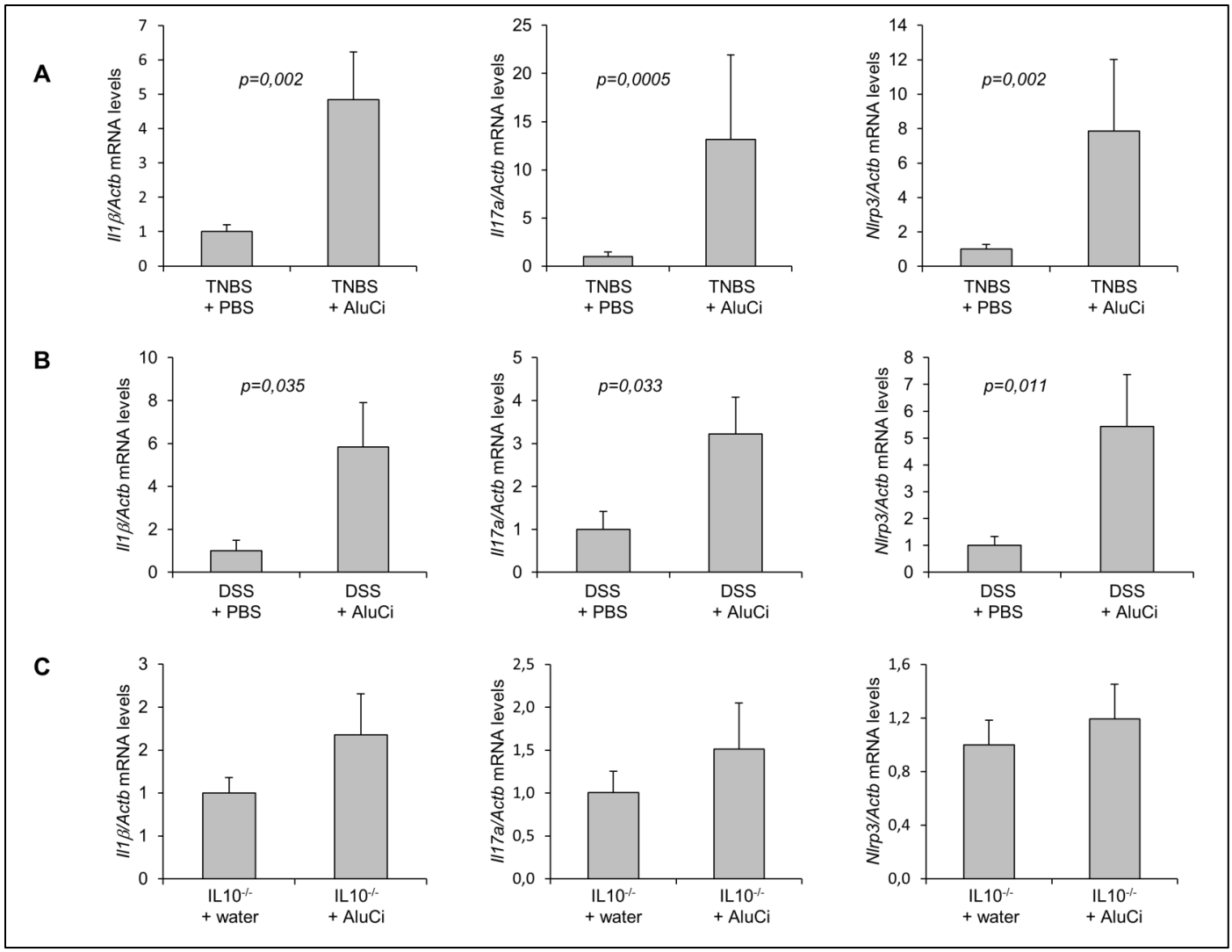

Figure 5: AluCi increases the expression of pro-inflammatory cytokines in colitis. *Il1β, Il17a* and *Nlrp3* mRNA levels from homogenized colons of: (**A**) mice treated with TNBS and PBS or treated with TNBS and AluCi, (**B**) mice treated with DSS and PBS or treated with DSS and AluCi, and **(C)** IL10$^{-/-}$ mice treated or not with AluCi.

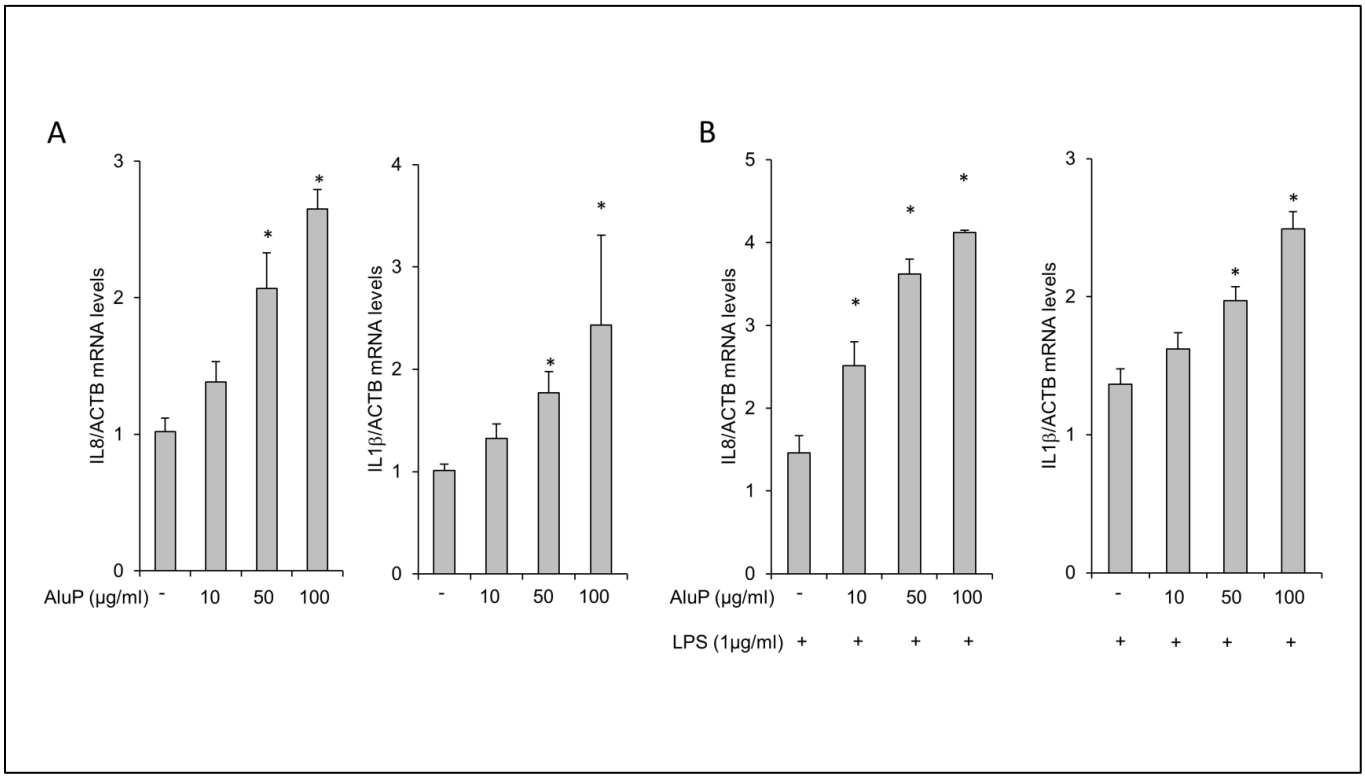

Figure 6: AluP stimulates the expression of IL8 and IL1β by intestinal epithelial cells and enhances their response to bacterial stimuli. (**A**) Caco-2 cells were incubated with increasing doses of AluP (from 10 to 100 µg of Al element/mL). qPCR assay on Caco-2 cell lysates showed a dose-dependent increase of IL8 and IL1β expression in presence of aluminum. (**B**) Caco-2 cells were co-stimulated with increasing doses of AluP (from 10 to 100 µg/mL) and LPS. qPCR assay on Caco-2 cell lysates showed a dose-dependent increase of IL8 and IL1β expression in presence of aluminum compared with LPS stimulation alone. *p <0.05 vs controls.

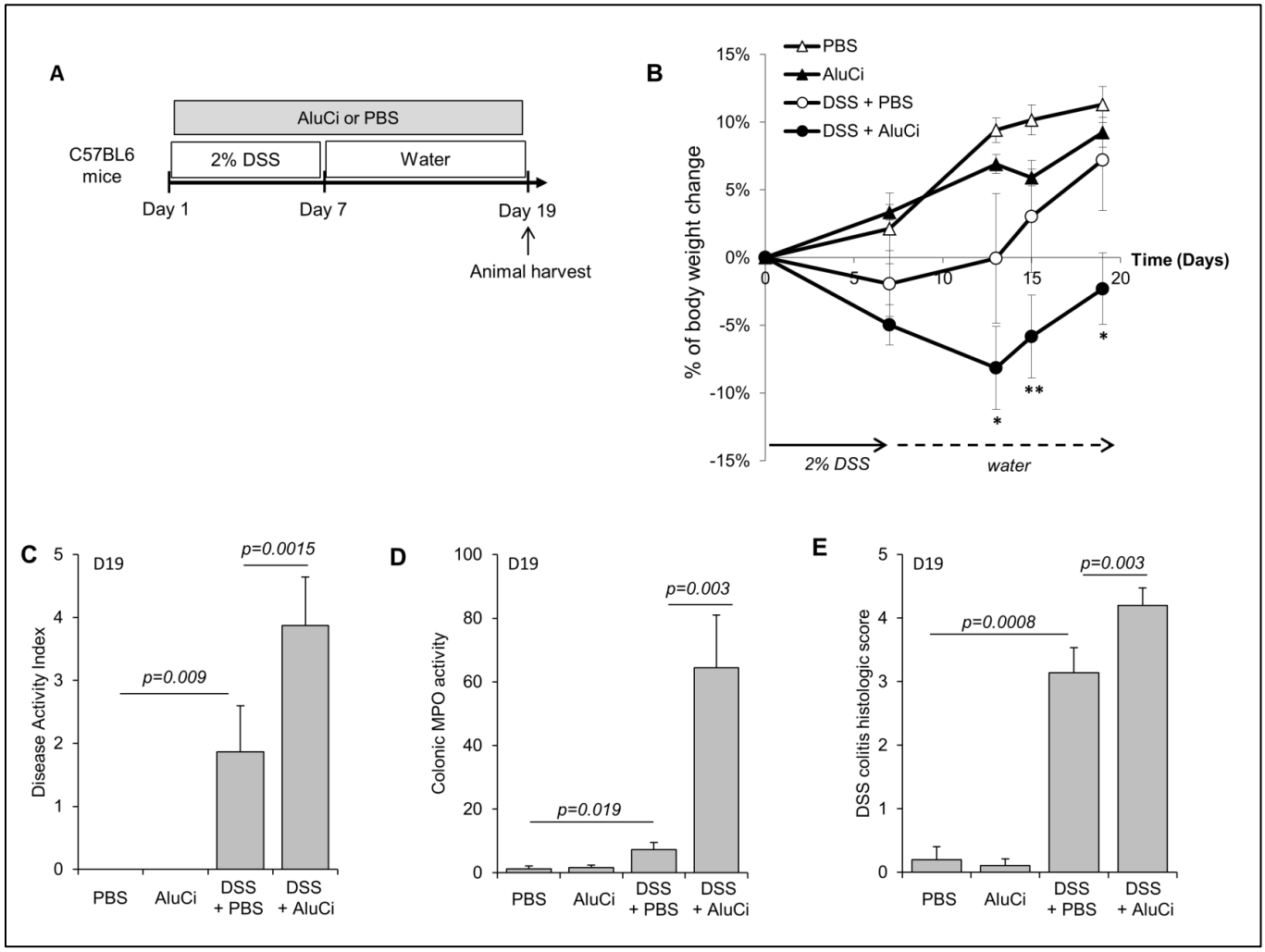

Figure 7: AluCi extends duration of DSS-induced colitis. (**A**) C57BL6 mice (n=10-15/group) were treated with 2% DSS for 7 days, followed by regular drinking water for 12 days. In parallel, mice were treated with AluCi (1.5 mg of Al element/kg/day) or PBS once a day until the end of the experiment. (**B**) Body weight was scored at baseline, D7, D13, D15 and D19. * means p <0.05; ** means p < 0.01 between DSS + PBS and DSS + AluCi. (**C**) A disease activity index that included body weight variation, presence of blood in stools and stool consistency was calculated at day 19. (**D**) MPO was measured in colonic samples harvested on day 19. (**E**) Histopathological changes in the colon tissues were examined by MGG staining and scoring of histopathology, as described in Methods.

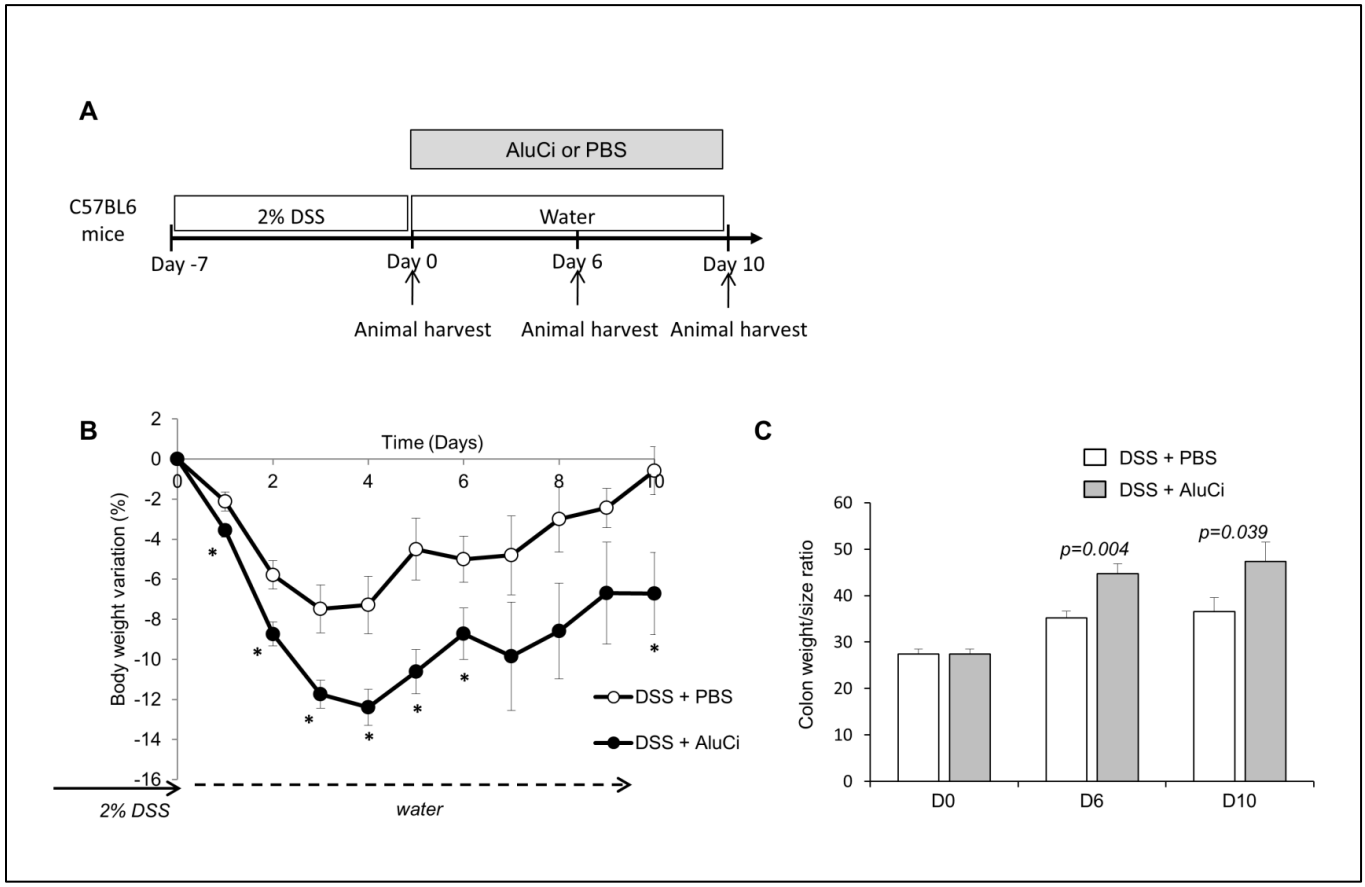

Figure 8: AluCi decreases mucosal repair. (**A**) C57BL6 mice were treated with 2% DSS for 7 days, followed by regular drinking water for 10 days. AluCi (1.5 mg of Al element/kg/day) and PBS treatment were started only after DSS discontinuation on day 7. (**B**) Body weight was scored daily. * means $p < 0.05$. (**C**) Colon length and weight were measured from mice euthanized on day 0, day 6 and day 10 after the start of aluminum treatment and the colon weight/size ratio was calculated.

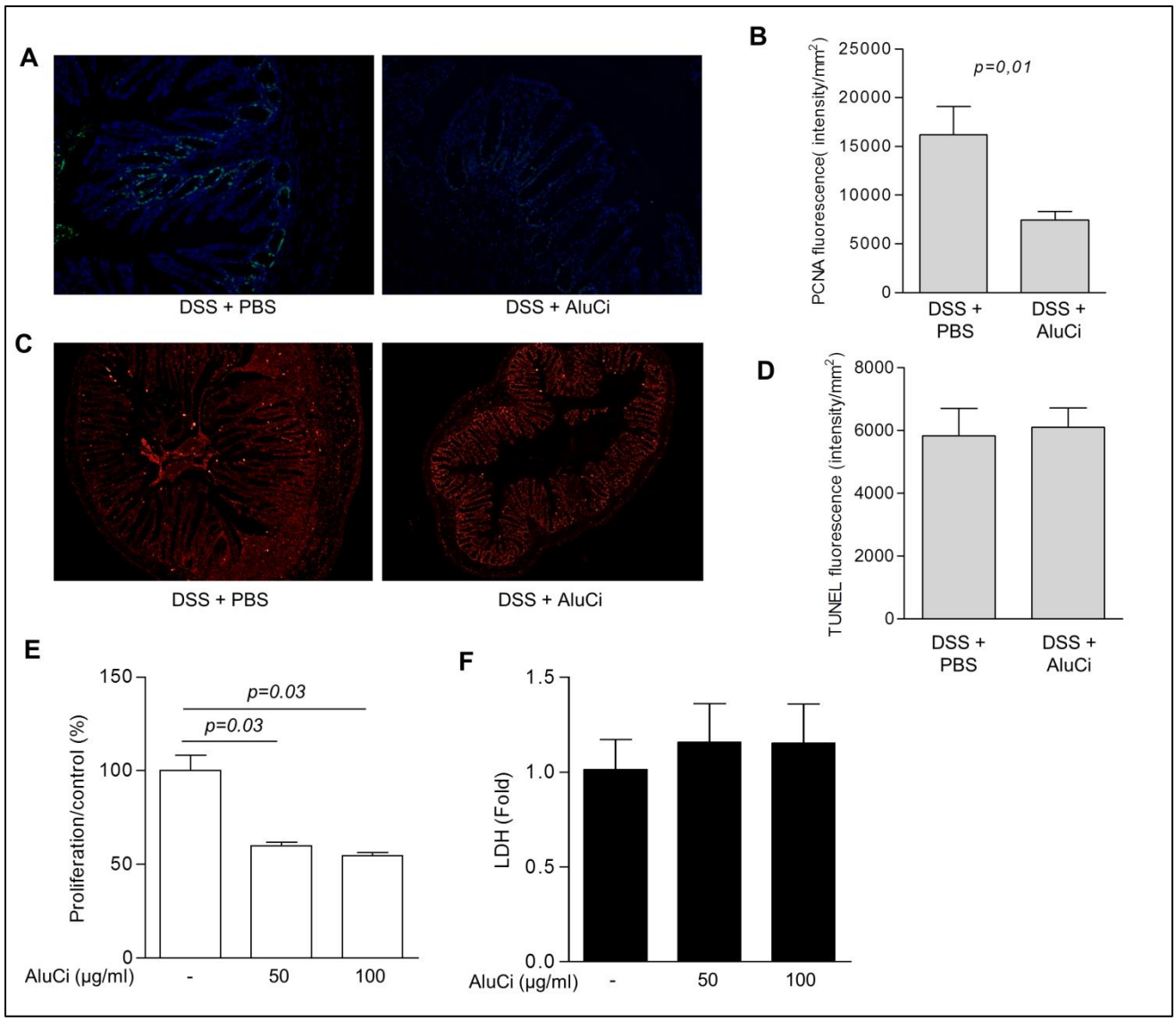

Figure 9: AluCi inhibits epithelial cell proliferation *in vivo* and *in vitro*. C57BL6 mice were fed with AluCi or PBS for 10 days after DSS-induced colitis. (**A,B**) PCNA immunostaining of colon sections (**A**) and its quantification (**B**) showed a decrease of epithelial cell proliferation in mice having received aluminum as compared to mice administered PBS. (**C,D**) TUNEL immunostaining of the same colons (**C**) and its quantification (**D**) shows no significant difference in epithelial cell apoptosis. Caco2 cells were incubated with increasing doses of AluCi (50 and 100 µg/mL) for 5 days. (**E**) MTT assay showed a decrease of epithelial cell proliferation. (**F**) LDH activity assay in the supernatants did not reveal any significant variation.

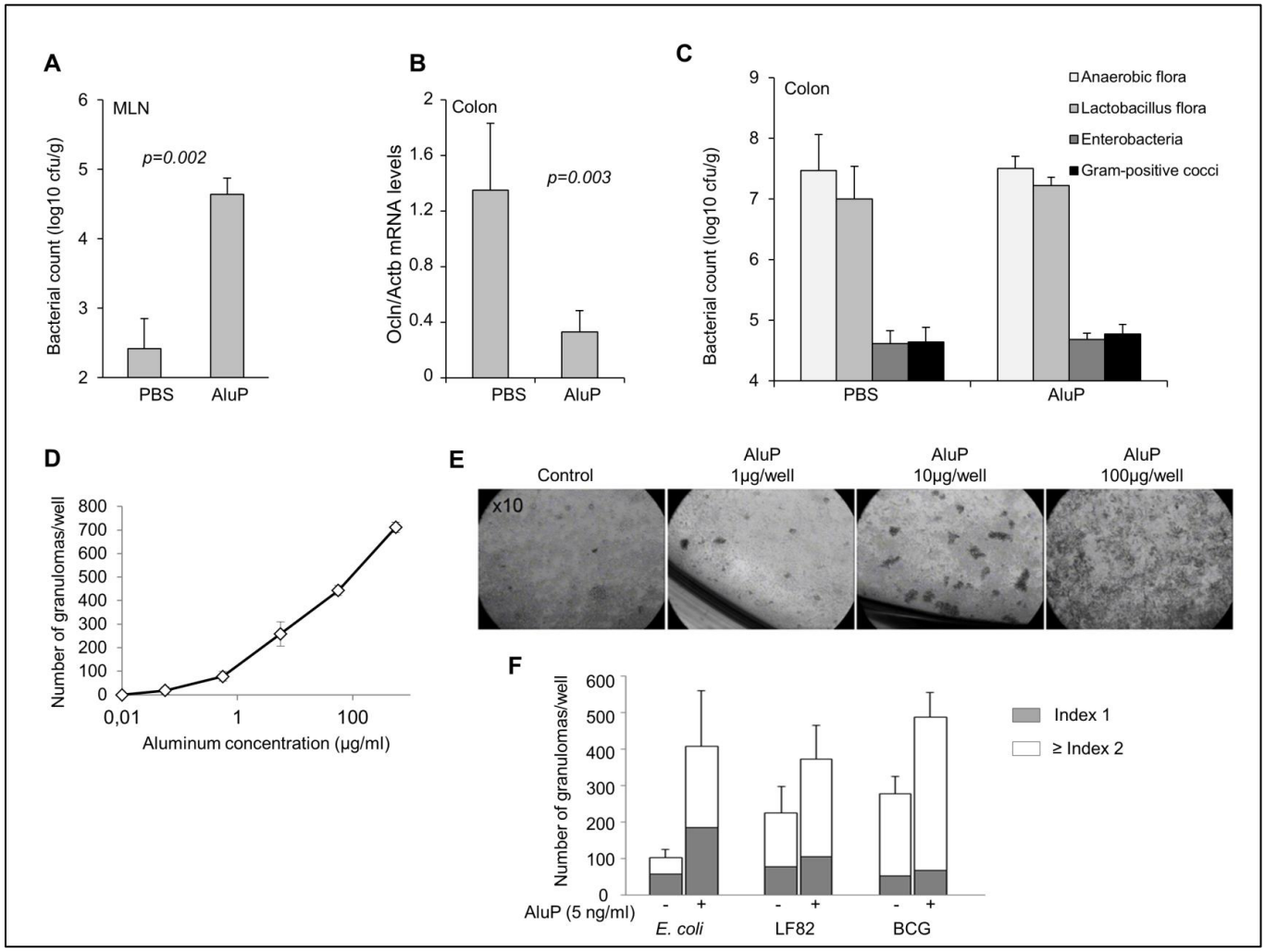

Figure 10: aluminum alters intestinal barrier integrity and induces granuloma formation. C57BL6 mice were fed with AluP (1.5 mg of Al element/kg/day, n=9) or PBS (n=4) for 4 weeks. Bacterial counts in MLN and colon were determined after 4 weeks. (**A**) Bacterial counts in MLN were significantly higher in aluminum-treated mice than in PBS-treated mice. (**B**) RT-qPCR assay of homogenized colons showed a decrease of *Ocln* mRNA in mice treated with aluminum as compared to PBS-treated mice. (**C**) Bacterial count of specific strains in the colonic mucosa showed no difference between aluminum-treated and PBS-treated mice. (**D**,) Human PBMCs were incubated for 4 days with increasing doses of AluP (from 1 to 100 µg of Al element/well; 1.5 mL medium/well). Quantitative analysis of the number of granulomas showed a dose-dependent enhancement of granuloma number in response to aluminum. (**E**) Representative light microscopy pictures (x10) of the culture wells after 4 days of reaction reveal large multicellular structures (granulomas) in presence of aluminum. (**F**) Human PBMCs were incubated for 5 days

with non-pathogenic *E. coli* K-12 strain DH5α, AIEC strain LF82 or BCG, alone or in presence of a low dose of aluminum (5ng of Al element/mL). The number of granulomas according to their size (Index 1, small size, Index 2, big size) was counted.

5. Supplementary tables and figure:

Supplementary Table 1: clinical scores for determination of disease activity index in the model of DSS-induced colitis

Score	Weight loss
0	No weight loss
1	Weight loss of 1-5%
2	6-10%
3	11-20%
4	More than 20%

Score	Stool consistency	Bleeding
0	Well-formed pellets	Negative hemoccult
2	Pasty and semi-formed stools	Positive hemoccult
4	Watery diarrhea	Rectal bleeding

Supplementary Table 2: DNA sequences of primers used in the study

Name	**Forward nucleotide sequence**	**Reverse nucleotide sequence**
ACTb	TCACCCACACTGTGCCCATCTACG	CAGCGGAACCGCTCATTGCCAATG
IL1b	TTGTTGAGCCAGGCCTCTCT	CCAAATGTGGCCGTGGTT
IL8	AAGGAACCATCTCACTGTGTGTAAAC	AAATCAGGAAGGCTGCCAAGA
Actb	TGG AATCCTGTGGCATCCATGAAAC	TAAAACGCAGCTCAGTAACAGTCCG
Tnfa	TG GGAGTAGACAAGGTACAACCC	CATCTTCTCAAAATTCGAGTGACAA
Il1b	CAA CCAACAAGTGATATTCTCCATG	GATCCACACTCTCCAGCTGCA
*Il17*a	CAGCAGCGATCATCCCTCAAAG	CAGGACCAGGATCTCTTGCTG
Nlrp3	TGAACCTGGGCAACAATGATC	CTGCTGTTTCAGCACCTCACA
Il6	GTTCTCTGGGAAATCGTGGA	CAGAATTGCCATTGCACAAC
Occludin	CCCTGACCA CTATGAAACAG	TTGATCTGAAGTGATAGGTG

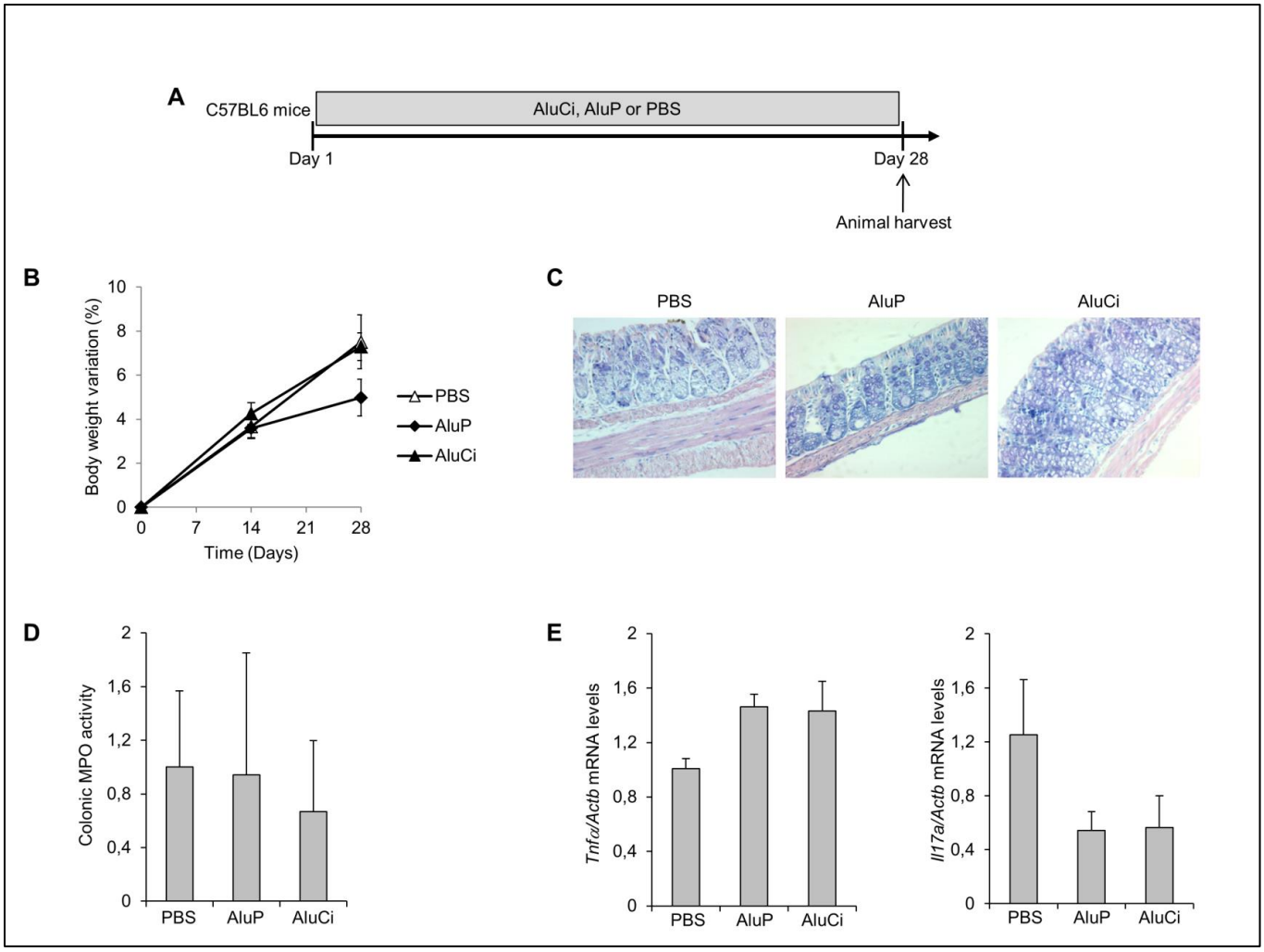

Supplementary Figure 1: aluminum does not induce colonic inflammation. (**A**) C57BL6 mice (n=5-10/group) were fed with aluminum citrate (AluCi) or aluminum phosphate (AluP) (1.5 mg of Al element/kg/day) or with PBS for 28 days. At day 28, colitis parameters were assessed. (**B**) Body weight was scored each week. (**C**) Histopathological changes in colon tissues were examined by MGG staining. (**D**) MPO activity was measured in colonic lesions. Results are expressed compared to PBS-treated mice. (**E**) Transcriptional expression of *Tnfα* and *Il17a* from homogenized colons of mice treated with PBS, AluP or AluCi was analyzed by RT-qPCR.

E. Conclusion:

L'épithélium intestinal est une des principales interfaces du corps humain avec le milieu extérieur. Ce milieu extérieur est caractérisé dans les pays industrialisés par l'augmentation de la teneur en microparticules provenant de la pollution ou des aliments industriels. L'influence de ces microparticules sur l'homéostasie intestinale et le développement de l'inflammation intestinale est encore méconnue. De plus, les éléments précis pouvant être toxiques au sein de ce groupe de microparticules ne sont pas identifiés.

Une approche première bibliographique nous a permis d'identifier l'aluminium comme étant un des composants principal de cette pollution aux microparticules. L'industrie de l'aluminium rejette dans l'atmosphère un nombre très important de microparticules. L'aluminium est solubilisé dans le sol par les pluies acides et contamine les végétaux. Il est aussi utilisé dans l'industrie alimentaire dans de nombreux produits comme additif alimentaire. Ensuite, l'analyse bibliographique des propriétés de l'aluminium nous a montré que ce métal pouvait interagir avec le système immunitaire avec un effet pro-inflammatoire.

Nous avons ensuite choisi de tester l'effet de l'aluminium administré par voie orale sur l'homéostasie et l'inflammation intestinales à l'aide de modèles animaux et cellulaires. Dans ce travail expérimental nous montrons que l'aluminium aggrave l'inflammation intestinale chez la souris dans un modèle de colite chimique induite par le TNBS et dans un modèle de colite chronique chez les souris $IL10^{-/-}$. Dans ces modèles, l'aluminium augmente l'intensité et la durée de l'inflammation intestinale au niveau macroscopique et microscopique, augmente l'activité myeloperoxydase au niveau de colon, augmente l'expression des cytokines pro-inflammatoires et diminue le renouvellement cellulaire. L'aluminium diminue aussi la cicatrisation muqueuse dans

un modèle de colite chimique induite par le DSS chez la souris. En l'absence d'inflammation muqueuse, l'aluminium altère les fonctions de la barrière intestinale en augmentant la perméabilité intestinale. *In vitro*, l'aluminium induit la formation de granulomes et présente une action synergique avec le lipopolysaccharide bactérien entrainant la stimulation de la secrétion de cytokines pro-inflammatoire par les cellules épithéliales intestinales.

Ces données expérimentales montrant un effet délétère de l'aluminium sur l'épithélium intestinal avec aggravation de l'inflammation intestinale et diminution de la cicatrisation muqueuse suggère que ce métal devrait être considéré comme un facteur de risque environnemental au cours des MICI.

III. L'hypothèse génétique et les facteurs moléculaires

A. Facteurs génétiques et MICI :

Bien que leur origine reste mal connue, l'hypothèse actuelle présente les MICI comme des maladies multifactorielles, secondaires à une réponse immunitaire muqueuse anormale dirigée contre la flore intestinale, survenant chez des individus génétiquement prédisposés [1, 8, 23, 104]. La fréquence des formes familiales de MICI et la concordance de 50 à 60 % pour la maladie de Crohn observée chez des jumeaux monozygotes, illustrent l'importance des facteurs génétiques.

Au cours des dernières décennies, des avancées majeures dans la compréhension des facteurs génétiques impliqués dans les MICI ont été réalisées (FIGURE 5) [1, 105]. Ces progrès ont été permis par le développement des technologies de séquençage et d'analyse de l'ADN, ainsi que l'utilisation de base de données multinationales permettant l'analyse comparative de millier d'individus dans des études d'association pan-génomique (GWAS pour genome wide association studies). Ces études identifient des polymorphismes concernant la variation d'un seul nucléotide (SNPs, pour single nucleotide polymorphisms). Les dernières études d'associations pan-génomiques ont identifié plus de 163 locus de gène associés aux MICI (110 sont associés à la MC et à la RCH, 30 spécifiquement à la MC et 23 spécifiquement à la RCH) [106]. Ces différents gènes codent pour des protéines impliquées dans des processus biologiques variés et l'identification des voies de signalisation mise en jeu a permis de mieux comprendre les mécanismes à l'origine de l'inflammation intestinale observée dans les MICI.

Le nombre toujours plus important de gènes de susceptibilité pour les MICI mis en évidence dans les GWAS indique l'importance de l'influence génétique au cours de ces maladies. A l'inverse, de nombreux SNPs retrouvés comme à risque correspondent à des séquences non

codantes ou à des gènes dont la fonction reste méconnue. L'analyse seule des gènes ne suffit pas et l'exploration de l'interaction des protéines codées par ces gènes entre-elles pourrait permettre de mieux identifier les voies de signalisation impliquées dans l'inflammation intestinale.

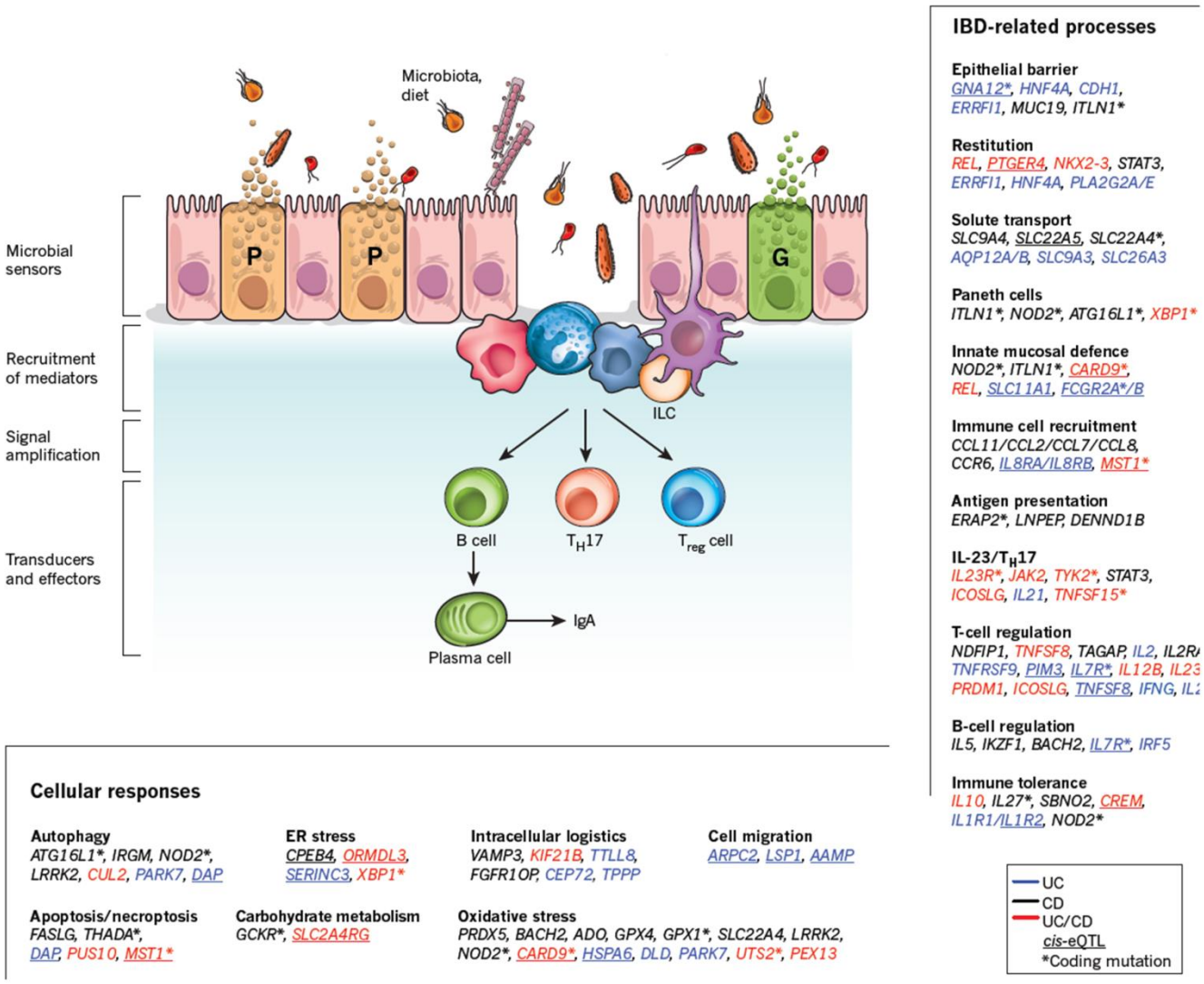

FIGURE 5 : gènes de susceptibilité des MICI et physiopathologie [25].

B. Facteurs moléculaires issus des études génétiques :

L'ère moderne de la recherche concernant les facteurs génétiques dans les MICI a débuté en 2001 avec la découverte de NOD2 (nucleotide-binding oligomerization domaincontaining 2) comme premier gène de susceptibilité pour la Maladie de Crohn [107]. Le gène NOD2 code pour un récepteur intracellulaire reconnaissant le muramyl dipeptide (MDP), un composé bactérien présent dans le peptidoglycane des bactéries Gram-positive et –négative. La stimulation par le MDP induit entre autre l'autophagie qui contrôle la réplication bactérienne et la présentation des antigènes au système immunitaire [108] et module les réponses immunitaires innée et adaptative [109]. L'association entre NOD2 et la MC d'abord identifiée par une approche de gène candidat à ensuite été répliquée dans les études pan-génomiques.

Depuis la découverte de NOD2, les études génétiques ont identifié l'autophagie comme une des voies de signalisation jouant un rôle majeur dans la réponse immunitaire au cours des MICI. Deux gènes liés à l'autophagie appelés ATG16L1 et IRGM sont significativement associés aux MICI dans les GWAS [35, 110, 111]. L'autophagie est impliquée dans la dégradation et le recyclage des composants du cytosol, permettant de maintenir une homéostasie intracellulaire. Elle joue aussi un rôle dans la défense contre les infections bactériennes. La protéine codée par ATG16L1 est un des composants majeur de la machinerie de l'autophagie et la mutation T300A du gène ATG16L1 est significativement associée à un sur risque de MC. Par la suite, des études expérimentales ont démontré que les cellules épithéliales et dendritiques qui contenaient les variants à risque de NOD2 ou ATG16L1 présentaient un déficit de l'autophagie antibactérienne [108].

Par la suite, d'autres voies de signalisation potentiellement impliquées dans l'inflammation intestinale ont été identifiées dans les études d'association pan-génomique.

Récemment, le gène codant pour l'IL23R a été significativement associé aux MICI [105]. Ce gène encode une sous-unité du récepteur de la cytokine pro-inflammatoire IL-23 impliquée dans la stimulation des lymphocytes Th17. La voie de signalisation de l'IL-23 et des lymphocytes Th17 est d'ailleurs très probablement impliquée dans la physiopathologie des MICI avec plusieurs gènes participants à cette voie, retrouvés comme associés aux MICI dans les GWAS (IL23R, IL12B, JAK2, STAT3). D'autres gènes de susceptibilité régulant les fonctions immunitaires ont été mis en évidence par les études génétiques incluant IL1R2, REL, SMAD3, PRDM1 et CARD9 [106]. En particulier, le gène CARD9 code pour une sous-unité des caspases impliquées dans la régulation des voies de mort cellulaire dont l'apoptose, voie de signalisation déjà impliquée dans les MICI.

C. Voies de mort cellulaire et caspase-8 :

L'apoptose est une voie de signalisation entrainant la mort organisée des cellules. Après l'activation du complexe intracellulaire DISC (death-inducing signaling complex) par les récepteurs transmembranaires aux TNFα ou autres molécules pro-apoptotiques, une activation en cascade des caspases par phosphorylation va aboutir à la dégradation de la cellule avec la formation des corps apoptotiques. L'apoptose est un processus cellulaire important pour l'élaboration de l'architecture du tractus gastrointestinal, le renouvellement de l'épithélium intestinal et le maintien de son homoeostasie [112, 113]. L'épithélium intestinal est une des structures majeures permettant de réguler la perméabilité intestinale et les interactions hôte-bactéries [114]. Plusieurs travaux cliniques et expérimentaux ont montré que l'apoptose était impliquée dans les phénomènes inflammatoires rencontrés au cours des MICI [115-117]. Des travaux expérimentaux récents ont montré qu'un déficit en certaines protéines du complexe DISC

comme FADD, c-FLIP ou la caspase-8 pouvait entrainer une dérégulation de l'homéostasie intestinale et le développement d'une inflammation muqueuse [112, 118-121]. En particulier, il a été suggéré que la caspase-8 contrôlerait la nécroptose (voie de mort cellulaire non organisée) des cellules de Paneth au niveau de l'intestin grêle et que son déficit entrainerait une inflammation intestinale [112].

Les caspases sont des protéases à cystéines qui régulent le développement embryonnaire, la différentiation cellulaire, l'homéostasie tissulaire et l'élimination des cellules endommagées. L'activation des caspases et l'activité qui en résulte sont hautement régulées et l'inhabilité d'une cellule à moduler efficacement l'activité des caspases peut mener à une apoptose dérégulée à l'origine de phénomènes pathologiques comme la carcinogenèse, l'auto-immunité, ou l'inflammation [118, 122, 123].

La caspase-8 est une des caspases principales initiatrices de l'apoptose par la voie extrinsèque et possède un rôle majeur de régulation de la survie cellulaire après activation des récepteurs au TNFα [124, 125]. L'importance de la caspase-8 est souligné par le fait que la délétion complète du gène caspase-8 entraine une mortalité embryonnaire chez la souris [126]. *In vitro*, l'absence ou l'inhibition de la caspase-8 dans différents types cellulaires entraine l'activation d'une autre voie de mort cellulaire appelée necroptosis et qui pourrait favoriser le développement de l'inflammation intestinale [119].

La caspase-8 présente en dehors de son activité pro-apoptotique des fonctions indépendantes des voies de mort cellulaire qui pourraient avoir une importance pour l'homéostasie tissulaire. En effet, i*n vitro,* il a été démontré que la caspase-8 entrainait l'activation de la transcription par l'intermédiaire de la voie NF-κB, favorisait la prolifération des lymphocytes T et augmentait la migration cellulaire et l'adhésion des cellules cancéreuses. La caspase-8 régule aussi l'endocytose dépendante de la clathrine des cellules épithéliales

intestinales [124, 127-129]. De plus, l'absence de la caspase-8 entraine *in vitro* une activation aberrante de l'autophagie dans les lymphocytes [130]. La caspase-8 est donc impliquée dans plusieurs processus intracellulaires qui sont importants pour l'homéostasie intestinale et qui participent à la physiopathologie de l'inflammation intestinale chronique. Cependant, l'importance physiologique des fonctions non-apoptotiques de la caspase-8 sur l'homéostasie et l'inflammation intestinale reste méconnue.

Après un travail de recherche bibliographique, nous avons donc choisi de nous intéresser à la caspase-8 et à ses fonctions non-apoptotiques et apoptotiques dans le maintien de l'homéostasie intestinale à l'aide d'un modèle de souris spécifiquement inactivé pour la caspase-8 au niveau des cellules épithéliales intestinales.

D. *Caspase-8 controls attachment and integrity of the intestinal epithelium upon microbial challenge.*

G Pineton de Chambrun[1,7], C Manthey[1], J Wong[2], M Guma[2], M Spehlmann[1], C McAllister[1], A Till[4,5], E Hanson[1], D Stupack[3], PB Ernst[6], T Stappenbeck[6], P Desreumaux[7], MF Kagnoff[1], M Karin[2], JY Wang[4], and L Eckmann[1]

[1]Departments of Medicine, University of California, San Diego, La Jolla, California, USA
[2]Pharmacology, University of California, San Diego, La Jolla, California, USA
[3]Pathology, University of California, San Diego, La Jolla, California, USA
[4]Moores Cancer Center, University of California, San Diego, La Jolla, California, USA
[5]Division of Biological Sciences, University of California, San Diego, La Jolla, California, USA
[6]San Diego Center for Systems Biology, University of California, San Diego, La Jolla, California, USA
[7]Inserm U995, Université Lille Nord de France, Lille, France

Référence de l'article :

Caspase-8 controls attachment and integrity of the intestinal epithelium upon microbial challenge. Pineton de Chambrun G, Manthey C, Wong J, Guma M, Spehlmann M, McAllister C, Till A, Hanson E, Stupack D, Ernst PB, Stappenbeck T, Desreumaux P, Kagnoff M, Karin M, Wang J, Eckmann L. *Nature cell biology. Manuscript ready for submission*

1. Introduction:

Caspases, signaling proteases that cleave selected host proteins after aspartic acid residues, are key regulators of controlled cell death in mammals, with indispensable functions in embryonic development, tissue homoeostasis, and removal of damaged or infected cells. Failures in caspase functions or regulation have been associated with a wide range of diseases from cancer and autoimmunity to neurodegeneration and immunodeficiency.[118, 122, 123] Mammals have at least 16 caspases with distinct functions, but they typically act in concerted fashion within proteolytic signaling cascades wherein upstream initiator caspases, including caspases-2, -8, -9- and -10, are activated by cell surface receptors upon cognate ligand binding ("extrinsic pathway") or mitochondrial dysfunction ("intrinsic pathway"), and then activate downstream effector caspases, such as caspases-3, -6, and –7, which cleave and inactivate key proteins involved in cell death initiation,

Caspase-8 is the central initiator caspase of the extrinsic pathway. It has a vital role in determining the fate of cells following activation of members of the TNF receptor family, collectively referred to as death receptors.[124, 125] Deletion of the *Casp8* gene in mice leads to embryonic lethality due to a critical role of the caspase in regulating endothelial death and survival.[126] Although caspase-8 is clearly important in mediating cell death receptor-mediate apoptosis, its absence does not merely prevent apoptosis. Instead, it functions as a molecular switch between different types of programmed cell death, since caspase-8 deficiency leads to necroptosis, a form of necrotic cell death characterized by features loss of membrane integrity and release of cytoplasmic contents.[119] Furthermore, beyond its well-documented in vitro and in vivo role in cell death, several in vitro studies have suggested that it may have functions unrelated to death regulation. For example, caspase-8 induces transcription through the NF-κB pathway and proliferation of T cells, promotes cell migration and cell-matrix adhesion in cancer

cells and regulates clathrin-dependent endocytosis.[124, 127-129] The physiological importance of these observations remains poorly understood.

The intestinal tract provides an attractive system to explore caspase functions, because it constitutes a uniquely vulnerable interface between host and external environment. The intestinal epithelium, which forms a single-cell boundary between these different domains, is self-renewing with high cell turnover, in which proliferation of stem cells in the crypts is balanced by programmed cell death at the villus tips in the small intestine or the surface in the colon. In transit, epithelial cells migrate and differentiate into several lineages. These highly orchestrated events occur in the face of constant exposure to abundant commensal microbes and intermittent infection with microbial pathogens that attach to or invade the epithelium by subverting various signaling pathways. The constant microbial stimulation leads to a finely balanced state of physiological inflammation with concurrent immune activation and suppression in the intestinal mucosa characterized by significant expression of proinflammatory cytokines and high numbers of mucosal lymphocytes and phagocytic cells.[131] The precarious nature of this balance is underlined by the observation that numerous body-wide defects in immune regulation lead primarily to intestinal inflammation and damage.[132]

Inactivation of proteins that participate in cell death regulation, such as key component of the death-inducing signaling complex (DISC), FADD, c-FLIP, and caspase-8, disrupts intestinal homeostasis and leads to inflammation.[112, 118-121] In particular, epithelial caspase-8 deficiency has been suggested to lead to Paneth cell loss in the small intestine.[112] These cells produce an array of antibacterial molecules, suggesting that their disappearance may impact host defense against bacterial infection, although this has not been directly investigated. The importance of cell death regulation in intestinal homeostasis is further underlined by identification by two genes involved in regulating autophagic cell death, *IRGM* and *ATG16L1*, as

susceptibility genes for the development of inflammatory bowel disease (IBD),[1, 106] a chronic remitting and relapsing condition related to dysregulated mucosal responses to the gut microbiota. Although caspase-8 has so far not been implicated in IBD pathogenesis, its disruption provides a powerful model for determining the relative importance of cell death regulation and cell death-independent actions of this central initiator caspase. Accordingly, we set out to investigate these activities of caspase-8 in the face of microbial challenges in the intestinal tract.

In this study, we demonstrate that caspase-8 has a novel physiological function in maintaining firm attachment of the epithelium to the basal membrane in response to microbial stimulation. This function is independent of cell death, and instead involves regulation of clathrin-dependent endocytosis of adhesion molecules and their autophagic degradation. These findings considerably broaden the range of functions of caspase-8 as a cell death-independent regulator of physiological processes. Furthermore, systems biology analysis suggests that it occupies a central position in a subnetwork of IBD susceptibility genes, thus providing a novel conceptual framework in understanding the mechanisms by which these genes may predispose to intestinal disease.

2. Results

Caspase-8 is dispensable for normal intestinal development and epithelial differentiation but is critical for mucosal integrity upon bacterial pathogen challenge

To investigate the physiological functions of caspase-8 in intestinal epithelial cells (IECs), we generated conditional knock-out mice (*Casp8*$^{\Delta IEC}$) by crossing *Casp8*$^{fl/fl}$ mice[133] to *Tg(Vil-cre)*^{997Gum} mice (villin-Cre).[134] Immunoblotting confirmed that caspase-8 was effectively ablated in the epithelium of small intestine and colon in *Casp8*$^{\Delta IEC}$ mice, whereas expression was normal in mesenteric lymph node cells (Fig. 1a,b). *Casp8*$^{\Delta IEC}$ mice were born at the expected frequency and displayed no macroscopic abnormalities (Fig. 1c, Supplemental Fig. 1a,b). At 6 weeks of age, the intestinal tract of *Casp8*$^{\Delta IEC}$ mice was histologically normal, including normal villus lengths and crypt depths, and normal numbers and appearance of goblet and Paneth cells (Fig. 1d,e, Supplemental Fig. S1c). Thus, caspase-8 is dispensable for normal intestinal development, IEC differentiation, and intestinal homeostasis until at least early adulthood in mice.

In the absence of a spontaneous phenotype, we questioned whether caspase-8 may have physiological functions under microbial challenge conditions. The murine pathogen, *Citrobacter rodentium*, is commonly used as an intestinal infection model, because it effectively colonizes the intestinal tract of mice, and causes a self-limiting infection characterized by mucosal inflammation and epithelial hyperplasia.[135] After oral *C. rodentium* infection, *Casp8*$^{\Delta IEC}$ mice showed significantly more weight loss (Fig. 2a) and mortality (40% vs. 0%) than *Casp8*$^{fl/fl}$ controls, and had significantly higher bacterial numbers in stool, mesenteric lymph nodes, liver, and spleen (Fig. 2b,c). Histological analysis revealed marked mucosal inflammation with immune cell infiltration, ulceration, and submucosal edema in the colon of *Casp8*$^{\Delta IEC}$ mice after 7 days, whereas control mice had only minimal changes at that time (Fig. 2d). Surprisingly,

Casp8$^{\Delta IEC}$ mice, but not controls, also displayed marked inflammation in the small intestine with villus destruction, epithelial detachment at the villus tips, and mucosal infiltration with immune cells (Fig. 2e). Thus, although caspase-8 had no apparent constitutive physiological functions, its absence led to severe intestinal damage and inflammation upon microbial challenge.

Bacterial stimulation causes acute epithelial detachment in the absence of caspase-8

The development of small intestinal inflammation in *Casp8*$^{\Delta IEC}$ mice in response to *C. rodentium* infection suggested that a soluble bacterial factor may be involved, since this Gram-negative pathogen colonizes mostly the cecum and colon, but not the small intestine. To test this hypothesis and begin to define the mechanism of infection-induced inflammation, we stimulated mice with the major cell wall component of Gram-negative bacteria, lipopolysaccharide (LPS). Within 2-4 h after LPS injection, *Casp8*$^{\Delta IEC}$ mice, but not controls, had a greatly enlarged small intestine with extensive luminal fluid accumulation (Fig. 3a, Supplemental Fig. S2a). Microscopic examination of the luminal contents revealed numerous single rounded cells in *Casp8*$^{\Delta IEC}$ mice, but not *Casp8*$^{fl/fl}$ controls (Fig. 3b). Concurrently, *Casp8*$^{\Delta IEC}$ mice displayed massive epithelial detachment from the basal membrane at the small intestinal villus tips within 1 h after LPS injection (Fig. 3c, Supplemental Fig. S2b). By 4 h, we observed complete villus destruction, epithelial ulcerations, and massive mucosal infiltration with inflammatory cells (Fig. 3c). In contrast, the small intestine of the *Casp8*$^{fl/fl}$ controls was morphologically normal throughout the 4 h observation period.

To exclude the possibility that the dramatic LPS-induced epithelial phenotype in *Casp8*$^{\Delta IEC}$ mice was related to any unrecognized developmental abnormalities, we constructed mice with an inducible epithelial deletion of *Casp8* by crossing *Casp8*$^{fl/fl}$ mice to mice bearing a tamoxifen-inducible villin-Cre.[136] Tamoxifen treatment induced complete loss of caspase-8 in

the small intestinal epithelium in the mice (Supplemental Fig. S3a). LPS stimulation of tamoxifen-induced mice caused massive small intestinal dilation, luminal fluid and cell accumulation, and epithelial detachment with villus destruction and mucosal inflammation (Supplemental Fig. S3b-e). LPS stimulation of littermates not pretreated with tamoxifen did not lead to apparent abnormalities. These data confirm that acute loss of epithelial caspase-8 was sufficient to cause the observed intestinal phenotype after LPS stimulation.

To further characterize the LPS-induced epithelial detachment in *Casp8*$^{\Delta IEC}$ mice, we conducted transmission electron microscopy (TEM) and immunofluorescence studies of the small intestine. IECs were observed by TEM to detach from the basal membrane in sheets without initial loss of cell-to-cell contact with neighboring cells (Fig. 3d, Supplementary Fig. S2c,d). The ultrastructural morphology of the detaching cells was not notably different from cells still attached to the basal membrane. Signs of apoptosis or necroptosis were not observed. Consistent with this, immunostaining for activated caspase-3 and TUNEL analysis for DNA fragments were negative in most detached cells (Fig. 3e,f). At the villus tips of *Casp8*$^{fl/fl}$ controls, we did observe a small number of attached cells positive for activated caspase-3 by 2 h after LPS injection, but such cells were not found in the attached or detached populations of *Casp8*$^{\Delta IEC}$ mice. We conclude from these studies that LPS-induced epithelial detachment in the small intestine of *Casp8*$^{\Delta IEC}$ mice occurred in live cells and was not secondary to cell death.

LPS-induced epithelial detachment in Casp8$^{\Delta IEC}$ mice depends on TNFα signaling

Activation of caspase-8 and the associated signaling pathways occurs in response to binding of TNFα and other cytokines to their cognate death receptors.[124, 125] To investigate the importance of TNFα signaling in LPS-induced IEC detachment in *Casp8*$^{\Delta IEC}$ mice, we generated double-mutant mice (*Casp8*$^{\Delta IEC}$ x *Tnfr1*$^{-/-}$) by crossing them with mice deficient for

Tnfr1, the major TNFα receptor that mediates cell death signals in most cell types.[137, 138] Four hours after LPS challenge, *Casp8*$^{\Delta IEC}$ x *Tnfr1*$^{-/-}$ mice were protected from small intestinal dilatation and fluid accumulation, epithelial detachment and ulceration, and mucosal inflammation seen in *Casp8*$^{\Delta IEC}$ mice (Fig. 4a,b and Supplementary Fig. S4a), suggesting that TNFα signaling was required for mediating the LPS-induced epithelial phenotype. To determine whether TNFα was not only necessary but also sufficient, we injected TNFα directly into *Casp8*$^{\Delta IEC}$ mice. Injection pheno-copied the LPS-induced events in *Casp8*$^{\Delta IEC}$ mice, as evidenced by marked small intestinal dilatation, epithelial detachment, and mucosal inflammation compared to TNFα stimulated *Casp8*$^{fl/fl}$ controls (Fig. 4c, Supplementary Fig. S4c-g).

Death receptor activation in caspase-8 deficient cells can induce necroptosis.[126] Although we did not find any signs of cell death in detaching epithelial cells of *Casp8*$^{\Delta IEC}$ mice (Fig. 3d-f, Supplemental Fig. 2d), we nonetheless wanted to further exclude this possibility by using the RIPK3 inhibitor, necrostatin-1, which was shown to block necroptosis in vitro and in vivo.[139] Injection of necrostatin-1 before LPS stimulation did not alter the epithelial detachment phenotype in *Casp8*$^{\Delta IEC}$ (Fig. 4d, Supplementary Fig. S5). To confirm that necrostatin could inhibit necroptosis in primary intestinal epithelial cells, we established enteroids from inducible *Casp8*$^{\Delta IEC}$ mice, induced caspase-8 deletion with tamoxifen, and stimulated them with TNFα. Cells were not visibly affected for the first 4 h after stimulation, but were observed to undergo cell death with features of necrosis after 24 h, suggesting that caspase-8 deficiency led to delayed cell death in this system (Fig. 4e). Necrostatin blocked the delayed cell death, confirming that the inhibitor had the expected activity on intestinal epithelial cells. Together, these results indicate that LPS-induced IEC detachment in the absence of caspase-8 is mediated by TNFα signaling, but is independent of necroptosis pathways.

Dysregulated endocytosis leads to epithelial β-integrin loss and detachment upon LPS stimulation of Casp8$^{\Delta IEC}$ mice

Detachment of live epithelial cells was the major phenotype in microbially-stimulated *Casp8*$^{\Delta IEC}$ mice, which prompted us to explore epithelial attachment mechanisms that might be regulated by caspase-8. Adhesion molecules, especially integrins, anchor the epithelium to the basal membrane.[140] Therefore, we examined the levels and localization of β1-integrin, the most abundant adhesion molecule in IEC[140], by confocal microscopy. As expected, β1-integrin was localized at the basal membrane of IEC in the small intestine of *Casp8*$^{fl/fl}$ controls (Fig. 5a). A similar pattern was also seen in *Casp8*$^{\Delta IEC}$ mice, although the staining intensity was somewhat weaker. Importantly, 2 h after LPS injection, epithelial β1-integrin staining had completely disappeared in the small intestine of *Casp8*$^{\Delta IEC}$ mice, whereas no changes were seen in *Casp8*$^{fl/fl}$ controls (Fig. 5a), suggesting that β-integrins are differentially degraded in caspase-8 deficient IEC upon microbial stimulation. Organoid culture from *Casp8*$^{ind\Delta IEC}$ mice confirm that β1-integrin quantity is decreased in epithelial cells lacking caspase-8 and that TNFα stimulation increased β1-integrin degradation in crypts with caspase-8 deficiency (Supplemental Fig. 6a and Fig. 7c).

Surface localization and abundance of integrins is dynamically regulated by uptake and recycling.[140] Prior *in vitro* studies had suggested that caspase-8 can cleave two proteins, adaptin-α and clathrin heavy chain, that are components of an endocytosis-related protein complex important for uptake, recycling and destruction of membrane proteins.[127] Consequently, we speculated that degradation of these critical endocytosis proteins by caspase-8 limits endocytotic uptake of surface integrins and thus maintains surface levels under physiological conditions, while loss of caspase-8 compromises the normal degradation of

endocytosis mediators and thereby promotes endocytosis and integrin uptake. To test this idea, we first examined the expression and degradation of adaptin-α and clathrin heavy chain by immunoblotting. Control *Casp8*$^{fl/fl}$ mice displayed constitutive degradation of both proteins in whole tissue extracts and isolated epithelial cells in the small intestine, whereas *Casp8*$^{\Delta IEC}$ mice showed very little degradation (Fig. 6a-c). In contrast, adaptin-γ, an adaptin protein that lacks caspase-8 cleavage sites and is involved in trafficking of endosomes rather than cell membrane endocytosis[127, 141], was not cleaved in controls or *Casp8*$^{\Delta IEC}$ mice (Fig. 6f). LPS stimulation further increased degradation of adaptin-α and clathrin heavy chain in *Casp8*$^{fl/fl}$ controls, but not in *Casp8*$^{\Delta IEC}$ mice (Fig. 6d-e, Supplemental Fig.6b). Furthermore, the cell-autonomous nature of caspase-8 dependent CHC degradation was confirmed in TNFα-stimulated enteroid cultures (Fig. 6g). These results show that the molecular defects in the endocytotic machinery observed in the absence of caspase-8 under resting conditions are exacerbated upon microbial stimulation.

To determine the importance of dysregulated endocytosis in the epithelial integrin loss, we employed an inhibitor of clathrin-dependent endocytosis, chlorpromazine.[142] Treatment with chlorpromazine completely prevented small intestinal dilatation, luminal fluid and cell accumulation, epithelial detachment, and mucosal destruction and inflammation in response to LPS stimulation of *Casp8*$^{\Delta IEC}$ mice (Fig. 5b-d). These data suggest that dysregulation of clathrin-dependent endocytosis and loss of β-integrins are important for LPS-induced epithelial detachment in *Casp8*$^{\Delta IEC}$ mice, while caspase-8 dependent degradation of the central endocytosis proteins, adaptin-α and clathrin heavy chain, prevents this process in caspase-8 proficient controls.

Autophagy plays a key role in epithelial detachment in response to LPS stimulation of Casp8$^{\Delta IEC}$ mice

The disappearance of β1-integrins from the cell membrane without concomitant intracellular appearance in the LPS-stimulated *Casp8*$^{\Delta IEC}$ mice (Fig. 5) suggested that dysregulated endocytosis was not solely responsible for the phenotype, but that a second mechanism may be involved that leads to protein degradation (Supplemental Fig. 6a and Fig7c). Caspase-8 deficient lymphocytes exhibit increased autophagy[130], which is an important cellular mechanism of controlled protein degradation and recycling. Moreover, clathrin-dependent endocytosis can participate in autophagosome formation.[143] Potential interactions between caspase-8, the endocytosis machinery, cell adhesion proteins and components of the autophagy pathway were also revealed by querying mammalian interactome data (see Material and Methods section). Thus, the corresponding networks revealed multiple direct protein-protein interactions between autophagy core proteins, including light chain 3 (LC3) family members (e.g. MAP1LC3A/B and GABARAP subfamily) and autophagy receptors (e.g. SQSTM1/p62 and OPTN). Notably, direct interactions with LC3 proteins and the autophagy core protein, ATG16L1, were most pronounced for clathrin components and the AP2 endocytosis complex. Furthermore, several cell adhesion proteins, including β1-integrin (ITGB1) and catenin, displayed interactions with autophagy receptors (Fig. 7a). Together, these observations underline that a close connection exists between endocytosis and autophagy.

To determine whether autophagy was activated in epithelial cells of *Casp8*$^{\Delta IEC}$ mice, we performed immunoblot analysis for LC3, whose lipidated form (LC3-II) is a marker of autophagosome formation.[144] LPS injection strongly induced epithelial LC3-II in *Casp8*$^{\Delta IEC}$ mice, but not in *Casp8*$^{fl/fl}$ controls (Fig. 7b, Supplemental Fig. 7a). Moreover, TEM analysis showed rounded, double membrane-lined vesicular structures indicative of autophagosomes in

the IEC cytoplasm of stimulated *Casp8*$^{\Delta IEC}$ mice (Fig. 7c, Supplemental Fig. 7b). These findings suggest that caspase-8 deficiency is associated with increased autophagy in the epithelium upon microbial stimulation.

We then sought to determine the functional consequences of excessive autophagic activation observed in *Casp8*$^{\Delta IEC}$ mice. We generated epithelium-selective, double-mutant mice (*Casp8*$^{\Delta IEC}$ x *Atg7*$^{\Delta IEC}$) deficient for caspase-8 and autophagy-related protein 7 (ATG7), a central component of the autophagy machinery.[145] Loss of ATG7 prevented LPS-induced autophagy in the absence of caspase-8 (Fig. 7d). In parallel, the double-mutant mice were protected against LPS-stimulated luminal fluid and cell accumulation, epithelial detachment, villus destruction, and mucosal inflammation in the small intestine (Fig. 7e,f). Organoid experiments confirmed that in double deficient epithelial cells loss of Atg7 protects from β1-integrin degradation (Supplemental Fig. 7c). These findings indicate that suppression of autophagy reversed the epithelial detachment phenotype of microbially-stimulated *Casp8*$^{\Delta IEC}$ mice, providing support for the notion that autophagy-related degradation of endocytosed adhesion molecules (such as β-integrins) contributes to their loss and subsequent cell detachment (Fig. 7g).

Suppression of autophagy prevents infection-induced and spontaneous intestinal inflammation in the absence of epithelial caspase-8

Having demonstrated the importance of autophagic activation in LPS-stimulated epithelial detachment in *Casp8*$^{\Delta IEC}$ mice, we then explored the role of epithelial autophagy in the exacerbated inflammatory response to microbial infection. *Casp8*$^{\Delta IEC}$ x *Atg7*$^{\Delta IEC}$ mice were protected from weight loss and mortality seen in *Casp8*$^{\Delta IEC}$ mice after oral *C. rodentium* infection (Fig. 8a). Bacterial counts in mesenteric lymph nodes, liver and spleen after 7 days were markedly reduced in the double-mutant mice compared to *Casp8*$^{\Delta IEC}$ mice, and were similar to

those in *Casp8*$^{fl/fl}$ controls (Fig. 8b). Furthermore, the severe infection-induced inflammation previously observed in the colon and small intestine of *Casp8*$^{\Delta IEC}$ mice was prevented in *Casp8*$^{\Delta IEC}$ x *Atg7*$^{\Delta IEC}$ mice (Fig. 8c,d). Thus, suppression of epithelial autophagy completely reversed the inflammatory phenotype associated with caspase-8 deficiency upon pathogen infection.

Epithelial caspase-8 deficiency was previously shown to cause spontaneous intestinal inflammation.[112] Although our *Casp8*$^{\Delta IEC}$ mice were morphologically normal at 6 weeks (when we conducted the experiments), we explored whether they might have subtle functional defects which may later lead to overt inflammation. Analysis of serum endotoxin indicated that *Casp8*$^{\Delta IEC}$ mice had moderately increased LPS levels compared with *Casp8*$^{fl/fl}$ mice (Supplemental Fig. 8a) suggestive of a modest defect in the intestinal epithelial barrier. Moreover, *Casp8*$^{\Delta IEC}$ mice exhibited increased epithelial proliferation in the small intestine (Supplemental Fig. 8b), which also indicates disturbed epithelial homeostasis. Surveillance of the mice for extended periods revealed that 30-40% developed spontaneous disease with marked weight loss and high mortality over 2-4 months (Supplemental Fig. 8c). Diseased *Casp8*$^{\Delta IEC}$ mice had marked mucosal inflammation in jejunum, ileum, and colon (Supplemental Fig. 8e,f), consistent with prior data.[112] *Casp8*$^{fl/fl}$ mice remained disease-free throughout the entire observation period. Importantly, *Casp8*$^{\Delta IEC}$ x *Atg7*$^{\Delta IEC}$ double-mutant mice were completely protected against spontaneous disease, because they did not lose weight or showed signs of intestinal inflammation even after four or more months (Supplemental Fig. 8d,f). We conclude from these observations that caspase-8 deficiency can cause spontaneous intestinal inflammation, which, like infection-induced inflammation, is mediated by autophagic processes in the intestinal epithelium.

3. Discussion:

Identification of mechanisms that regulate intestinal homeostasis and control intestinal inflammation is one of the critical questions in the mucosal immunology field. The ability of the intestinal epithelium to function as a barrier between the external environment and the closely regulated internal milieu is one of the major component participating to intestinal homeostasis.[114, 146] Indeed, a single cell layer of IECs is the first line of defence against the luminal content and the host. IECs are challenged by the complex task of on the one hand to adsorb water and nutrients from the lumen but on the other hand to protect the host from pathogenic microbes and toxic compounds.[147] Perturbations of epithelial homeostasis or function lead to the development of intestinal disorders such as IBD, celiac disease, infectious gastrointestinal diseases and intestinal cancer.[148] Investigations in the field of intestinal homeostasis have mainly focused on immune system regulation, tight junction regulation, cytokines production such as TNFα and dysbiosis.

Cell death signaling proteins have been recently identified as critical regulators of intestinal homeostasis.[118] It is well known that apoptosis is important for the turnover of IECs and for shaping the morphology of the gastrointestinal tract.[149] The epithelium is constantly renewed by new cells derived from stem cells at the crypt base, which migrate upwards to either the villus of the small intestine or crypt mouth of the colon, from where they are shed by induction of cell controlled cell death.[150] Although epithelial cells are continuously shed from the surface of the intestine, the intestinal epithelium maintains the integrity of the epithelial barrier. It was demonstrated that stimulation by TNFα which may activate apoptosis and other death pathways, can trigger a disturbance of these barrier functions by increasing rates of cell shedding.[150] Recent works have also shown that disturbance of intracellular protein complexes classically involved in cell death signaling may favor intestinal inflammation.[119] It was

demonstrated that mice with IEC-specific knockout of FADD, an adaptor protein required for death-receptor-induced apoptosis, spontaneously developed severe erosive colitis.[121] Also, another adaptor, c-FLIP, a catalytically inactive homolog of caspase-8 blocks apoptosis by binding to and inhibiting caspase-8 and plays a role in the NF-kB–dependent protection of cells from death receptor signaling.[120] IEC-specific deletion of c-Flip in mice resulted in perinatal lethality as a result of the enhanced apoptosis and programmed necrosis of the IEC. Finally, caspase-8 itself has been shown to control Paneth cell necroptosis and small intestinal inflammation.[112]

Our results confirmed that cell death signaling proteins are important for intestinal homeostasis. Here, we demonstrated that caspase-8 is necessary for maintaining intestinal barrier integrity under bacterial stimulation. Interestingly, we observed that the effect of caspase-8 deletion on IECs does not involved apoptosis or necroptosis. Indeed, the LPS-induced detachment of IECs we observed is a really early phenomenon occurring less than 2 hours after bacterial stimulation without any sign of macroscopic or microscopic cell death before and just after IEC detachment. Moreover, treatment of mice with necrostatin-1 that prevents necroptosis does not rescue the LPS-induced IEC detachment.

In this study, we demonstrated that caspase-8 contributes to intestinal homeostasis through its non-apoptotic effects. Previous work showed that caspase-8 regulates the clathrin-dependent endocytosis pathway by cleaving proteins involved in this endocytosis such as clathrin and adaptin-α.[127] Clathrin-dependent endocytosis through adaptors such as AP-1 and AP-2 that contains adaptin proteins, leads to internalization of coated vesicles from plasma membrane into cytoplasm.[141] Our results indicated that caspase-8 constitutively cleaved clathrin-dependent endocytosis proteins in IECs *in vivo* in mice, limiting the internalization of plasma membrane and transmembrane proteins such as adhesion molecules that are critical for IECs adhesion. Indeed,

clathrin heavy chain and adaptin-α play important roles in endocytotic uptake and recycling of membrane proteins[127, 141], and their increased degradation predictably impairs uptake, while loss of degradation in caspase-8 deficient mice promote uptake.[127] In absence of caspase-8, IECs demonstrates no cleavage of clathrin heavy chain or adaptin-α with no functional consequences in young mice. However, after bacterial stimulation this defect in endocytosis regulation leads to adhesion molecules internalization and IECs detachment without activation of cell death pathways. This barrier breach is rapidly followed by villi destruction and mucosal inflammation. We hypothesized that the constitutive cleavage of clathrin-dependent endocytosis proteins was due to basal stimulation of cells with TNFα. *In vitro*, HT-29 epithelial cells without any stimulation did not present any cleavage of adaptin-α protein. However, rapidly after TNFα stimulation we observed in HT-29 cells a cleavage of adaptin-α that is caspase-8 specific. Indeed, this cleavage was abolished in HT-29 cells with a downregulation of *casp8* gene expression stimulated with TNFα (data not shown). Moreover, we observed that the LPS-induced IEC detachment is dependent on TNFR1 activation as $Casp8^{\Delta IEC}$ x $Tnfr1^{-/-}$ mice are prevented from IECs detachment and intestinal inflammation.

Although the non-repression of endocytosis pathway seems to play an important role in homeostasis disturbance in absence of caspase-8, it is not sufficient as about 60% of $Casp8^{\Delta IEC}$ mice do not developed any intestinal disease. We suspected that after bacterial stimulation another mechanism was involved in the IECs detachment phenotype. Several previous studies described an association between caspase-8 and autophagy, a critical process involved in cell survival, immunity, and protein degradation.[130, 151, 152] Lymphocytes lacking caspase-8 demonstrated an aberrant activation of autophagy and defect in proliferation.[130] Our results showed that IECs lacking caspase-8 and stimulated by LPS present an abnormal activation of autophagy. This activation of autophagy leads to the formation of autophagosomes that need lipid

membrane to grow. Interestingly, a previous study clearly demonstrated that plasma membrane that is internalized by clathrin-dependent endocytosis is used in autophagosome formation.[143] Our bioinformatic analysis also suggests that autophagy and adhesion molecule share protein interactions together and with caspase-8. Thus, after LPS stimulation in absence of caspase-8 abnormal activation of autophagy in IECs leads to consumption of internalized plasma membrane and degradation of adhesion molecule ultimately followed by cell detachment. Confirmation of the involvement of autophagy came from the inactivation of autophagy with deletion of *Atg7* gene that prevents LPS-induced IECs detachment in mice.

After few weeks, about 40% of mice lacking caspase-8 in IECs developed a spontaneous intestinal inflammation predominantly in the terminal ileum and proximal colon. As we demonstrated that bacterial stimulation leads to massive IECs detachment, we may hypothesized that like in other spontaneous models (i.e. IL-10 knockout mice) microbiota plays a role and explains why not all mice developed a spontaneous disease.[153] This spontaneous intestinal inflammation observed in *Casp8*$^{\Delta IEC}$ mice is of particular importance as it shares many features with human Crohn's disease. Indeed, Crohn's disease patients present mostly an ileocolonic disease similar to what we observed in *Casp8*$^{\Delta IEC}$ mice.[7] They have intestinal barrier impairment with increased intestinal permeability whereas *Casp8*$^{\Delta IEC}$ mice have also increased IECs proliferation and increased serum endotoxin level suggesting a defect in intestinal barrier. It is well known that microbiota play a fundamental role in IBD pathogenesis and we showed that bacterial stimulation are critical for IECs detachment and mucosal inflammation in *Casp8*$^{\Delta IEC}$ mice.[7] TNFα secretion is also involved in Crohn's disease inflammation and anti-TNFα agents are to date the most powerful treatment for IBD patients.[154] Our results suggested an important role of TNFα secretion in the IECs detachment phenotype. To further investigate the implication of caspase-8 in human IBD pathogenesis we performed bioinformatic analysis looking for

protein-protein interactions between *CASP8* gene and identified IBD risk genes, using the HIPPIE human proteome interaction data base (see materials and methods section). IBD risk genes (1442 genes including some pseudogenes and some withdrawn entries) were selected from >160 IBD risk loci identified and described by Jostins et al.[106] Association to one of these functional categories: endocytosis, cell adhesion, autophagy using GO terms was determined for each IBD risk gene. Of the 1442 IBD genes, 1028 are contained in the protein-protein interactome data set. These 1028 proteins cluster in one big main interaction network with CASP8 in the very Centre (Supplemental Fig. 9). Interestingly, CASP8 gene has proximity to genes linked to autophagy, endocytosis and cell adhesion. Among these close interactors, there is the Clathrin heavy chain gene (CLTC) supporting a possible functional role of caspase-8 in regulating Clathrin-dependent endocytosis. Finally, our results demonstrated that autophagy participates to intestinal inflammation in the *Casp8*$^{\Delta IEC}$ mice. Autophagy has also been suspected to be involved in IBD pathogenesis with ATG16L1 and IRGM gene characterized as susceptibility gene for IBD in large genome wide association studies.[1, 106] The exact implication of autophagy in Crohn's disease is still poorly understood and both impairment of autophagy or abnormal activation of autophagy, have been suspected.[155, 156] Our results support the hypothesis that abnormal activation of autophagy in IECs favors intestinal inflammation. Overall, these data suggest that caspase-8 may be a critical regulator of human intestinal homeostasis that may play a role in development of inflammation observed in human IBD.

In conclusion, caspase-8 controls IECs adhesion and maintains intestinal barrier integrity in response to infectious stimuli by regulating clathrin-dependent endocytosis and autophagy. Overall, this work demonstrates a major physiological role of caspase-8 in maintaining intestinal homeostasis and controlling intestinal inflammation and suggests that modulation of caspase-8

expression or autophagy in IECs may serve as new therapeutic targets against intestinal inflammation.

4. Material and Methods:

Mouse strains and treatment

IEC-specific caspase-8 deficient mice (*Casp8*$^{\Delta IEC}$) were generated in our laboratory by breeding *Casp8*$^{fl/fl}$ mice[133] with villin-Cre mice[134] as described by Günther et al[112]. Tamoxifen-inducible IEC-specific caspase-8 deficient mice were generated by breeding floxed caspase-8 mice to villin-*CreERT2* mice. For the induction of the CreERT2 line (villin-*CreERT2* × *Casp8*$^{fl/fl}$), tamoxifen (Sigma) was emulsified in ethanol then in sunflower oil at a concentration of (10mg/ml). Tamoxifen was administered by gavage (5mg/mouse) for 3 consecutive days. In all experiments, littermates carrying the *loxP*-flanked alleles but not expressing Cre recombinase were used as controls. Cre-mediated recombination was genotyped by PCR on tail DNA. Villin-Cre mice and *Tnfr1* knockout mice were purchased from The Jackson Laboratory. *Casp8*$^{\Delta IEC}$ × *Tnfr1*$^{-/-}$ mice were obtained by crossing *Casp8*$^{\Delta IEC}$ mice to *Tnfr1* knockout mice. *Atg7* $^{fl/fl}$ mice were a gift from Dr. Tomoki Chiba (Department of molecular oncology, Tokyo Metropolitan Institute of Medical Science). IEC-specific caspase-8 and atg7 deficient mice (*Casp8*$^{\Delta IEC}$ × *Atg7*$^{\Delta IEC}$) were generated by crossing *Casp8* $^{fl/fl}$ mice to *Atg7*$^{fl/fl}$ mice and then breeding *Casp8* $^{fl/fl}$ × *Atg7*$^{fl/fl}$ with villin-Cre mice. *Casp8*$^{fl/fl}$, *Casp8*$^{\Delta IEC}$, *Tnfr1*$^{-/-}$, *Atg7* $^{fl/fl}$, villin-Cre, *Casp8*$^{\Delta IEC}$ × *Tnfr1*$^{-/-}$ and *Casp8*$^{\Delta IEC}$ × *Atg7*$^{\Delta IEC}$ mice were maintained in specific pathogen-free conditions at University of California, San Diego. Mice were given a single i.p. injection of 20mg/kg LPS in sterile PBS, using sterile PBS alone as a control. Recombinant mouse TNFα (200 ng.g^{-1}), necrostatin-1 (2 mg.kg^{-1}) and chlorpromazine (4 mg.kg^{-1}) were injected i.p. Mice were sacrificed at 1, 2 and 4 h after injection unless otherwise indicated. All animal studies were approved by the University of California, San Diego Institutional Animal Care and Use Committee.

Reagents

LPS from Escherichia coli O111:B4, necrostatin-1, chlorpromazine, tamoxifen, alcian blue and cycloheximide were from Sigma-Aldrich (St. Louis, MO). Recombinant mouse TNFα was purchased from Enzo Life Sciences (Farmingdale, NY). Recombinant human TNFα was purchased from Peprotech (Rocky Hill, NJ). Alexa Fluor 488 Phalloidin, mouse specific caspase-8, cleaved caspase 3 (Asp175), Actin-β, Sqstm1/p62 and LC3B antibodies were from Cell Signaling Technology (Danvers, MA). Anti-mouse Integrin beta 1 (KMI6) antibody was purchased from eBioscience (San Diego, CA). Mouse anti-adaptin-α, anti-adaptin-γ and anti-clathrin heavy chain antibodies were purchased from BD biosciences (San Jose, CA). Prolong Gold Antifade Reagent with DAPI was purchased from Invitrogen. Cell proliferation labeling reagent bromodeoxyuridine was purchased from GE Healthcare Biosciences (Pittsburgh, PA).

Citrobacter rodentium infection

C. rodentium was grown overnight in Luria-Bertani broth at 37°C, harvested by centrifugation, and resuspended in fresh Luria-Bertani broth at a concentration of $5x10^7$/ml. Six week old *Casp8*$^{\Delta IEC}$ and *Casp8*$^{fl/fl}$ mice were infected with 200 µl of the bacterial suspension (10^7 bacteria) by oral gavage. Mice weight was recorded each day during infection. After 6 or 7 days of *C. rodentium* infection, mice were euthanized. Before sacrifice, to determine bacterial numbers in the stool, fecal pellets were collected from individual mice over a 2- to 3-h period, weighed, and homogenized in 5 ml of phosphate-buffered saline (PBS). For determining bacterial numbers in the spleen, mesenteric lymph nodes and liver, each organ was removed in its entirety and homogenized in 2 ml of sterile PBS. Serial dilutions of the homogenates were plated onto MacConkey agar, and the numbers of CFU were determined after overnight incubation at 37°C.

Macroscopic analysis

After LPS injection mice were euthanized and abdominal cavity was opened. Pictures of intra-abdominal organs were taken in order to analyze the morphology of small intestine and colon. Small intestine was dissected and the luminal content was collected in pre-weighted small plastic tubes. After collection, tubes were weighted and luminal content weight was obtained by subtraction. Then luminal content of the small intestine of each mouse was diluted in 1ml of PBS and analyzed under optical microscope. Presence of luminal cells was assessed, and cells were counted using a hemocytometer.

Histology, immunochemistry, immunofluorescence and electron microscopy

Small intestine and colon were opened longitudinally, cleaned, and processed as Swiss rolls[135]. Ileal Swiss rolls were taken from the distal third of the small intestine. Tissues were fixed in 10% formalin and embedded in paraffin, and 5-mm sections were stained with H&E. For alcian blue staining, slides were deparaffinized and hydrated to distilled water. Slides were then stained in alcian blue solution for 30 minutes and counterstained in nuclear fast red solution (Sigma Aldrich) for 5 minutes. After coloration, slides were dehydrated and mounted with resinous mounting medium. For cleaved caspase 3 staining, samples were deparaffinized, subjected to Ag retrieval, and incubated with Ab overnight, after which HRP-conjugated secondary Ab was added for 2 h followed by incubation with 3,39-diaminobenzidine (Vector Laboratories) and counterstaining with hematoxylin. Immunofluorescence of cryosections was performed after fixation of tissue sections with cold acetone. Then sections were blocked with goat serum and incubated in primary antibody overnight at 4°C. Slides were then incubated with fluorochrome-conjugated secondary antibodies (Cell Signaling Tcehnology, Danvers, MA). Finally, slides were counterstained and mounted with Prolong Gold Antifade Reagent with DAPI (Invitrogen).

Confocal laser scanning microscopy (Olympus FV1000) was used for analysis. Cell death was analysed using the *in situ* cell death detection kit (Roche) for TUNEL. For electron microscopy, glutaraldehyde-fixed material was used. After embedding in Epon Araldite, ultrathin sections were cut and analysed using a Zeiss EM10C electron microscope.

Microscopic analysis

After LPS i.p. injection, mice were euthanized and small intestine was opened longitudinally, processed as a Swiss roll, immediately fixed in 10% buffered formalin and embedded in paraffin wax. Villus and crypt lengths were measured in each Swiss roll using three digital images per Swiss roll representing three different parts of the small intestine and containing at least 10 villi. Values of villus length were divided by the values of adjacent crypts length to obtain a villus/crypt ratio. Values of villus/crypt ratio were averaged to give a final mean villus/crypt ratio for each mouse. Histological mucosal damage in each small intestine was graded on a seven point scale adapted from Chiu *et al [157]* as follows: grade 0, normal mucosa; grade 1, development of subepithelial spaces near the tips of the villi; grade 2, extension of the subepithelial space with moderate epithelial lifting from the lamina propria, but without breach in the epithelial layer; grade 3, significant epithelial lifting along the length of the villi with breach of the epithelial layer and IECs floating in the lumen; grade 4, shortening of the villi with exposed lamina propria and numerous IECs floating in the lumen; grade 5, disappearance of the villi with immune cell infiltration of the mucosa; and grade 6, intense mucosal infiltration by immune cells, haemorrhage, and ulceration. All samples were evaluated and scored by one blinded investigator. Samples were examined in our laboratory under an microscope. Digital images were captured. Villus and crypt lengths were measured using the ImageJ 1.46 software.

IEC isolation and immunoblotting

IECs were isolated in an EDTA separation solution. Briefly, small intestines and colons were dissected and flushed with a fresh sterile PBS solution to remove faecal contents. The intestinal segments were then cut in half longitudinally, then into 0.5-1 cm pieces and shaken in PBS supplemented with 1.5 mM EDTA and 5% fetal calf serum for 5 minutes at 37°C. Supernatant was collected, mixed with a cold PBS solution and maintained at 4°C until the end of the isolation protocol. Small intestinal pieces were then reincubated in EDTA separation solution for 5 minutes at 37°C. Isolation steps were repeated 4 times. Isolated IECs were then recovered by centrifugation at 1300 rpm for 5 minutes and were used for preparation of protein extracts. Protein extracts were prepared using homemade RIPA lysis buffer supplemented with protease and phosphatase inhibitor tablets (Roche). Protein extracts were separated by SDS–PAGE (10%) and transferred to nitrocellulose transfer membranes (Whatman). Membranes were probed with the following primary antibodies: caspase-8, actin-β, sqstm1/p62, LC3B (Cell Signaling Technology), anti-adaptin-α, anti-adaptin-γ and anti-clathrin heavy chain (BD biosciences). Then secondary HRP-linked anti-rabbit or anti-mouse antibodies (Cell Signaling) were used.

Organoid culture

Organoid culture of small intestine was established as previously described (Sato et al, 2009). Briefly, crypts were extracted from small intestine of Vil-Cre-ERT2 Casp8 floxed mice and Vil-Cre-ERT2 Casp8 Atg7 double-floxed mice after 30 min incubation in PBS (pH 7.4) containing 2 mM EDTA in 6°C. Organoids were plated in Matrigel (BD Bioscience) and maintained in DMEM/F12 media (Life Technologies) containing B27 and N2 supplements (Life Technologies), 1.25 mM N-acetyl L-cysteine (Sigma), 100 ng/ml noggin (Peprotech), 50 ng/ml mEGF (Biosource), and 10% Rspo1-Fc-conditioned medium (the Rspo1-Fc-expressing cell line was a

generous gift from Dr. Calvin Kuo, Stanford). Casp8 deletion or Casp8 Atg7 double deletion in organoids was induced with 1 μM 4-hydroxytamoxifen (4OHT, Sigma). Two days after 4OHT treatment, organoids were challenged with TNF or PBS for various time points. Organoids were then released from Matrigel with ice cold DMEM/F12 media, washed once with ice cold PBS, pelleted, and lyzed with RIPA buffer plus protease inhibitor cocktail. Protein lysates were subjected to SDS-PAGE and immunoblotting.

Interaction Network assembly

In order to analyze potential direct interactions between proteins belonging to different functional categories, we queried 17 genes (caspase-8, eight adhesion proteins, eight endocytotic proteins) for their first degree interactors using the Human Integrated Protein-Protein Interaction rEference HIPPIE (http://cbdm.mdc-berlin.de/tools/hippie/index.php) [PMID: 22348130] and identified autophagy core and receptor proteins within these interactors. The interaction network was visualized using the force-directed layout (Biolayout) within Cytoscape (http://www.cytoscape.org). [PMID: 14597658].

Endotoxin and proliferation assays

For endotoxin assays, blood from *Casp8*$^{\Delta IEC}$, *Casp8*$^{fl/fl}$ and DSS treated mice was collected by tail puncture and centrifuge to obtain serum samples. Determination of serum endotoxin levels was done using a LAL Chromogenic Endotoxin Quantitation Kit (Thermo scientific). For BrdU staining, mice were injected i.p. with 2 mg/mouse BrdU (GE Healthcare Biosciences) 2 h before sacrifice. Paraffin-embedded small intestine sections were stained using a BrdU *In-Situ* Detection Kit (BD Pharmingen). To quantify IEC proliferation by BrdU labeling index, we calculated the number of BrdU^{+} cells per crypt in at least 10 well-oriented crypts per small intestine section.

Values of $BrdU^+$ cells per crypt were averaged to give a final mean $BrdU^+$ cells per crypt for each mouse.

Statistical Analysis

Data are expressed as mean ± SEM. Differences between groups of mice were evaluated with the Mann-Whitney test or *t* test, as appropriate. Differences with a *P* value of < 0.05 were considered significant. Statistical analyses were performed using Graphpad Prism 6 software (GraphPad Software Inc, La Jolla, CA).

5. Figures and Supplementary Figures:

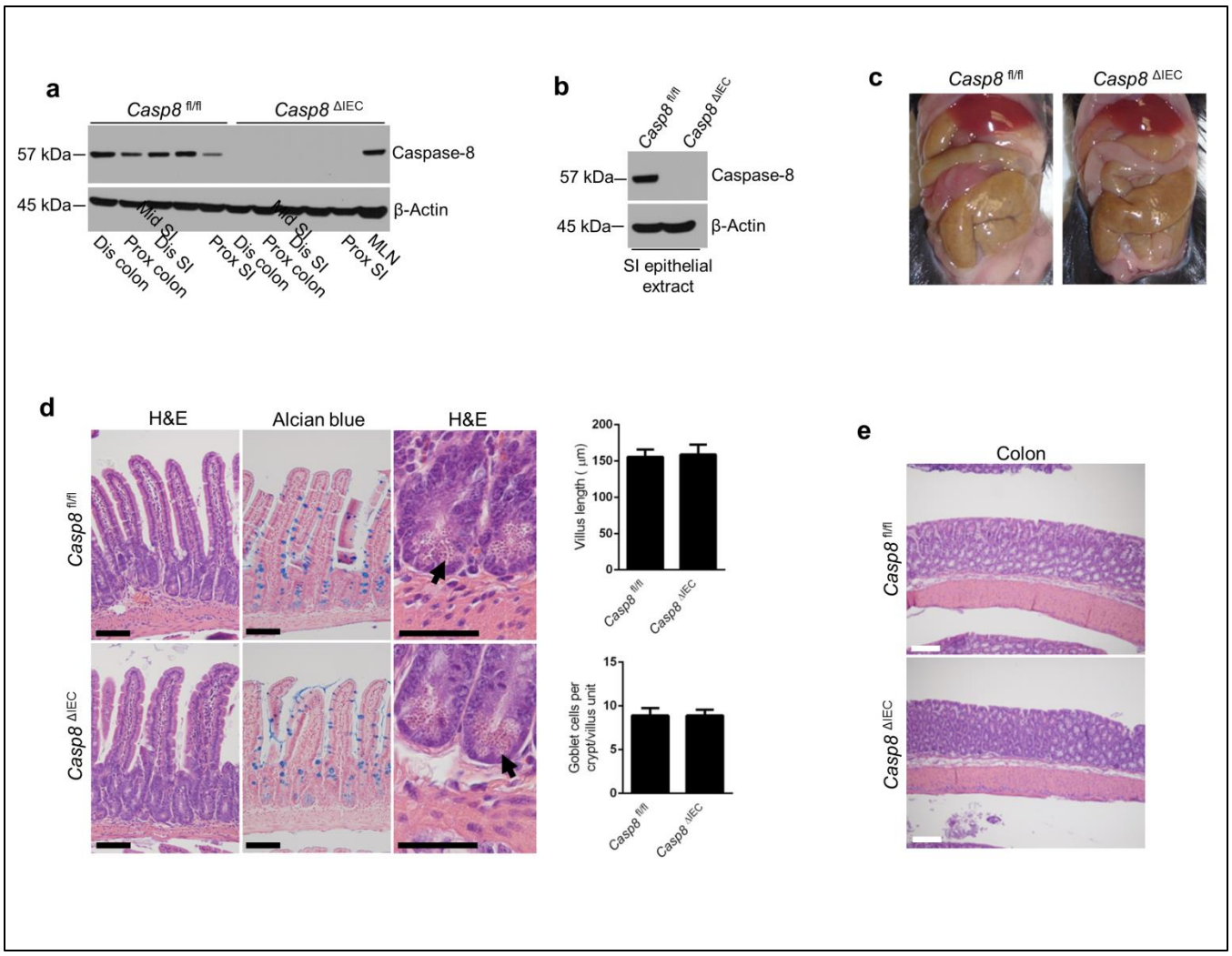

Figure 1: Normal intestinal development and epithelial differentiation in Casp8$^{\Delta IEC}$ mice. a, Colon and small intestine samples of *Casp8*$^{\Delta IEC}$ and *Casp8*$^{fl/fl}$ mice were lysed for western blot analysis with anti-caspase-8 and anti-β-actin antibodies. Mesenteric lymph node (MLN) lysate of *Casp8*$^{\Delta IEC}$ mice was used as positive control of caspase-8 expression in other cell types than IECs. **b**, IECs were isolated from small intestine of *Casp8*$^{fl/fl}$ and *Casp8*$^{\Delta IEC}$ mice and lysed for western blot analysis with anti-caspase-8 and anti-β-actin antibodies to confirm the absence of caspase-8 proteins in *Casp8*$^{\Delta IEC}$ mice. **c**, Representative pictures of 6 weeks old *Casp8*$^{fl/fl}$ and *Casp8*$^{\Delta IEC}$ mice without any stimulation after sacrifice and dissection showing no difference in abdominal cavity. **d**, Representative H&E (left and right pictures) and alcian blue (middle pictures) stained Swiss roll sections showing normal villi and crypts morphology with presence of paneth cells and goblet cells in *Casp8*$^{\Delta IEC}$ mice. Scale bars, 50µm for left and middle pictures

and 25µm for right pictures. No difference is observed for Villi length (µm) and number of goblet cells per crypt between *Casp8*$^{\Delta IEC}$ (n=4) and *Casp8*$^{fl/fl}$ (n=4) mice ($p>0.05$). **e**, Representative H&E stained Swiss roll sections of small intestine and colon of 6 weeks old *Casp8*$^{fl/fl}$ and *Casp8*$^{\Delta IEC}$ mice without any stimulation showing no major microscopic abnormalities in *Casp8*$^{\Delta IEC}$ mice.

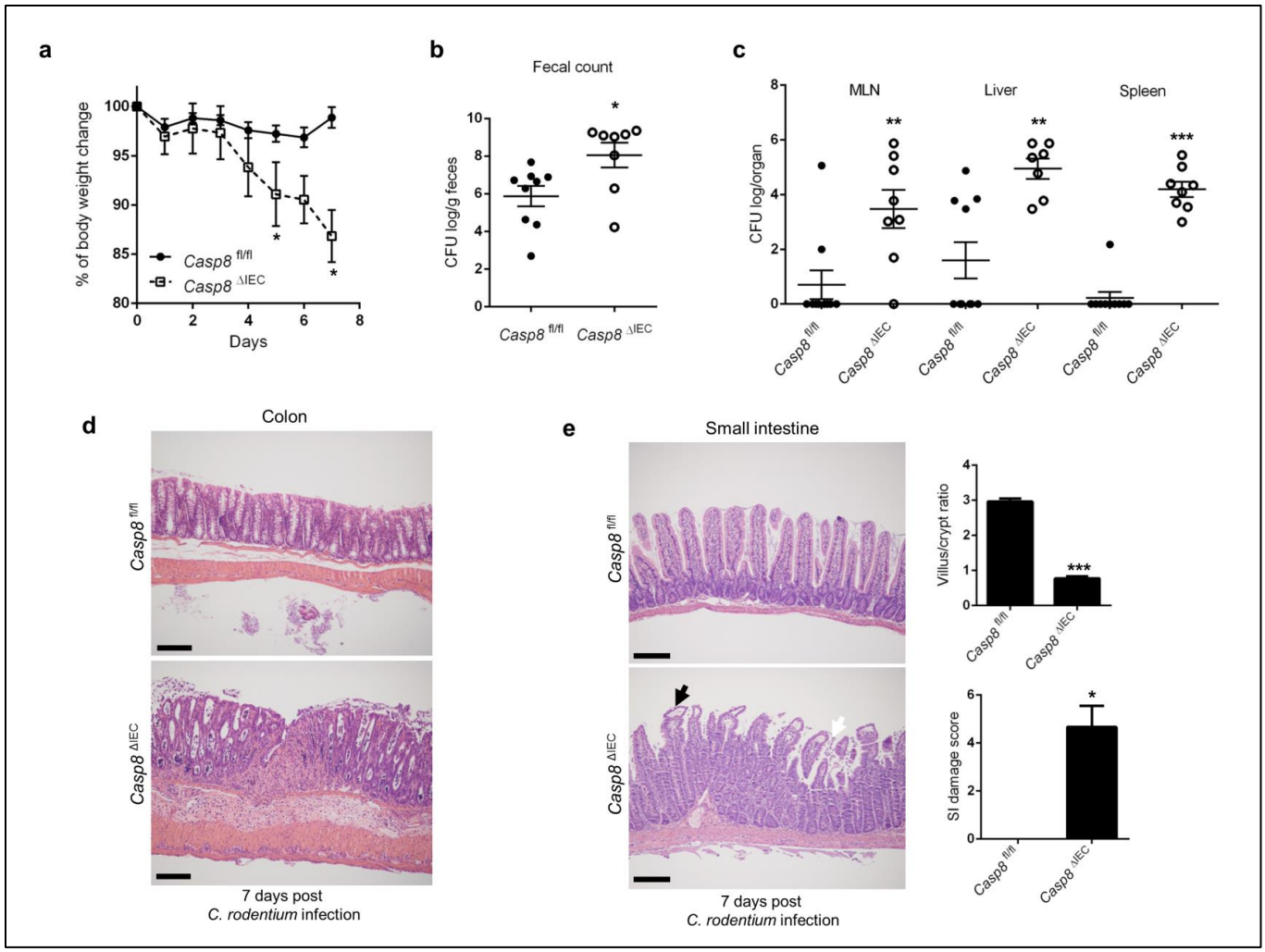

Figure 2: Citrobacter rodentium causes severe intestinal inflammation in *Casp8*$^{\Delta IEC}$ mice. a, *Casp8*$^{fl/fl}$ (filled circle and solid line, n=5) and *Casp8*$^{\Delta IEC}$ (empty square and dotted line, n=8) mice were infected orally with *Citrobacter rodentium* (10^7 bacteria per mouse) and then followed for 7 days with measurement each day of animal weight and percentage of weight loss. *Casp8*$^{\Delta IEC}$ mice show a significant loss of weight during *C. rodentium* infection compared with *Casp8*$^{fl/fl}$ mice. *p<0.05. Experiments were performed twice with similar results. **b**, **c**, Just before sacrifice, fecal pellets (**b**) were collected from individual mice, weighed, and homogenized in 5 ml of PBS. At sacrifice, spleen, mesenteric lymph nodes (MLN) and liver (**c**) was removed and homogenized in 2 ml of sterile PBS. Serial dilutions of the homogenates were plated onto MacConkey agar, and the numbers of *C. rodentium* CFU were determined after overnight incubation at 37°C. *Casp8*$^{\Delta IEC}$ mice (empty circle) have higher numbers of *C. rodentium* CFU in feces, liver, spleen

and MLN compared with *Casp8*$^{fl/fl}$ mice (filled circle). Of note, CFU numbers in Liver, spleen and MLN of *Casp8*$^{fl/fl}$ mice are very low showing no bacterial translocation in control animals. *p<0.05, **p<0.01, ***p<0.001. **d**, Representative H&E stained sections of *Casp8*$^{fl/fl}$ and *Casp8*$^{\Delta IEC}$ mice colons 7 days after *C. rodentium* infection showing critical mucosal inflammation in *Casp8*$^{\Delta IEC}$ mice colon section with immune cell infiltration and epithelial ulceration compared to control section. Scale bars, 100µm. **e**, Representative H&E stained sections of *Casp8*$^{fl/fl}$ and *Casp8*$^{\Delta IEC}$ mice small intestine 7 days after *C. rodentium* infection showing also mucosal inflammation in *Casp8*$^{\Delta IEC}$ mice small intestine section with shortening of the villi, development of subepithelial spaces near the tips of the villi (black arrow), epithelial cell detachment (white arrow) and immune cell infiltration. Scale bars, 100µm. Villus crypt ratio is decreased and intestinal damage score is significantly increased in *Casp8*$^{\Delta IEC}$ mice compared with *Casp8*$^{fl/fl}$ mice 7 days after *C. rodentium* infection. *p<0.05, ***p<0.001.

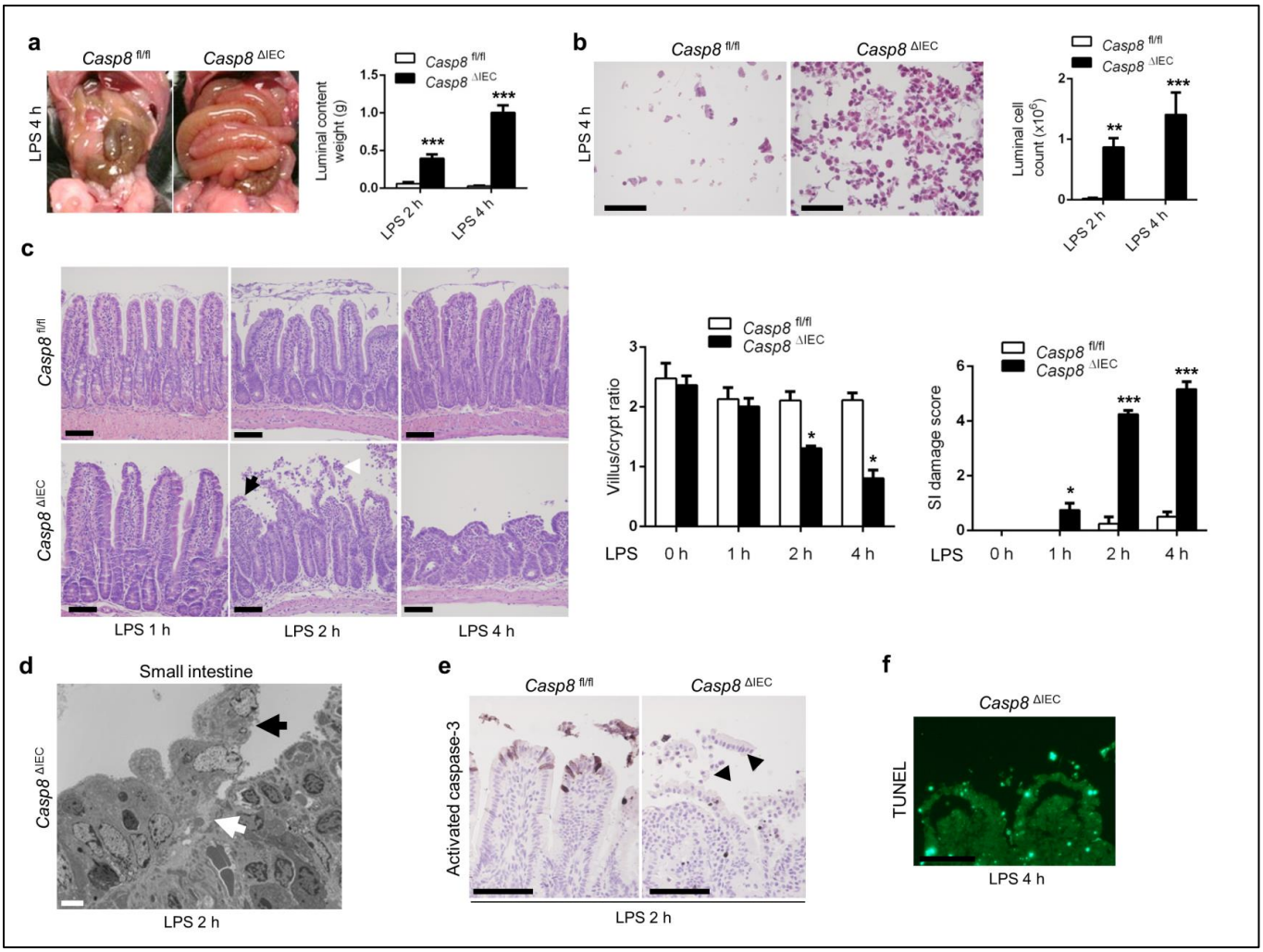

Figure 3: LPS stimulation leads to acute epithelial detachment in *Casp8*$^{\Delta IEC}$ mice. a, Animals were euthanized 4 hours after LPS i.p. injection (20mg/kg). Representative pictures of intestinal macroscopic findings in *Casp8*$^{fl/fl}$ and *Casp8*$^{\Delta IEC}$ mice showing massive dilatation of *Casp8*$^{\Delta IEC}$ mice small intestine after LPS injection compared with controls. Luminal content weight of small intestine of each animal was evaluated using pre-weighted small plastic tubes, 2 h (n=4 per group) and 4 h (n=7 per group) after LPS injection. ***p<0.001. **b**, Evaluation of cells in the small intestine luminal fluid collected after LPS injection. Representative pictures of small intestinal fluid smears showing numerous round-shaped cells floating in the luminal content of *Casp8*$^{\Delta IEC}$ mice whereas only small sheets of IECs with normal structure are observed in *Casp8*$^{fl/fl}$ mice (due to collection techniques). Black scale bars, 50µm. Number of luminal cells in each small intestine luminal content was evaluated 2 h (n=4 per group) and 4 h (n=7 per group)

after LPS injection. **p<0.01, ***p<0.001. **c**, Representative H&E stained sections of *Casp8*$^{fl/fl}$ and *Casp8*$^{\Delta IEC}$ mice small intestine, 1 h, 2h, and 4 h after LPS i.p injection showing IECs detachment (white arrow) with breach of the epithelia layer (black arrow) in *Casp8*$^{\Delta IEC}$ mice starting 2 h after LPS injection and leading to villi destruction and small intestinal inflammation no more than 4 h after LPS injection. Villus/crypt ratio decreases and small intestine damage score increases over time in *Casp8*$^{\Delta IEC}$ mice compared with controls. *p<0.05, ***p<0.001. Results are representative of 4 independent experiments. **d**, Representative electron microscopy picture of *Casp8*$^{\Delta IEC}$ mice small intestinal villus, 2 h after LPS i.p. injection showing IECs detachment from basal membrane (black arrow) with persistence of cell to cell adhesion (white arrow). **e**, Representative small intestine sections stained with activated caspase-3, 2 h after LPS i.p; injection showing no staining in already detached IECs in *Casp8*$^{\Delta IEC}$ mice (black arrows). **f**, Representative of TUNEL stained small intestine section of *Casp8*$^{\Delta IEC}$ mice showing absence of TUNEL staining in the majority of already detached IECs, 4 h after LPS i.p. injection. Black scale bars, 50µm. White scale bar, 5µm.

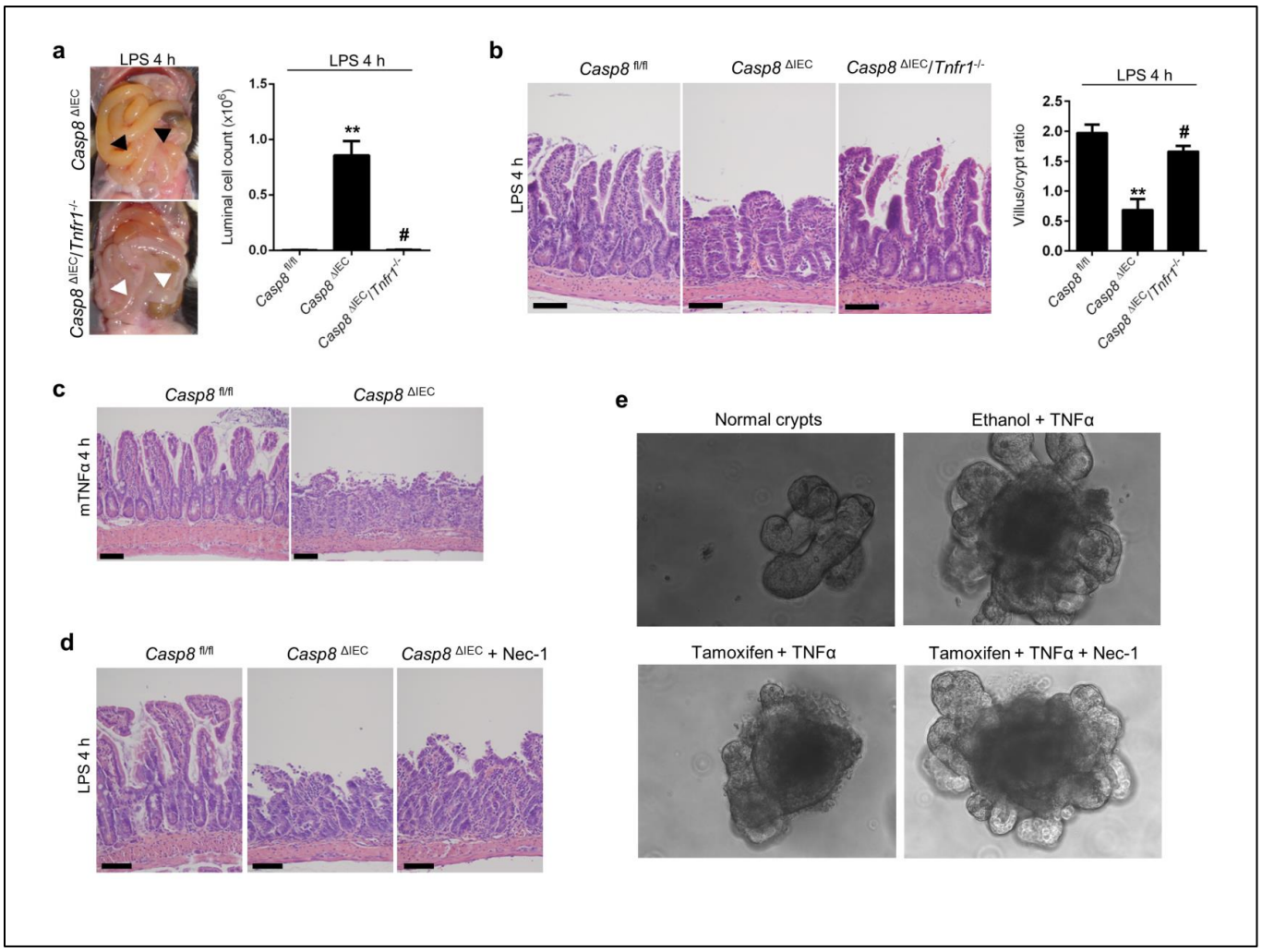

Figure 4: LPS-induced epithelial detachment in *Casp8*$^{\Delta IEC}$ mice requires TNFα signaling.

a, Representative macroscopic pictures of *Casp8*$^{\Delta IEC}$ and *Casp8*$^{\Delta IEC}$ x *Tnfr1*$^{-/-}$ mice 4 h after LPS i.p. treatment showing absence of small intestine dilatation in *Casp8*$^{\Delta IEC}$ x *Tnfr1*$^{-/-}$ mice (white arrows) compared with *Casp8*$^{\Delta IEC}$ mice (black arrows). Prevention of IEC detachment in *Casp8*$^{\Delta IEC}$ x *Tnfr1*$^{-/-}$ was confirmed by significant decrease of luminal cell count compared with *Casp8*$^{\Delta IEC}$ mice (n=4-7 mice per group). **p<0.01 *vs.* control, $^{\#}$p<0.05 *vs. Casp8*$^{\Delta IEC}$ mice. **b**, Representative H&E stained sections of small intestine of *Casp8*$^{fl/fl}$, *Casp8*$^{\Delta IEC}$ and *Casp8*$^{\Delta IEC}$ x *Tnfr1*$^{-/-}$ mice 4 h after LPS i.p. injection showing prevention of villi destruction and ileitis in *Casp8*$^{\Delta IEC}$ x *Tnfr1*$^{-/-}$ mice (right panel). This was confirmed by a significant increase of villus/crypt ratio in *Casp8*$^{\Delta IEC}$ x *Tnfr1*$^{-/-}$ mice compared with *Casp8*$^{\Delta IEC}$ mice. **p<0.01 *vs.* control, $^{\#}$p<0.05 *vs. Casp8*$^{\Delta IEC}$ mice. Results are representative of two independent experiments.

c, Representative H&E stained sections of small intestine of *Casp8*$^{fl/fl}$ and *Casp8*$^{\Delta IEC}$ mice 4 h after recombinant mouse TNFα (mTNFα) injection i.p. (200 ng.g^{-1}) showing villi destruction and IEC detachment only in *Casp8*$^{\Delta IEC}$ mice. **d**, Representative H&E stained sections of small intestine of *Casp8*$^{fl/fl}$, *Casp8*$^{\Delta IEC}$ mice and *Casp8*$^{\Delta IEC}$ mice treated with necrostatin-1 i.p. 4 h after LPS injection showing no effect of necrostatin-1 for prevention of IEC detachment. Scale bars, 50µm. **e**, Organoids culture was established from IECs of *Casp8*$^{ind\Delta IEC}$ mice (Normal crypts) and treated with ethanol or tamoxifen plus TNFα for 22 hours. Crypts treated with tamoxifen and TNFα demonstrated cell death that was prevented by Nec-1 treatment.

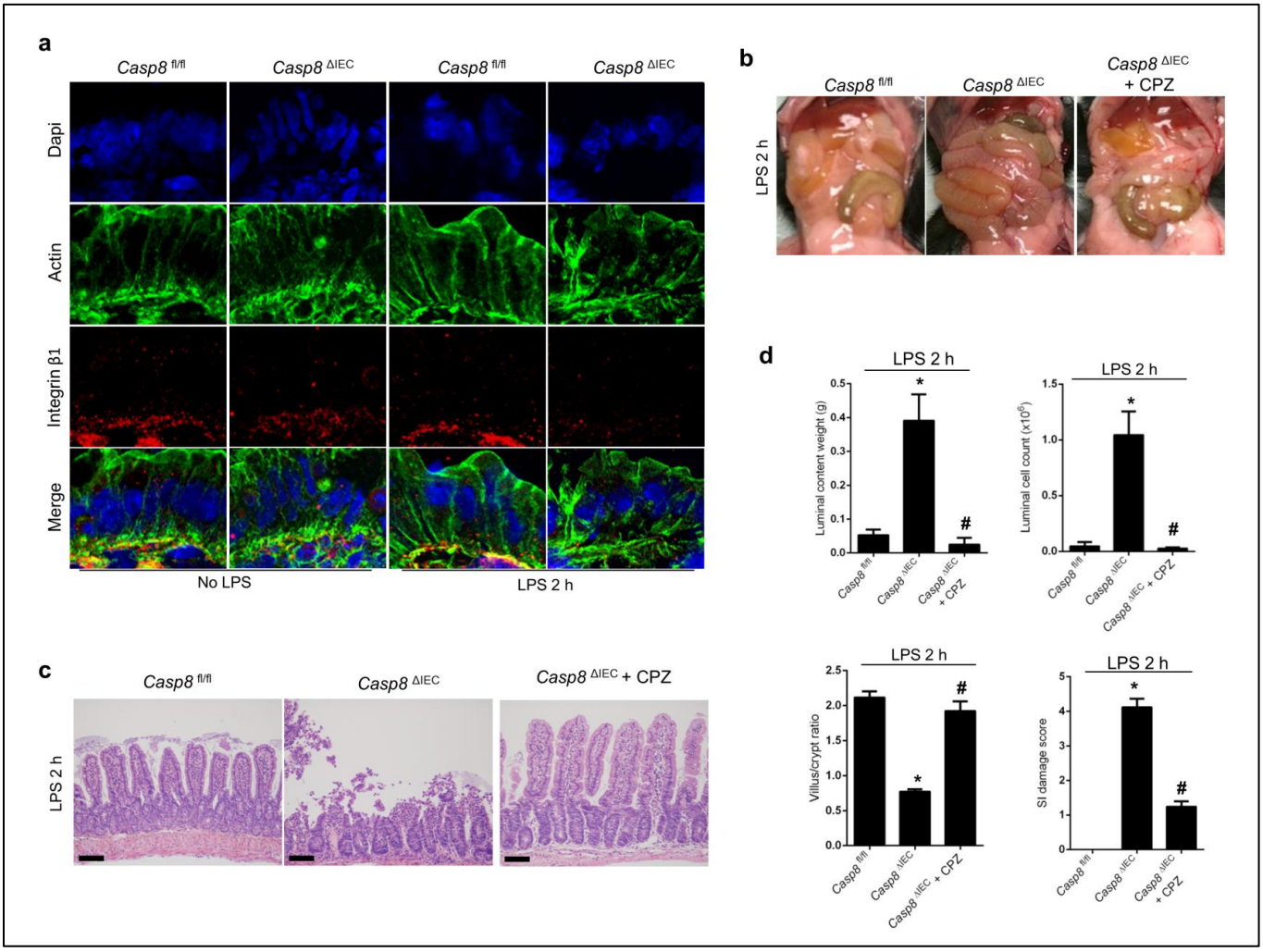

Figure 5: LPS-induced epithelial detachment in *Casp8*$^{\Delta IEC}$ mice is mediated by uncontrolled endocytosis of β1-integrins. a, Frozen small intestine sections of *Casp8*$^{fl/fl}$ and *Casp8*$^{\Delta IEC}$ mice collected before and 2h after LPS i.p injection, were stained with anti-β1-integrin and anti-β-actin primary antibodies, and then with fluorescent secondary antibodies before visualization under confocal microscope. Slides were counterstained with DAPI. Fluorescent staining of β1-integrins (red) is present at the basal side of IECs along the basal membrane in *Casp8*$^{fl/fl}$ mice but also in *Casp8*$^{\Delta IEC}$ mice without LPS, although the staining is weaker. After LPS injection, a complete disappearance of β1-integrins fluorescent staining is observed in *Casp8*$^{\Delta IEC}$ mice, but not in control animals. **b**, Representative macroscopic pictures of *Casp8*$^{fl/fl}$, *Casp8*$^{\Delta IEC}$ and chlorpromazine-treated *Casp8*$^{\Delta IEC}$ mice small intestine 2 hours after LPS i.p. injection showing

prevention of small intestine major dilatation in chlorpromazine-treated *Casp8*$^{\Delta IEC}$ mice compared with *Casp8*$^{\Delta IEC}$ mice. **c**, Representative H&E stained sections of small intestine of *Casp8*$^{fl/fl}$ and *Casp8*$^{\Delta IEC}$ mice collected 2 hours after LPS i.p. injection. Black scale bars, 50µm. *Casp8*$^{\Delta IEC}$ mice were either treated with LPS alone or with concomitant i.p. injection of chlorpromazine, an endocytosis inhibitor. Treatment with chlorpromazine prevents IECs detachment observed in *Casp8*$^{\Delta IEC}$ mice. **d**, This was confirmed by decreased small intestine luminal cell count and increased villus/crypt ratio in *Casp8*$^{\Delta IEC}$ *mice* treated with chlorpromazine compared with *Casp8*$^{\Delta IEC}$ mice treated with LPS alone. Two hours after LPS i.p. injection, small intestines of *Casp8*$^{fl/fl}$, *Casp8*$^{\Delta IEC}$ and chlorpromazine-treated *Casp8*$^{\Delta IEC}$ mice were harvested and luminal content from each small intestine was collected and weighted. Chlorpromazine significantly prevents the increase in luminal content weighted observed in *Casp8*$^{\Delta IEC}$ mice (n=4 mice per group). * $p<0.05$ *vs.* controls, $^{\#}$ $p<0.05$ *vs. Casp8*$^{\Delta IEC}$ mice. **c**, Small intestine damage score was evaluated in *Casp8*$^{fl/fl}$, *Casp8*$^{\Delta IEC}$ and chlorpromazine-treated *Casp8*$^{\Delta IEC}$ mice 2 hours after LPS i.p. injection. Chlorpromazine significantly prevents the increase of small intestine damage score observed in *Casp8*$^{\Delta IEC}$ mice. * $p<0.05$ *vs.* controls, $^{\#}$ $p<0.05$ *vs. Casp8*$^{\Delta IEC}$ mice.

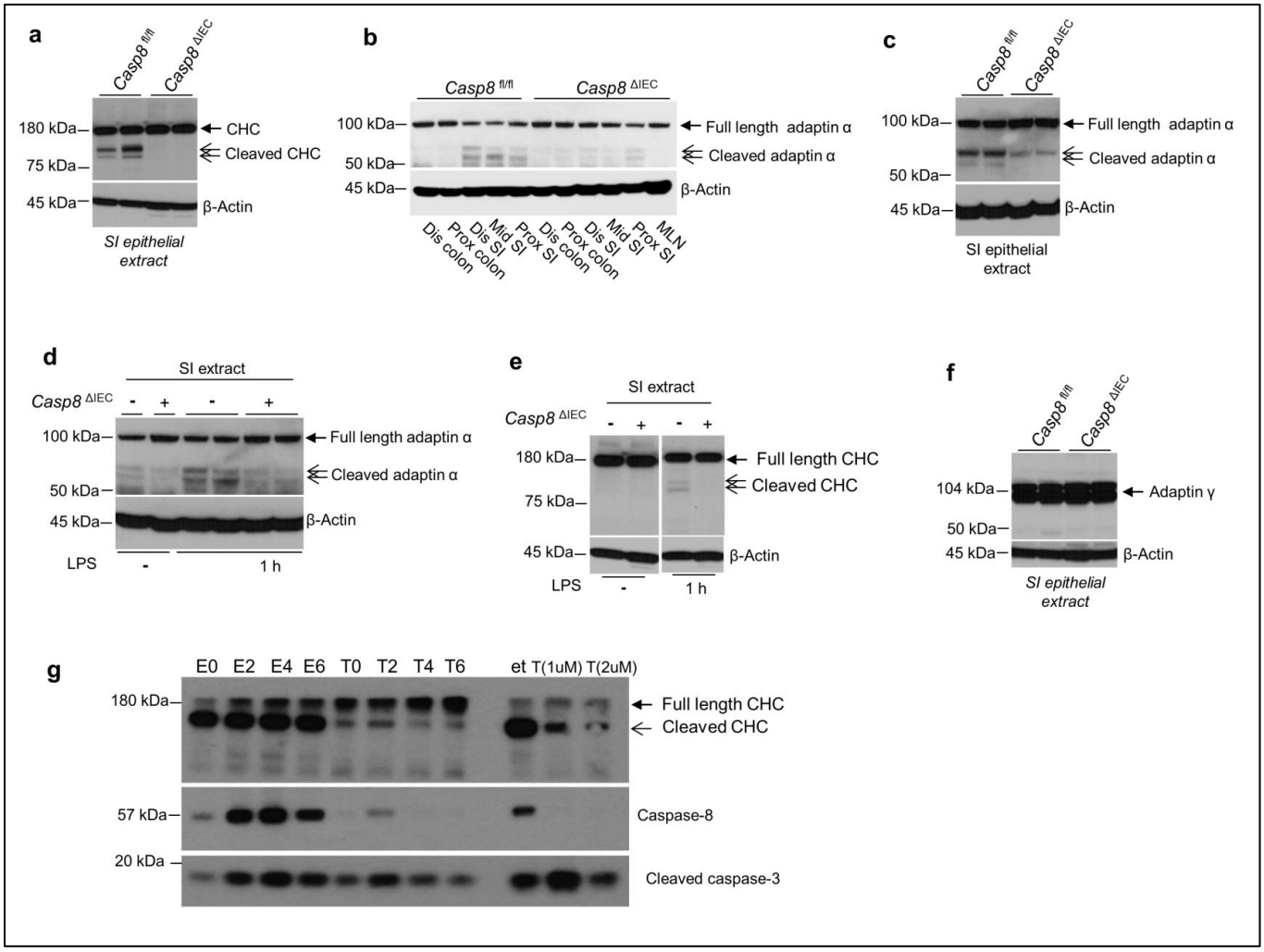

Figure 6: Caspase-8 constitutively cleaves clathrin-dependent endocytosis proteins. a, **c**, **f** IECs were isolated from small intestine of *Casp8*$^{fl/fl}$ and *Casp8*$^{\Delta IEC}$ mice and used for western blot with anti-clathrin heavy chain (**a**), anti-adaptin-α (**c**), and anti-adaptin-γ (**f**) antibodies. β-actin was used as loading control in each experiment. Only controls mice present a cleavage of adaptin-α and clathrin heavy chain proteins, but not of adaptin-γ, which is not involved in the clathrin-dependent endocytosis. Western blot analysis show representative pictures of 2 independent experiments. **b**, Colon and small intestine samples of *Casp8*$^{\Delta IEC}$ and *Casp8*$^{fl/fl}$ mice were lysed for western blot analysis with anti-adaptin-α antibody. Constitutive cleavage of adaptin-α were observed in small intestine of *Casp8*$^{fl/fl}$ mice, but not in *Casp8*$^{\Delta IEC}$ mice. MLN samples from *Casp8*$^{\Delta IEC}$ mice which present good caspase-8 expression, did not present any degradation of adaptin-α meaning that constitutive degradation of adaptin-α is specific to intestinal epithelial cells. **d**, **e**, Small intestine samples of *Casp8*$^{\Delta IEC}$ and *Casp8*$^{fl/fl}$ mice were

collected before and 1 h after LPS i.p. injection and lysed for western blot analysis with anti-adaptin-α, anti-clathrin heavy chain and anti-β-actin antibodies. Increased cleavage of adaptin-α and clathrin heavy chain is observed in control animals after LPS treatment whereas no cleavage of these proteins is observed in *Casp8*$^{\Delta IEC}$ mice after LPS treatment. **g**, Enteroids cultures were established from IEC of *Casp8*^{indΔIEC} mice and then treated with ethanol or tamoxifen. Crypts were then harvested and used for western blot with anti-clathrin heavy chain (CHC), anti-caspase-8, and anti-cleaved caspase-3 antibodies. Time course experiment (from 0 to 6 hours) and dose experiments (with 1 or 2 µM of tamoxifen) were performed. Only crypts treated with ethanol present a constitutive cleavage of the Clathrin heavy chain.

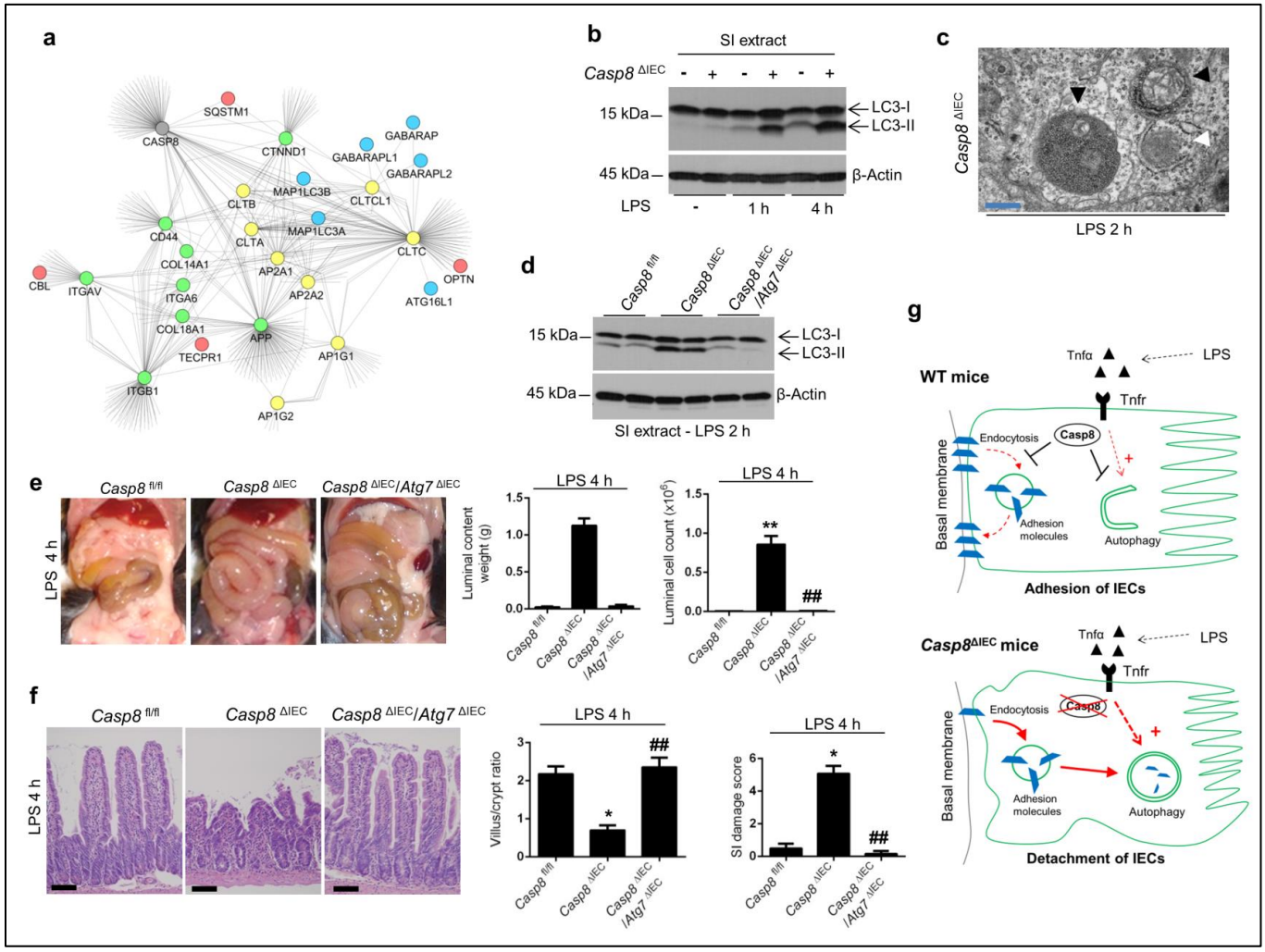

Figure 7: Autophagy plays a key role in LPS-induced epithelial detachment in *Casp8*$^{\Delta IEC}$ mice. a, Protein interaction network. 17 query genes (caspase-8, grey; adhesion molecules, green; endocytotic proteins, yellow) were interrogated for their direct interactors using the HIPPIE interactome data base. Within these interactors, proteins belonging to the autophagy core machinery (blue) or autophagy receptors (red) are displayed by large symbols, while other interacting proteins are minimized for clarity. Black edges represent direct protein-protein interactions. **b**, Small intestine (SI) samples of *Casp8*$^{\Delta IEC}$ and *Casp8*$^{fl/fl}$ mice collected before, 1 hour and 4 hours after LPS i.p. injection were lysed for western blot analysis with anti-LC3 and anti-β-actin antibodies. LC3-I represents the basal cytosolic form of LC3 protein and LC3-II represents the autophagosome associated form. **c**, Representative electron microscope picture of LPS-treated *Casp8*$^{\Delta IEC}$ mice IEC cytoplasm section showing presence of autophagosomes as

double membrane structures engulfing organelles. Blue scale bar, 0.5 µm. **d**, Small intestine samples of *Casp8*$^{\Delta IEC}$, *Casp8*$^{fl/fl}$ and *Casp8*$^{\Delta IEC}$ x *Atg7*$^{\Delta IEC}$ mice collected 2 hours after LPS i.p. injection were lysed for western blot analysis with anti-LC3 and anti-β-actin antibodies. **e**, Representative pictures of intestinal macroscopic findings in *Casp8*$^{fl/fl}$, *Casp8*$^{\Delta IEC}$ and *Casp8*$^{\Delta IEC}$ x *Atg7*$^{\Delta IEC}$ mice 4 hours after LPS i.p. injection (20mg/kg) showing absence of small intestine dilatation in *Casp8*$^{\Delta IEC}$ x *Atg7*$^{\Delta IEC}$ mice compared with *Casp8*$^{\Delta IEC}$ mice. Luminal content weight of small intestine of each animal (n=3-4 per group) was evaluated using pre-weighted small plastic tubes, 4 h after LPS injection. Small intestine luminal cell count was evaluated in each animal (n=4-7 per group), 4 hours after LPS injections. **$p<0.01$ *vs.* control, $^{\#\#}p<0.01$ *vs.* *Casp8*$^{\Delta IEC}$ mice. **f**, Representative H&E stained sections of *Casp8*$^{fl/fl}$, *Casp8*$^{\Delta IEC}$ and *Casp8*$^{\Delta IEC}$ x *Atg7*$^{\Delta IEC}$ mice small intestine collected 4 hours after LPS i.p. injection showing absence of IECs detachment and mucosal inflammation in *Casp8*$^{\Delta IEC}$ x *Atg7*$^{\Delta IEC}$ mice compared with *Casp8*$^{\Delta IEC}$ mice. Black scale bars, 50 µm. Villus/crypt ratio is increased and small intestine (SI) damage score is decreased in *Casp8*$^{\Delta IEC}$ x *Atg7*$^{\Delta IEC}$ mice compared with *Casp8*$^{\Delta IEC}$ mice (n=5-6 per group). *$p<0.05$ *vs.* control, $^{\#\#}p<0.01$ *vs.* *Casp8*$^{\Delta IEC}$ mice. Data are representative of two independent experiments. **g**, Scheme representing the hypothesized model of IECs detachment in *Casp8*$^{\Delta IEC}$ mice after LPS stimulation involving uncontrolled activation of clathrin-dependent endocytosis and autophagy.

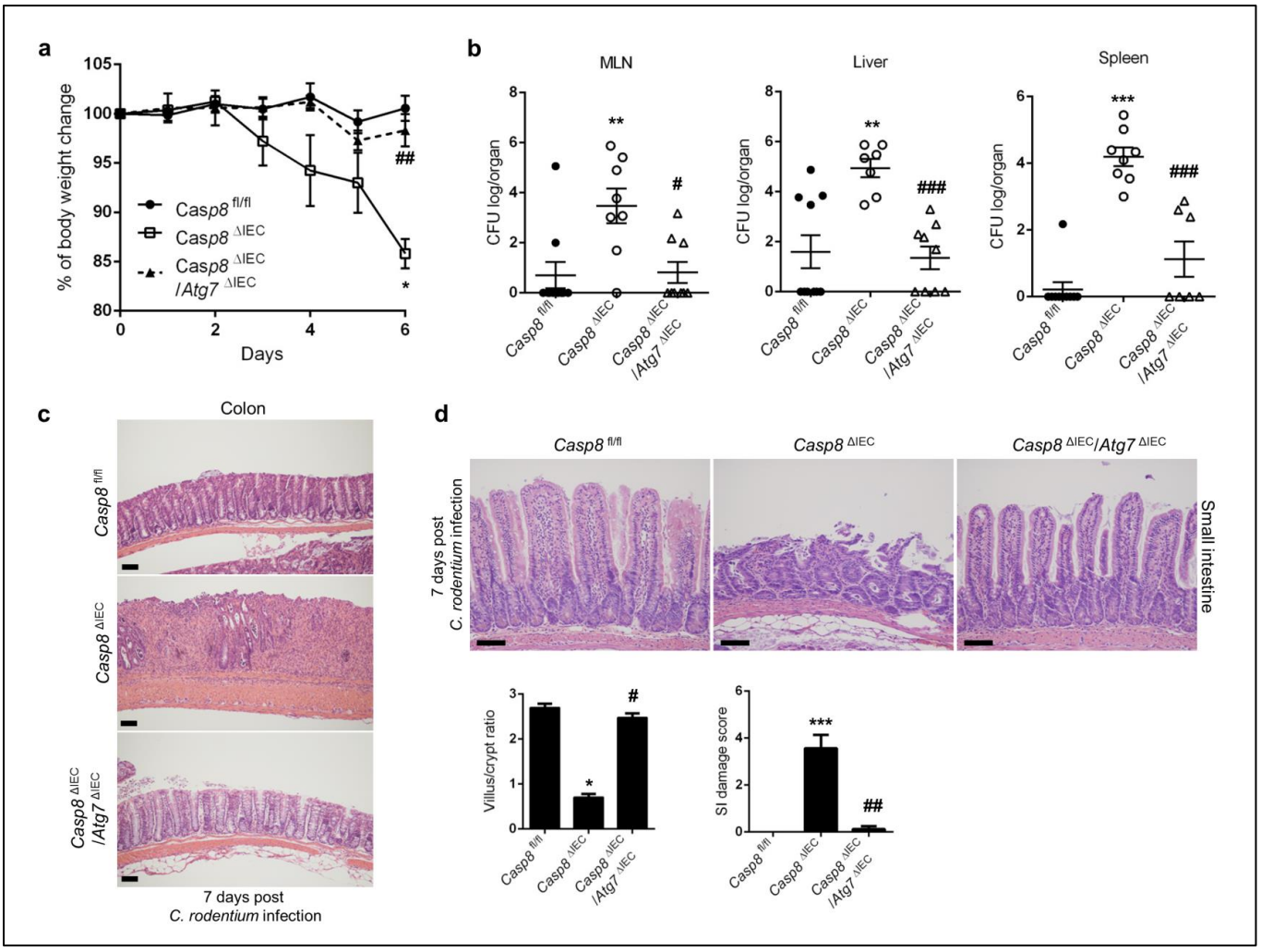

Figure 8: Suppression of autophagy prevents microbially-induced intestinal inflammation in the absence of epithelial caspase-8. a, *Casp8*$^{fl/fl}$ (filled circle and solid line, n=5), *Casp8*$^{\Delta IEC}$ (empty square and solid line, n=3) and *Casp8*$^{\Delta IEC}$ x *Atg7*$^{\Delta IEC}$ mice (filled triangle and dotted line, n=5) were infected orally with *Citrobacter rodentium* (10^7 bacteria per mouse) and then followed for 6 days with measurement each day of animal weight and percentage of weight loss. *Casp8*$^{\Delta IEC}$ mice show a significant loss of weight during *C. rodentium* infection, which is not observed in *Casp8*$^{\Delta IEC}$ x *Atg7*$^{\Delta IEC}$ mice. *p<0.05 vs. controls and $^{\#\#}$p<0.01 vs. *Casp8*$^{\Delta IEC}$ mice. Experiments were performed twice with similar results. **b**, At sacrifice, spleen, mesenteric lymph nodes (MLN) and liver (c) was removed and homogenized in 2 ml of sterile PBS. Serial dilutions of the homogenates were plated onto MacConkey agar, and the numbers of *C. rodentium* CFU were determined after overnight incubation at 37°C. *Casp8*$^{\Delta IEC}$ x *Atg7*$^{\Delta IEC}$ mice (empty triangle, n=9) have lower numbers of *C. rodentium* CFU in liver, spleen and MLN compared with *Casp8*$^{\Delta IEC}$

mice (empty circle, n=9). This experiment also confirmed that *Casp8*$^{\Delta IEC}$ mice have higher numbers of *C. rodentium* CFU in Liver, spleen and MLN compared with *Casp8*$^{fl/fl}$ mice (filled circle, n=10). Of note, CFU numbers in Liver, spleen and MLN of *Casp8*$^{fl/fl}$ and *Casp8*$^{\Delta IEC}$ x *Atg7*$^{\Delta IEC}$ mice are very low demonstrating no bacterial translocation in control animals. **p<0.01, ***p<0.001 vs. controls and $^{###}$p<0.001 vs. *Casp8*$^{\Delta IEC}$ mice. **c**, Representative H&E stained sections of *Casp8*$^{fl/fl}$, *Casp8*$^{\Delta IEC}$ and *Casp8*$^{\Delta IEC}$ x *Atg7*$^{\Delta IEC}$ mice colons 7 days after *C. rodentium* infection showing critical mucosal inflammation in *Casp8*$^{\Delta IEC}$ mice but not in *Casp8*$^{\Delta IEC}$ x *Atg7*$^{\Delta IEC}$ mice. Scale bars, 50 µm. **d**, Representative H&E stained sections of *Casp8*$^{fl/fl}$, *Casp8*$^{\Delta IEC}$ and *Casp8*$^{\Delta IEC}$ x *Atg7*$^{\Delta IEC}$ mice small intestine 7 days after *C. rodentium* infection showing critical mucosal inflammation in *Casp8*$^{\Delta IEC}$ mice, but not in *Casp8*$^{\Delta IEC}$ x *Atg7*$^{\Delta IEC}$ mice. Scale bars, 50 µm. Villus/crypt ratio is increased and intestinal damage score is significantly decreased in *Casp8*$^{\Delta IEC}$ x *Atg7*$^{\Delta IEC}$ mice compared with *Casp8*$^{\Delta IEC}$ mice 7 days after *C. rodentium* infection. $^{#}$p<0.05, $^{##}$p<0.01.

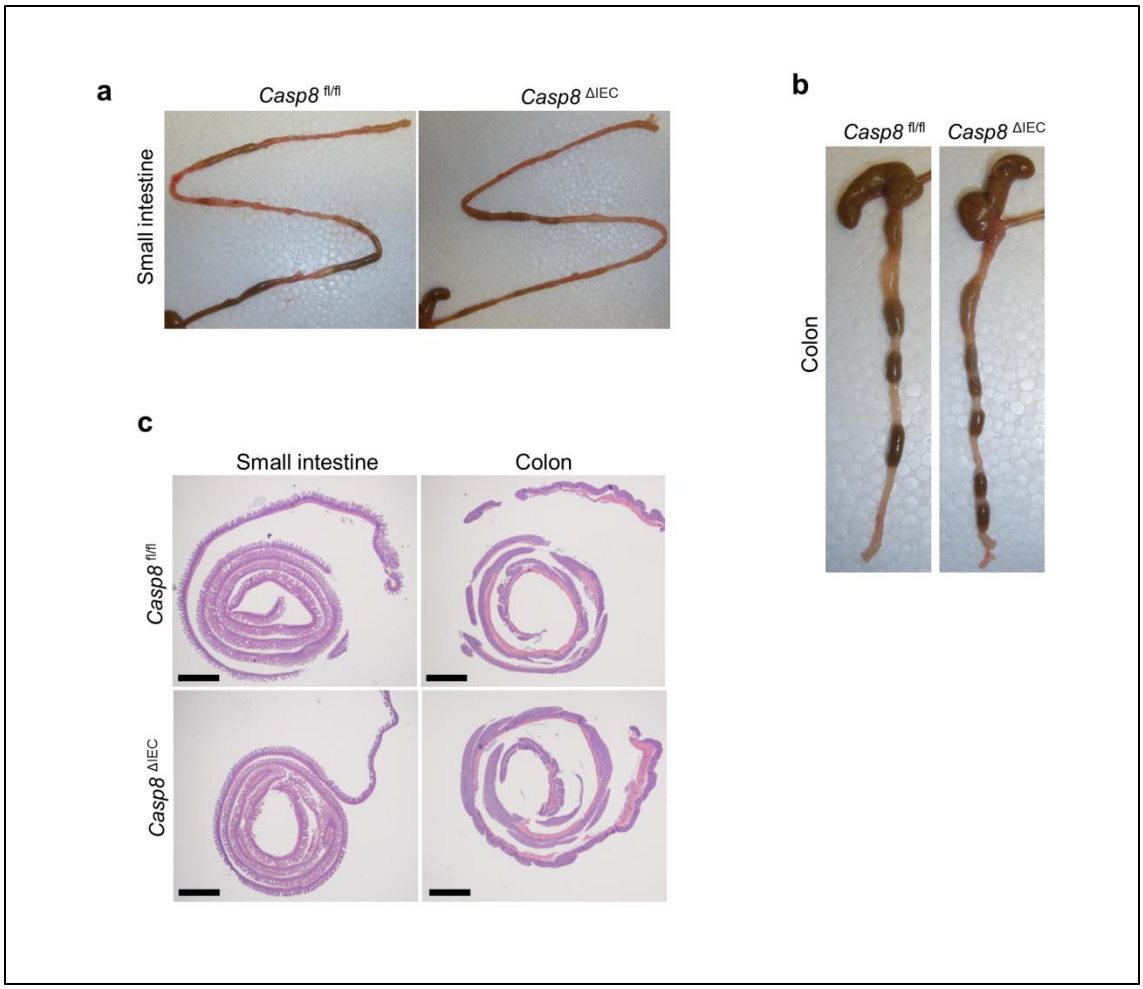

Supplemental figure 1: Colon and small intestine of *Casp8*$^{\Delta IEC}$ mice are macroscopically and microscopically normal. a, **b**, Representative pictures of 6 weeks old *Casp8*$^{fl/fl}$ and *Casp8*$^{\Delta IEC}$ mice without any stimulation after sacrifice and dissection showing no difference in small intestine (**a**) and colon (**b**) morphology. **c**, Representative H&E stained Swiss roll sections of small intestine and colon of 6 weeks old *Casp8*$^{fl/fl}$ and *Casp8*$^{\Delta IEC}$ mice without any stimulation showing no major microscopic abnormalities in *Casp8*$^{\Delta IEC}$ mice.

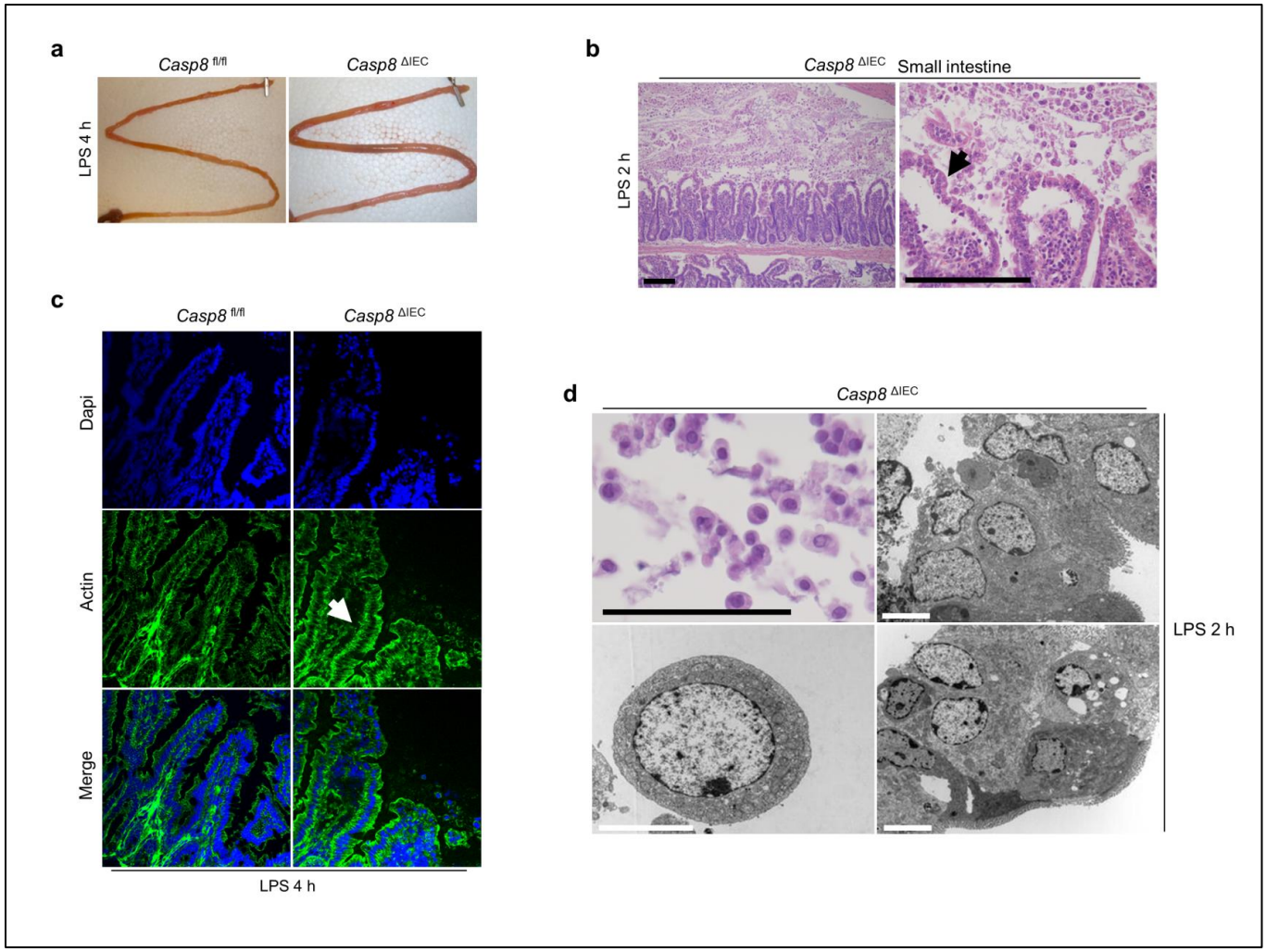

Supplemental figure 2: LPS induces intestinal epithelial cell detachment in *Casp8*$^{\Delta IEC}$ mice which is not related to cell death. a, Representative pictures of dissected small intestine from *Casp8*$^{fl/fl}$ and *Casp8*$^{\Delta IEC}$ mice euthanized 4 hours after LPS i.p. injection. Small intestine of *Casp8*$^{\Delta IEC}$ mice showed a marked dilation with presence of an important amount of fluid in its lumen. **b**, Representative H&E stained Swiss roll sections of *Casp8*$^{\Delta IEC}$ mice small intestine 2 hours after LPS i.p. injection showing detachment of the epithelial layer (black arrow) with IECs floating in the intestinal lumen. Black scale bars, 100 µm. **c**, Frozen small intestine sections of *Casp8*$^{fl/fl}$ and *Casp8*$^{\Delta IEC}$ mice collected 4 hours after LPS i.p injection, were stained with phalloidin, and then counterstained with DAPI. *Casp8*$^{fl/fl}$ small intestine showed normal morphology after LPS treatment and *Casp8*$^{\Delta IEC}$ small intestine presented a clear detachment of IECs form basal membrane (white arrow) with preservation of cell-cell adhesion and cell morphology. **d**, Representative smear of LPS-treated *Casp8*$^{\Delta IEC}$ small intestine luminal content

(Upper left panel) showing numerous round-shaped cells (detached IECs) without sign of apoptosis or other death pathway induction. Black scale bar, 50 µm. Other panels: Representative electron microscope pictures of already detached IECs in LPS-treated *Casp8*$^{\Delta IEC}$ mice showing normal morphology of these cells with persistence of cell-cell adhesion (upper and lower right panels). No sign of cell death such as apoptosis or necroptosis is observed in these detached IECs. White scale bars, 5 µm.

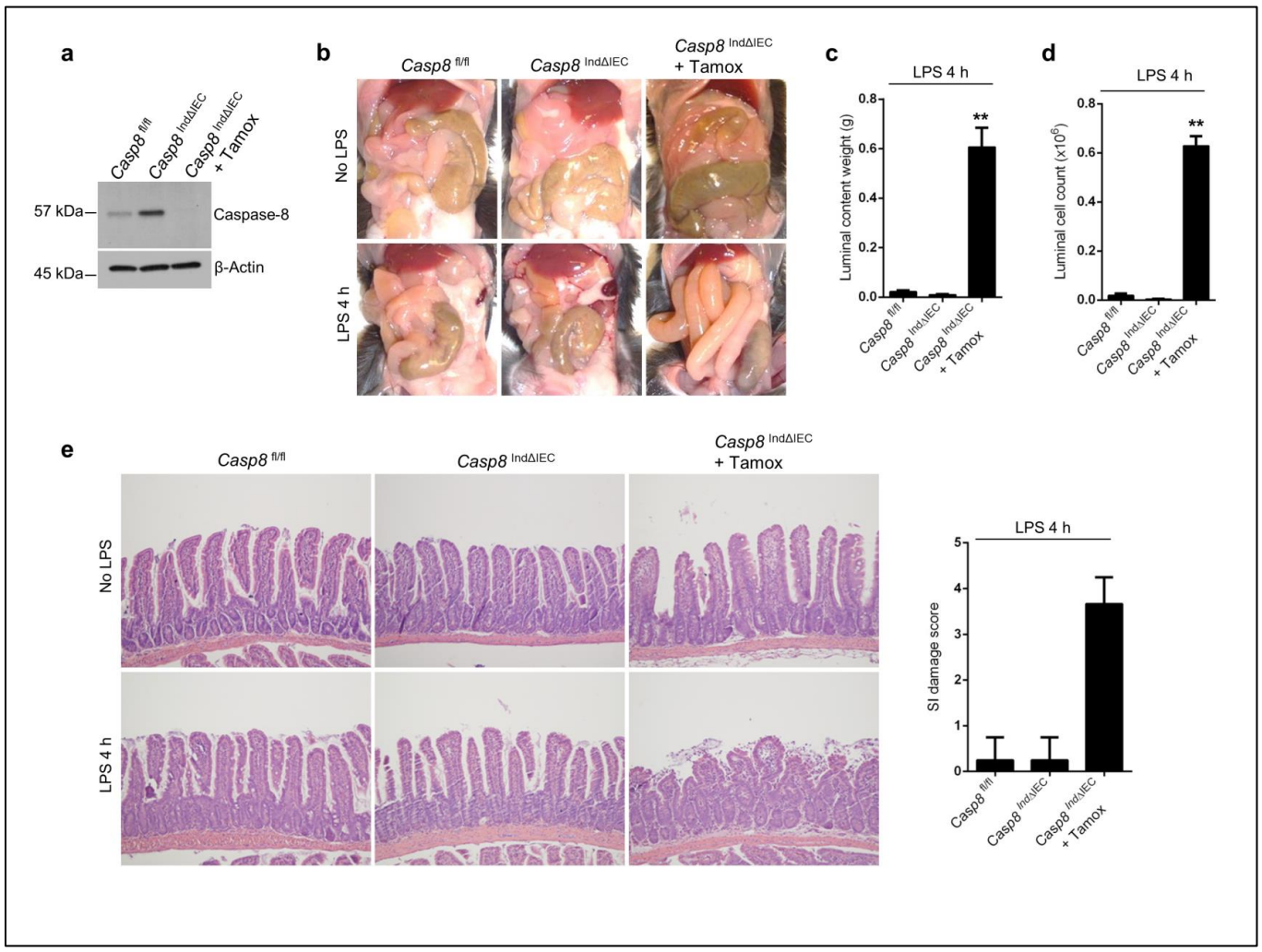

Supplemental figure 3: LPS stimulation leads to acute epithelial detachment in tamoxifen treated *Casp8*$^{\mathbf{indΔIEC}}$ mice. a, Small intestine samples from *Casp8*$^{fl/fl}$, *Casp8*^{indΔIEC} and Tamoxifen-treated *Casp8*^{indΔIEC} mice were lysed for western blot analysis with anti-caspase-8 and anti-β-actin antibodies. Tamoxifen treatment in *Casp8*^{indΔIEC} mice leads to induction of Cre recombinase in IECs and deletion of casp8 gene which is confirmed by absence of caspase-8 proteins in small intestine of Tamoxifen-treated *Casp8*^{indΔIEC} mice. **b**, Representative macroscopic pictures of small intestine from *Casp8*$^{fl/fl}$, *Casp8*^{indΔIEC} and Tamoxifen-treated *Casp8*^{indΔIEC} mice without or 4 hours after LPS i.p. injection showing small intestinal dilatation in only Tamoxifen-treated *Casp8*^{indΔIEC} mice after LPS stimulation. **c**, **d**, Four hours after LPS i.p. injection small intestine luminal content from *Casp8*$^{fl/fl}$, *Casp8*^{indΔIEC} and Tamoxifen-treated *Casp8*^{indΔIEC} mice was collected, weighted (**c**) and cells present in the luminal fluid were counted (**d**) under optical microscope (n=3-4 per groups). Tamoxifen-treated *Casp8*^{indΔIEC} mice present a significant

increase in small intestine luminal content weight and luminal cell count compared with *Casp8*$^{fl/fl}$ and *Casp8*^{indΔIEC} mice. ** p<0.01 by ANOVA test. **e**, **f**, Representative H&E stained sections of *Casp8*$^{fl/fl}$, *Casp8*^{indΔIEC} and Tamoxifen-treated *Casp8*^{indΔIEC} mice small intestine (**e**), without or 4 h after LPS i.p injection showing IECs detachment and villi destruction in Tamoxifen-treated *Casp8*^{indΔIEC} mice after LPS injection. Small intestine damage score (**f**) increases in Tamoxifen-treated *Casp8*^{indΔIEC} mice compared with controls after LPS stimulation (n=3-4 per groups).

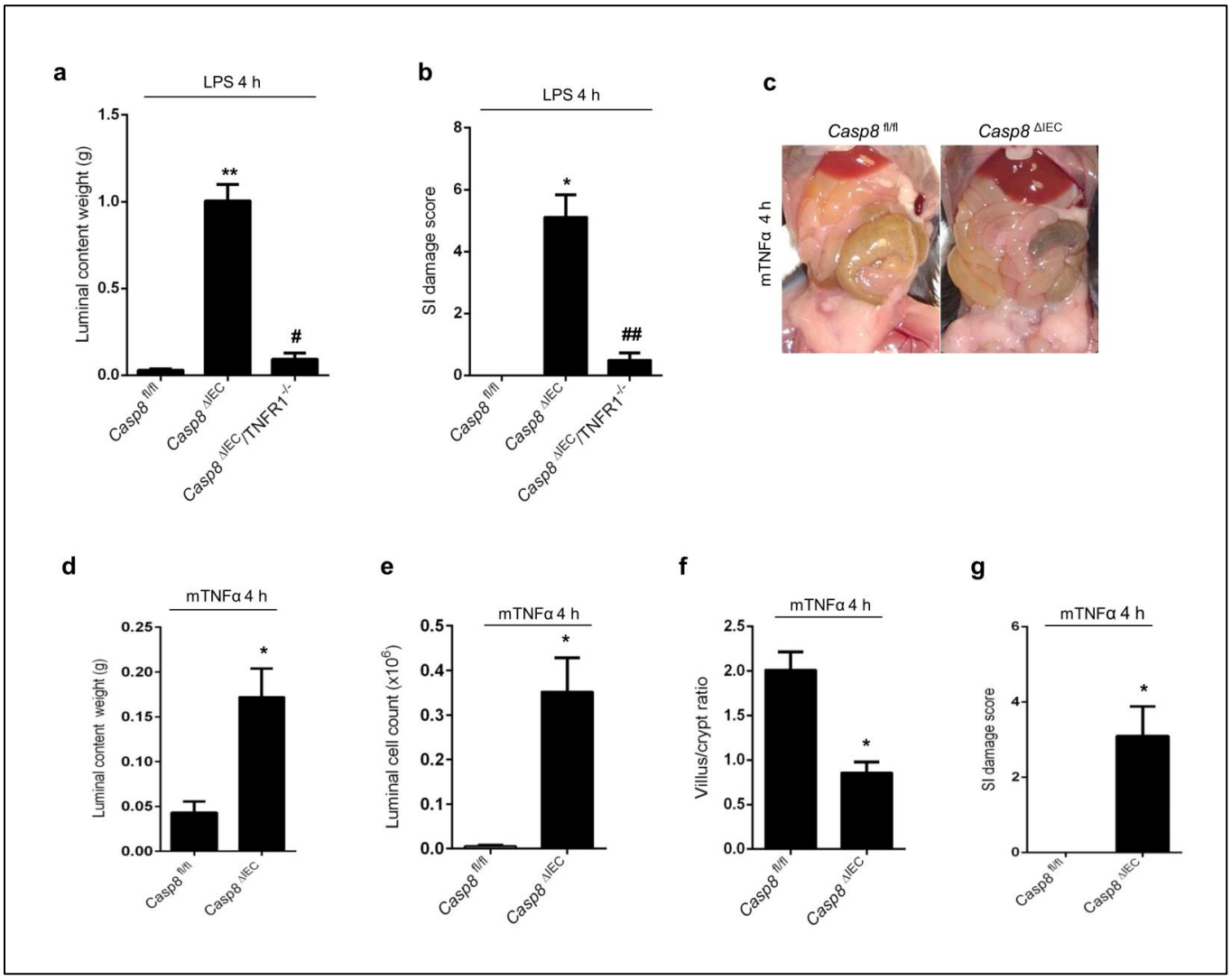

Supplemental figure 4: LPS-induced small intestine damage in *Casp8*$^{\Delta IEC}$ mice requires TNFα signaling. Increase of luminal content weight (**a**) and small intestine damage score (**b**) observed in *Casp8*$^{\Delta IEC}$ mice 4 hours after LPS i.p. injection is prevented in *Casp8*$^{\Delta IEC}$ x *Tnfr1*$^{-/-}$ mice (n= 4-7 mice per group). ** p<0.01 *vs.* controls, $^{\#}$ p<0.05 *vs. Casp8*$^{\Delta IEC}$ mice, * p<0.05 *vs.* controls and ## p<0.01 *vs. Casp8*$^{\Delta IEC}$ mice. Data are representative of two independent experiments. **c**, Representative macroscopic pictures of *Casp8*$^{fl/fl}$ and *Casp8*$^{\Delta IEC}$ mice small intestine 4 hours after mTNFα i.p. injection showing moderate small intestine dilatation only in *Casp8*$^{\Delta IEC}$ mice. **d**, **e**, Four hours after mTNFα i.p. injection, small intestines of *Casp8*$^{fl/fl}$ and *Casp8*$^{\Delta IEC}$ mice were harvested and luminal content from each small intestine was collected and weighted. A significant increase in luminal content weighted and in small intestine luminal cell count is observed in *Casp8*$^{\Delta IEC}$ mice compared with control mice (n=4-5 mice per group). *

p<0.05 *vs.* controls. **f**, **g**, Small intestine villus/crypt ratio and damage score were evaluated in *Casp8*$^{fl/fl}$ and *Casp8*$^{\Delta IEC}$ mice 4 hours after mTNFα i.p. injection. A significant decrease in the villus/crypt ratio and a significant increase in the damage score are observed in *Casp8*$^{\Delta IEC}$ mice compared with control mice (n=4-5 mice per group). * p<0.05 *vs.* controls. Data are representative of two independent experiments.

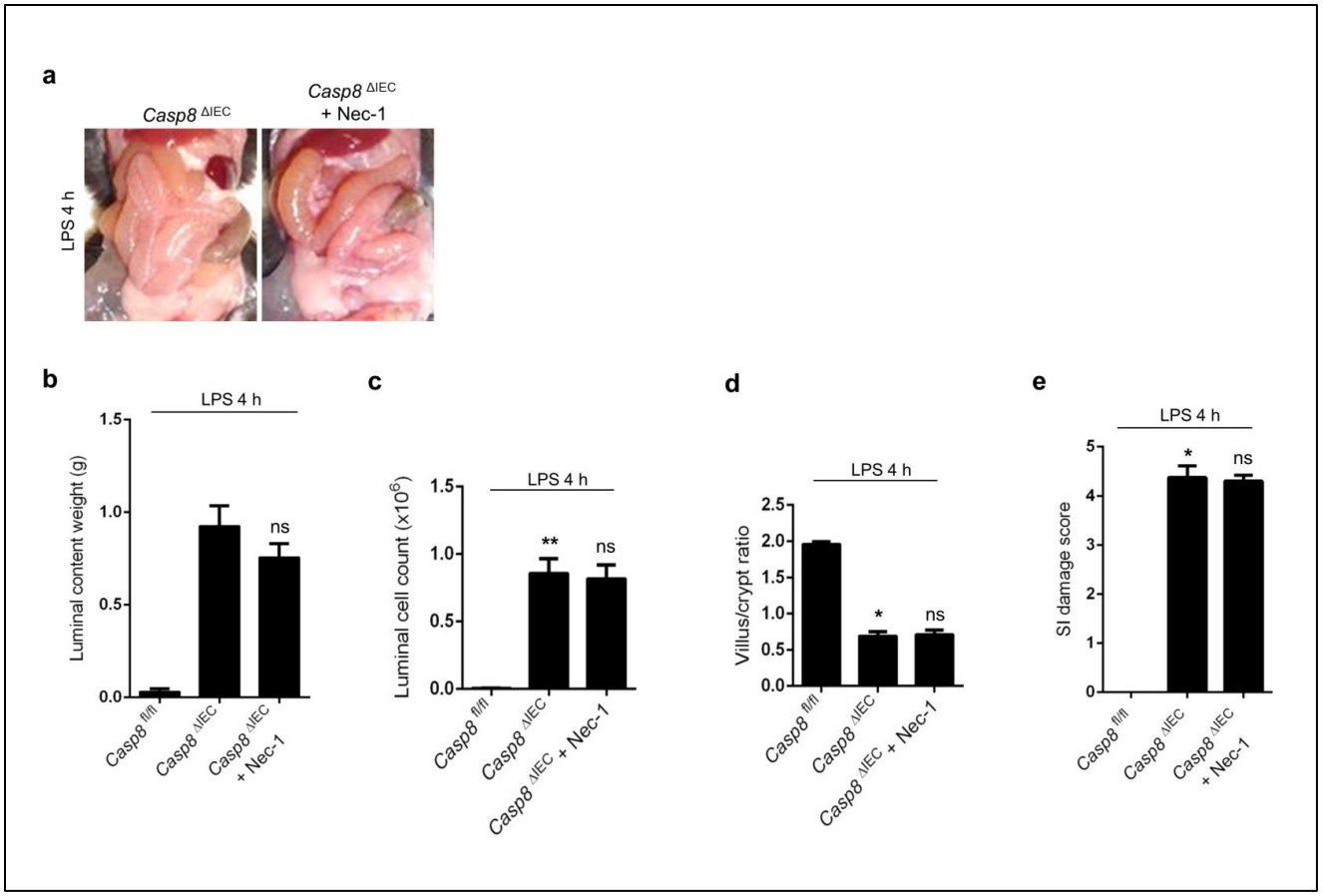

Supplemental figure 5: Necrostatin-1 does not prevent LPS-induced intestinal inflammation in *Casp8*$^{\Delta IEC}$ mice. a, Representative macroscopic pictures of *Casp8*$^{\Delta IEC}$ and necrostatin-1-treated *Casp8*$^{\Delta IEC}$ mice small intestine 4 hours after LPS i.p. injection showing no prevention of small intestine major dilatation after necrostatin-1 treatment. **b**, **c**, Four hours after LPS i.p. injection, small intestines of *Casp8*$^{fl/fl}$, *Casp8*$^{\Delta IEC}$ and necrostatin-1-treated *Casp8*$^{\Delta IEC}$ mice were harvested and luminal content from each small intestine was collected and weighted. An increase in luminal content weighted and small intestine cell count is observed in *Casp8*$^{\Delta IEC}$ mice compared with control mice, which is not prevented by necrostatin-1 pretreatment (n=3-5 mice per group). **d**, **e**, Small intestine villus crypt ratio and damage score were evaluated in *Casp8*$^{fl/fl}$, *Casp8*$^{\Delta IEC}$ and necrostatin-1-treated *Casp8*$^{\Delta IEC}$ mice 4 hours after LPS i.p. injection. Necrostatin-1 does not prevent decrease of villus crypt ratio and increase of small intestine damage score observed in *Casp8*$^{\Delta IEC}$ mice. *p<0.05 and **p<0.01 *vs.* control; ns, not significant vs. *Casp8*$^{\Delta IEC}$ mice.

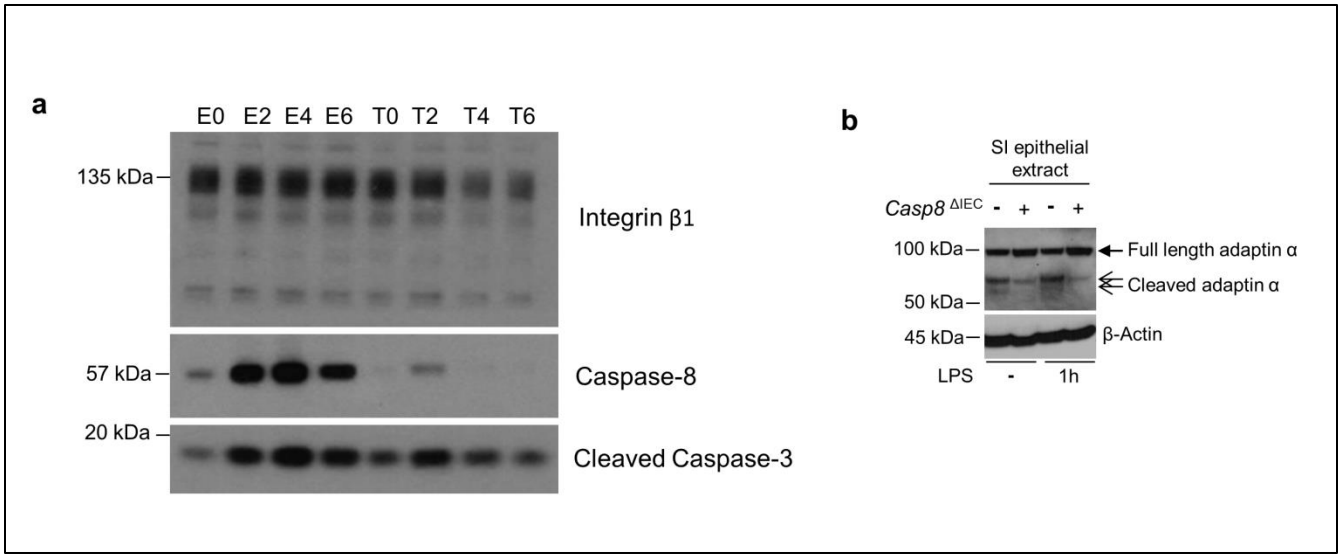

Supplemental figure 6: Degradation of β1-integrins in enteroids lacking caspase-8 and increased degradation of adaptin-α in IECs of *Casp8*$^{fl/fl}$ mice after LPS stimulation. a, Enteroids cultures were established from IEC of *Casp8*^{indΔIEC} mice and then treated with ethanol or tamoxifen. Crypts were then harvested and used for western blot with anti-integrin β1, anti-caspase-8, and anti-cleaved caspase-3 antibodies. A time course experiment (from 0 to 6 hours) was performed. Crypts treated with tamoxifen presented a decreased quantity of integrin β1 protein after 4 and 6 hours. **b**, IECs were isolated from small intestine of *Casp8*$^{fl/fl}$ and *Casp8*^{ΔIEC} mice before and 1 h after LPS i.p. injection and used for western blot with anti-adaptin-α and anti-β-actin antibodies.

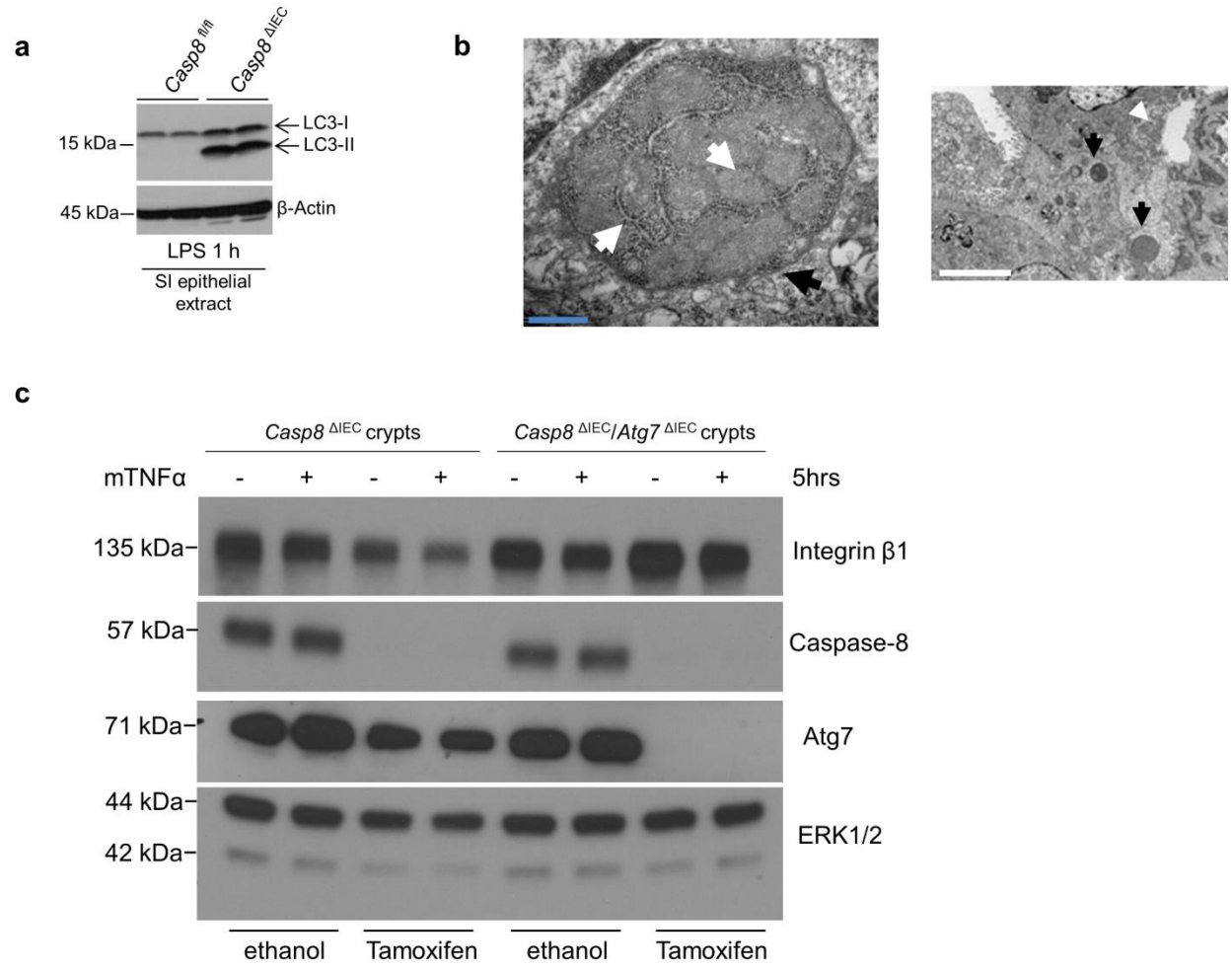

Supplemental figure 7: LPS stimulation induces activation of autophagy and formation of autophagosomes in IECs of *Casp8*$^{\Delta IEC}$ mice. a, IECs were isolated from small intestine of *Casp8*$^{fl/fl}$ and *Casp8*$^{\Delta IEC}$ mice on hour after LPS i.p. injection and lysed for western blot analysis with anti-LC3 and anti-β-actin antibodies. LC3-I represents the basal cytosolic form of LC3 protein and LC3-II represents the autophagosome associated form. **b**, Representative electron microscope picture of LPS-treated *Casp8*$^{\Delta IEC}$ mice IEC cytoplasm section (left panel) showing an autophagosome with double membranes (black arrow) engulfing organelles such as mitochondria or endoplasmic reticulum (white arrows). Representative electron microscope picture of LPS-treated *Casp8*$^{\Delta IEC}$ mice villi section (right panel) showing autophagosomes in the cytoplasm of IECs (black arrows) and detachment of an intestinal epithelial cell from basal membrane (white

arrow). **c**, Enteroids cultures were established from IECs of *Casp8*$^{ind\Delta IEC}$ mice and *Casp8*$^{ind\Delta IEC}$ x *Atg7*$^{ind\Delta IEC}$ mice and then treated with ethanol or tamoxifen with or without mTNFα for 5 hours. Crypts were then harvested and used for western blot with anti-integrin β1, anti-caspase-8, anti-Atg7 and anti-ERK1/2 antibodies. Crypts from *Casp8*$^{ind\Delta IEC}$ mice treated with tamoxifen and TNFα presented degradation of integrin-β1 protein that was also observed but at a low degree in crypts from *Casp8*$^{ind\Delta IEC}$ mice treated only with tamoxifen. These crypts presented a complete lack in caspase-8. Integrin-β1 degradation was completely prevented in crypts from *Casp8*$^{ind\Delta IEC}$ x *Atg7*$^{ind\Delta IEC}$ mice treated with tamoxifen that lack caspase-8 and Atg7.

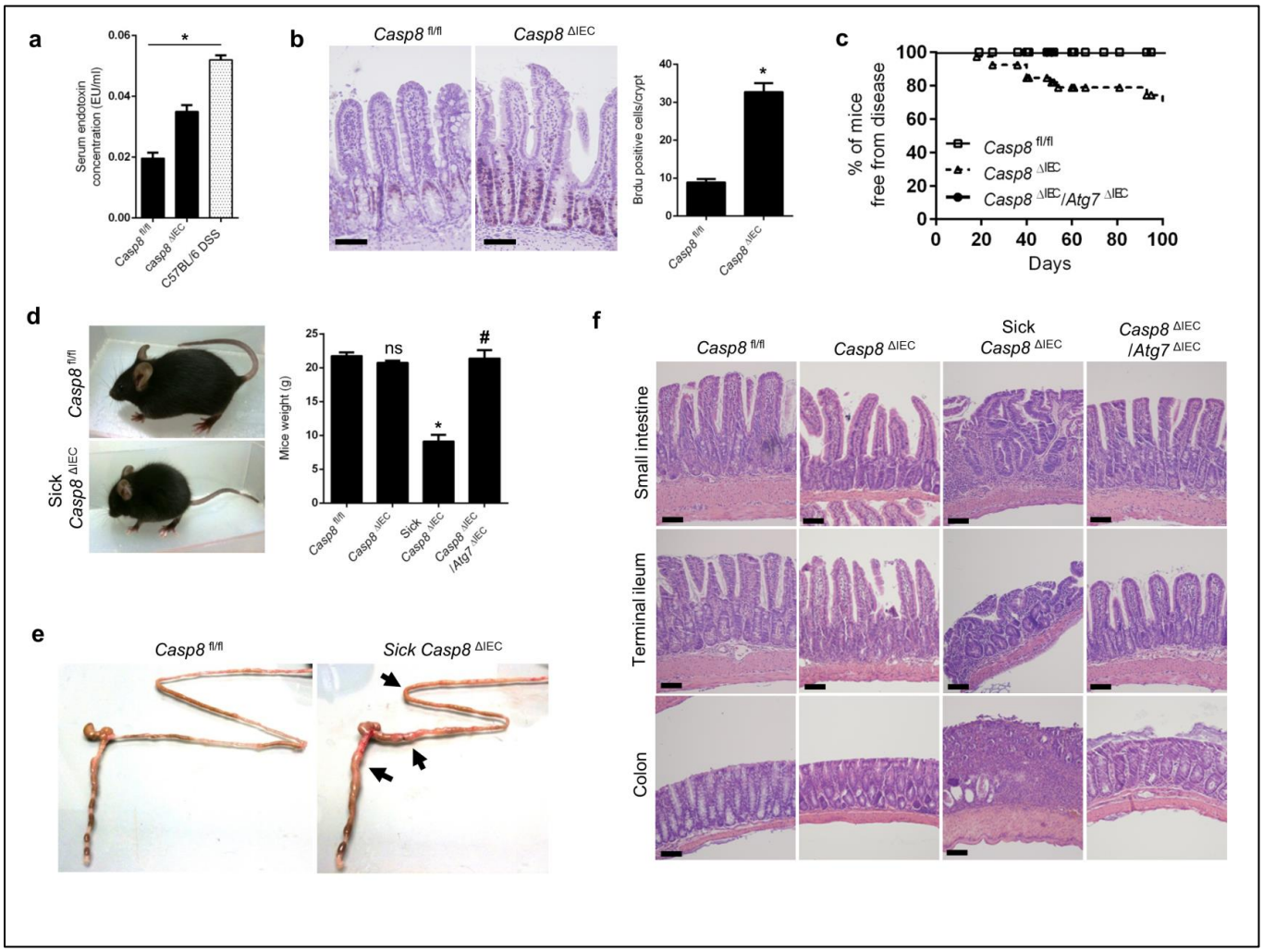

Supplemental Figure 8: Suppression of autophagy prevents spontaneous intestinal inflammation developed in *Casp8*$^{\Delta IEC}$ mice. a, Blood was collected from *Casp8*$^{fl/fl}$, *Casp8*$^{\Delta IEC}$ and DSS-treated C57BL/6 mice. After centrifugation, serum was collected and used for endotoxin measurement. *p<0.05. **b**, Representative BrdU stained sections of *Casp8*$^{fl/fl}$ and *Casp8*$^{\Delta IEC}$ mice, 2 hours after BrdU i.p. injection. Scale bars, 50 µm. For each animal (n=4 per group), mean number of BrdU+ cells per crypt (counting cells in at least 10 crypts per mouse) was determined showing an increased IEC proliferation in *Casp8*$^{\Delta IEC}$ mice. *p<0.05. **c**, *Casp8*$^{\Delta IEC}$ mice develop spontaneous disease with weight loss. Kaplan Meier analysis of disease free survival in *Casp8*$^{fl/fl}$ (empty square and solid line, n=43), *Casp8*$^{\Delta IEC}$ (empty triangle and dotted line, n=40) and *Casp8*$^{\Delta IEC}$ x *Atg7*$^{\Delta IEC}$ mice (filled circle and solid line, n=11) showing appearance of disease only in *Casp8*$^{\Delta IEC}$ mice. Log-rank test, p<0.0003. The disease observed in about 30-40% of *Casp8*$^{\Delta IEC}$ mice starts around 6 week of age and leads frequently to animal death in 2 to

10 weeks. **d**, Representative pictures of *Casp8*$^{fl/fl}$ mice and *Casp8*$^{\Delta IEC}$ mice presenting spontaneous disease. Disease observed in *Casp8*$^{\Delta IEC}$ mice is characterized by a significant weight loss in sick *Casp8*$^{\Delta IEC}$ mice compared with controls, healthy *Casp8*$^{\Delta IEC}$ mice and *Casp8*$^{\Delta IEC}$ x *Atg7*$^{\Delta IEC}$ mice. ns, not significant vs. controls, *$p<0.05$ vs. controls and $^{\#}p<0.05$ vs. sick *Casp8*$^{\Delta IEC}$ mice. **e**, Spontaneous disease observed in *Casp8*$^{\Delta IEC}$ mice is due to development of intestinal inflammation characterized by macroscopic inflammation of small intestine and colon with maximum lesions observed in the ileocolonic region. **f**, Representative H&E stained small intestine, terminal ileum and colon sections of *Casp8*$^{fl/fl}$, *Casp8*$^{\Delta IEC}$ and *Casp8*$^{\Delta IEC}$ x *Atg7*$^{\Delta IEC}$ mice (>2 month old) showing mucosal inflammation in colon, and small intestine only in *Casp8*$^{\Delta IEC}$ mice with macroscopic disease (weight loss). Scale bars, 50 µm.

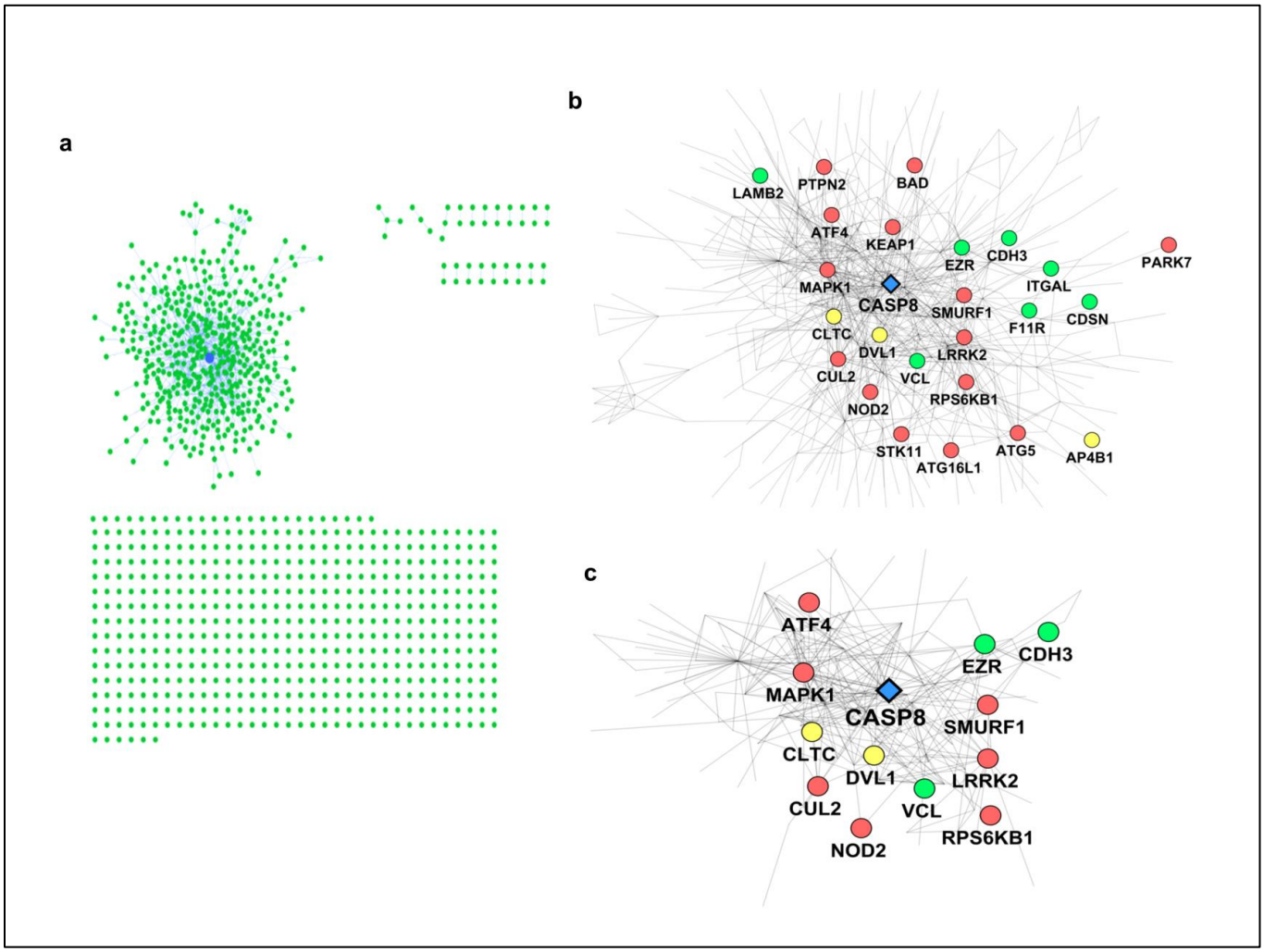

Supplemental figure 9: Protein-protein interaction networking demonstrates multiple and close interactions between IBD genes and human *CASP8* gene. a, The HIPPIE human proteome interaction data base was used to analyze protein-protein interactions between *CASP8* gene and identified IBD risk genes. IBD risk genes (1442 genes including some pseudogenes and some withdrawn entries) were selected from >160 IBD risk loci identified and described by Jostins et al[106]. Association to one of these functional categories: endocytosis, cell adhesion, autophagy using GO terms was determined for each IBD risk gene. Of the 1442 IBD genes, 1028 are contained in the protein-protein interactome data set. These 1028 proteins cluster in one big main interaction network (upper left) with CASP8 (blue node) in the very Centre. Other proteins either have no interactions (cloud of unconnected nodes at bottom) or have small number of interactions (upper right corner). **b**, Focus on the main interaction network that contains CASP8 and 478 IBD risk genes. CASP8 (blue diamond) is in the center of this network and has

proximity to genes linked to autophagy (red circles), endocytosis (yellow circles) and cell adhesion (green circles). **c**, Interaction network between CASP8 and IBD risk genes with no more than 2nd degree neighbours. Among these close interactors, there is the Clathrin heavy chain gene (CLTC) supporting a possible functional role of caspase-8 in regulating Clathrin-dependent endocytosis.

E. *TLR3, TRIF and Caspase 8 determine double-stranded RNA induced epithelial cell death and survival in vivo.*

C McAllister[1], O Lakhdari[1], G Pineton de Chambrun[1, 2, 3], MG Gareau[1], A Broquet[1], GH Lee[1], S Shenouda[1], L Eckmann[1] and MF Kagnoff[1]

[1]Department of Medicine, University of California, San Diego, USA
[2]Univ Lille Nord de France, Lille, France
[3]Hepato-Gastroenterology Department, CHU Lille, Lille, France

Référence de l'article :

TLR3, TRIF, and caspase 8 determine double-stranded RNA-induced epithelial cell death and survival in vivo. McAllister CS, Lakhdari O, Pineton de Chambrun G, Gareau MG, Broquet A, Lee GH, Shenouda S, Eckmann L, Kagnoff MF. *J Immunol.* 2013 Jan 1;190(1):418-27. doi: 10.4049/jimmunol.1202756. Epub 2012 Dec 3.

1. Introduction

The intestinal mucosa in the small intestine contains finger-like projections termed villi that are lined by a single-cell layer of intestinal epithelial cells (IECs) that separate the intestinal lumen from the underlying immune cell-rich lamina propria. IECs are armed with numerous pathogen pattern-recognition receptors (PRRs) that detect and activate host responses to protect against viral and bacterial pathogens and their products [158]. Double-stranded RNA (dsRNA) is a virus-associated molecular pattern that is recognized by the endosomal, extra-cytoplasmic PRR, TLR3, and intracellular cytoplasmic RIG-like sensors [159, 160]. Interestingly, dsRNA signaling through TLR3 has been reported to induce small intestinal mucosal damage in mice [161].

TLR3 signals through the adaptor molecule TRIF, whereas the RIG-like RNA sensors, RIG-I and Mda5, signal through the adaptor molecule MAVS (IPS-1) [159]. These pathways activate IRF3 and NF-κB transcription factors and result in the production of type I interferons and proinflammatory cytokines. Furthermore, activation of host signaling pathways can induce apoptosis, likely as a means to kill infected host cells to shut down virus production [162]. While NF-κB can have both pro- and anti-apoptotic effects within cells, IRF3 has been shown to interact with BAX to directly induce apoptosis after viral infection [163]. Additionally, i*n vitro* studies have shown that TRIF, unlike the TLR adaptor protein MyD88, interacts with caspase 8 through the RIP1 signaling molecule to directly induce apoptosis [164-167].

PRR signaling pathways can also induce TNFα that can act upon other cells to either induce survival through NF-κB signaling or death through apoptosis or necroptosis [168]. Interestingly, TNF injection induces IEC apoptosis *in vivo* in mice [169]. This effect is dependent upon TNF receptor 1 (TNFR-1) and more pronounced in the proximal than distal small intestine, possibly due to the expression pattern of the TNFR-1 [170]. Signaling through

TNFR-1 leads to the recruitment of a signaling complex that activates caspase 8, which then mediates apoptosis by activating effector caspases including caspase 3 [168].

We investigated the mucosal signaling pathways activated by dsRNA that cause small intestinal damage *in vivo*. We report that dsRNA rapidly induces intestinal villus epithelial cell apoptosis and cell loss in the proximal small intestine that results in marked villus shortening and significant diarrhea, with subsequent recovery. dsRNA-induced IEC apoptosis *in vivo* was strictly dependent on TLR3 and TRIF signaling through Caspase 8 in IECs, and independent of other TLR signaling pathways, as well as TNFα, dendritic cells (DCs), NK cells, and other hematopoietic cells. Interestingly, this pathway proved to be host protective since, in the absence of downstream signaling of Caspase 8, dsRNA caused marked destruction of the small intestinal mucosa and death.

2. Results

dsRNA induces IEC apoptosis in the proximal small intestine.

We used the synthetic dsRNA viral nucleic acid mimic poly(I:C) (pIC) as a probe of the host's antiviral strategies in the small intestine. Administration of pIC i.p. resulted in villus shortening in the proximal small intestine, which was maximal between 3 and 6 h after injection and recovered thereafter (Fig. 1 A-C). The dramatic reduction in villus length correlated with decreased numbers of IECs per villus (Fig. S1 A-C). The relatively rapid loss of IECs and ensuing recovery suggested a dsRNA-activated pathway that causes IEC loss, perhaps as a host response to rid the epithelium of virus infected cells, while concurrently maintaining a relatively intact IEC layer.

To determine if apoptosis explained the decreased numbers of IECs, we evaluated cleaved caspase 3 staining of small intestinal tissue sections [171] (Fig. 1 D-F). IEC apoptosis preceded villus shortening with a peak at 2 h after pIC i.p. (Fig. 1 G). Apoptotic IECs predominately localized in the mid to upper villus region, with little apoptosis in the lower villus region and no increase in apoptosis in either the crypt region (i.e., the site of epithelial stem cells) or the subepithelial lamina propria (Fig. 1 E). Cleavage of caspase 8, an initiator caspase, was also observed at 2 h post treatment (Fig. S1 D-E). Apoptosis of villus IECs and villus shortening were less pronounced but still significant in the distal small intestine (Fig. S1 F–I), likely reflecting shorter villi with decreased numbers of IECs in the distal small intestine.

pIC treated mice had significant fluid accumulation in the small intestine and diarrhea that peaked at 4-6 h and returned to normal thereafter (Fig. 1 H-J). To address the cause of this increase in intestinal fluid accumulation, Ussing chamber studies were done to measure the small intestinal secretory state and mucosal permeability. Baseline Isc, indicative of active ion secretion, was elevated in mice treated with pIC compared to PBS controls (Fig. 1K). In contrast,

conductance indicative of ion permeability (Fig. 1 L) and FITC-flux indicative of macromolecular permeability (Fig. 1 M) were not significantly altered by pIC treatment, suggesting an increased secretory state. Together, these data suggest that increased luminal fluid accumulation in the proximal small bowel resulted from increased secretory state in these mice in the context of intact tight junctions and mechanisms of endocytosis.

We next investigated if the mode of pIC delivery determined IEC apoptosis, as injection by the i.p. route suggested the possible involvement of intraperitoneal macrophages or other cell subsets specific to the peritoneal cavity in inducing villus shortening and IEC apoptosis. However, there was no dependence on i.p. injection, as either i.p. or retro-orbital sinus injection of pIC induced significant villus shortening in the proximal small intestine and IEC apoptosis (Fig. S1 J-M, N and O). Moreover, Cy3 labeled pIC was detected in the lamina propria of proximal small intestinal villi after retro-orbital injection (Fig. S1 P-R). Administration of pIC by oral gavage did not induce villus shortening or IEC apoptosis (Fig. S1 M-O).

TLR3-TRIF signaling is required for IEC apoptosis.

We found that TLR3 was required for dsRNA-induced intestinal damage as reported before by others [161]. Indeed, $TLR3^{-/-}$ were completely resistant to dsRNA-induced IEC apoptosis and villus shortening (Fig.2 A, B, D and E). Further, dsRNA did not induce IEC apoptosis or villus shortening in mice lacking TRIF, the downstream adaptor molecule for TLR3 (Fig. 2 C, F). Villus length and the number IECs with cleaved caspase 3 staining per villus were quantified and confirmed the essential involvement of TLR3-TRIF signaling in pIC activated villus shortening and apoptosis in the proximal small intestine (Fig 2 G and H). Neither $TLR3^{-/-}$ nor $TRIF^{-/-}$ mice developed small intestinal fluid accumulation or diarrhea. There was no

difference in IEC proliferation between WT and TLR3$^{-/-}$ mice after pIC, indicating that pIC did not damage the proliferative capacity of crypt cells (Fig. 2 I-L).

We assessed the requirement for other RNA sensors to determine if they had a contributory role in pIC-activated IEC apoptosis in the small intestine. MAVS (IPS-1), the signaling adaptor for RIG-like receptors, was not required for villus shortening or caspase 3 cleavage (Fig. 2 M, N). PKR is an IFN-inducible protein kinase that can act as a general translation inhibitor and induce apoptosis in response to activation by dsRNA (35). Mice deficient in PKR had similar levels of villus shortening and numbers of caspase 3 cleaved cells as WT mice (Fig. 2 M, N) indicating that PKR-dependent translation inhibition or signaling was not required for pIC activated IEC apoptosis and villus shortening.

Apoptosis of small intestinal IECs induced by TLR ligands.

High levels of TNF result in IEC apoptosis (12) and, consistent with this, i.p. injection of 5 μg, but not 1 μg, of TNF induced IEC apoptosis in WT mice (Figs. 3 E–G). Since several TLR ligands that signal through MyD88 induce the release of TNF (2), we evaluated IEC apoptosis induced by other TLR ligands and found that pIC induced significantly higher levels of IEC apoptosis than TLR7 ligand R848, TLR9 ligand ODN, and TLR4 ligand LPS (Fig. 3 A-D, G). Moreover, pIC induced TNF levels orders of magnitude lower than those TLR ligands, with LPS inducing the highest TNF levels (Fig. 3 H). While others observed higher serum TNF levels after pIC (4) we established that this was likely due to endotoxin contamination of pIC in their studies. However, we found such levels of endotoxin contamination did not significantly affect IEC apoptosis or villus shortening (Fig. S2).

pIC-induced IEC apoptosis is independent of TNF, IL-6 and IL-1 signaling

We definitively excluded the involvement of TNF in pIC-induced apoptosis using mice deficient in TNF (TNF−/−) that did not produce TNF following dsRNA treatment (Fig. 3 L). TNF−/− mice were as sensitive as WT mice to dsRNA-induced IEC apoptosis (Fig. 3 I–K). These results, confirmed that TNF has no role in pIC-induced small intestinal IEC apoptosis. We also confirmed that IL-6 and IL-1β, two cytokines that were increased after pIC, are not required for dsRNA-induced IEC apoptosis using IL-6−/− and IL-1R−/− mice (Fig. S3).

IEC apoptosis is independent of IL-15 and NK cells.

IL-15 signaling and NK cell mediated killing were reported to be required for dsRNA-induced small intestinal villus shortening and epithelial cell injury [161]. To evaluate the role of IL-15 in our model, we utilized mice genetically deficient in IL-15 production. Surprisingly, IL-$15^{-/-}$ mice demonstrated the same level of sensitivity to pIC as WT mice (Fig. 4 A-D). To assess the role of $NK1.1^{+}$ cells in dsRNA-induced IEC apoptosis, those cells were depleted using antibody to NK1.1. We observed the same level of IEC apoptosis and small intestinal damage in NK1.1 depleted mice as in littermates treated with control IgG (Fig. 4 E-H). NK1.1+ cell depletion was confirmed by immunohistochemistry (Fig. S4 A–C).

IEC apoptosis does not require type I interferon signaling or IRF3.

IFN-β expression in the small intestinal mucosa was increased in WT but not $TLR3^{-/-}$ mice after pIC (Fig. 4 I). Because type I IFN signaling was reported to potentiate virus induced apoptosis [172], we assessed the involvement of type I IFN signaling in pIC-induced IEC apoptosis and villus shortening. There was no significant difference between $IFNAR^{-/-}$ and WT mice in villus shortening or apoptosis (Fig. 4 J-M).

Antiviral signaling through MAVS can activate IRF3 in a manner that results in IRF3 interacting with BAX and localizing to mitochondria to induce apoptosis [163]. Because TLR3 signaling also activates IRF3 [173], we tested if this pathway was involved in pIC activated IEC apoptosis. We found no evidence to suggest the involvement of IRF3 or BAX, since neither $IRF3^{-/-}$ nor $BAX^{-/-}$ mice manifested differences in villus length or IEC apoptosis compared to WT mice after pIC treatment (Fig. 4 N-R).

NF-κB signaling in IECs does not affect villus IEC apoptosis, but is required to protect IECs in the small intestinal crypts from apoptosis.

TLR3-TRIF signaling can activate the transcription factor NF-κB [173]. To assess the involvement of NF-κB signaling in pIC induced apoptosis of IECs, we used mice conditionally deficient in IKKα and β in small intestinal IECs [174, 175]. The magnitude of IEC apoptosis in the villi of mice lacking in IEC NF-κB signaling and control mice was similar after pIC (Fig. 5 B and E), whereas $IKK\alpha/\beta^{-/-}$ mice had increased levels of IEC apoptosis in the small intestinal crypts (Fig. 5 B, F). To assess the contribution of IKKα and IKKβ to this phenotype, we used $IKK\alpha^{\Delta IEC}$ and $IKK\beta^{\Delta IEC}$ mice deficient selectively in IKKα or IKKβ, respectively, in the IECs and determined that increased crypt apoptosis after pIC was dependent on the absence of IκKβ signaling (Fig. 5 D and F). This same pattern of IκKβ-dependence for crypt, but not IEC, apoptosis was observed in response to TNFa (Fig. G-J).

TLR3 signaling in cells of non-hematopoietic origin is required for IEC apoptosis.

NK 1.1 cell depletion demonstrated that NK1.1 cells were not involved in pIC activated IEC apoptosis (Fig. 4 E-H). To exclude the contribution of other immune cell subsets, we assessed the sensitivity of $RAG1^{-/-}$ mice that lack B and T cells and certain IEL subsets [176] to

dsRNA-induced IEC apoptosis. RAG1$^{-/-}$ mice were not protected and appeared more sensitive than WT mice to dsRNA induced villus shortening and IEC apoptosis (Fig. S4 D-F). We also assessed the sensitivity of DC depleted mice [177] to pIC activated IEC apoptosis. DTR mice treated with diphtheria toxin (DTX) to deplete DCs showed similar levels of IEC apoptosis as WT mice in response to pIC (Fig. S4 K-O). Interestingly, DC-depleted mice had significantly decreased serum TNFa levels after pIC treatment (Fig. S4 P). DC depletion was confirmed by immunohistochemistry (Fig. S4 Q, R).

To determine if other cells of hematopoietic origin contribute to dsRNA-induced IEC apoptosis, we generated TLR3$^{-/-}$ bone marrow chimera mice. As shown in figure 6 C, WT mice reconstituted with TLR3-deficient bone marrow (TLR3$^{-/-}$ BM→ WT) were as sensitive to IEC apoptosis as WT mice (Fig 6 A and C). Additionally, TLR3$^{-/-}$ mice reconstituted with WT bone marrow (WT BM→TLR3$^{-/-}$) did not show increased IEC apoptosis in response to pIC (Fig. 6 B and D). Numbers of cleaved caspase 3 positive IECs per villus in these mice demonstrated that IEC apoptosis was not dependent on WT cells of hematopoietic origin (Fig. 6 E). Successful bone marrow transfer was confirmed by evaluating serum TNF levels in mice after treatment with pIC (Fig 6 F). WT mice showed TNF levels consistent with previous experiments and TLR3$^{-/-}$ mice showed no induction of TNF, whereas TLR3$^{-/-}$→WT mice had levels of TNF comparable to TLR3$^{-/-}$ mice and WT→TLR3$^{-/-}$ mice had TNF levels comparable to WT mice (Fig. 6 F).

Caspase 8 coordinates IEC apoptosis and preserves the integrity of the intestinal epithelium following dsRNA treatment.

We observed activated caspase 8 at early time points following pIC treatment (Fig. S1 D, E). TRIF has been shown to activate apoptosis through caspase 8, the same initiator caspase that

mediates TNF-induced apoptosis [165, 167]. Interestingly, in the absence of caspase 8, alternative cell death pathways, involving necroptosis, can be activated [178]. To assess the importance of caspase 8 in pIC-activated IEC apoptosis and subsequent small intestinal damage, we generated mice that lack caspase 8 in IECs. Control mice with floxed caspase 8 behaved like WT mice following pIC treatment at 1.5 h (Fig. 7 B, C). However, mice lacking caspase 8 in IECs did not have significant levels of IEC caspase 3 activation or epithelial apoptosis at this time point (Fig 7 E). Interestingly, by 2.5 h post treatment, these mice developed complete destruction of the small intestinal villi, with an apparent loss of the villus epithelium (Fig. 7 F), and died within 6 h of treatment (data not shown). These results demonstrate that caspase 8 is required to regulate IEC apoptosis and to maintain the integrity of the intestinal epithelium following pIC activated TLR3/TRIF signaling in IECs. In the absence of Caspase 8, alternative pathways result in complete loss of the epithelium and ensuing death.

3. Discussion

We elucidated the signaling pathways and mechanisms by which the viral dsRNA mimic pIC selectively causes small intestinal mucosal damage *in vivo*. Small intestinal mucosal changes after encountering pIC were characterized by a rapid onset of epithelial cell apoptosis, the loss of IECs from villus structures, accompanying marked loss of villus height, and significant diarrhea with recovery over the following 24-48 h. IEC apoptosis and villus shortening after pIC treatment were strictly dependent on signaling through the TLR3/TRIF pathway and caspase 8 as demonstrated using $TLR3^{-/-}$, $TRIF^{-/-}$, and caspase $8^{\Delta IEC}$ mice. While this apoptotic pathway has been studied *in vitro* [178], we demonstrate an *in vivo* system where it dramatically impacts the structure and function of the small intestine.

Induction of type I interferon in IECs is an important antiviral mechanism [179, 180]. Moreover, activation of NF-κB in IECs is important both for the induction of IEC innate proinflammatory chemokines and cytokines and for IEC resistance to apoptosis [174, 175, 181, 182]. However, pIC-induced IEC apoptosis and villus shortening were independent of those pathways. Further, while IRF3 can induce apoptosis in response to viral infection through a BAX-dependent pathway in fibroblast cell lines [163], we found no role for BAX and IRF3 in pIC-induced apoptosis of small intestinal IECs. TNF is also well known for its ability to induce IEC apoptosis [169], but dsRNA-induced IEC apoptosis was completely independent of TNF as well as other cytokines like IL-6 and IL-1. Moreover, pIC-induced apoptosis of small intestinal villus IECs *in vivo* was independent of TLR signaling pathways that use the adaptor molecule MyD88, the TRIF signaling arm of TLR4 and pIC signaling through PKR.

dsRNA-induced small intestinal epithelial cell apoptosis, mucosal remodeling and recovery after pIC *in vivo* required signaling downstream of TLR3/TRIF through caspase 8. In the absence of an intact signaling pathway through caspase 8 downstream of TLR3/TRIF, there

was severe damage to the epithelium and small intestinal mucosa. This suggests the TLR3/TRIF/caspase 8 apoptotic pathway has an important function as a protective mechanism that maintains the integrity of the intestinal epithelium after dsRNA activated TLR3/TRIF signaling. Since TRIF can interact directly with RIP3 as well as RIP1 [165], the increased damage to the small intestinal mucosa in the absence of caspase 8 may be mediated by activation of alternative death pathways, possibly involving RIP3-dependent necroptosis. In this regard, RIP-3 has been shown to signal necroptosis in caspase 8 deficient mice treated with TNF, and after virus infection *in vivo* [112, 126, 183, 184].

Cells generated in the stem cell compartment in the crypts of the small intestine proliferate and migrate upwards to populate the villi where they differentiate and ultimately are shed from the upper villus tips. Apoptosis of IECs after pIC was largely confined to the mid to upper villus region. Using mice conditionally deficient in IKKα, IKKβ, or both in IECs, we showed that activation of the consensus NF-κB pathway protected crypt IECs but not villus IECs from pIC-induced apoptosis. Moreover, the marked sensitivity to dsRNA-induced apoptosis of mid to upper villus IECs in the small intestine occurred in the absence of additional stimuli. This differs from many other cell types and tissues that require two stimuli to induce apoptosis (e.g., the activation of death receptors and translation inhibition) [168]. For example, this is the case *in vivo* for hepatocytes where both TNF and D-galactosamine, a translation inhibitor, are required to induce apoptosis [185]. Even in certain cancer cells, dsRNA-induced apoptosis through TLR3 requires a translation inhibitor (e.g. cyclohexamide) [186]. In those cells, pro-survival signals from NF-κB signaling appear to protect from the activation of apoptosis by caspase-8 [168, 187]. It is possible that the different susceptibility of crypt and villus IECs to apoptosis may reflect differences in the negative regulation of NF-κB signaling in villus IECs or different NF-κB isoforms throughout the crypt villus axis, where an increased fraction of p50 homodimers may

act to negatively regulate NF-κB targets in the villi [188, 189]. In this regard, NF-κB signaling likely is tightly regulated in villus IECs since these cells ultimately must undergo detachment-dependent apoptosis, termed anoikis, at the villus tips as a part of their lifecycle and NF-κB signaling has been shown to decrease anoikis [190].

Infection with enteric viruses like rotavirus causes significant loss of small intestinal villus epithelial cells, villus shortening and concomitant diarrhea [191, 192] similar to that noted herein. Other R*eoviridae* also contain a dsRNA genome whereas other viruses that induce gastroenteritis, including norovirus, produce dsRNA during their replication cycle [193-195]. The likely relevance of the model using parenterally administered synthetic dsRNA to enteric virus infection is strengthened further since circulating dsRNA is found in rotavirus infected humans and animals. Our findings with dsRNA suggest a host protective role for the TLR3/TRIF/Caspase 8 activated apoptosis pathway in IECs in viral infection *in vivo*. This would include a rapid shedding of apoptotic virus infected cells and shortening of villi which also decreases the epithelial surface area available for virus infection, while maintaining epithelial integrity with a functional secretory epithelium that generates fluid in the intestinal lumen to flush out luminal virus with the diarrheal fluid. Conversely, while $TLR3^{-/-}$ and $TRIF^{-/-}$ mice are protected from dsRNA induced epithelial cell apoptosis, villus remodeling and diarrhea, therapeutic approaches designed to inhibit TLR3 signaling could result in decreased virus clearance, as was reported in $TLR3^{-/-}$ mice infected with murine rotavirus [196].

The mechanisms we show are responsible for pIC-induced small intestinal epithelial cell death and villus shortening and differ from those proposed by Zhou et al [161, 197]. Their model was based on a mix of *in vitro* and *in vivo* experiments in which pIC signaling through TLR3 was proposed to increase IL-15 production by IECs and Rae1, a ligand for NKG2D on IECs. Further, IEC produced IL-15 was proposed to increase NKG2D on IELs, with co-culture of isolated IECs

and IELs resulting in killing of IECs *in vitro* at 24 h. Support for their model of pIC induced small intestinal injury was based on an the *in vivo* finding that antibody to IL-15 Rα partially decreased villus shortening in pIC injected mice [197]. Whereas dsRNA has been reported to induce IL-15 *in vivo* [198], using IL-15$^{-/-}$ mice we showed that pIC-induced apoptosis and villus shortening after pIC was totally independent of IL-15. Zhou et al further reported decreased small intestinal villus damage in response to dsRNA after NK1.1 cell depletion, whereas NK1.1 cell depletion did not affect dsRNA induced IEC apoptosis or villus shortening in our studies. Additionally, using bone marrow chimera mice we showed that cells of hematopoietic origin were not required for IEC apoptosis.

Finally, the relevance of our findings can be envisioned to extend beyond viral RNA triggers of TLR3/TRIF signaling. In this regard mRNA released from necrotic cells was shown to activate TLR3 signaling [199]. Further, RNA from necrotic cells in rheumatoid arthritis synovial tissues activated TLR3-dependent signaling [200]. In other studies, endogenous RNA from injured tissues and cells activated TLR3 signaling, and resulted in cell death. For example, endogenous RNA, derived from lung tissue or necrotic neutrophils, signaled through TLR3 in the absence of exogenous virus and increased lung damage, proinflammatory cytokine production and death in a model of hyperoxia lung injury [201]. TLR3 also functioned as an endogenous sensor of tissue necrosis, independent of viral activation, in models of septic peritonitis and ischemic gut injury. Importantly, injury and mortality were attenuated in anti-TLR3 antibody treated and TLR3$^{-/-}$ mice [202]. Taken together with our results, these studies indicate that dsRNA associated with either virus infection or tissue injury and inflammation can have a dramatic impact on intestinal mucosal tissues.

4. Materials and Methods

Reagents

Low molecular weight pIC was from Invivogen (San Diego, CA) and used in all studies unless indicated otherwise. pIC sodium salt (S-pIC) was from Sigma-Aldrich (St. Louis, MO). R848, ODN 1826 and LPS from *E. coli* O111:B4 were from Invivogen. pIC was heated to 50°C for 10 minutes and allowed to cool to room temperature to anneal. Cleaved caspase 3 antibody was from Cell Signaling (Danvers, MA). Recombinant mouse TNFα was purchased from Peprotech (Rocky Hill, NJ).

Mouse strains and treatment

Wild type (WT) C57BL/6J, $TRIF^{lps2/lps2}$ ($TRIF^{-/-}$) [203], $BAX^{-/-}$[204], $RAG1^{-/-}$ [205], $IL\text{-}6^{-/-}$ [206] and $IL\text{-}1R^{-/-}$ [207] mice from The Jackson Laboratory, $IL\text{-}15^{-/-}$ mice [208] from Taconic, and $IFNAR^{-/-}$ [209], $PKR^{-/-}$[210], $MyD88^{-/-}$ [211], $TLR3^{-/-}$ [212], DTR [177], IκK-$\beta^{\Delta IEC}$ [175], IκK-$\alpha^{\Delta IEC}$ [213], $TLR4^{-/-}$ [214], $IRF3^{-/-}$ mice [215] and $MAVS^{-/-}$ [216] mice were maintained in specific pathogen free conditions at UCSD. Mice were given a single intraperitoneal (i.p.) injection of 30 mg/kg pIC, 10 mg/kg R848, 5 mg/kg ODN 1826 or 20 mg/kg LPS in a volume (ul) of sterile phosphate buffered saline or saline solution equal to 10x body weight (g), using sterile PBS or saline injection alone as a control. In one series of experiments pIC was injected in the retro-orbital sinus of anesthetized mice. Recombinant TNFα was injected retro-orbitally in anesthetized mice. Mice were sacrificed at 3-6 h after injection unless otherwise indicated. All animal studies were approved by the UCSD Institutional Animal Care and Use Committee.

Histology and Immunohistochemistry

Proximal small intestine starting 2 cm distal to the pylorus and continuing for the first third of the small intestine was processed as Swiss rolls [135]. Distal small intestine Swiss rolls were taken from the distal third of the small intestine. Tissues were fixed in 10% formalin and embedded in paraffin, and 5-µm sections were stained with H&E. For cleaved caspase3 staining samples were deparaffinized, subjected to antigen retrieval and incubated with antibody overnight, after which HRP conjugated secondary antibody was added for 2 h followed by incubation with 3,3'-diaminobenzidine (DAB) and counter-staining with hematoxylin. For CD11c staining, small intestine Swiss rolls were frozen in OCT (Tissue-Tek). Frozen sections were fixed in neutral buffered formalin for 10 min, washed and blocked with 3% BSA in PBS. Sections were incubated overnight with CD11c antibody (BD Pharmingen) or hamster negative control (AbD Serotec) then washed and stained with Cy3 goat anti-Armenian hamster (Jackson Immunoresearch).

Microscopy analysis

Villus lengths were measured in each Swiss roll and the ten longest villi were averaged to give a final mean villus length. Cleaved caspase 3 stained cells that were completely black were counted as positive cells and ten representative villi were counted and averaged to provide a value for each mouse. Samples were examined in our laboratory under an Olympus BX41microscope. Digital images were processed using Adobe Photoshop 9.0 (Adobe Systems) or Power Point (Microsoft), with the same settings being applied for test and control antibody.

Ussing chamber studies

Segments of proximal small intestine were cut along the mesenteric border and mounted in Ussing chambers (Physiological instruments, San Diego, CA), exposing 0.09 cm^2 of tissue area

to 4 mL of circulating oxygenated Ringer's buffer maintained at 37°C. The buffer consisted (in mM) of: 140 Na^+, 5.2 K^+, 1.2 Ca^{2+}, 0.8 Mg^{2+}, 120 Cl^-, 25 HCO_3^-, 2.4 $H_2PO_4^-$, 0.4 HPO_4^{2-}. Additionally, glucose (10 mM) was added to the serosal buffer as a source of energy, osmotically balanced by mannitol (10 mM) in the mucosal buffer. Agar–salt bridges were used to monitor the potential difference across the tissue and to inject the required short-circuit current (Isc) to maintain the potential difference at zero. This was registered by an automated voltage clamp and continuously recorded by computer. Baseline Isc values were obtained at equilibrium, 15 min after the tissues were mounted and expressed as $\mu A/cm^2$. Conductance (G) was also determined at baseline as an indicator of ion flux and expressed as mS/cm^2. FITC labeled dextran (4 kDa, Sigma) was used as a probe to assess macromolecular permeability, and was added (2.2mg/mL final concentration) to the luminal buffer once equilibrium was reached. Serosal samples (240 uL) were taken at 30 min intervals for 2h and replaced with fresh buffer to maintain constant volume. Fluorescence was measured by end point assay (Victor4X, Perkin Elmer) and the flux of FITC-dextran from the mucosa to the serosa was calculated as the average value of two consecutive stable flux periods (60–90 and 90–120 min) and expressed as $pmol/cm^2/h$. [217].

Cytokine detection

Serum samples were collected 1h after treatment and stored at -80°C. Cytokine measurements used the mouse ultra-sensitive TNF kit or proinflammatory 7-plex kit from Meso Scale Discovery (Gaithersburg, MD) and cytokine levels were determined using a Meso Scale Discover Sector Imager 6000.

RNA extraction and quantitative real-time PCR

Total cellular RNA was extracted using Trizol (Life Technologies, Carlsbad, CA), according to the manufacturer's instructions. 1 mg RNA total RNA was used for iScript (BioRad Laboratories, Hercules, CA) reverse transcription and the cDNA was used for quantitative Real Time PCR (qPCR) using SYBR green Master mix (Applied Biosystems, Foster City, CA) and GAPDH forward primer ATCAACGACCCCTTCATTGACC and GAPDH reverse primer CCAGTAGACTCCACGAGATACTCAGC or IFN-β forward primer CTGAGCAGCTGAATGGAAAG and IFN-β reverse primer CTTGAAGTCCGCCCTGTAGGT. Denaturation was 5 min at 95˚C followed by 40 cycles of amplification at 95˚C for 30 s and 60˚C for 30 s using an ABI StepOnePlus (Applied Biosystems). IFN-β induction was calculated using the ΔΔCt method and values were normalized to PBS treated mice.

IEC isolation

To isolate IECs, the proximal small intestine beginning 2 cm distal to the pylorus was cut into 0.5-1 cm pieces, which were then shaken in RPMI 1640 containing 1 mM DTT and 2 mM EDTA at 37°C. Supernatant was removed and centrifuged and the resultant pellet was washed in ice-cold PBS and snap-frozen in Trizol. The remaining fraction was centrifuged and used as the lamina propria fraction.

Natural killer and dendritic cell depletion

To deplete NK cells, mice were injected with 200 μg purified anti-NK1.1 (PK136) mAb (eBioscience, San Diego, CA) 24 h before injection of pIC. $NK1.1^+$ cell depletion was confirmed by FACS. Three h after PBS or pIC treatment, spleens were harvested and homogenized. Total spleen cell suspensions were labeled with PE conjugated anti-NK1.1and anti-CD49b eFluor 450

antibodies (eBioscience) and analyzed using a BD FACScan (BD Biosciences). Antibody to NK1.1, NK1.1 PE, CD49b (integrin 2α), control IgG2 and IgG2a PE were from eBioscience (San Diego, CA). DTR [177] mice were treated with 4 ng/g diphtheria toxin i.p. (Sigma Aldrich) 24 h prior to pIC injection. DC depletion was confirmed by immunohistochemistry as described above.

Bone marrow chimeras

To generate bone marrow chimeric mice, WT or TLR3 recipients were exposed to a single lethal dose of 9 Gy total body irradiation from a ^{137}Cesium source. Six hours later these mice were injected i.v. with 2-5×10^6 bone marrow cells from TLR3$^{-/-}$ or WT mice. Mice were rested for 8 weeks before use.

Statistical Analysis

Data are expressed as mean ± standard deviation. Two groups were compared using unpaired Student *t* test. Analysis of variance with Bonferonni posttest was used for multiple group comparisons. Significant differences were reported where $p < 0.05$.

5. Figures and Supplementary Figures

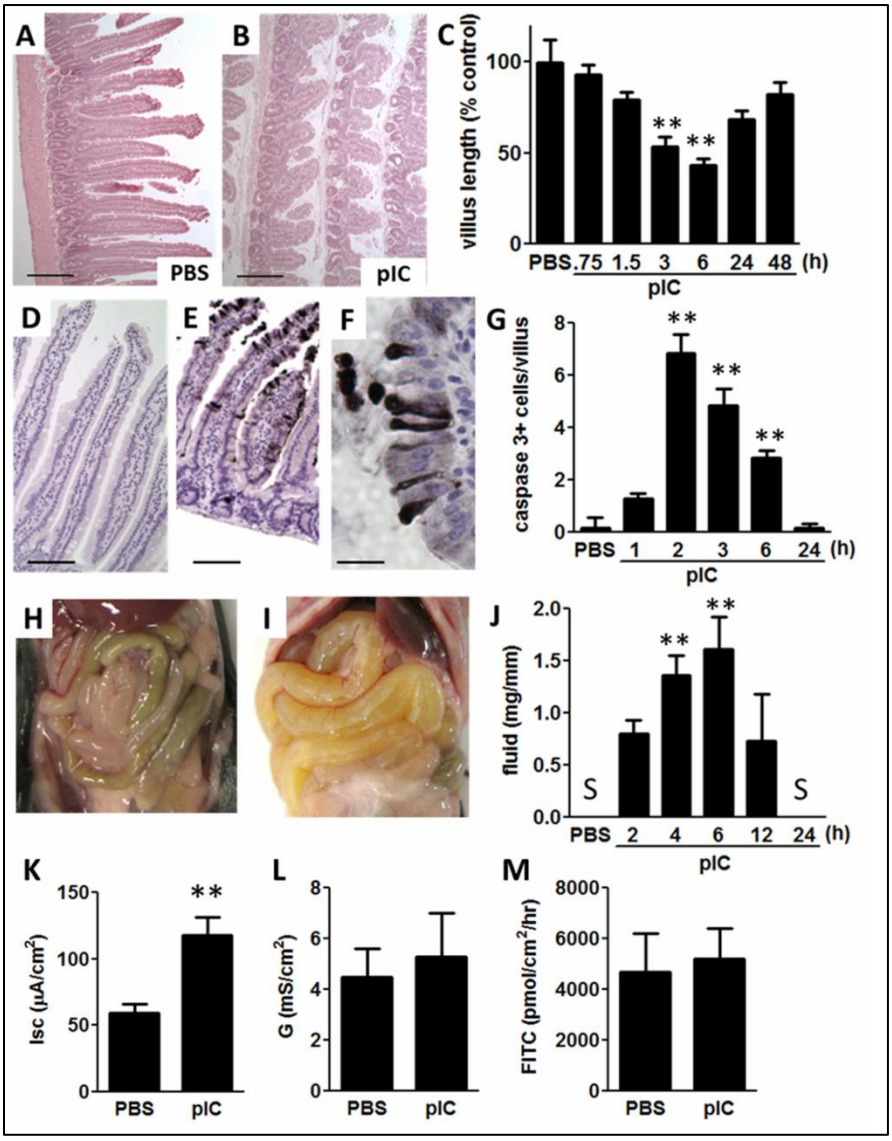

Figure 1: pIC induces IEC apoptosis and small intestinal villus shortening. H&E stained sections of proximal WT mouse small intestine 3 h after (A) PBS or (B) pIC 30 μg/g i.p. Scale bar 200 μm. (C) Mean villus length at indicated times after pIC. (D) Cleaved caspase 3 stained sections of proximal small intestinal mucosa 2 h after (D) PBS or (E, F) pIC. (D, E) Scale bar 100 μm and (F) 25 μm. (G) Cleaved caspase 3 labeled cells per villus at specified times after pIC. Representative images of the peritoneal cavity of (H) PBS or (I) pIC 30 μg/g i.p. injected mice at 6 h. (J) Fluid weight per length of the entire small intestine at the indicated times after pIC. Values are mean ± SD, n=3–6 mice per time. ** $p < 0.01$ vs PBS. S = solid contents, no fluid.

Ussing chamber measurements of (K) short circuit current (Isc), (L) conductance (G) and (M) macromolecular permeability to 4 kDa FITC-dextran in proximal small intestine pieces isolated from mice treated with PBS or 30 μg/g i.p. pIC for 3 h. Graphs show mean ± SEM, n = 5 samples per treatment group.

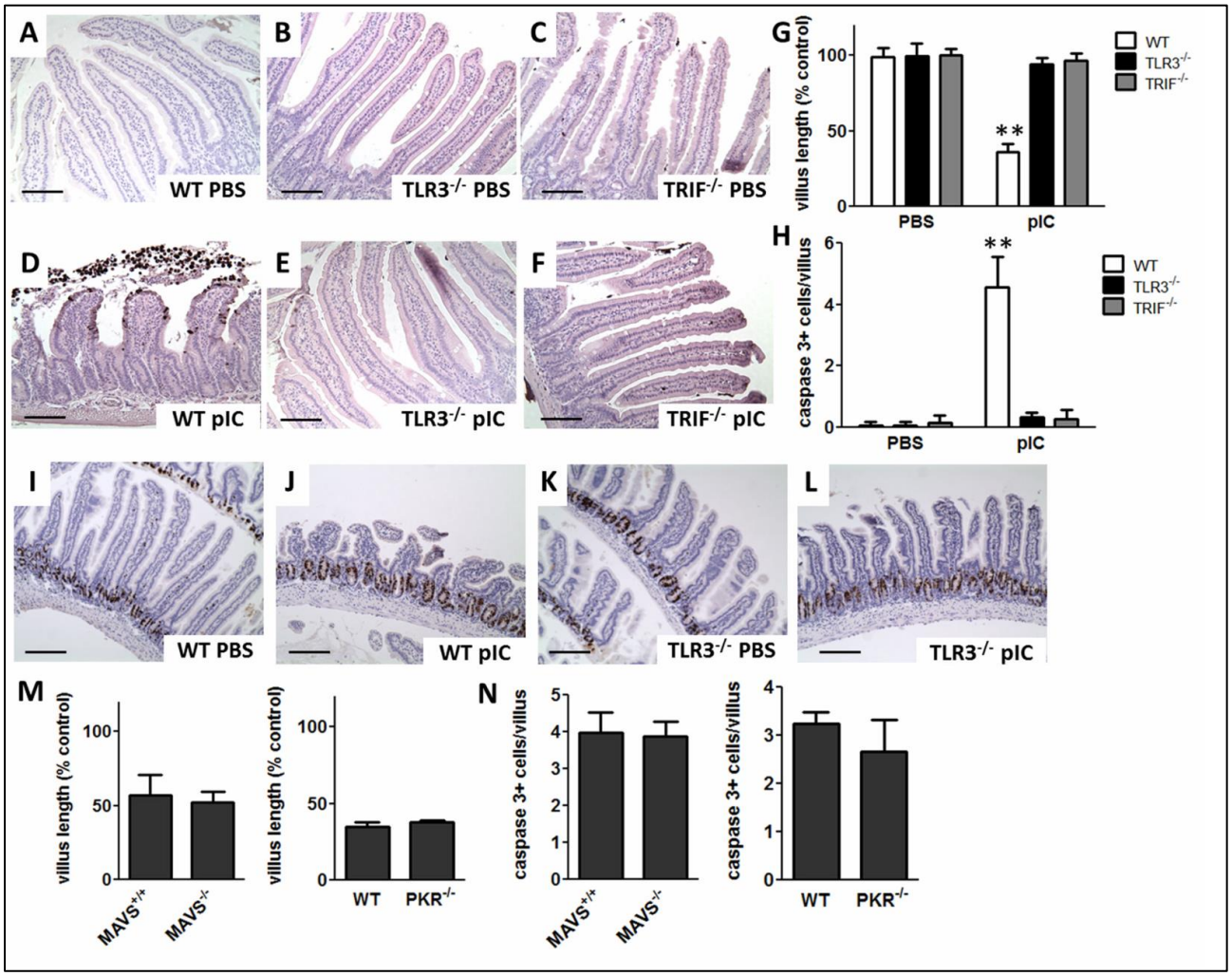

Figure 2: TLR3-TRIF signaling is required for pIC-induced small intestinal villus shortening and IEC apoptosis. Cleaved caspase 3 stained sections of proximal small intestine from (A–C) PBS and (D–F) 30 μg/g pIC i.p. treated WT, TLR3−/− and TRIF−/− mice at 3 h. Scale bar 100 μm. (G) Villus length and (H) cleaved caspase 3 labeled cells per villus after PBS or 30 μg/g pIC i.p. at 3 h. Data are mean ± SD, n=3–4 mice/group. ** $p < 0.01$ vs PBS treated mice and pIC treated TLR3−/− and TRIF−/− mice. BrdU stained sections from the proximal small intestine 6 h after (I) PBS i.p. or (J) 30 μg/g pIC i.p. in WT mice, (K) PBS i.p. or (L) 30 μg/g pIC i.p. in TLR3−/− mice. Scale bar 200 μm. (M) Villus length of MAVS+/+, MAVS−/−, WT and PKR−/− mice at 3 h after 30 μg/g pIC i.p. (N) Cleaved caspase 3 labeled cells per villus for pIC treated MAVS+/+, MAVS−/−, WT and PKR−/− mice at 3 h after 30 μg/g pIC i.p. Mean ± SD, n=5–8 mice/group.

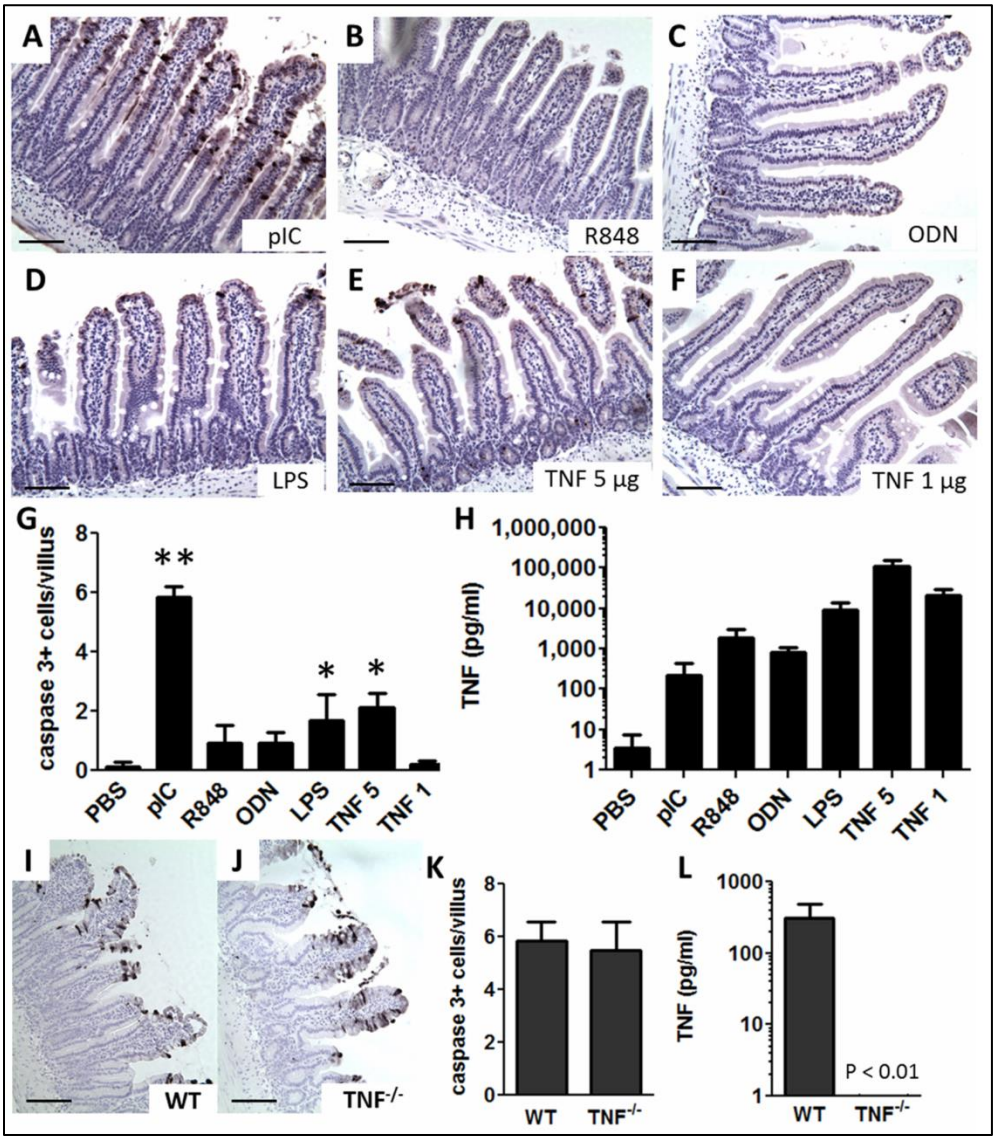

Figure 3: pIC-induced IEC apoptosis is TNF independent. Cleaved caspase 3 stained proximal small intestine sections from WT mice injected i.p. with (A) TLR3 ligand pIC, (B) TLR7 ligand R848, (C) TLR9 ligand ODN 1826, (D) TLR4 ligand LPS, (E) 5 µg TNF or (F) 1 µg TNF after 2 h. Scale bar 100 µm. (G) Cleaved caspase 3 labeled cells per villus in WT mouse proximal small intestine sections 3 h following treatment as described in (A–F). (H) Serum TNF levels at 1 h after treatments described in (A–F). Data are mean ± SD for 4–9 mice/group. ** $p < 0.01$ vs PBS, other TLR ligands and TNF-treated mice, * $p < 0.05$ vs PBS. Cleaved caspase 3 stained proximal small intestine sections from (I) WT and (J) TNF−/− mice at 3 h after i.p. injection of 30 µg/g pIC. Scale bar 100 µm. (K) Cleaved caspase 3 labeled cells per villus in proximal small intestine sections 3 h after 30 µg/g i.p. pIC. (L) Serum TNF levels at 1 h

following i.p. injection of 30 μg/g pIC in WT and TNF−/− mice. Values are mean ± SD, n=9–14 mice/group.

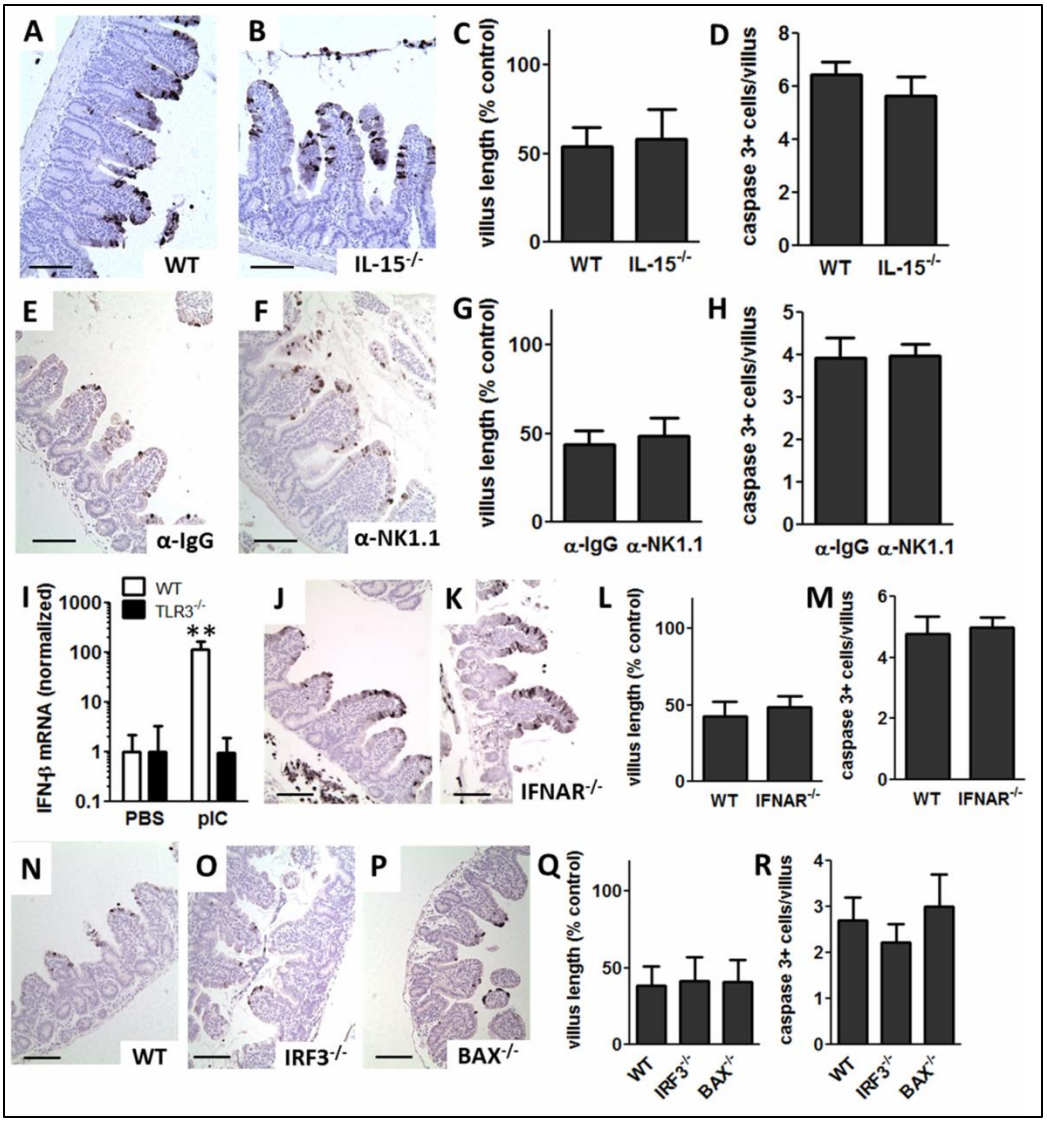

Figure 4: IL-15 signaling, NK+ cells and type I IFN signaling are not required for pIC induced villus shortening and IEC apoptosis. Cleaved caspase 3 stained proximal small intestine sections from (A) WT and (B) IL-15−/− mice 3 h after 30 μg/g i.p. pIC. (C) Proximal small intestine villus length and (D) cleaved caspase 3 labeled cells per villus following the treatments in (A) and (B) at 3 h. Cleaved caspase 3 stained proximal small intestine sections for WT mice treated with (E) antibody isotype control IgG2a or (F) NK1.1 antibody for 24 h prior to 3 h 30 μg/g i.p. pIC treatment. (G) Proximal small intestine villus length and (H) cleaved caspase 3 labeled cells per villus for mice treated as in (E) and (F). Data are mean ± SD, n=5–9 mice/group. (I) IFN-β mRNA levels normalized to GAPDH using quantitative real time PCR analysis of WT and TLR3−/−mice treated with PBS or 30 μg/g i.p. pIC. RT used RNA extracted from samples 3 h post treatment. Data are mean ± SD of normalized data, n=3–4 mice/group. **

$p < 0.01$ vs WT PBS and TLR3−/− pIC. Cleaved caspase 3 stained proximal small intestine sections from (J) WT, (K) IFNAR−/−, (N) WT, (O) IRF3−/− and (P) BAX−/− mice 3 h after 30 μg/g i.p. pIC. (L and Q) Proximal small intestine villus length and (M and R) cleaved caspase 3 labeled cells per villus from these pIC-treated mice at 3 h. Graphs show mean ± SD, n=4–5 mice/ group. Scale bar 100 μm.

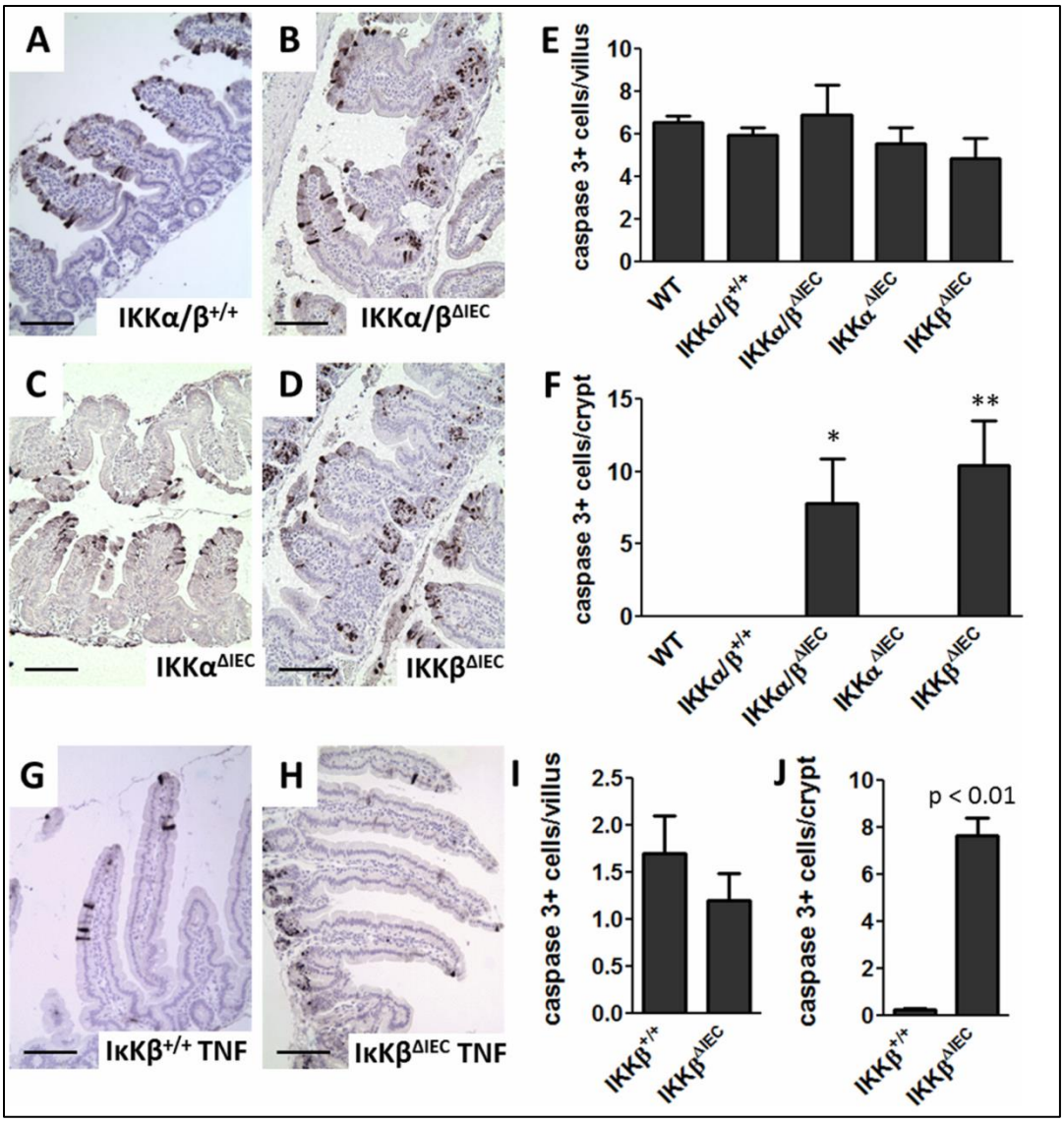

Figure 5: pIC- and TNF-induced IEC apoptosis is independent of NF-κB signaling, but NFκB signaling protects crypt cells from apoptosis. Cleaved caspase 3 stained proximal small intestine sections from (A) IKKα/β+/+ control, (B) IKKα/βΔIEC, (C) IKKαΔIEC and (D) IKKβΔIEC mice at 3 h after 30 μg/g i.p. pIC. Cleaved caspase 3 labeled cells 3 h after 30 μg/g i.p. pIC treatment (E) per villus and (F) per crypt. Data are mean ± SD, n=3–5 mice/group. * $p < 0.05$ or ** $p < 0.01$ compared to WT, IKKα/β+/+ and IKKαΔIEC. Cleaved caspase 3 stained proximal small intestine sections from (G) IKKβ+/+ and (H) IKKβΔIEC mice 3 h after 5 μg i.p. TNF. Cleaved caspase 3 labeled cells (I) per villus or (J) per crypt for IKKβ+/+ and IKKβΔIEC mice 3 h after 5 μg i.p. TNF. Values are mean ± SD, n=3–5 mice/group. Scale bar 100 μm.

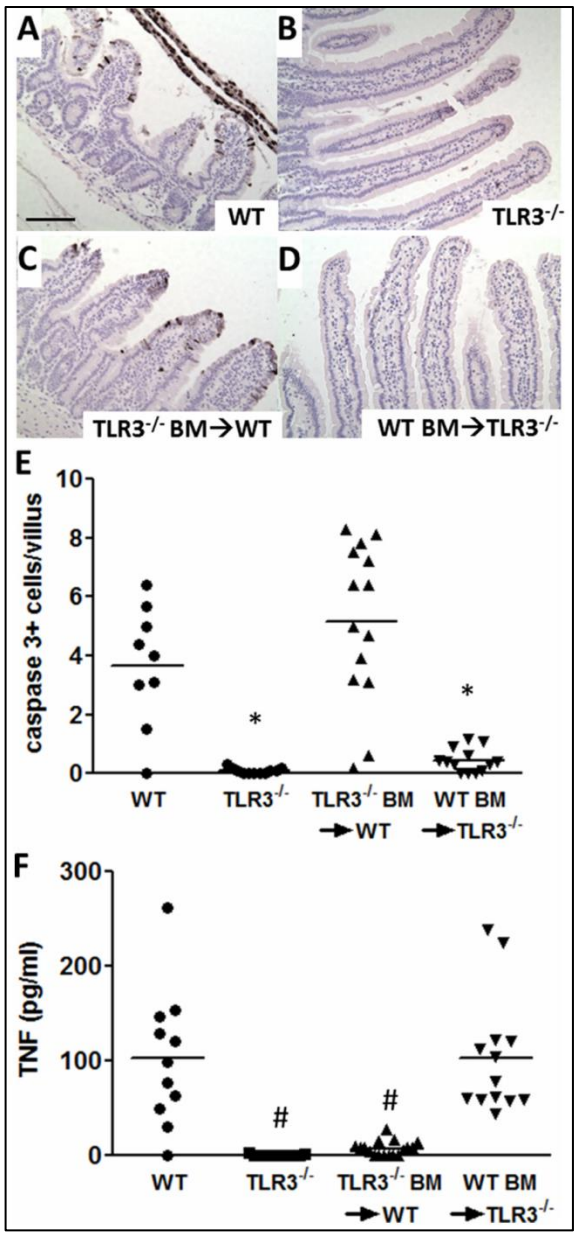

Figure 6: Cells of hematopoietic origin are not required for pIC-induced IEC apoptosis. Cleaved caspase 3 staining of (A) WT, (B) TLR3−/−, (C) TLR3−/− bone marrow reconstituted WT (TLR3−/− BM→WT), and (D) WT bone marrow reconstituted TLR3−/− (WT BM→TLR3−/−) mice following 30 μg/g pIC treatment for 3 h. Scale bar 100 μm. (E) Cleaved caspase 3 positive cells per villus and (F) TNF cytokine levels for each group. Graph show results from each mouse. Bar is mean value. *P < 0.01 compared to WT and TLR3−/− BM→WT. # P < 0.01 compared to WT and WT BM→TLR3−/−.

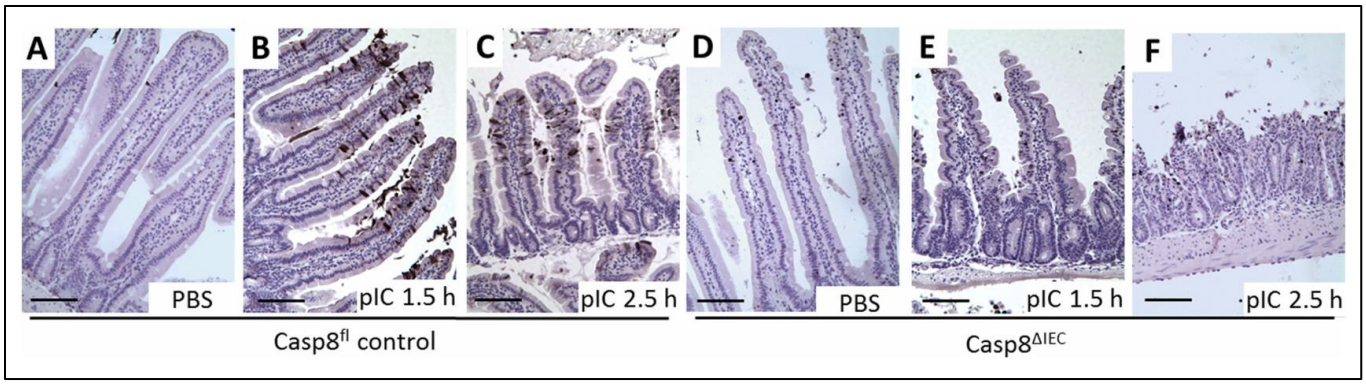

Figure 7: Caspase 8 is required for IEC apoptosis and preservation of the epithelium after pIC treatment. Cleaved caspase 3 stained proximal small intestine sections from Caspase 8fl control mice treated with (A) PBS or 30 µg/g i.p pIC for (B) 1.5 h or (C) 2.5 h and mice lacking caspase 8 in their IECs (casp8ΔIEC) treated with (D) PBS or 30 µg/g i.p pIC for (E) 1.5 h or (F) 2.5 h. Scale bar 100 µm.

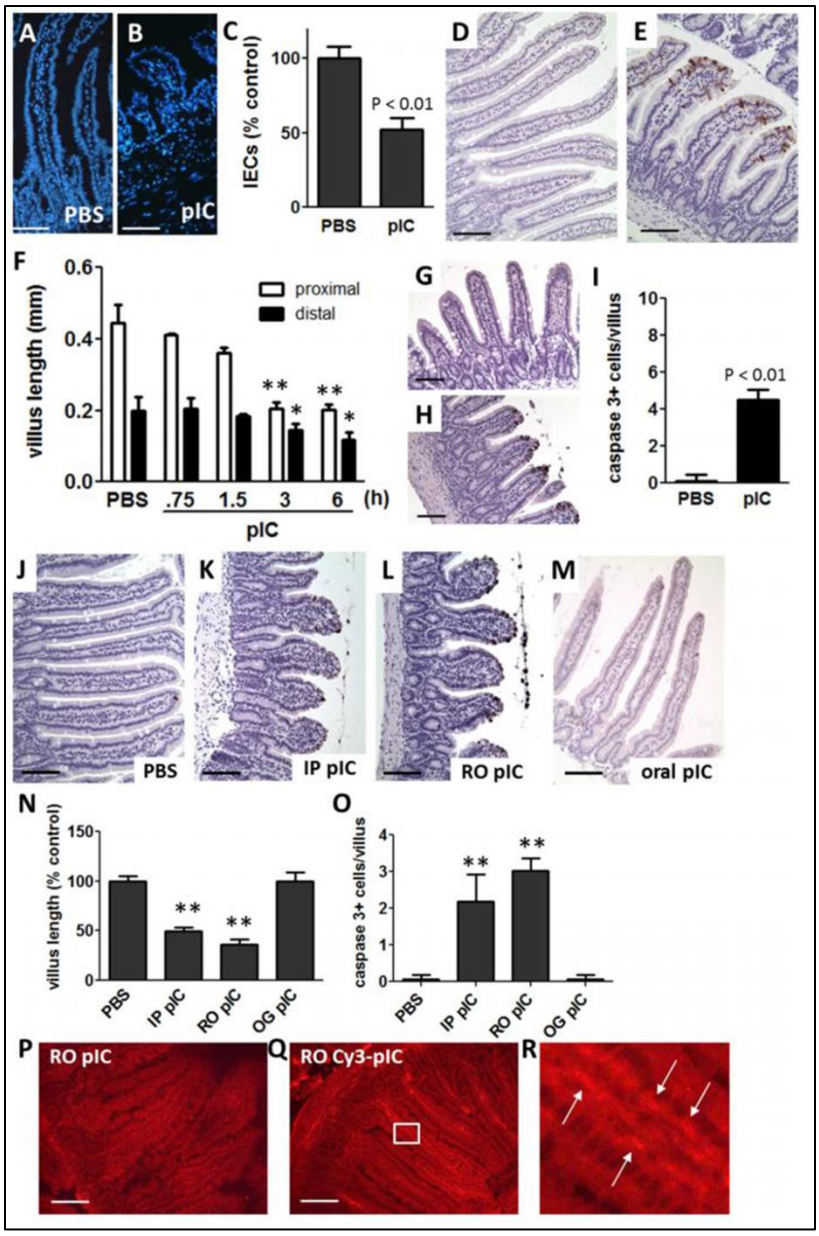

Supplementary Figure 1: pIC-induced villus shortening in the small intestine is due to a loss of IECs. Nuclear staining of proximal small intestine sections at 6 h after (A) PBS or (B) 30 µg/g i.p. pIC treatment. (C) Percentage of IECs per villus in PBS or 30 µg/g i.p. pIC treated mice at 6 h. Data are mean ± SD, n = 3-5 mice/group. Cleaved caspase 8 stained small intestine sections from mice treated for 2 h with (D) PBS or (E) 30 µg/g i.p. pIC. (F) Villus length in the proximal or distal small intestine after PBS or 30 µg/g i.p. pIC treatment at the indicated time points. Data are mean ± SD, n = 3-5 mice/group. ** $p < 0.01$ vs proximal PBS. Cleaved caspase 3 stained sections from the distal small intestine at 2 h after (G) PBS or (H) 30 µg/g i.p. pIC treatment. (I)

Mean ± SD of cleaved caspase 3 stained distal small intestine sections at 2 h for the treatment groups described in (G) and (H), n = 4 mice/group. Cleaved caspase 3 stained proximal small intestine sections from WT mice 3 h after (J) PBS, (K) 30 μg/g i.p. (IP) pIC injection, (L) 30 μg/g retro-orbital (RO) pIC injection or 6 h after (M) 100 μg/g oral gavage (OG), (N) Proximal small intestine villus length and (O) cleaved caspase 3 labeled cells per villus at 3 h for mice treated as described in (A-D). Data are mean ± SD, n=3-5 mice/group. ** $p < 0.01$ vs PBS and OG pIC. Fluorescence microscopy of frozen proximal small intestine sections harvested 20 minutes after 30 μg/g RO injection with (P) pIC or (Q) pIC labeled with Cy3. (R) Expanded view of the boxed region from (Q) with arrows indicating staining in Cy3-pIC injected mice. Scale bar 100 μm.

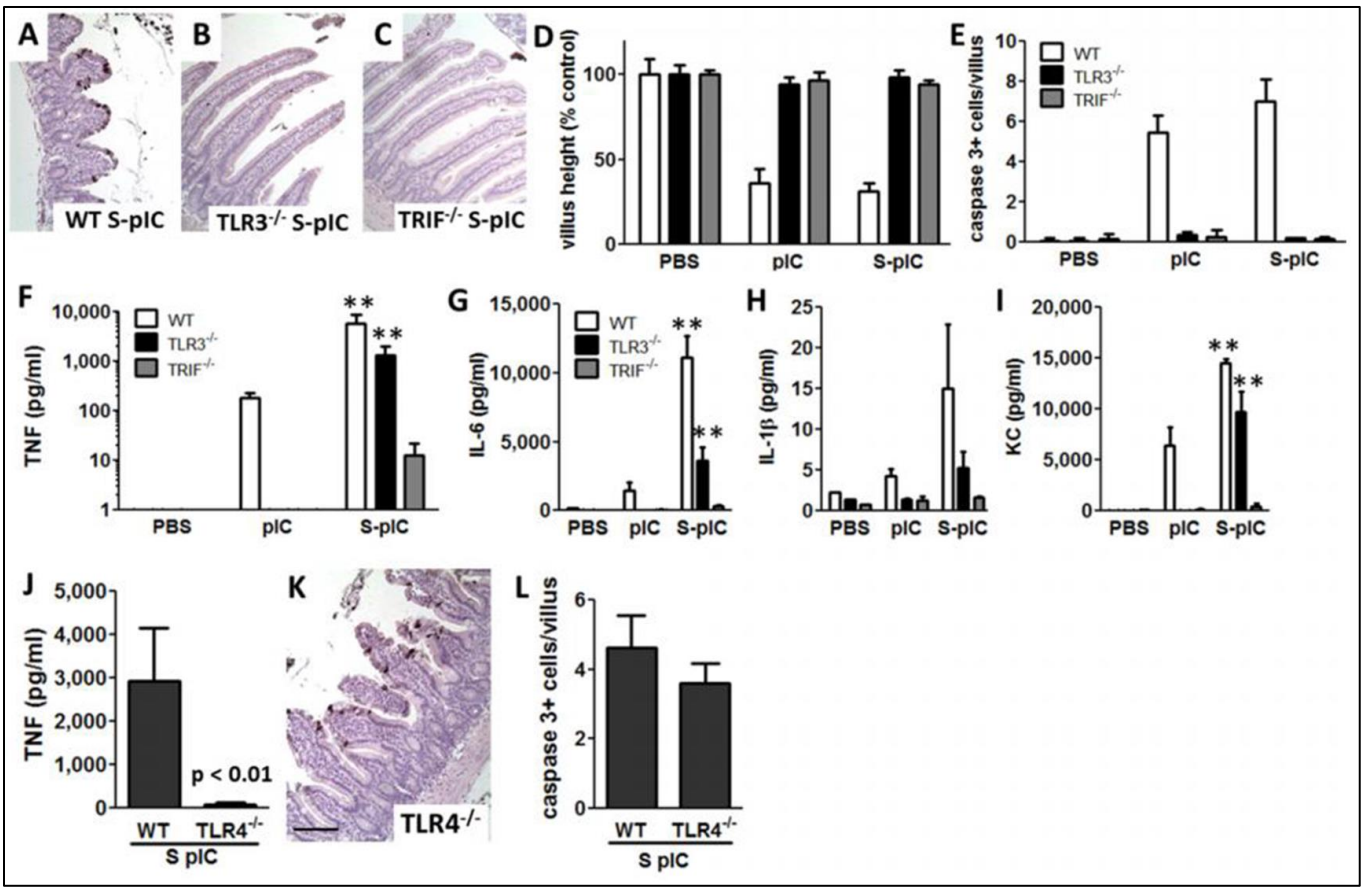

Supplementary Figure 2: Endotoxin contamination of pIC results in high levels of serum TNF but does not affect IEC apoptosis or villus shortening. Cleaved caspase 3 stained proximal small intestine sections from (A) WT, (B) TLR3-/- and (C) TRIF-/- mice 3 h after treatment with 30 μg/g pIC produced standardly without endotoxin purification (termed S-pIC). (D) Villus length and (E) cleaved caspase 3 positive cells per villus 3 h after treatment of WT, TLR3-/- and TRIF-/- mice with 30 μg/g PIC or S-pIC. Circulating levels of (F) TNF, (G) IL-6, (H) IL-1β and (I) KC in the same treatment groups at 1 h. Values are mean ± SD, n= 3-4 mice/group. ** $p < 0.01$ compared to pIC for each strain. (J) Serum TNF at 1 h after treatment of WT and TLR4-/- mice with 30 μg/g S-pIC. Values are mean ± SD, n=4 mice/group. (K) Cleaved caspase 3 stained proximal small intestine sections from TLR4-/- mice treated with 30 μg/g S-pIC for 3 h. (L) No significant difference in cleaved caspase 3 positive cells per villus at 3 h after treatment of WT and TLR4-/- mice with 30 μg/g S-pIC. Values are mean ± SD, n=4 mice/group. Scale bar 100 μm.

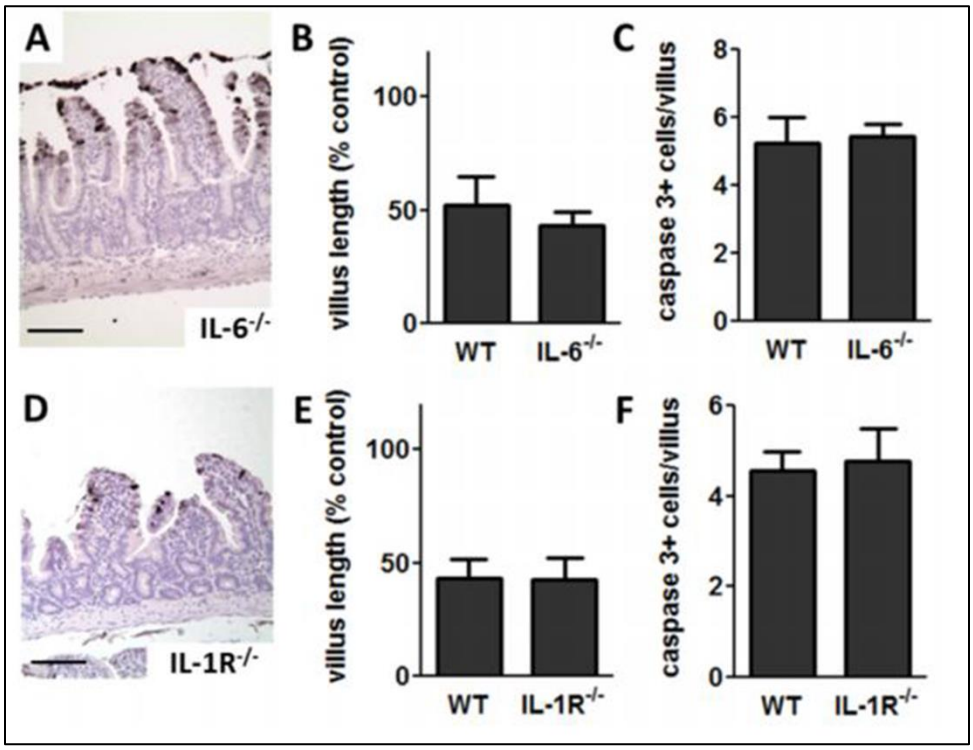

Supplementary Figure 3: IL-6 and IL-1 signaling are not required for pIC-induced IEC apoptosis. (A) Cleaved caspase 3 stained proximal small intestine sections from (A) IL-6-/- and (D) IL-1R-/- mice 3 h after 30 μg/g i.p. pIC. Mean ± SD of (B) proximal small intestine villus length and (C) cleaved caspase 3 labeled cells per villus 3 h after 30 μg/g i.p. pIC in WT and IL-6-/- mice, n=4-6 mice/group. Mean ± SD of (E) villus length and (F) cleaved caspase 3 labeled cells per villus 3 h after 30 μg/g i.p. pIC in WT and IL-1R-/- mice, n=5-7 mice/group. Scale bar 100 μm.

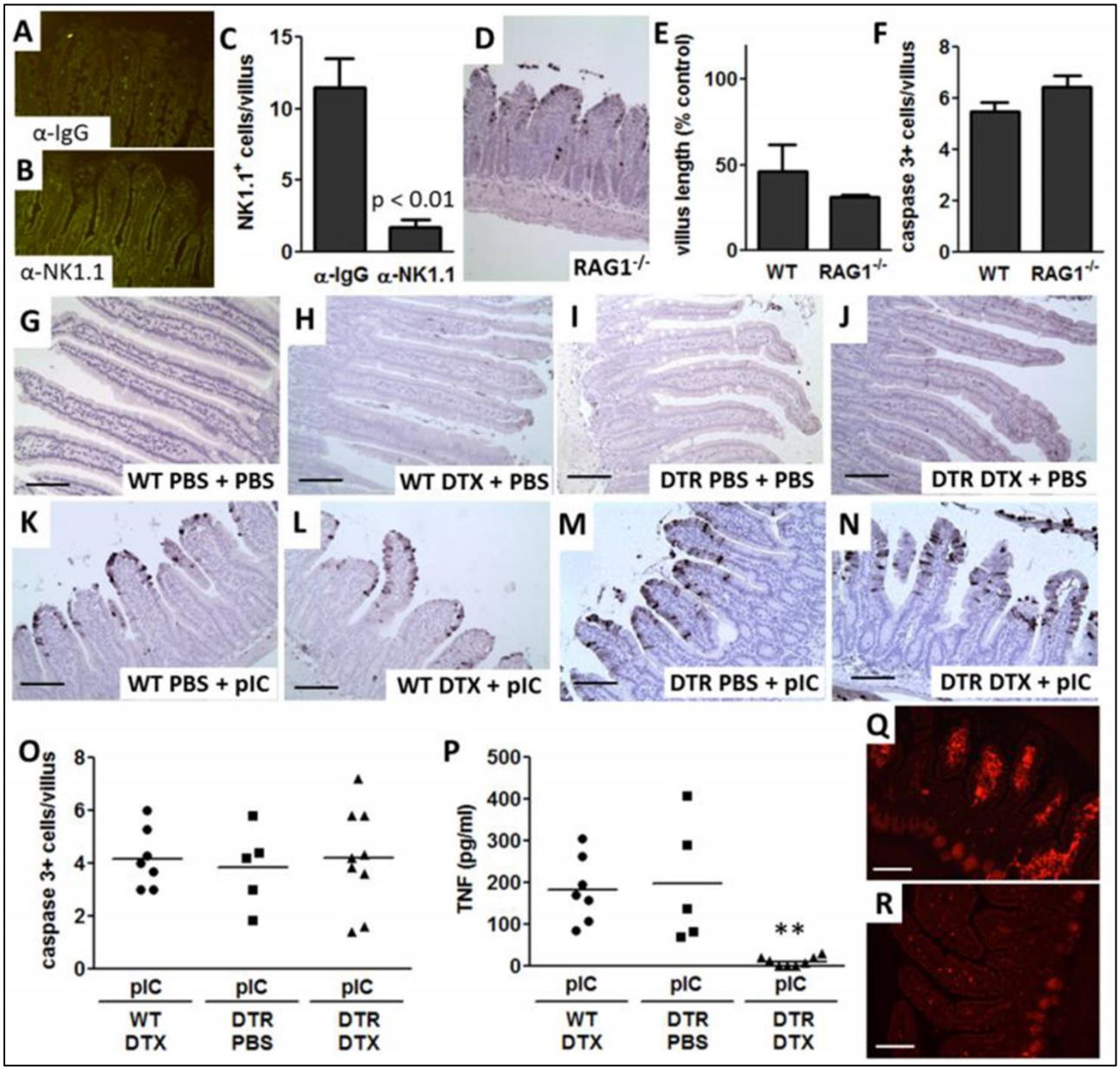

Supplementary Figure 4: Functional T and B cells and dendritic cells are not required for IEC apoptosis. Proximal small intestine sections from WT mice pretreated for 24 h with (A) negative control IgG or (B) NK1.1 antibody stained with FITC-conjugated NK1.1 antibody. (C) Mean ± SD NK1.1 positive cells per villus from 2 mice per treatment group. (D) Cleaved caspase 3 stained proximal small intestine sections from Rag1-/-mice at 3 h after 30 μg/g i.p. pIC. (E) Proximal small intestine villus length and (F) cleaved caspase 3 labeled cells per villus for WT and RAG1-/- mice at 3 h after 30 μg/g i.p. pIC. Data show mean ± SD, n=4-5 mice/group. Cleaved caspase 3 stained proximal small intestine sections from (G) WT mice pretreated for 24

h with PBS and then treated with PBS i.p. for 3 h, (H) WT mice pretreated with diphtheria toxin (DTX) and then treated with PBS i.p. pIC for 3 h, (I) DTR mice pretreated with PBS and then treated with PBS i.p. for 3 h, (J) DTR mice pretreated with DTX and then treated with PBS i.p. for 3 h, (K) WT mice pretreated with PBS and treated with 30 μg/g i.p. pIC for 3 h, (L) WT mice pretreated with DTX and then treated with 30 μg/g i.p. pIC for 3 h, (M) DTR mice pretreated with PBS and then treated with 30 μg/g i.p. pIC for 3 h, and (N) DTR mice pretreated with DTX and then treated with 30 μg/g i.p. pIC for 3 h. (O) Cleaved caspase 3 labeled cells per villus and (P) serum TNF levels at 1 h for mice treated as in F-H showing values for each mouse. Bar is mean value. ** $p < 0.01$ vs WT DTX and DTR PBS. Proximal small intestine sections from DTR mice pretreated for 24 h with (Q) PBS or (R) DTX stained with CD11c antibody. Scale bar 100 μm.

F. Conclusion :

Les découvertes récentes concernant la physiopathologie des MICI démontrent l'importance des études génétiques permettant d'identifier les voies de signalisation à l'origine de l'inflammation intestinale. Certains des gènes de susceptibilité aux MICI identifiés dans les études d'association pan-génomiques sont impliqués dans les voies de mort cellulaire incluant l'apoptose et les caspases. Nous avons choisi de nous intéresser à ces voies de signalisation intracellulaires et à leur implication dans le développement de l'inflammation intestinale sachant que ces voies de signalisation sont étroitement liées avec le TNFα, protéine clairement impliquée dans les MICI. Nous nous sommes focalisés plus particulièrement sur la caspase-8 qui présente des fonctions pro-apoptotiques et d'autres fonctions essentielles indépendantes de l'apoptose. A l'aide de souris présentant un déficit de la caspase-8 au niveau des cellules épithéliales intestinales nos travaux ont permis de montrer son importance dans le maintien de l'homéostasie intestinale et le développement de l'inflammation intestinale.

Dans notre travail, nous avons montré que les souris déficientes pour la caspase-8 au niveau des cellules épithéliales développaient une inflammation iléo-colique spontanée majorée par les agents bactériens et dépendante du TNFα. Cette inflammation intestinale était due à un détachement des cellules épithéliales intestinales faisant suite à la stimulation par des composés bactériens. En l'absence de caspase-8 on mettait en évidence au niveau des cellules épithéliales intestinales une augmentation de l'endocytose et la dégradation des intégrines de surface assurant l'adhésion des cellules à la matrice extracellulaire. Nous avons aussi démontré que les cellules épithéliales intestinales déficientes en caspase-8 présentaient une hyperactivation de l'autophagie. La dégradation des intégrines de surface associée à une activation dérégulée de

l'autophagie en l'absence de caspase-8 et en présence de composés bactériens était responsable du détachement des cellules épithéliales intestinales et de l'inflammation muqueuse.

Nous avons ensuite étudié l'effet de la caspase-8 dans un modèle de stimulation de l'épithélium intestinal par de l'ARN viral double brins. Dans ce modèle les souris traitées par de l'ARN viral double brin présentent une diminution de la hauteur de leur villosités intestinales du fait d'une apoptose induite par l'activation du récepteur transmembranaire TLR3 et de la transduction du signal par la protéine cytosolique TRIF. Cette apoptose permet une élimination des cellules infectées et la régénération de l'épithélium intestinal par la suite. En l'absence de caspase-8 au niveau des cellules épithéliales intestinales, la stimulation par l'ARN viral double brins entraine une destruction épithéliale marquée, l'apparition d'une inflammation muqueuse et la mort des animaux. La caspase-8 est donc nécessaire à cette apoptose induite par TLR3 et TRIF et l'absence de la caspase-8 entraine une mort cellulaire dérégulée avec apparition d'une inflammation intestinale.

L'ensemble de ces résultats suggèrent que la caspase-8 est un facteur important pour le maintien de l'homéostasie intestinale en réponse à des agressions bactériennes ou virales et que son déficit ou le dysfonctionnement des voies de signalisation l'impliquant sont responsables du développement d'une inflammation muqueuse.

G. Caspase-8 : données préliminaires chez l'homme :

Les données expérimentales obtenues chez la souris concernant la caspase-8 montrent que cette protéine pourrait être impliquée dans la physiopathologie des MICI. Par contre, peu de données sont actuellement disponibles concernant la caspase-8 chez l'homme et plus particulièrement les patients atteints de MICI. Une étude récente publiée en 2014 dans l'American Journal of Gastroenterology s'est intéressé à la caspase-8 et la nécroptose chez des enfants atteints de MICI [218]. Cette étude montre que dans les zones inflammatoires de l'intestin des enfants atteints de MC ou de RCH, il existe une augmentation de RIP3 témoignant de l'activation de la nécroptose et une diminution de la caspase-8. Nous avons donc choisi de poursuivre l'étude de la caspase-8 chez les patients adultes atteints de MC et de RCH.

Pour ce travail nous avons utilisé des prélèvements d'intestins grêles et de côlons de patients atteints de MICI et de patients contrôles (cancer, diverticule), obtenus lors d'une résection intestinale. Tout d'abord, nous avons utilisé des sections d'intestins pour réaliser un marquage immunohistochimique avec un anticorps anti-caspase-8. Chez les patients témoins, le marquage était principalement présent au niveau des cellules épithéliales intestinales (FIGURE 6). L'analyse des prélèvements de patients atteints de MC et de RCH montrait une diminution du marquage caspase-8 au niveau des cellules épithéliales intestinales principalement au niveau des tissus lésés mais aussi au niveau des tissus sains en comparaison aux patients contrôles (FIGURE 7-9). Nous avons ensuite confirmé cette diminution de la caspase-8 dans la muqueuse des patients atteints de MC et de RCH par western-blot (FIGURE 10 et 11). Finalement, nous avons extrait les cellules épithéliales intestinales du côlon de patients atteints de MICI et de patients contrôles. Nous avons ensuite mesuré l'expression de l'ARN caspase-8 par PCR en temps réel au niveau des cellules épithéliales intestinales. L'expression de la caspase-8 était significativement

diminuée dans les cellules épithéliales intestinales des côlons de patients atteints de MC et de RCH comparés aux contrôles (FIGURE 12).

Ces données préliminaires suggèrent qu'il existe un déficit de la caspase-8 dans l'intestin des patients atteints de MICI. Parallèlement aux données expérimentales animales précédemment décrites, ces résultats sont en faveur d'un rôle de la caspase-8 dans le développement de l'inflammation intestinale au cours des MICI.

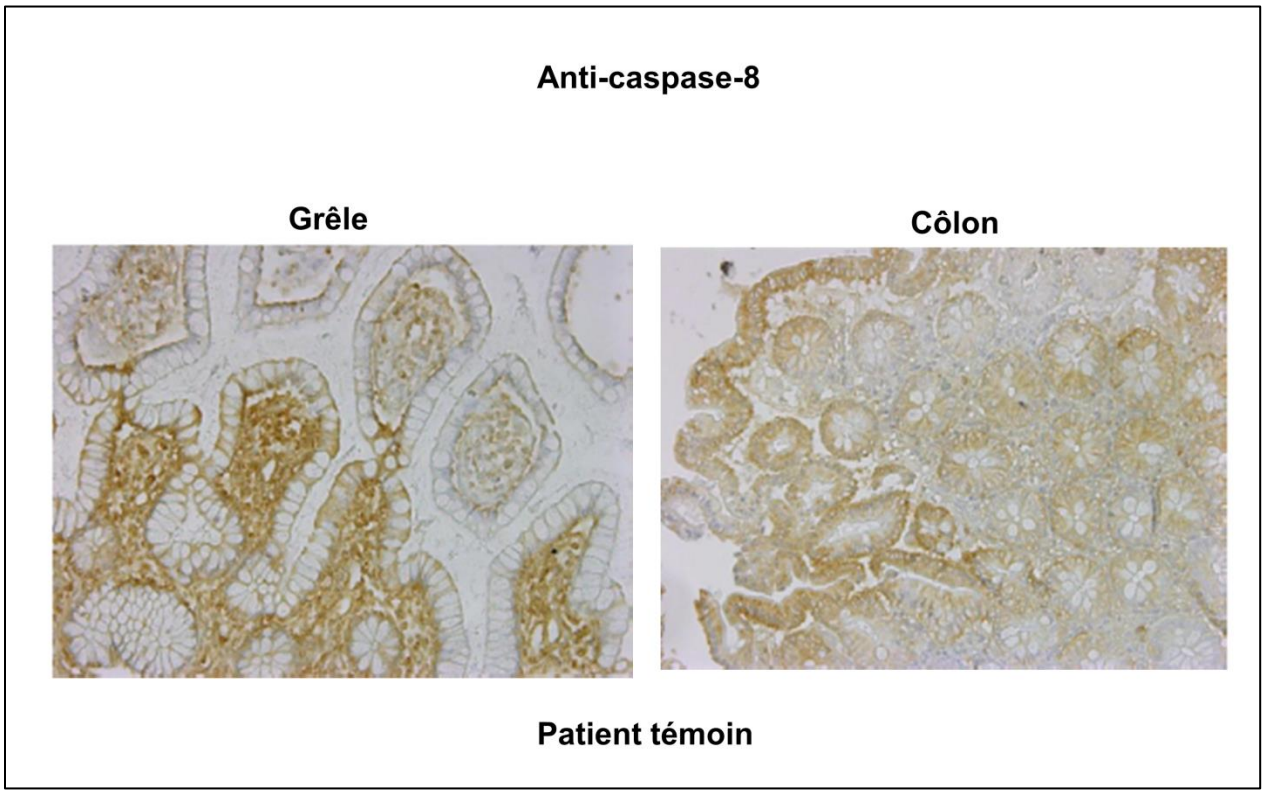

FIGURE 6 : marquage immunohistochimique de coupe d'intestin grêle et de côlon avec un anticorps anti-caspase-8 chez un sujet sain.

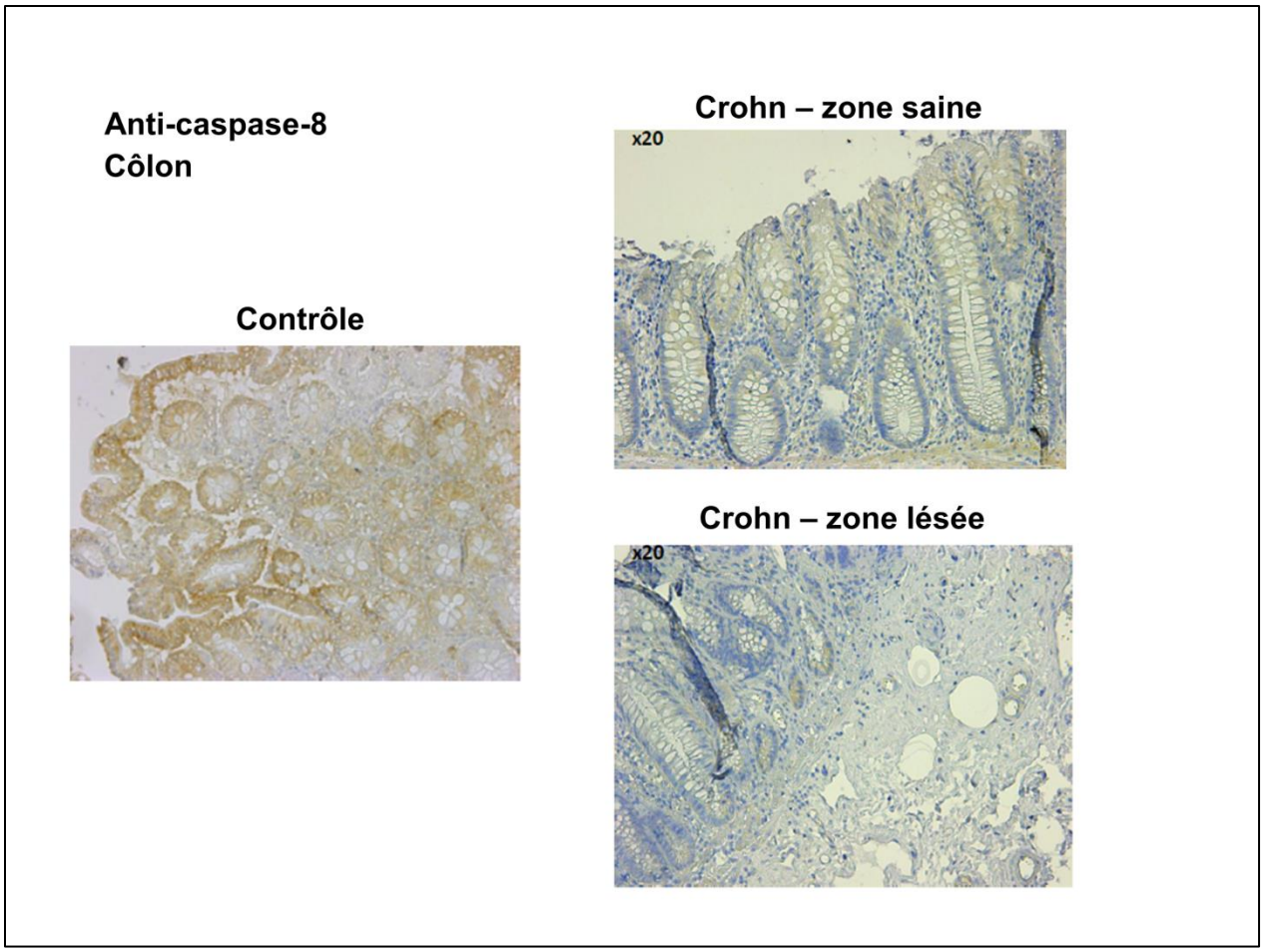

FIGURE 7 : marquage immunohistochimique de coupe de muqueuse colique avec un anticorps anti-caspase-8 chez des sujets sains et des patients atteints de MC.

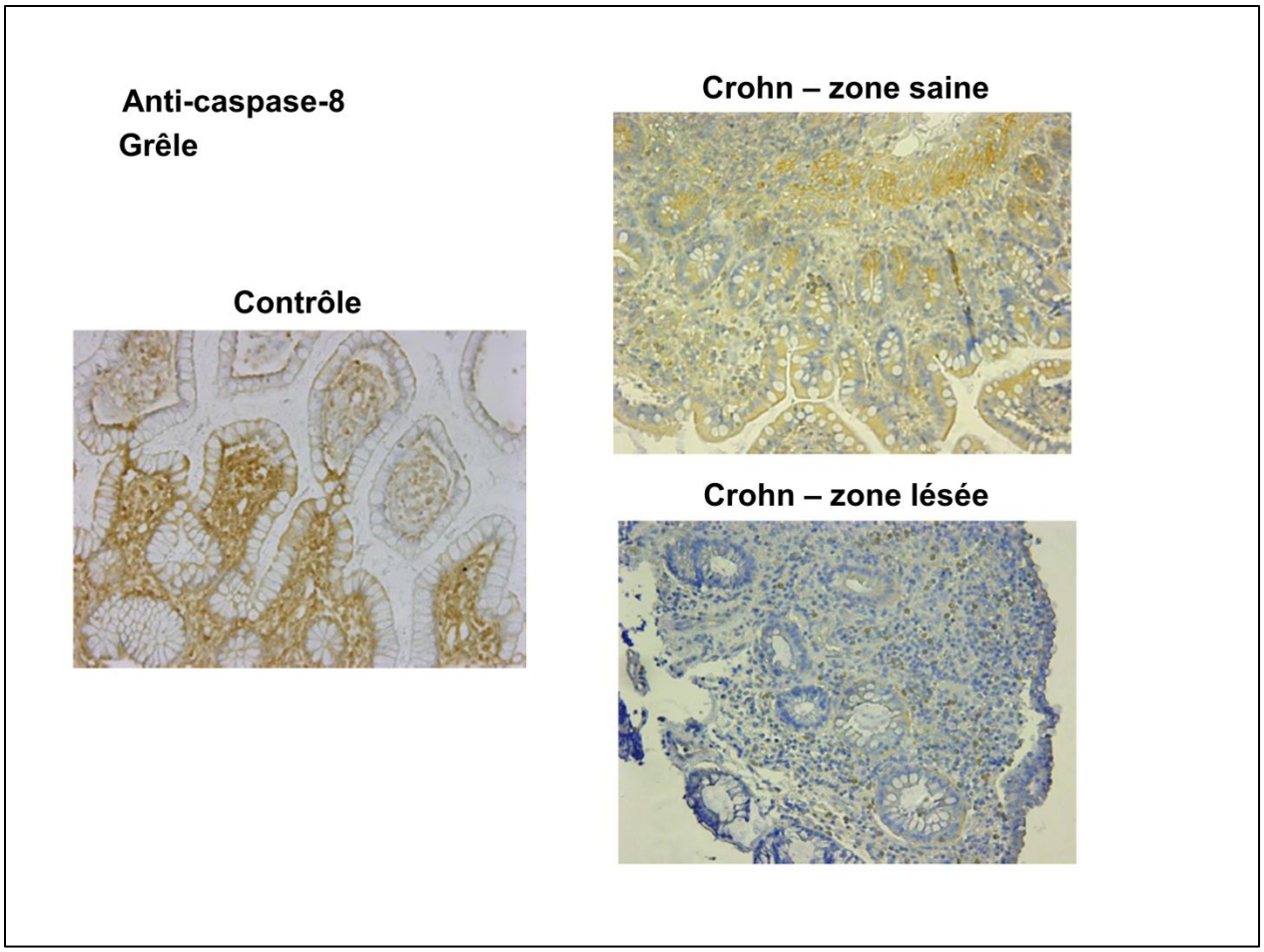

FIGURE 8 : marquage immunohistochimique de coupe de muqueuse grêlique avec un anticorps anti-caspase-8 chez des sujets sains et des patients atteints de MC.

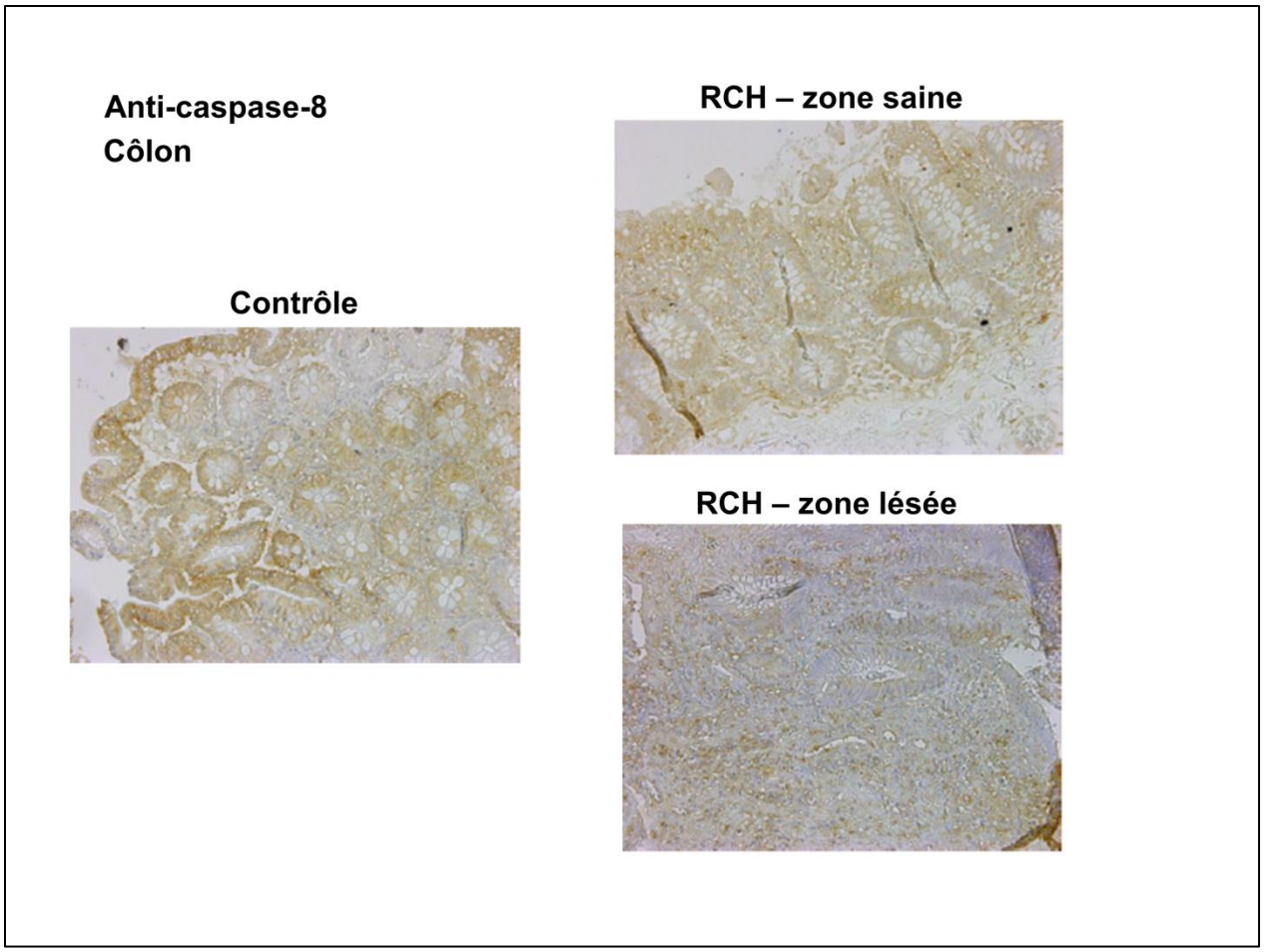

FIGURE 9 : marquage immunohistochimique de coupe de muqueuse colique avec un anticorps anti-caspase-8 chez des sujets sains et des patients atteints de RCH.

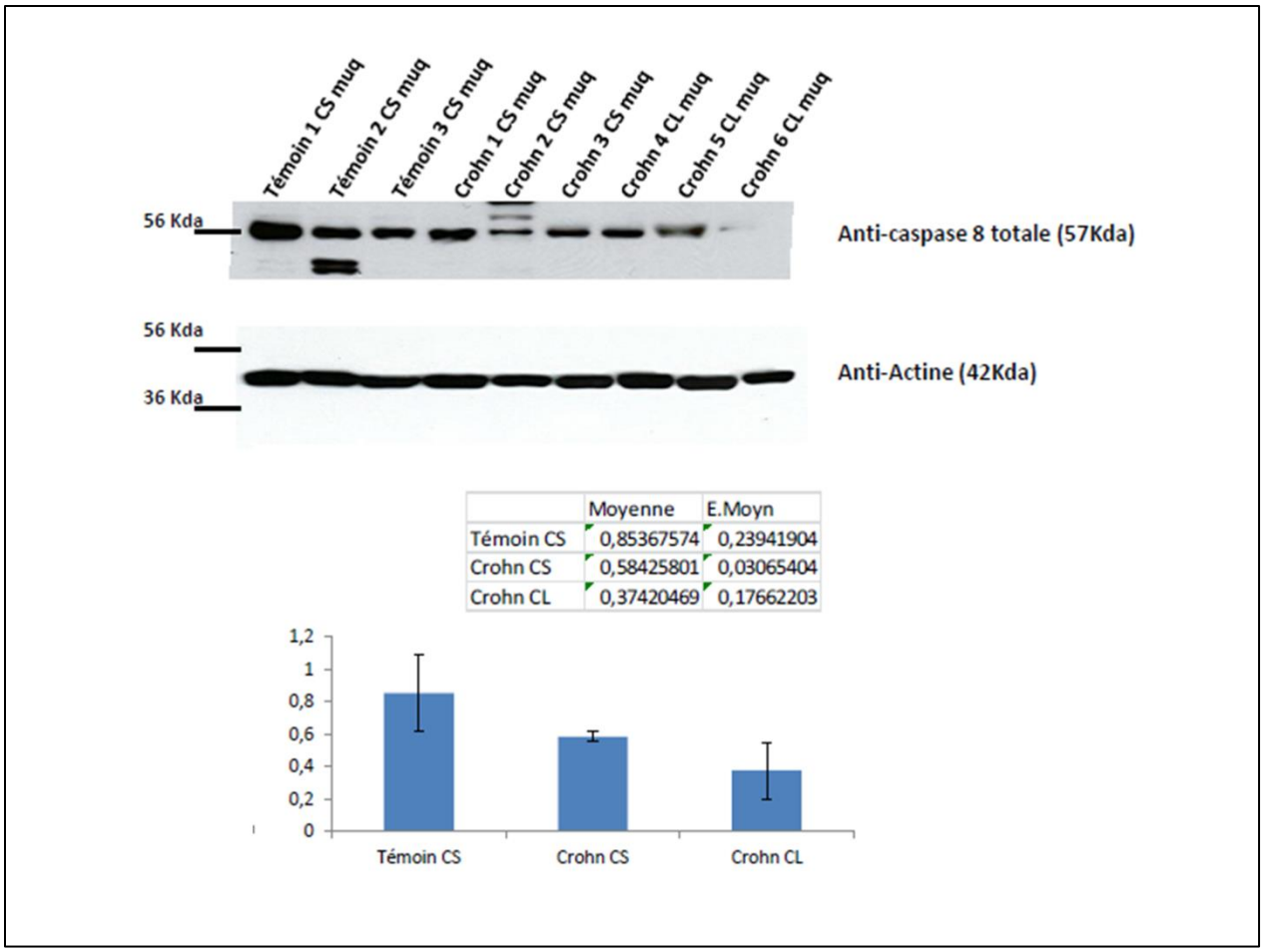

FIGURE 10 : analyse en Western-blot de l'expression de la caspase-8 dans la muqueuse colique de sujets sains et de patients atteints de MC (muqueuse saine, CS et muqueuse lésée, CL).

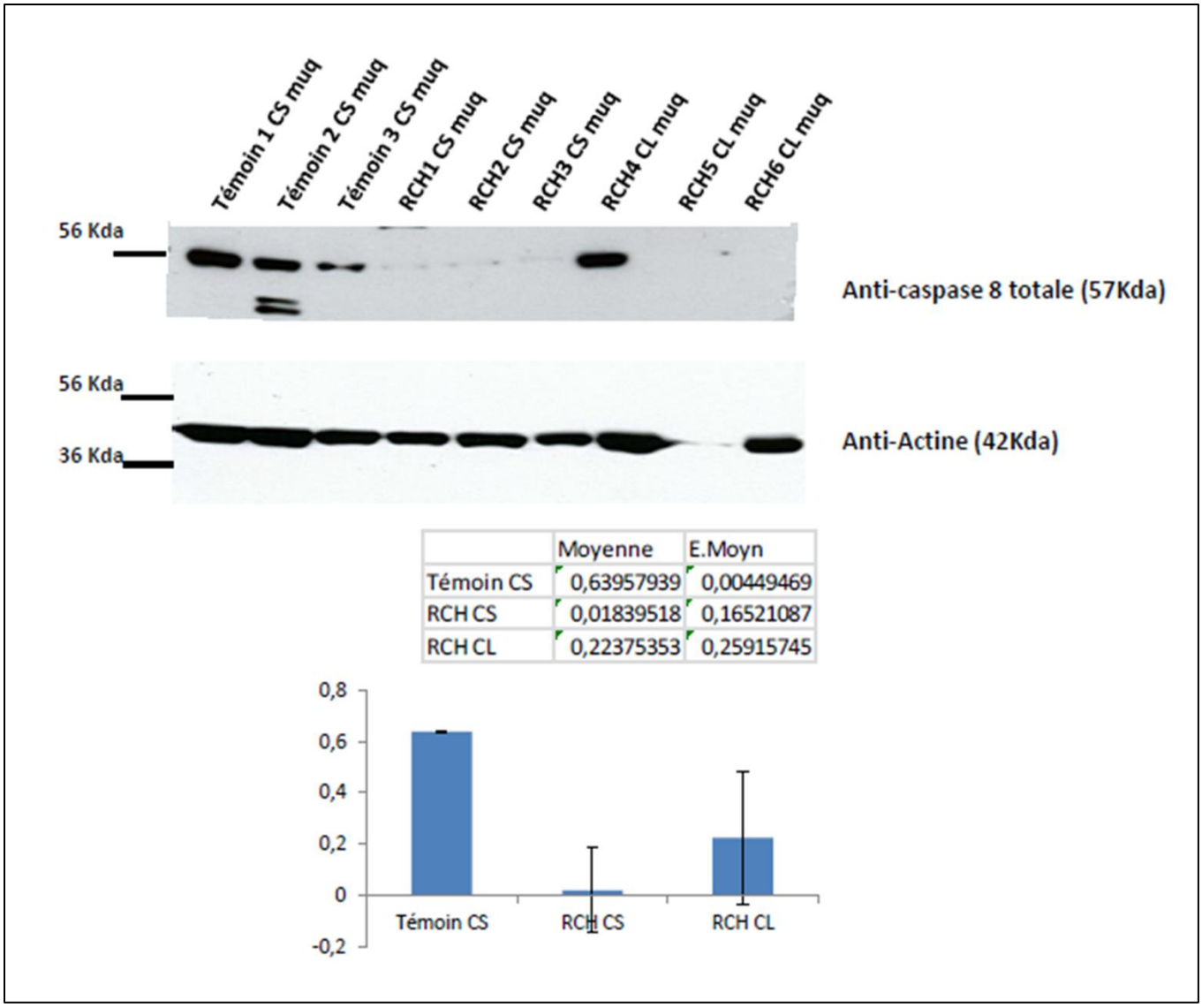

FIGURE 11 : analyse en Western-blot de l'expression de la caspase-8 dans la muqueuse colique de sujets sains et de patients atteints de RCH (muqueuse saine, CS et muqueuse lésée, CL).

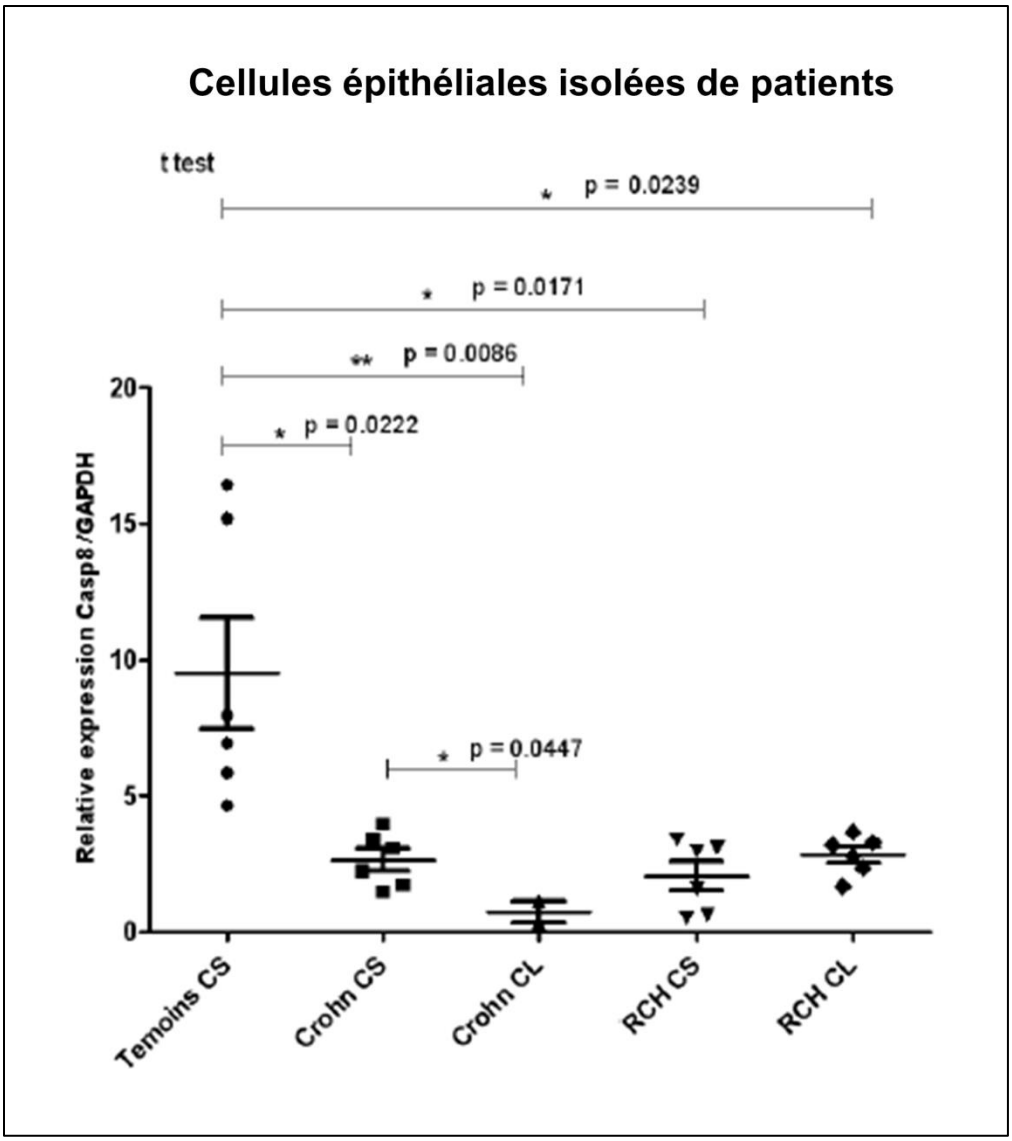

FIGURE 12 : analyse par PCR en temps réel de l'expression de l'ARN caspase-8 dans les cellules épithéliales isolées de la muqueuse colique de sujets sains et de patients atteints de MICI (Crohn et RCH en zone saine, CS et en zone lésée, CL).

IV. L'hypothèse microbienne

A. Rôle de la flore intestinale dans les MICI :

L'interaction entre l'homme et les bactéries commensales digestives est appelée homéostasie intestinale. Dans les conditions normales du développement humain, la flore bactérienne, variée et complexe, colonisant progressivement le tube digestif, participe à l'éducation du système immunitaire intestinal [219]. L'intégrité de la muqueuse intestinale est assurée ensuite par un équilibre entre les bactéries « bénéfiques » et pathogènes au niveau de la flore luminale et par l'intégrité de la barrière muqueuse intestinale composée de la couche jointive de cellules épithéliales, la couche de mucus et les différents peptides antimicrobiens. L'apparition d'une dysbiose ou d'une altération de la barrière intestinale, va conduire à une rupture de l'homéostasie intestinale facilitant la prolifération de bactéries pathogènes, leur adhésion à la muqueuse digestive et leur passage à travers l'épithélium [219]. Une invasion bactérienne anormale entraine une réponse inflammatoire muqueuse pouvant persister et s'amplifier en cas de susceptibilité génétique.

De nombreuses données supportent actuellement le rôle de la flore intestinale dans la physiopathologie des MICI [220-223]. Les patients atteints de MC présentent une amélioration clinique après dérivation du flux fécal lors de la mise en place d'une stomie et la remise en continuité du tube digestif est souvent suivie d'une récurrence de l'inflammation intestinale [224, 225]. De plus, l'iléon terminal et le côlon qui sont les segments intestinaux qui présentent la plus grande quantité de bactéries sont atteints plus fréquemment au cours des MICI.[5] Ces différentes observations sont en faveur du déclenchement de l'inflammation intestinale par les bactéries et autres microbes présents dans la lumière intestinale.

Comme les bactéries sont les éléments microbiens les plus abondants présents dans la lumière intestinale, de nombreuses études se sont intéressées à la composition de la flore luminale et adhérente à la muqueuse chez les patients atteints de MICI [226-231]. Plusieurs agents pathogènes pouvant être mis en évidence dans la lumière digestive, comme *Mycobacterium avium paratuberculosis*, ont été incriminés dans le développement des MICI sans qu'aucun n'ait pu être formellement impliqué [232] Par contre, il a été clairement démontré que les patients atteints de MICI avaient une augmentation de nombre de bactéries adhérentes à la muqueuse et une altération de la composition de leur microbiote intestinal comparés aux sujets sains [230, 231]. Cette altération du microbiote fécal est appelée dysbiose. Chez les patients atteints de MICI, la dysbiose est caractérisée par une augmentation des souches de bactéroïdes, d'*Escherichia coli* adhérente et invasive et d'entérocoques et par une diminution des souches de bifidobactéries et lactobacilles [226, 228, 230]. Ce déséquilibre entre les bactéries « pathogènes » et les bactéries « bénéfiques » pourrait être à l'origine de l'inflammation muqueuse.

Il a aussi été démontré que les patients atteints de MICI présentaient une perte de tolérance envers les bactéries commensales du tube digestif [233, 234]. Les études génétiques chez les patients atteints de MICI ont permis une meilleure compréhension des interactions entre l'hôte et la flore commensale. En effet, Les patients atteints de MICI présentent des anomalies au niveau de gènes impliqués dans la reconnaissance et l'élimination des bactéries [108, 235-237].

Finalement, les modèles animaux apportent eux aussi des éléments en faveur d'une implication de la flore intestinale dans les MICI. Dans les modèles murins de colite, la flore commensale est nécessaire au développement de l'inflammation intestinale et les souris élevées dans un milieu stérile sans germes ne développent pas de colite [238].

En résumé, les données de la littérature suggèrent que la flore intestinale participe activement au développement et à l'entretien de l'inflammation intestinale chez des sujets

génétiquement prédisposés. Bien que le mécanisme exact soit encore inconnu, les hypothèses sont une infection persistante par un agent pathogène spécifique, une dysbiose, l'augmentation de l'exposition aux antigènes bactériens due à une altération de la barrière intestinale et une réponse immunitaire aberrante dirigée contre la flore commensale.

B. Rôle du microbiote dans les modèles « aluminium » et « caspase-8 » :

1. Aluminium et flore intestinale

L'aluminium entraine une altération de l'homéostasie intestinale avec une modification de la flore adhérente colique chez la souris.

Nous avons supposé que l'aluminium pouvait participer au déclenchement d'une inflammation intestinale par l'altération de la barrière épithéliale conduisant à la perturbation de l'homéostasie intestinale. Nous avons réalisé une étude quantitative et qualitative de la flore bactérienne adhérente au niveau de la muqueuse colique chez des souris C57Bl/6 exposées à l'aluminium phosphate pendant 4 semaines. Aucune différence n'est observée en ce qui concerne la mesure quantitative de la flore anaérobie totale, des lactobacilles, des entérobactéries et des cocci gram+ dans les prélèvements de côlon des animaux contrôles et traités par l'aluminium (FIGURE 13). Par contre, l'analyse qualitative de la flore adhérente colique montre une fréquence plus élevée de bifidobactéries et d'entérocoques chez les animaux traités par l'aluminium comparés aux contrôles (FIGURES 14a et 14b).

Chez la souris, la flore colique est principalement constituée de lactobacilles et de bifidobactéries. Si la flore luminale est extrêmement riche avec plus de 109 bactéries, la flore adhérente à la muqueuse colique est paradoxalement beaucoup plus faible. Cette différence s'explique par les propriétés défensives de la barrière intestinale. L'augmentation de fréquence

des bifidobactéries et des entérocoques que nous observons au niveau de la flore adhérente témoignerait donc d'une altération de la barrière muqueuse avec un enrichissement du nombre de bactéries au contact de l'épithélium.

L'aluminium diminue la croissance des bifidobactéries in vitro

Nous avons démontré que l'aluminium entrainait une altération de la barrière intestinale. D'autre part, au cours de la MC, un déséquilibre de flore au niveau intestinal a été mis en évidence [239]. Nous avons voulu approfondir cette observation en étudiant l'effet de l'aluminium sur la croissance bactérienne. Nous avons supposé que l'aluminium pouvait augmenter la croissance de bactéries pro-inflammatoires et diminuer à l'inverse la croissance de bactéries commensales « bénéfiques ».

Nous avons isolé des souches bactériennes de type lactobacille, entérobactérie (*E. sakazakii*) et bifidobactérie présentes dans la flore adhérente de souris C57Bl/6. Ces souches ont été incubées en présence d'aluminium phosphate et une analyse séquentielle de la croissance bactérienne a ensuite été réalisée avec dénombrement. Aucun effet de l'aluminium sur la croissance de la souche lactobacillaire ni sur la croissance d'*E. sakazakii* n'a été observé (FIGURE 15b et 15c). Par contre, une diminution très nette de la croissance de la souche de type bifidobactérie est observée en présence d'aluminium à partir de la 24ème heure (FIGURE 15a).

En conclusion, l'aluminium est responsable d'une diminution de la croissance des bifidobactéries *in vitro*. Cette diminution pourrait expliquer une dysbiose colique en partie responsable de l'augmentation de souches bactériennes pro-inflammatoires telles que les entérocoques au niveau de la muqueuse colique et de l'aggravation d'une colite expérimentale chez la souris.

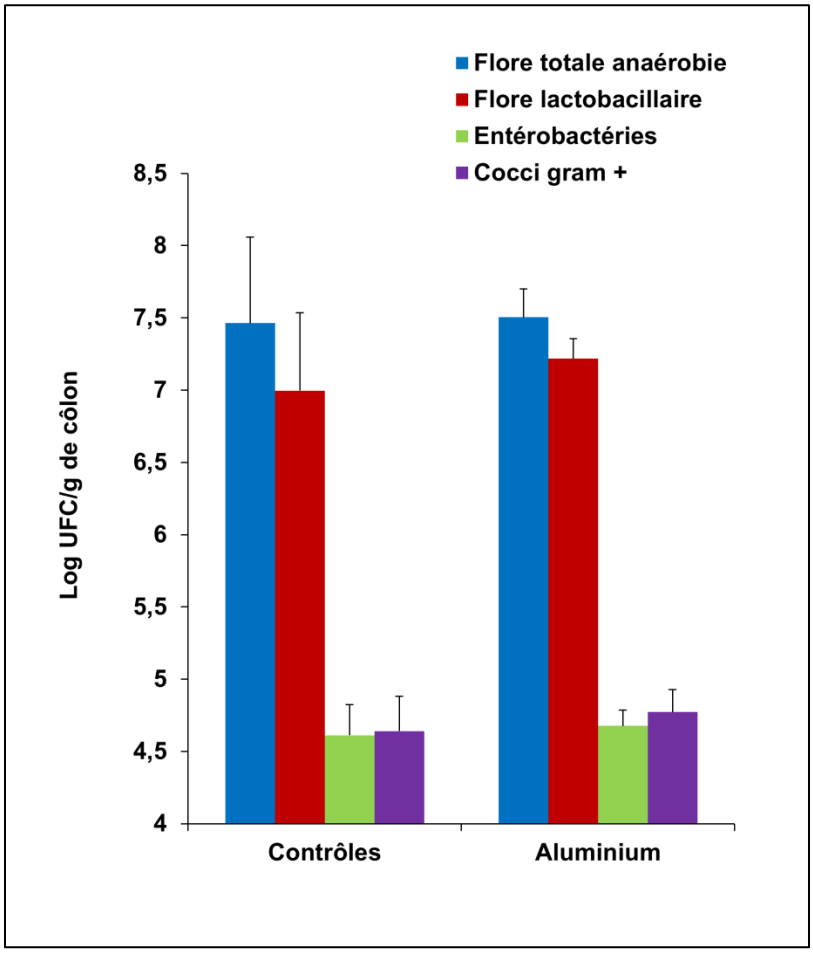

FIGURE 13 : Analyse quantitative de la flore adhérente colique de souris au cours d'une intoxication chronique par l'aluminium. Ce graphique représente la quantification de la flore totale anaérobie, de la flore lactobacillaire, des entérobactéries et des cocci gram+. L'histogramme représente les valeurs moyennes du nombre de colonies par gramme de côlon de chaque groupe.

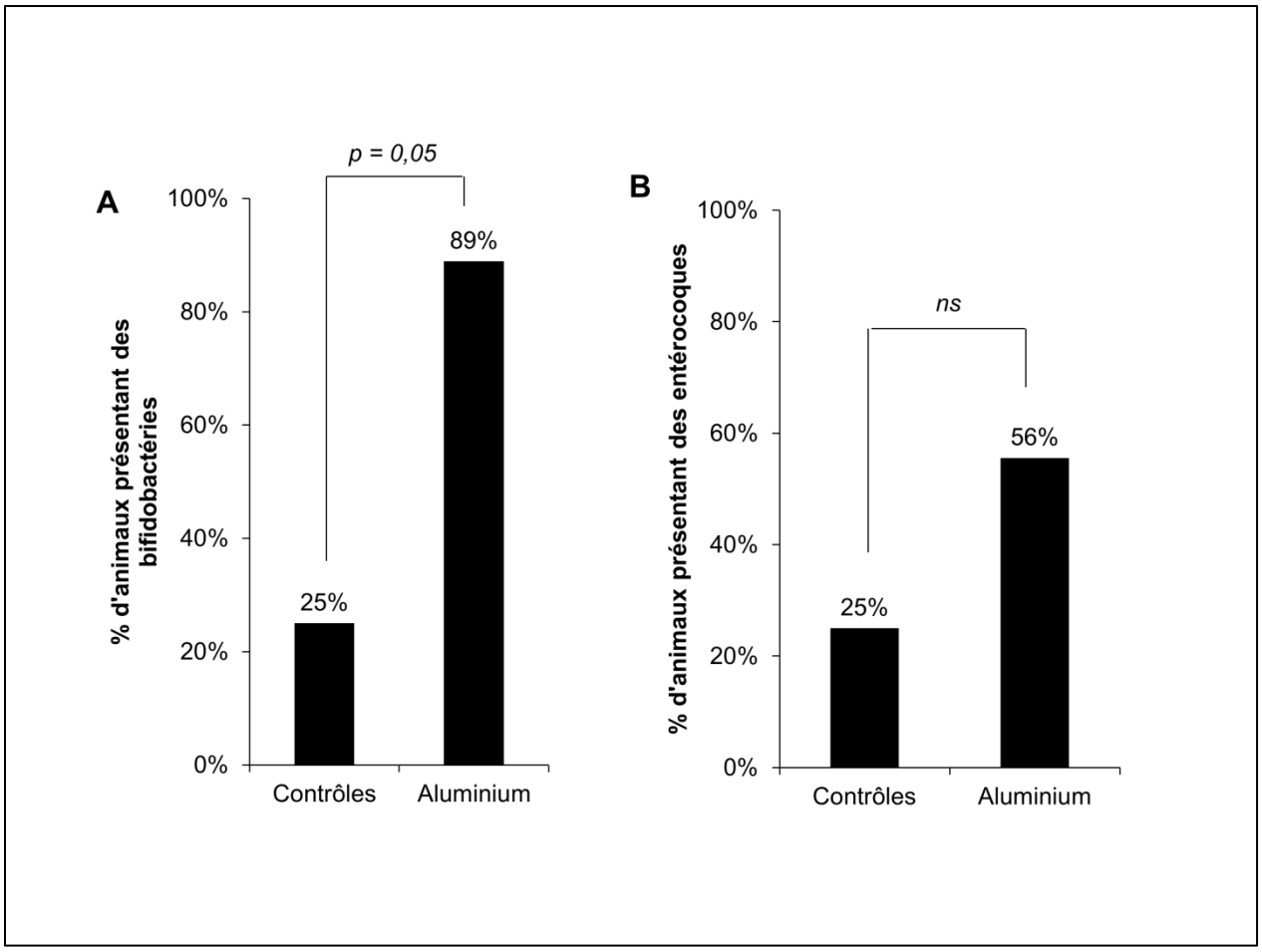

FIGURE 14 : L'aluminium favorise l'adhérence des bactéries au niveau de la muqueuse colique chez la souris. Représentation du pourcentage d'animaux de chaque groupe pour lesquels des bifidobactéries (**A**) et des entérocoques (**B**) ont été identifiés au niveau de la muqueuse colique de souris C57bl/6 après une intoxication orale d'aluminium phosphate de quatre semaines. L'identification bactérienne est réalisée après culture sur milieux spécifique.

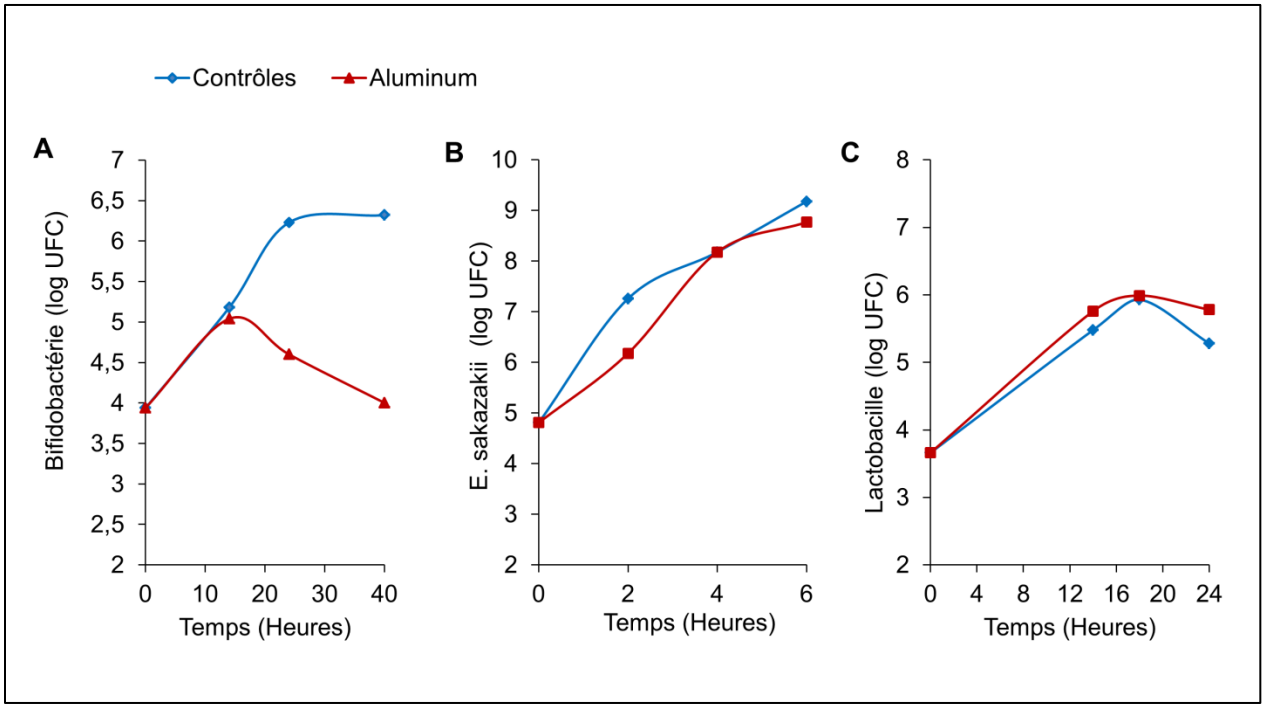

FIGURE 15 : L'aluminium diminue la croissance des bifidobactéries *in vitro*. Mesure de la croissance de trois souches bactériennes, une bifidobactérie (A), une entérobactérie (B) et un lactobacille (C), en présence d'aluminium phosphate stérile à la dose de 100µg/ml. Des dénombrements séquentiels sur gélose ont été réalisés à différents temps en fonction de la vitesse de croissance de chaque souche.

2. Caspase-8 et flore intestinale :

Dans un modèle de souris déficientes pour FADD, une des protéines du complexe apoptotique DISC, l'inflammation intestinale n'est observée qu'en présence d'une flore intestinale [121]. Effectivement, les souris déficientes pour FADD au niveau des cellules épithéliales intestinales, élevées dans un milieu stérile ne développent pas d'inflammation intestinale [121]. Nous avons aussi observé dans notre modèle de souris déficientes pour la caspase-8 l'importance des stimulations infectieuses pour le développement de l'inflammation intestinale. Nous avons observé que certaines souris déficientes pour la caspase-8 développaient une inflammation intestinale spontanée et que d'autres gardaient un phénotype sain. Pour étudier le rôle joué par la flore intestinale nous avons réalisé une expérience de cohabitât.

Des souris déficientes pour la caspase-8 au niveau des cellules épithéliales intestinales (*Casp8*$^{\Delta IEC}$) présentant un phénotype sain suggérant l'absence d'inflammation intestinale ont été séparées en deux groupes : un groupe contrôle restant dans leur cage initiale et un groupe « cohabitât » où les souris *Casp8*$^{\Delta IEC}$ saines étaient transférées dans une cage contenant une souris *Casp8*$^{\Delta IEC}$ malade. Chaque cage contenait en plus des souris contrôles sans déficit en caspase-8 (*Casp8*$^{fl/fl}$). Après seulement 4 jours de cohabitât, les souris *Casp8*$^{\Delta IEC}$ saines présentaient une perte de poids importante entrainant la mort des animaux alors que les souris *Casp8*$^{\Delta IEC}$ saines n'ayant pas changé de cage ne présentaient pas de perte de poids (FIGURE 16). Parallèlement, les souris *Casp8*$^{\Delta IEC}$ saines mises en cohabitât présentaient l'apparition de sang dans les selles et le sacrifice des animaux mettait en évidence une inflammation intestinale macroscopique qui n'était pas retrouvée chez les souris *Casp8*$^{\Delta IEC}$ saines contrôles (FIGURE 17 et 18).

Cette expérience démontre que l'inflammation intestinale se transmet entre des souris partageant la même flore commensale au sein de la même cage.

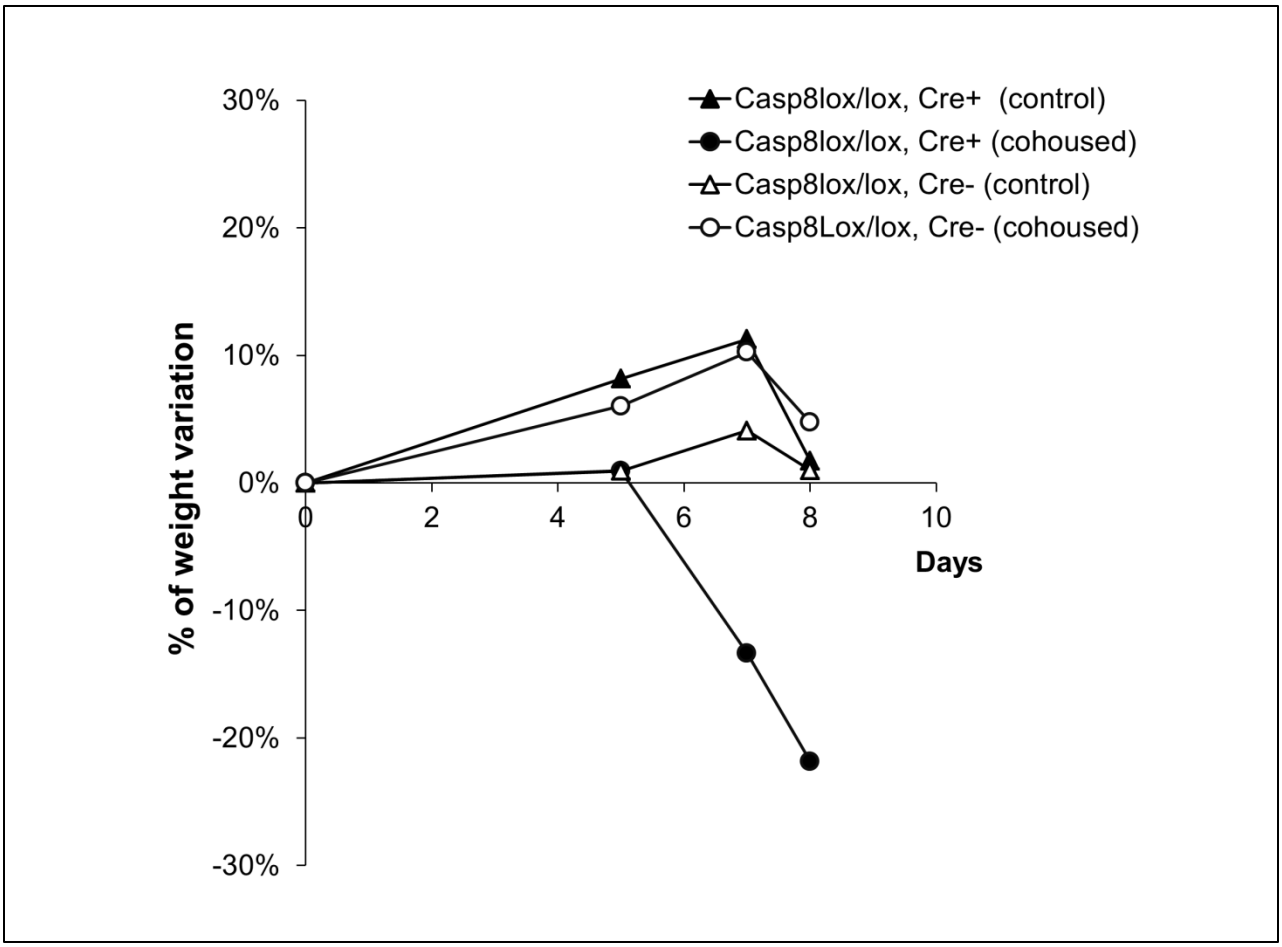

FIGURE 16 : variation du poids des souris au cours du temps. Les souris déficientes pour la caspase-8 non malades initialement et transférées en cohabitât (Casp8lox/lox, cre+, cohoused) avec des souris malades présentent une perte de poids importante par rapport au souris déficients pour la caspase-8 non malades maintenues dans leur cage initiale (Casp8lox/lox, cre+, control).

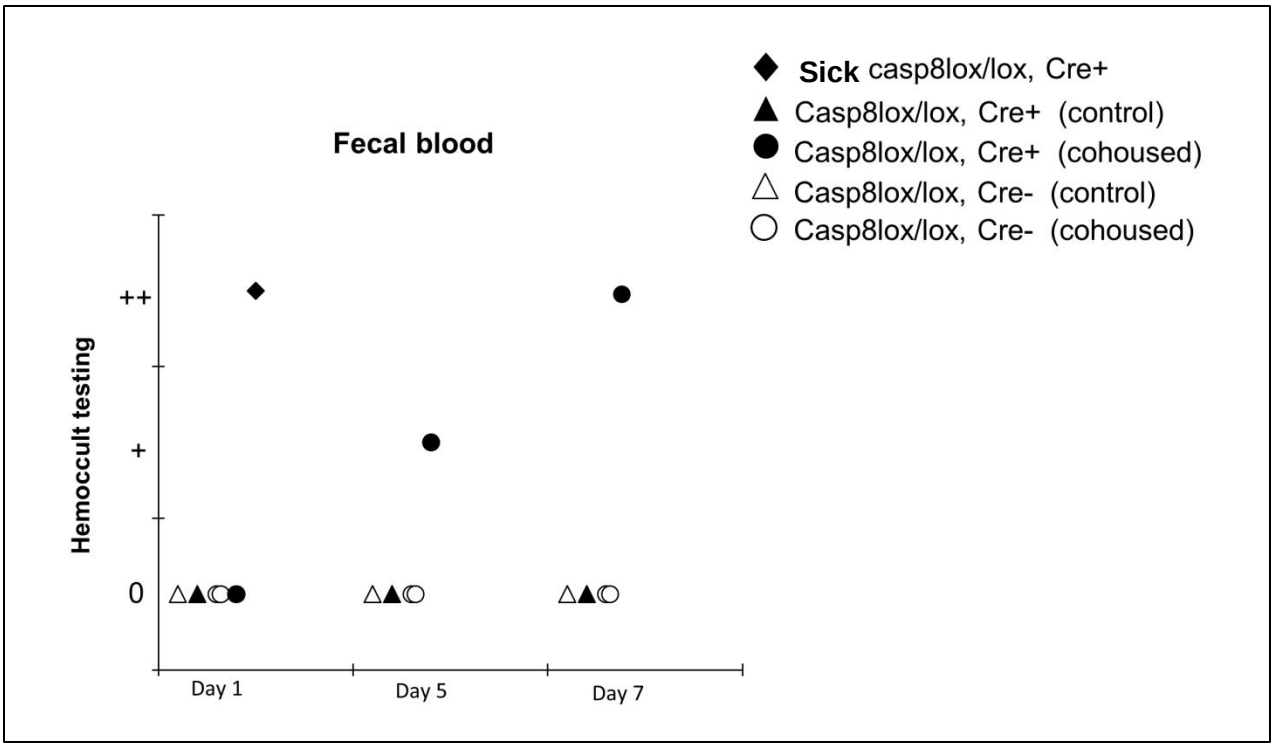

FIGURE 17 : Recherche de la présence de sang au niveau des selles de souris. La souris déficiente pour la caspase-8 initialement malade (Sick casp8lox/lox, cre+) présente du sang dans les selles dès le premier jour. On voit apparaitre progressivement du sang dans les selles des souris déficientes pour la caspase-8 non malades initialement et mises en cohabitât (Casp8lox/lox, cre+, cohoused).

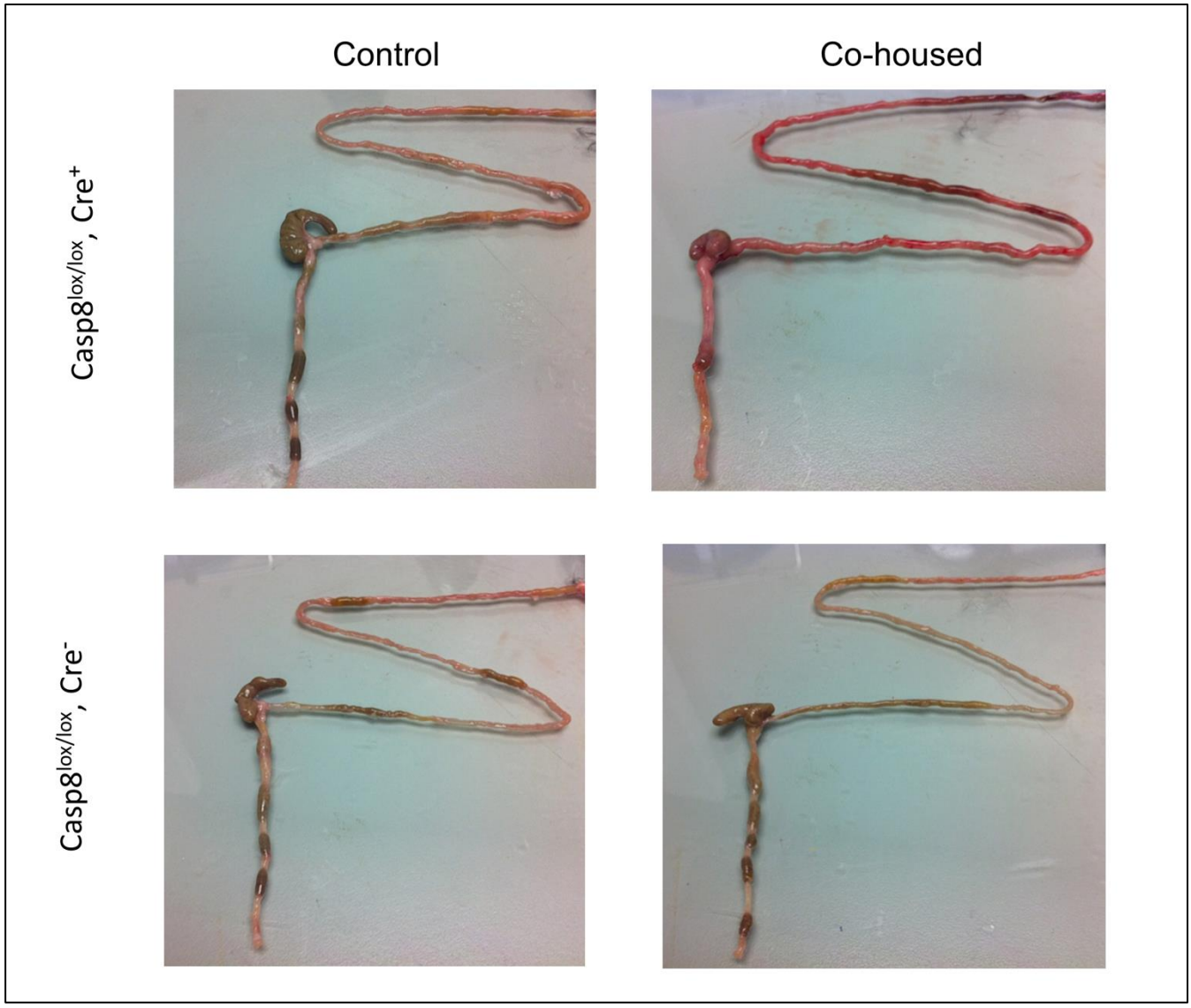

FIGURE 18 : analyse macroscopique de l'intestin des souris. Les souris déficientes pour la caspase-8 non malades initialement mise en cohabitât (Casp8lox/lox, cre+, cohoused) avec des souris malades développement dès le septième jour une inflammation iléocolique macroscopique alors que les souris déficientes pour la caspase-8 non malades initialement maintenues dans leur cage (Casp8lox/lox, cre+, control) ont une morphologie intestinale normale.

C. Syndrome de l'intestin irritable, probiotiques et *Saccharomyces cerevisiae* :

La flore intestinale commensale ou pathogène est impliquée dans de nombreuses pathologies et en particuliers dans la physiopathologie des MICI et du syndrome de l'intestin irritable. Le syndrome de l'intestin irritable est un trouble fonctionnel gastro-intestinal fréquent (5 à 15% de la population générale) caractérisé par la présence de douleurs abdominales chroniques et récurrentes associées à une modification du transit intestinal sans anomalie organique macroscopique [147, 240, 241]. Le diagnostic du syndrome de l'intestin irritable est défini selon les critères de Rome III par la présence de douleurs abdominales au moins 3 jours par mois pendant 3 mois et l'association à au moins deux des trois symptômes suivants : (1) Amélioration à la défécation, modification de la consistance (2) ou de la fréquence (3) des selles [242]. Au cours des dernières décennies, la plupart des études concernant la physiopathologie du syndrome de l'intestin irritable se sont focalisées sur les troubles de la motricité colique, l'hypersensibilité viscérale et l'interaction entre le cerveau et l'intestin [243]. Cependant des données plus récentes ont montré que d'autres mécanismes pourraient être impliqués comme l'inflammation intestinale, les infections digestives, une réponse immunitaire anormale, une modification de la flore intestinale ou des facteurs alimentaires [177, 243-248]. De plus, plusieurs études ont montré la présence d'anomalies microscopiques de la muqueuse intestinale chez des patients présentant les critères de Rome III [249, 250]. Le rôle de ces différents facteurs dans le développement du syndrome de l'intestin irritable est encore méconnu.

Bien que les troubles de la motricité intestinale restent considérés comme le mécanisme principal à l'origine du syndrome de l'intestin irritable, des données récentes sont en faveur d'un rôle de l'inflammation intestinale dans la physiopathologie de l'intestin irritable [243]. Effectivement, l'analyse immunohistochimique de la muqueuse de patients atteints du syndrome

de l'intestin irritable montrait la présence d'une infiltration par des cellules immunitaires activées incluant des lymphocytes T, des neutrophiles et des cellules mastocytaires [251]. Comme pour les MICI, d'autres études ont montré que la flore intestinale était probablement un acteur important dans la physiopathologie du syndrome de l'intestin irritable. Les patients ayant présenté un épisode de gastroentérite aigue sont plus à risque de développer un SSI. Il a aussi été démontré que la flore intestinale des patients atteints de SII était différente comparée à des sujets contrôles avec une diminution des bifidobactéries et une augmentation des entérobactéries [252-254]. La découverte de cette dysbiose [255, 256] a permis le développement d'approches thérapeutiques cherchant à moduler la flore intestinale chez les patients atteints de SII incluant l'utilisation des prébiotiques, des probiotiques et des antibiotiques [257, 258].

Les probiotiques sont des microorganismes vivants provenant de la flore intestinale ou de l'environnement qui sont capables d'apporter un bénéfice à l'hôte s'ils sont administrés à une dose suffisante [258]. Les mécanismes d'actions proposés pour l'effet bénéfique des probiotiques sont un renforcement de la barrière intestinale, une diminution du pouvoir pathogène de certaines bactéries et la modulation du système immunitaire intestinal [259, 260]. Des données expérimentales et cliniques suggèrent que des probiotiques appartenant à la famille des lactobacilles et des bifidobactéries pourraient être efficaces dans le traitement du SII. Une étude expérimentale a montré que la souche *Lactobacillus acidophilus* NCFM diminuait le seuil de douleur abdominale chez les rats via l'induction du récepteur aux opioïdes Mu et des récepteurs aux cannabinoïdes [261]. Ces récepteurs sont exprimés dans le côlon et jouent un rôle dans la modulation de l'inflammation et de la sensibilité viscérale. Au niveau clinique deux méta-analyses ont montré un bénéfice des probiotiques dans le SII. La première méta-analyse étudiait 19 essais randomisés contrôlés contre placébo chez 1650 patients atteints du SII et concluait à une efficacité des probiotiques par rapport au placébo (RR de l'absence d'amélioration = 0.71

[95% CI 0.57 to 0.88]) [262]. Une deuxième méta-analyse reprenant 42 essais randomisés contrôlés étudiant l'effet des bactéries produisant de l'acide lactique sur les symptômes du SII, montrait que 32 de ces études rapportaient un bénéfice de ces probiotiques sur au moins un des objectifs étudiés [263].

La flore intestinale est composée majoritairement de bactéries mais présente aussi des virus et des levures pouvant agir sur l'hôte et jouer un rôle dans les pathologies chroniques intestinales. Les patients atteints de MC présente dans environs 60% des cas des anticorps dirigés contre une levure *Saccharomyces cerevisiae* [264]. Des données récentes suggèrent qu'une autre levure cette fois-ci pathogène, *Candida albicans* pourrait être à l'origine de la production de ces anticorps chez les patients atteins de MC et donc participer au développement de cette pathologie [232]. A l'inverse, des levures ont aussi été testé comme probiotique dans différentes pathologies intestinales [265]. *Saccharomyces boulardii* une souche de levure très répandue dans l'environnement a montré des propriétés bénéfiques dans la prévention et le traitement des infections digestives et le traitement des MICI [265]. Dans ces pathologies, *S. boulardii* traite principalement la diarrhée grâce à ces propriétés anti-inflammatoire et immuno-régulatrice, en particulier par l'augmentation de l'expression du récepteur nucléaire PPARγ [266]. Les récepteurs PPARs (peroxisome proliferator activated receptors) sont des récepteurs nucléaires exprimés au niveau du côlon principalement au niveau des cellules épithéliales intestinales qui présentent des propriétés anti-inflammatoires [267]. Récemment, plusieurs études ont montré que PPARα présentait des effets anti-inflammatoire et anti-nociceptif après son activation par le palmitoylethanolamide dans des modèles animaux d'arthrite et d'inflammation [268-271].

Le rôle des levures et en particulier celui de *Saccharomyces cerevisiae* dans la modulation de l'inflammation et de la douleur intestinale au cours du syndrome de l'intestin irritable reste méconnue. Plusieurs études ont testé *Saccharomyces boulardii* dans le traitement de l'intestin

irritable et une seule de ces études démontrait une amélioration de la diarrhée chez une majorité de patients sans effet sur les douleurs abdominales [265, 272, 273]. Même si *S. cerevisiae* appartient à la même espèce que *S. boulardii* [274], ces deux souches sont très différentes d'un point de vue génétique, physiologique et métabolique [275, 276]. Dans notre travail nous avons donc décidé d'étudier les effets de *Saccharomyces cerevisiae* sur l'inflammation et la douleur abdominale dans un modèle animal de SII. Nous avons ensuite étudié l'utilisation de *Saccharomyces cerevisiae* pour le traitement des patients atteints de SSI dans un essai thérapeutique prospectif contrôlé contre placebo.

B. *Saccharomyces cerevisiae CNCM I-3856 strain decreases intestinal pain and induces PPAR alpha activation in the gut.*

Christel Rousseaux[1], Guillaume Pineton de Chambrun[2, 3], Caroline Dubuquoy[1], Laurent Dubuquoy[2], Pascal Vandekerckove[4] and Pierre Desreumaux[1, 2, 3].

[1]Intestinal Biotech Development, Lille, France

[2]Inserm U995, North of France University, Lille, France

[3]Gastroenterology department, Lille University Hospital, Lille France

[4]Lesaffre International, Lesaffre Human Care, France

Référence de l'article:

Rousseaux C, Pineton de Chambrun G, Dubuquoy C, Dubuquoy L, Vandekerckove P, Desreumaux P. Saccharomyces cerevisiae CNCMI-3856 strain decreases intestinal pain and induces PPAR alpha activation in the gut. Manuscript in preparation. 2014.

1. Introduction:

Nowadays, there is growing evidence suggesting a potential role of intestinal microbiota in numerous pathologies and more precisely in IBS pathophysiology and symptom generation [255, 256]. These qualitative and quantitative changes in intestinal microbiota may induce different effects on the intestinal mucosa including mucosal barrier defects and immune activation which may contribute to symptom generation. Studies in IBS patients have aimed to change intestinal microflora with different therapeutic approaches, such as the use of prebiotics, probiotics, synbiotics, and non-absorbable and systemic antibiotics [257, 258].

Probiotics are live microorganisms when given in sufficient amount confer a health benefit to the host [258]. Probiotics can enhance gut barrier function, inhibit pathogen binding and modulate gut inflammatory response. Experimental and clinical data suggest that specific probiotics belonging to the *Lactobacillus* and *Bifidobacterium* species may attenuate abdominal pain (ref). Previous studies have demonstrated that a specific strain of *Lactobacillus acidophilus* NCFM strain is able to decrease the pain perception threshold in rats via induction of Mu opioid receptors and cannabinoid receptors [261]. These receptors are expressed in the colon where they play role in the modulation of inflammation and pain.

Saccharomyces boulardii, a species of yeast widely distributed, has been described as a biotherapeutic agent since several clinical trials displayed its beneficial effects in the prevention and the treatment of intestinal infections and the treatment of inflammatory bowel disease [265]. All these diseases are characterized by acute diarrhoea. All *S. Boulardii* beneficial effects are correlated to its anti-inflammatory and immune-modulatory properties. Among the different mechanism of action involved in the regulation of inflammation, it has been demonstred that *S. boulardii* up-regulates the expression of PPARγ [266].

PPARs (peroxisome proliferator activated receptors) are nuclear receptors expressed in the colon and more specifically by the epithelial cells and are known to exert anti-inflammatory properties [267]. Recent studies have demonstrated that PPARα mediates anti-inflammatory and antinociceptive effects of PEA (palmitoylethanolamide) in animals with adjuvant-induced arthritis, formalin-evoked pain and carrageenan inflammation [268-271].

Roles of yeasts and more precisely of *Saccharomyces cerevisiae* strain on the modulation of intestinal pain remain unknown. Even if S. cerevisiae belongs to the same species than *S. boulardii* [274], it has been well-described that these two strains differ genetically, metabolically and physiologically [275, 276].

So the aim of this study was to evaluate the functional role of *Saccharomyces cerevisiae* CNCM I-3856 strain on intestinal pain in rats and their mechanisms of actions in healthy rats or rats with a hypersensitivity induced by butyrate instillations using the colorectal distension method. We have also investigated the function of PPARα in mediating this effect.

2. Results:

In vitro screening of potential analgesic and/or anti-inflammatory properties of yeasts

In a first step of experiments, we evaluated the capacity of 10 different strains of *Saccharomyces cerevisiae* (provided by Lesaffre company) on their ability to induce the expression of receptors involved in the regulation of pain and inflammation, known to be induced by probiotics (data not shown). We evaluated the level of expression of opioid receptors (MOR), cannabinoid receptors (CB1 and CB2), PPARs receptors (PPARγ and PPARα) after stimulation of HT-29 colonic cells by the different yeast strains.

In vitro, colonic epithelial HT-29 cells were stimulated by different strains of yeasts for 0 to 3h. IL-10 expression was induced at the mRNA level by the strain CNCM I-3856. These results confirm the good safety profile of the strain CNCMI-3856 (Fig. 1).

Then we evaluated the effect of yeasts stimulation on the expression of receptors involved in the regulation of pain, known to be regulated by probiotics: opioid receptors (MOR, KOR & DOR), cannabinoid receptors (CB1 & CB2) and PPARs (γ and α). In stimulated HT-29 cells, only the strain CNCMI-3856 was able to induce one receptor: PPARα (Fig. 1).

Moreover, we observed that the expression of a target gene of PPARα was induced by the CNCM I-3856 strain. CPT1 (Carnitine Palmitoyl Transferase) is an enzyme involved in the different steps of transfer and β-oxydation of fatty acids in the mitochondria. These results indicated that expression and activation of PPARα was induced by CNCM I-3856 at the mRNA level.

Evaluation of PPARα expression at the protein level after administration of CNCM I-3856 in vivo in rats

In vivo, in rats, after 15 days of oral administration the strain CNCM I-3856 at the dosage of 10^6 cells/day, we performed immunohistochemistry staining using a specific antibody directed against PPARα on colonic section embedded in paraffin (Fig. 2). We observed a strong and specific staining of the epithelial cells, confirming the results obtained in vitro.

Effect of Saccharomyces cerevisiae CNCM I-3856 strain on the activation of PPAR

In vivo, we used a model of transgenic mice which expressed the luciferase gene after PPAR activation. We administered the strain CNCM I-3856 by oral gavage to transgenic mice expressing in their whole body the element response of PPAR, the PPRE fused to the luciferase gene reporter.

As described in the figure 3, bioluminescent activity was located on the abdominal region, particularly in the gut region. The administration of GED-0507-34-levo at the dosage of 10^7 cells /day increases the spontaneous luciferase activity between untreated and CNCM I-3856- treated groups. In conclusion, oral administration of CNCM I-3956 at 10^7cells/day activates *in vivo* PPARα.

Effect of Saccharomyces cerevisiae CNCM I-3856 strain on the inflammation in the model of colitis induced by chemical agents

As we have observed *in vitro* the induction of receptors involved in the regulation of pain and inflammation, we evaluated *in vivo* the potential anti-inflammatory properties of CNCM I-3856. We evaluated the effect of oral administration of CNCM I-3856 (1mg/kg/day) in the model

of colitis induced by TNBS in C57bl6 mice. CNCM I-3856 was administered in a preventive mode 5 days before colitis induction and until euthanasia of the mice 4 days after colitis induction.

CNCM I-3856 exerts significant anti-inflammatory effects on colonic lesions at the macroscopic level compared to untreated colitic mice receiving only the vehicle, with respectively, 1.71±0.74 vs 3.89±0.41, p=0.038 (Fig. 4).

Similar results were obtained at the histological level showing a significant improvement of the colonic lesions in the group of mice having received CNCM I-3856 compared to mice having received only the vehicle, with respectively 1.5±0.26 vs 3.11±0.56, p=0.05 (Fig. 4).

In vivo, oral administration of CNCM I-3856 reduced significantly the inflammation in the gold standard model of colitis.

Effect of Saccharomyces cerevisiae CNCM I-3856 strain in the pain perception

We assessed the visceral perception of rats using a validated technique: colorectal distension. In untreated rats, a mean colorectal distension of 50 ± 2 mm Hg is required to induce pain, characterized by clearly visible abdominal contractions and elevation of the hindpart of the animal's body. Oral administration of the CNCM I-3856 strain (10^6 CFU/d) during 15 d decreased normal visceral perception, allowing a 20% increase in the pain threshold (p=0.013). This analgesic effect was enhanced as the CNCM I-3856 dosage was increased from 10^6CFU/d to 10^9 CFU/d (p<0.0001) (Fig. 5).

We then performed an experiment to estimate the time period necessary to *S. cerevisiae* CNCM I-3856 for enhancing the resistance to intestinal pain perception of healthy rats. The animals were fed with 10^6 or 10^7 cfu/day during 7, 10 or 15 days and then tested for intestinal nociception (fig. 6). Results showed that at 10^6 cfu/days the enhancement to intestinal pain was

significant after 15 days of feeding with yeast. A significant improving of intestinal nociception was obtained with the 10^7 cfu/day dosage after 10 days (Fig. 6). We evaluated the time-course of the analgesic effect induced by oral administration of CNCM I-3856 at the dosage of 10^7 cells/days. We observed that the analgesic effect was induced rapidly within 10 d, maintained for the duration of the treatment (from day 10 to 4 weeks of administration) and disappeared 3 d after the last CNCM I-3856 administration (Fig. 6).

In a model of chronic colonic hypersensitivity, elicited by butyrate enemas and mimicking irritable bowel syndrome (Fig. 7), the hypersensitivity of rats was improved by the CNCM I-3856 strain: treatment with CNCM I-3856 increased the colorectal distension threshold by 44% compared to that in untreated rats ($p<0.03$). Analgesic property of CNCM I-3856 after 15 days of feeding was similar to the injection of 1 mg/kg of morphine (Fig. 7).

Involvement of PPARα in the regulation of visceral pain perception induced by Saccharomyces cerevisiae CNCM I-3856 strain in the pain perception.

To evaluate the involvement of PPARα in the regulation of pain perception in analgesia-induced by CNCM I-5836, used at the optimal dosage (10^6 cells/days for 15 days), we performed 3 injections of a specific antagonist of PPARα, the GW6471 (30µg/kg) just 2 days before and for the third last injection just 30 min before the colorectal distension assay and we used as positive control, the fenofibrate (300mg/kg/day), a specific agonist of PPARα. Morphine was used also as positive control (intraperitoneal injection, 30 min before colorectal distension, 1mg/kg).

In untreated rats, a classical mean pressure value for colorectal distension around 50 mm Hg is required to induce visceral pain, characterized by clearly visible abdominal contractions and elevation of the hindpart of the animal's body. The positive control used in this experiment to validate the assay was the morphine, used at the dosage of 1mg/kg. The morphine induced a

significant analgesia in healthy rats compared to control rats with respectively 83±0.76 vs 52±1.45 p<0.001 (Fig. 8).

Injection of the specific PPARα antagonist in control rats, 30 minutes before colorectal distension, did not modify the pain threshold compared to control rats with respectively 53±1.9 vs 52±1.45, p=ns. In this experiment, oral administration of the CNCM I-3856 strain at the dosage of 10^6 cells/day for 15 days decreased significantly the normal visceral pain perception allowing a strong increase in the pain threshold of 21% compared to control rats with respectively 63±1.71 vs 52±1.45, p=0.01. In this model, we also demonstrated that oral administration of a specific PPARα agonist, the fenofibrate is able to induce significant analgesic effect (70±4.48 vs 52±1.45, p<0.01) (Fig. 8).

In the group of rats administered for 15 days with CNCM I-3658 the dosage of 10^6 cells/days received the 3 last days a concomitant intraperitoneal injection of the specific PPARα-antagonist before the colorectal distension assay, we observed that injections of GW6471, inhibited significantly the analgesic effect induced by the CNCM I-3856 strain compared to the rats receiving the CNCM I-3856 alone with respectively, 55.56±1.64 vs 63±1.71, p=0.02 (Figure 8). After injection of GW6471, the rats treated with CNCM I-5836 showed the same value for the pain threshold than the untreated control rats with respectively, 55.56±1.64 vs 52±1.45, ns (Fig. 8).

This experiment indicates that PPARα is involved in the regulation of pain perception induced by CNCM I-3856.

3. Materials and methods:

Cell lines

The colon carcinoma cell lines Caco-2 (ATCC HTB-39) and HT-29 (ATCC HTB-38) were routinely grown in DMEM supplemented respectively with 20% or 10% heat-FCS, and antibiotics. Cells were grown in monolayer, incubated at 37°C in 5% CO2 and 95% relative humidity. 200 000 cells/well were plated overnight to allow cell adhesion, after having change the medium, cells were stimulated for 0 to 20h with *S. cerevisiae* CNCMI-3856 strain.

Cell stimulation

S. cerevisiae CNCM I-3856 was resuspended in the culture medium (DMEM supplemented as described above) at the adequate concentration.

Gene expression at the mRNA level

Total RNA was isolated from epithelial colonic cells using Rneasy kit (Macherey Nagel, Hoerdt, France) according to the manufacturer's instructions. RNA quantification was performed using spectrophotometry. After treatment at 37°C for 30 min with 20-50 units of RNase-free DNase I (Roche Diagnostics Corporation, Indianapolis, IN, USA), oligo-dT primers (Roche Diagnostics Corporation, Indianapolis, USA) was used to synthesize single-stranded cDNA. mRNAs will be quantified using SYBR green Master Mix (Applera, Courtaboeuf, France) with human specific oligonucleotides for cytokines and PPARs (see table above) in a GeneAmp Abiprism 7000 (Applera, Courtaboeuf, France). In each assay, calibrated and no-template controls were included. Each sample was run in triplicate. SYBR green dye intensity will be analysed using the Abiprism 7000 SDS software (Applera, Courtaboeuf, France). All results were normalized to the unaffected housekeeping gene β-actin.

TNBS

Animal experiments were performed in accredited establishment at the Institut Pasteur from Lille (86/609/CEE) according to governmental guidelines. Animals were housed five per cage and had free access to standard mouse chow and tap water. For colitis induction, mice were anesthetized for 90–120 min and received an intrarectal administration of TNBS (40 µl, 150 mg/kg) dissolved in a 1:1 mixture of 0.9% NaCl with 100% ethanol (13, 18). Control mice received a 1:1 mixture of 0.9% NaCl with 100% ethanol or a saline solution using the same technique. Animals were killed 5 d after TNBS administration.

Macroscopic and histological indications of colitis were evaluated blindly by two investigators. The colon of each mouse was examined under a dissecting microscope (at a magnification of 5) to evaluate the macroscopic lesions according to the Wallace criteria. The Wallace score rates macroscopic lesions on a scale from 0 to 10 based on features reflecting inflammation, such as hyperemia, thickening of the bowel, and extent of ulceration. A colon specimen located precisely 2 cm above the anal canal was used for histological evaluation according to the Ameho criteria. This grading on a scale from 0 to 6 takes into account the degree of inflammation infiltrate, the presence of erosion, ulceration, or necrosis, and the depth and surface extension of lesions. *Saccharomyces cerevisiae* was administered orally once daily, starting 5 d before colitis induction.

Evaluation of analgesic properties in healthy rats

Nociception in animals was assessed by measuring the intracolonic pressure required to induce a behavioural response during colorectal distension (CRD) due to the inflation of a balloon introduced in the colon. This response is characterized by an elevation of the hind part of the animal body and clearly visible abdominal contraction corresponding to the severe

contractions [277-279]. Briefly, rats were anesthetized with volatile anaesthesia (2% isoflurane), the balloon (prepared as previously described in Bourdu & al, 2005 [278]) was inserted intrarectally in a minimally invasive manner to 7 cm from the anus, and the catheter will be taped to the base of the tail. After 5 minutes, rats were placed in the middle of a 40x40-cm Plexiglas box and the catheter was connected to an electronic barostat apparatus (Distender Series IIR™, G& J Electronics). Increasing pressure was continuously applied until pain behaviour was displayed or a cut-off pressure of 80 mm Hg was reached.

Time course protocol

To determine the time-course of analgesic effect induced by *S. cerevisiae* CNCMI-3856, we administered the strain by oral gavage (10^6 cells/day) to healthy rats. Evaluation of pain threshold by DCR began after 7 days of *S. cerevisiae* CNCM I-3856 administration and every three days until the analgesic effect was obtained. Then, the administration of *S. cerevisiae* CNCM I-3856was stopped and DCR was performed all the three days until the analgesic effect disappear.

Dose effect protocol

To evaluate the effective dosage of *S. cerevisiae* CNCM I-3856, we administered the *S. cerevisiae* CNCM I-3856 strains from 10^5 to 10^{10} cells/days for 15 days by oral gavage to healthy rats and we performed a DCR as previously described.

Evaluation of PPARα involvement in the analgesia induced by S. cerevisiae CNCM I-3856

Fenofibrate (300mg/kg/day), a specific PPARα agonist was used as a positive control to evaluate the effect of PPARα in the modulation of visceral pain perception. It was administered by oral gavage once daily.

To evaluate the role of PPARα in the induction of analgesia by *S. cerevisiae* CNCMI-3856, we co-administered the GW6471 (30µg in 50µl, subcutaneous injection), a specific antagonist of PPARα the 3 last days of two weeks administration of *S. cerevisiae* CNCM I-3856 used at optimal dosage (10^6 cells/day).

Evaluation of analgesic properties in rats with visceral hypersensitivity induced by butyrate instillations

For each enema, a catheter (2-mm Fogarty catheter) were placed in the colon at 7 cm from the anus, and animals received 1 ml of 200 mM of sodium butyrate at neutral pH (pH6.9) twice daily for 3 days. Healthy animals received saline solution.

According to a previous study [261], animals with visceral hypersensitivity were used (n=10/group). Treated animals received once a day for 7, 15 days by gastric gavage, 100µg of yeasts and the optimal dosage of their derivatives and control animals PBS by the same route and during the same time. Yeasts and their derivatives were resuspended in PBS. Butyrate or saline instillations started 7 days after the first gavage for three days. Colonic hypersensitivity was determined 14 days after the beginning of oral treatment thus 7 days after colonic instillations.

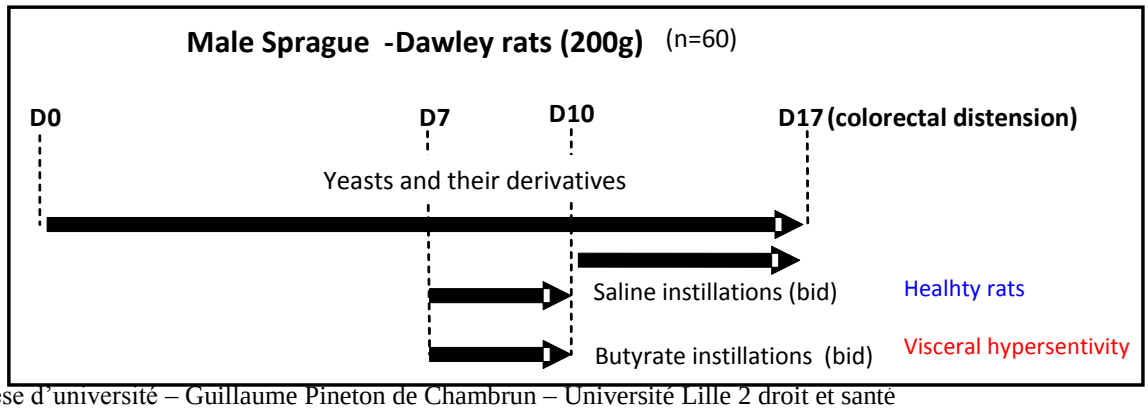

PPARα immunohistostaining

According to results obtained by PCR, data were extended at the protein level by immunohistochemistry using the relevant antibody. Immunohistochemistry were performed on colonic sections. After permeabilisation during 9 min by microwaves and 20 minutes of cooling in sodium citrate buffer, sections were incubated for 10 min with methanol and 3% of H2O2 to inhibit endogenous peroxidases and incubated for 15 min with avidin and 15 min with blocking buffer (0.1% BSA in milk) to minimize non-specific adsorption of the antibodies. The tissues were subsequently incubated with the rabbit polyclonal primary antibody directed against PPARα (1:200, Abcam) overnight at 4°C. Sections were then incubated for 30 min at room temperature with a swine anti-rabbit biotinylated secondary antibody (dilution 1:500, Dako Laboratories). Then slides were incubated with the complex avidin-biotin (Dako for 30 min) and revealed using DAB (Dako) for 4 min. Sections were rinsed twice for 5 min in PBS containing 0.05% Tween between each stage. Then slides were counterstained with hematoxylin solution and mounted for microscopy. Negative controls consist of staining with normal rabbit serum instead of specific antibody. Immunohistostaining was revealed under a microscope (Leica, Bensheim, Germany).

PPRE-luc mice

To study in vivo the PPAR activation under different conditions, we have developed a model of transgenic mice which expressed the luciferase gene after PPAR activation. The exogenous DNA contains 4 binding sites of the PPAR/RXR heterodimer (PPRE) upstream to the luciferase gene. Generation of these transgenic mice (PPRE-*Luc*) has been performed in collaboration with Professors Pierre Chambon and Johan Auwerx in mouse clinic institute (Illkirch, France), using classical techniques of microinjection of fertilized eggs.

All experiments were carried on with 15 to 16 month-old female PPRE-*Luc* transgenic mice. The animals were housed with free access to commercial rodent food and water.

Bioluminescence Reporter Imaging

Mice were visualized with a charge-coupled device camera (IVIS Imaging System 100 Series, Caliper Life Sciences). For the detection of bioluminescence, mice were anesthetized using a low dose of isofluran (2%). The mice then received an i.p. injection of 120 mg/kg D-luciferin (Euromedex) 2 min before bioluminescence quantification, to obtain a uniform biodistribution of the substrate. Mice were placed in the imaging chamber and a grayscale picture of the animals was first taken. Photon emission was then integrated over a period of 5 min. After this period, image analysis was performed using the Living Image® software. We evaluated the number of photon per second on a square representative to the rodent abdomen. *S. cerevisiae* CNCM I-3856 was administered by oral gavage (10^7 CFU/day).

4. Figures

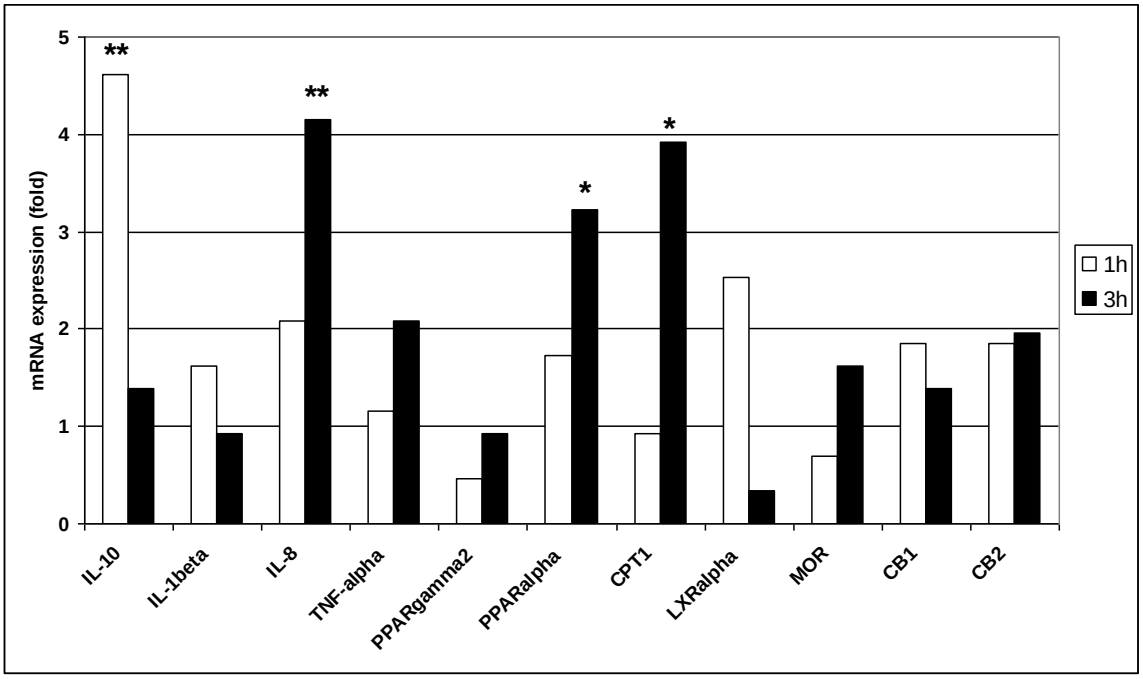

Figure 1: mRNA expression level for different receptors and cytokines in HT-29 cells after stimulation of with CNCM I-3856.

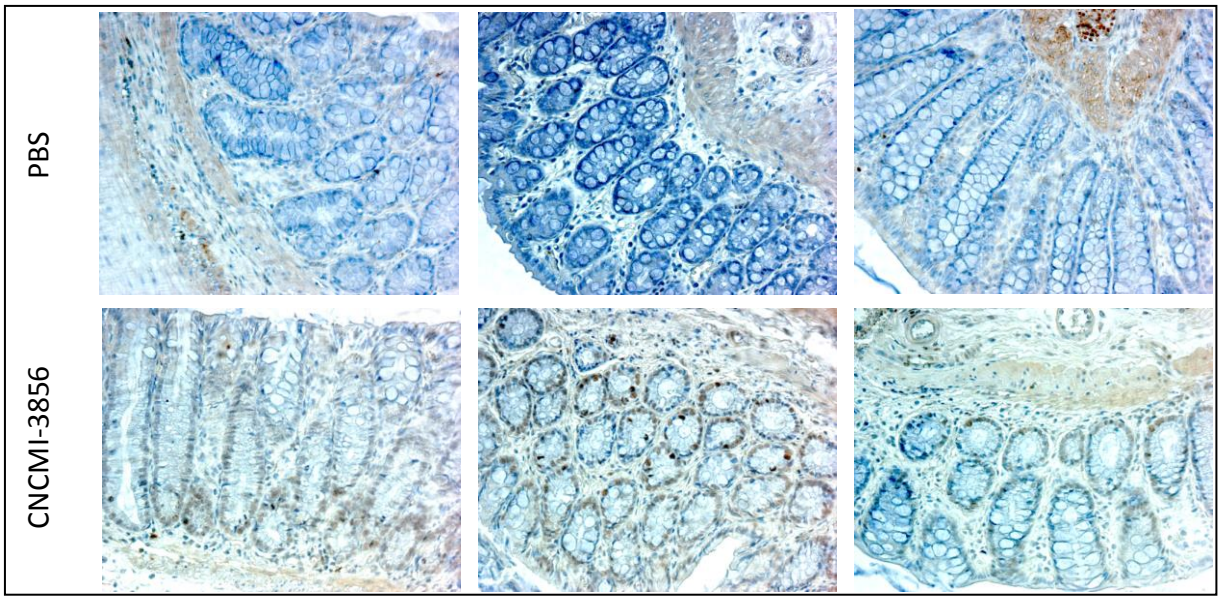

Figure 2: immunohistochemistry staining of colon section with anti-PPARα antibody.

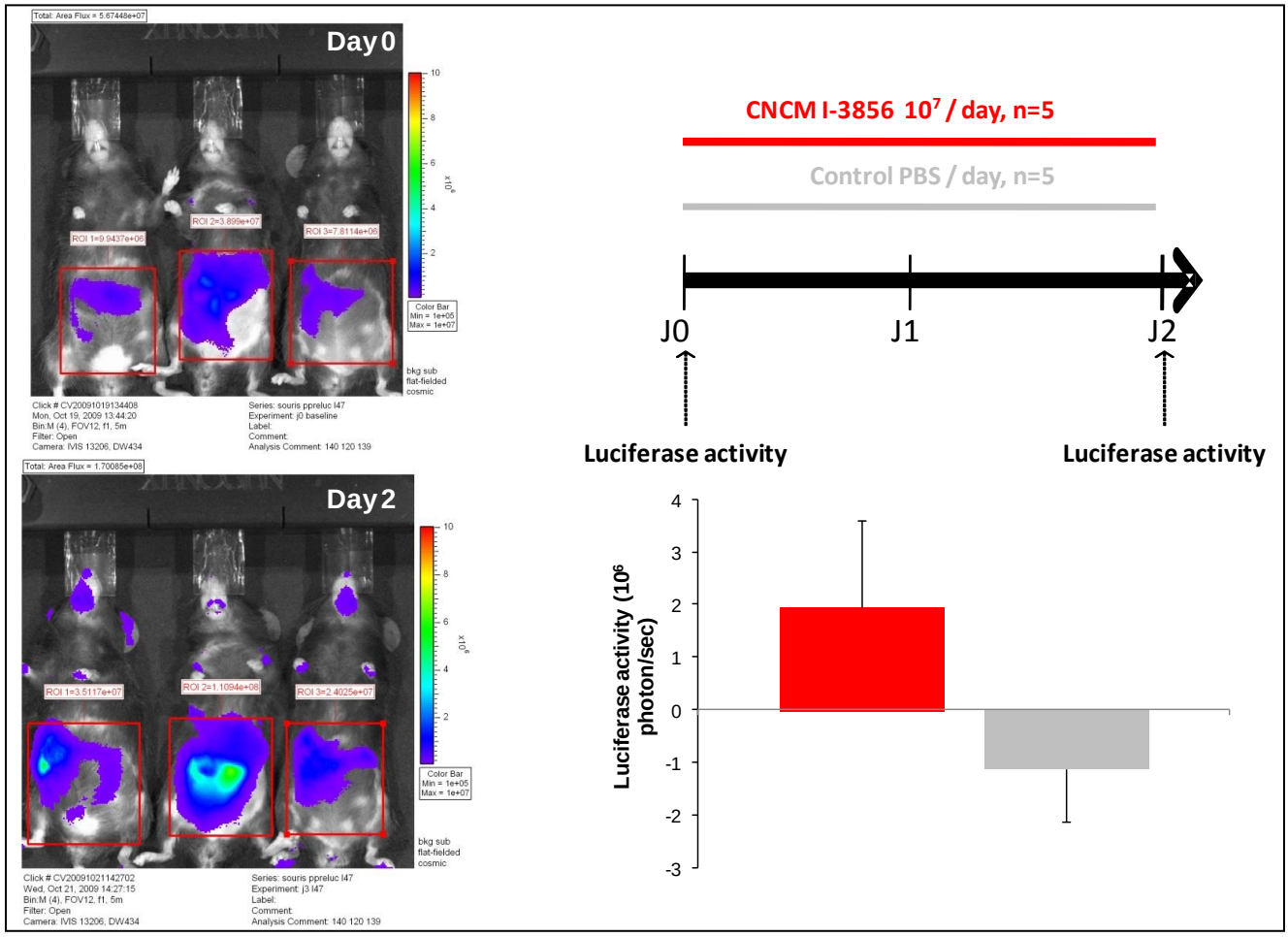

Figure 3: assessment of bioluminescent activity of the PPRE-*Luc* transgenic mice. The mice before treatment are considered as internal control and the luciferase activity was compared after CNCM I-3856 administration in the same mice. The qualitative assessment showed the activity of luciferase observed only in the abdominal region and the quantitative assessment showed the increase of bioluminescent activity after CNCM I-3856 administration.

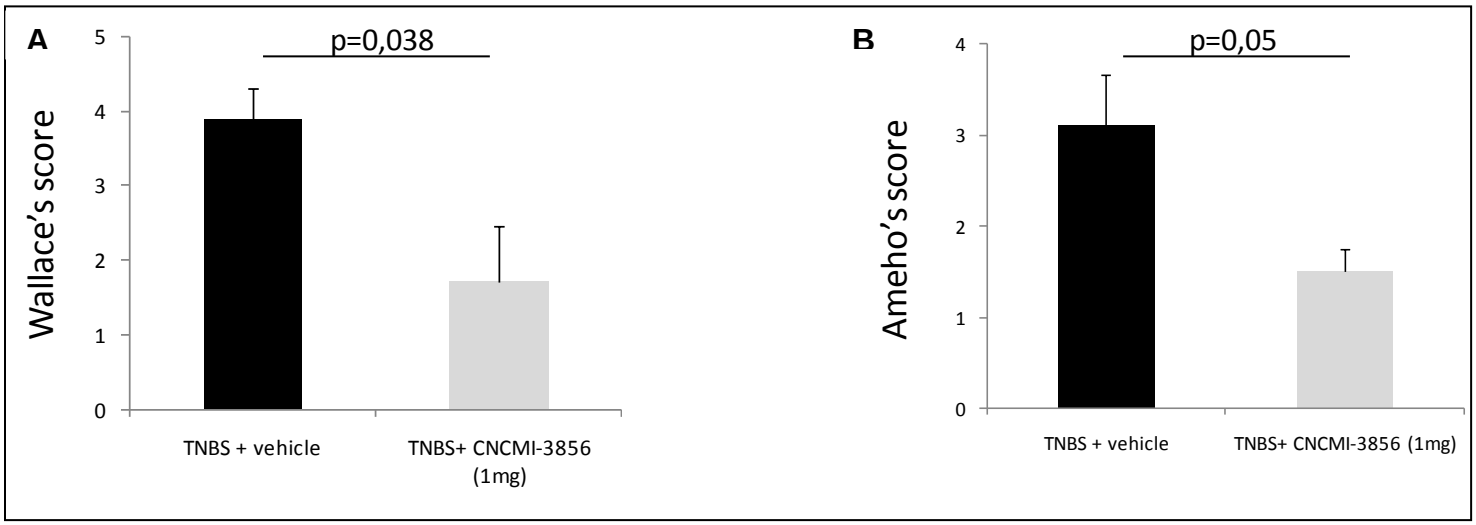

Figure 4: oral administration of CNCM I-3658 improves colitis induced by TNBS. Colitis was induced by intrarectal administration of TNBS in C57bl6 wild-type mice. Animals were killed 4 d later to evaluate the intensity of colitis. (A) Anti-inflammatory effect of oral administration of CNCM I-3856 (1mg/day) was compared to vehicle (CMC 0.5%) according to the macroscopic evaluation of the intensity of colonic lesions using the validated score of Wallace. Inflammation was also analyzed at the histological level using the validated score of Ameho (B). Statistical significances are indicated. Results are expressed as the mean ± SEM.

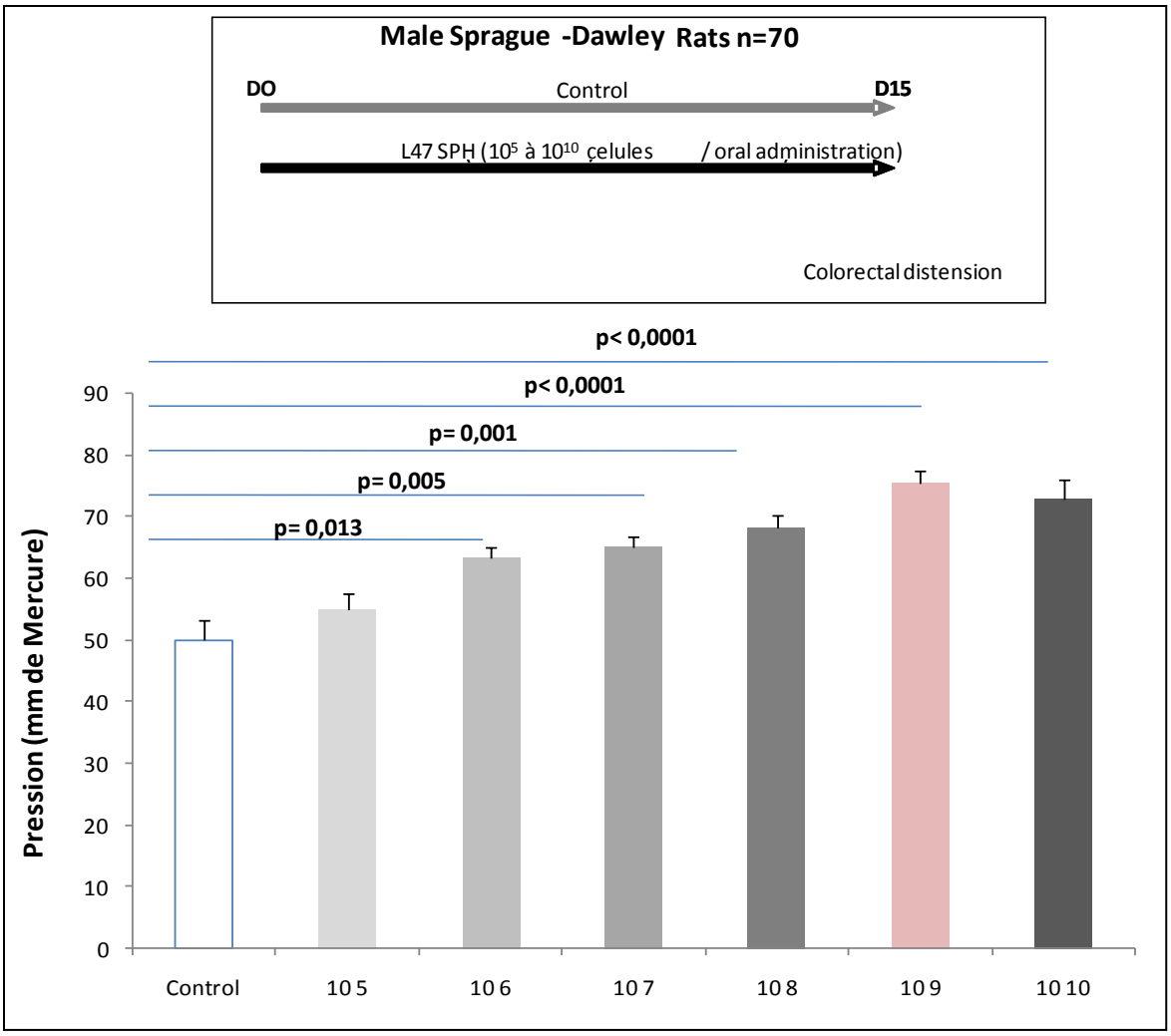

Figure 5: influence of *S. cerevisiae* CNCM I-3856 administered at different dosage from 10^5 to 10^{10} cfu/day on intestinal nociception in healthy rats after 17 days.

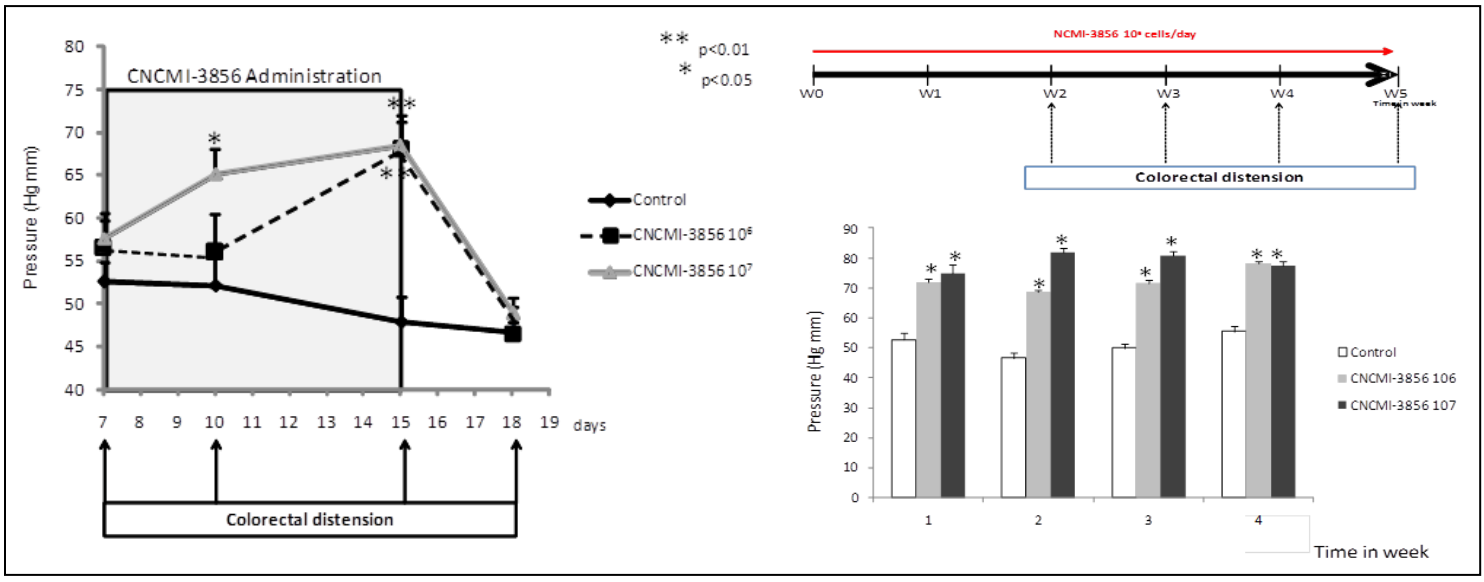

Figure 6: analgesic properties of *S. cerevisiae* CNCM I-3856 in time course experiment.

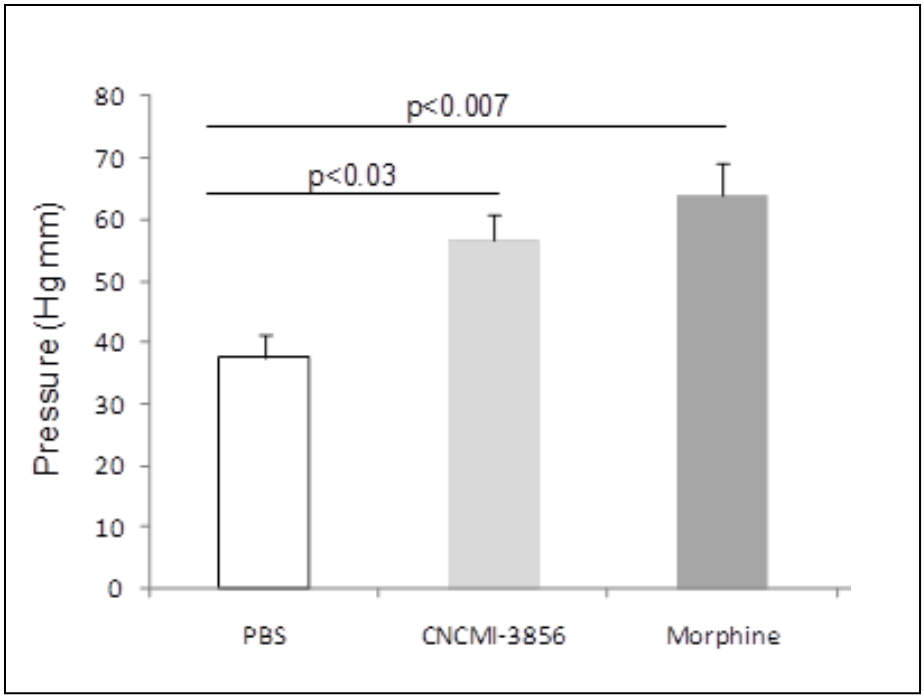

Figure 7: analgesic properties of *S. cerevisiae* CNCM I-3856 administered at 100 µg/day (10^6 cfu/day) on intestinal nociception in rats with induced hypersensitivity after 15 days.

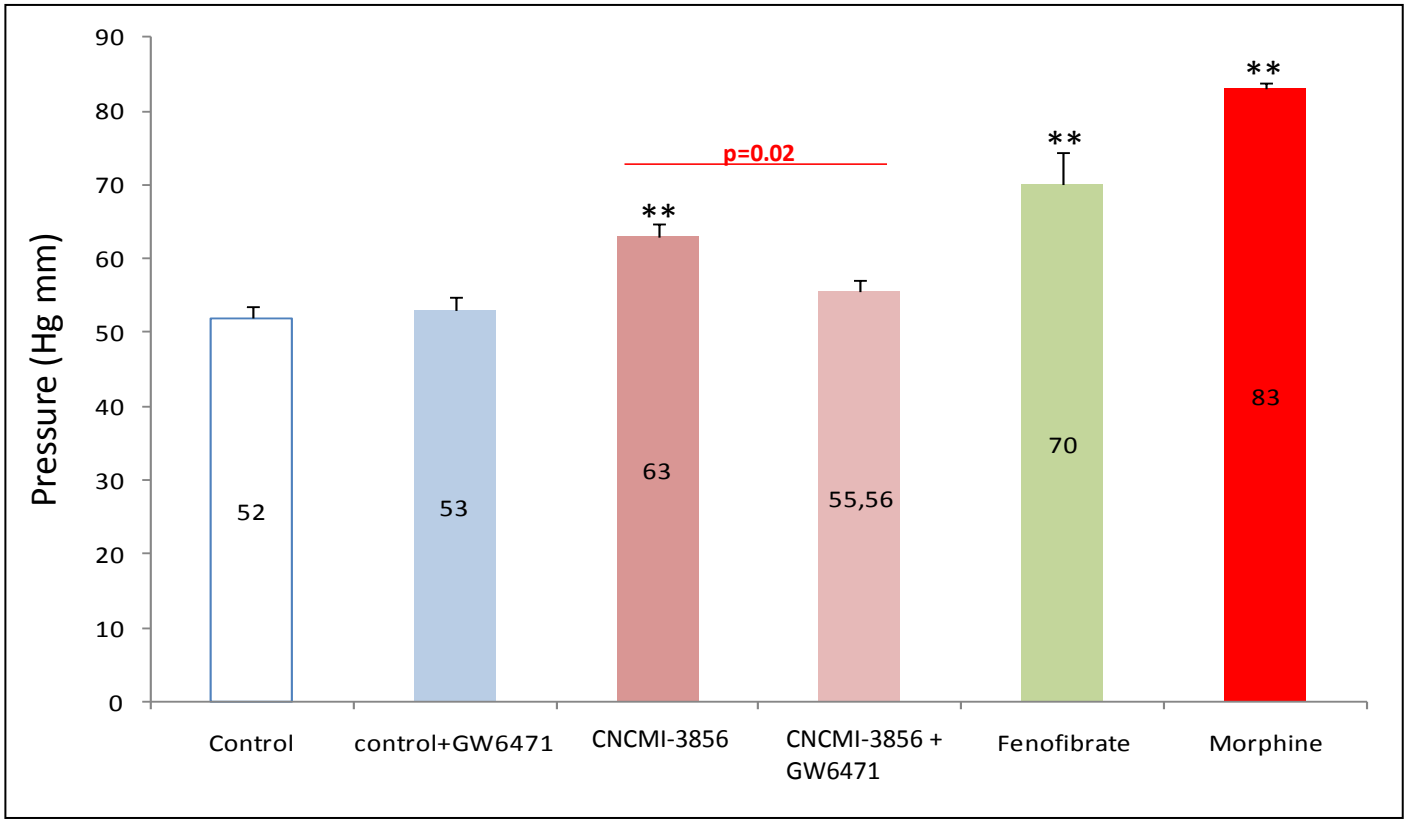

Figure 8: analgesic properties of *S. cerevisiae* CNCM I-3856 with or without PPARα antagonist (GW6471) on intestinal nociception in rats compared with fenofibrate, a PPARα agonist and morphine.

E. *Saccharomyces cerevisiae CNCM I-3856 reduces digestive discomfort and abdominal pain in subjects with irritable bowel syndrome: a randomized double-blinded placebo-controlled clinical trial.*

G Pineton de Chambrun[1, 2], C Neut[2, 3], M Cazaubiel[4], F Pelerin[5], P Justen[5] and P Desreumaux[1, 2]

[1]Department of Gastroenterology, Claude Huriez hospital, CHRU, Lille, France
[2]INSERM 995, University and CHU of Lille, France
[3]Department of microbiology, Faculty of Pharmacy, University of Lille, France
[4]Biofortis Silliker, Nantes, France
[5]Lesaffre International, Lesaffre Human Care, France

Référence de l'article :

Pineton de Chambrun G, Neut C, Cazaubiel C, Pelerin F, Justen P, Desreumaux P. *Saccharomyces cerevisiae* CNCM I-3856 reduces digestive discomfort and abdominal pain in subjects with irritable bowel syndrome: a randomized double-blinded placebo-controlled clinical trial. Dig Liv Dis. Submitted. 2014.

1. Introduction

Irritable bowel syndrome (IBS) is a common functional gastrointestinal disorder with a worldwide prevalence of 5-15%, accounting for 3% of visits to general practioners and about 40% of all gastroenterology outpatient consultations [242]. This high prevalence is associated with annual direct and indirect costs of more than 20 billion / year in USA corresponding to 3.5 million physician visits annually and one of the leading causes of work absenteeism. Despite the prevalence and impact of IBS in the community, pathogenesis remains unclear and efficacy of treatments is modest, focusing mainly on abdominal pain and bloating which are the dominant and most troublesome symptoms of IBS, using pharmacological and probiotic approaches [243].

Probiotics are live microorganisms when given in sufficient amount confer a health benefit to the host [258]. Probiotics can be bacteria, virus, parasites or yeasts. The main clinical feature of IBS is abdominal discomfort and/or abdominal pain. In these IBS patients, a recent systematic review of randomized controlled trials indicate that probiotics mainly belonging to the *Lactobacillus* and/or *Bifidobacterium* families have a trend for being efficacious, but the magnitude of benefit and the mechanisms of actions of strains are still unknown [262, 263].

In a previous study, we have shown that a specific strain of *Lactobacillus acidophilus* NCFM was able to decrease the visceral pain perception in rats via induction of Mu opioid receptor and cannabinoid receptor expression by colonic epithelial cells [261]. More recently, we reported that a new strain *Saccharomyces cerevisiae* CNCM I-3856 derived from baker's yeast had analgesic effects in the gut through a local activation of the peroxisome proliferator activated receptor alpha (manuscript in preparation). In this preclinical study, oral administration of CNCM I-3856 improved pain similarly to standard dosage of morphine in a model of colorectal distension in rats. This analgesic effect was dose dependent, appearing 15 days after the

beginning of probiotic administration and was transitory, disappearing 3 days after the last CNCM I-3856 administration.

Given this preclinical evidence of the analgesic effect of CNCM I-3856 in the gut, the aim of this study was to investigate whether oral administration of CNCM I-3856 is effective in alleviating IBS symptoms in a randomized double-blinded placebo-controlled clinical trial.

2. Materials and Methods

Patients

Patients were recruited in one investigative site Biofortis, Nantes, France. They were male and female subjects between 18-75 years of age with a diagnosis of IBS according to the Rome III criteria [242] and a pain/discomfort score strictly above 1 and strictly below 6 determined on a pain/discomfort scale using arbitrary graduation from 0 to 7 in the 7 days preceding the inclusion visit. They had normal blood count (erythrocytes, haemoglobin, haematocrit, mean corpuscular volume (MCV), thrombocytes and leucocytes), within reference values for serum creatinine, urea, alkaline phosphatase, total bilirubin, gamma-GT, ALT, ALP, TSH and CRP levels below twice the upper limit of the normal value of the laboratory. Treatments for diarrhoea, laxatives and antispasmodic drugs were not exclusion criteria on the condition that doses were stable and were not modified during the study. Menopausal female receiving a hormone treatment or contraception in non-menopausal female subjects must have started at least 3 months beforehand at stable doses without modification for the entire duration of the study.

Subjects were excluded if they had organic intestinal diseases, treatments likely to influence IBS, in particular by modifying intestinal sensitivity or motility (antidepressants, opioids, and narcotic analgesics), antibiotic therapy in progress or prescribed in the 8 weeks before inclusion in the study, long-term treatment with analgesics or NSAIDS. Subjects not willing to stop taking probiotics, prebiotics or synbiotics in the form of dietary supplements or convenience goods were not eligible. Pregnancy in progress, chronic alcoholism, vegetarian or vegan subjects, eating disorders such as anorexia or bulimia, documented food allergies were exclusion criteria.

Study design

It was a 13 week single-center double blind placebo-controlled clinical study randomizing 2 parallel groups of 100 IBS patients. During a 2-week run-in period, scores for abdominal pain/discomfort, bloating and flatulence, difficulty with defecation, stool frequency and consistency were recorded. Dietary recommendations were explained to each patient in particular concerning the consumption of fermented dairy products and certain cheeses (list of authorized and forbidden foods). After verification of inclusion/exclusion criteria, eligible IBS patients were randomized to consume daily for 8 weeks 1 capsule of *Saccharomyces cerevisiae* CNCM I-3856 (500mg, $8x10^9$ CFU/g) or a placebo (calcium phosphate). A total of 5 medical visits were regularly scheduled during the 13 week study including the 3 week follow-up period. The study protocol was conducted in accordance with the Declaration of Helsinki and approved by the Ethics Committee of Amiens, France. All subjects provided written informed consent before inclusion in the study.

Study products and compliance evaluation

Products studied were presented in capsule form, packaged in blister packs of 15. All capsules of active product or placebo were without flavour and had the same size, color and vegetal hydroxypropylmethylcellulose composition. They were to be taken by oral route, one capsule a day, the morning at breakfast time with a glass of water. The probiotic preparation specifically contained 500 mg per capsule of *Saccharomyces cerevisiae* CNCM I-3856 ($8x10^9$ CFU/g). The placebo consisted of a 500 mg dibasic calcium phosphate.

Patients had to return all their treatment units whether consumed or not to calculate compliance which was evaluated during the treatment period at W0 and W4.

Assessment of symptoms and study endpoints

The primary endpoint specified in the protocol was the evolution of abdominal pain/discomfort evaluated daily and assessed each week during the 13-week study according to a 7-point Likert scale [280]. Abdominal pain/discomfort scores were first analyzed using the area under the curve (AUC) in placebo and treatment groups where the score at W0 defined as a baseline value was added to the model to improve adjustment. A second analysis comparing the percentage of subjects who experienced an improvement in their abdominal pain/discomfort in the last 4 weeks of the treatment period was carried out using the Cochran-Mantel-Haenszel test. Improvement was defined as a reduction in the abdominal pain/discomfort score of 1 arbitrary unit for at least 50% of the time, i.e. for at least 2 weeks out of 4.

Secondary outcome measures were the weekly scores of bloating/distension and bowel movement difficulty recorded daily and weekly in the same condition using the 7-point Likert scales. Changes in stool frequency and consistency were followed using the Bristol Stool Scale [281]. The subjective global assessment of relief was measured at weekly intervals during the course of the study.

Safety variables

Adverse events were recorded by patients and transmitted immediately to the investigator to estimate the severity. Severe and non-severe adverse events were recorded on two different forms. The list of severe adverse events was transmitted to the authorities every six months throughout the study. The number of adverse events and their severity were compared between the treatment and placebo group (Fisher's exact test and chi-square test).

Collection of fecal samples

At V1, V3 and V4 (± 1 day), 60 subjects collected a stool specimen. These 60 subjects were distributed as follows: 10 subjects with constipation (IBS-C) who received the active product, 10 subjects with constipation (IBS-C) who received the placebo product, 10 subjects with diarrhoea (IBS-D) who received the active product, 10 subjects with diarrhoea (IBS-D) who received placebo product, 10 subjects with mixed IBS (IBS-M) who received the active product and 10 subjects with mixed IBS (IBS-M) who received the placebo product. These specimens were taken to perform a faecal calprotectin assay.

Sample size, randomization and statistical methods

On the basis of preclinical data obtained in a model of rectal distension in mice receiving *Saccharomyces cerevisiae* CNCM I-3856 (manuscript in preparation), a reduction of 20% in the abdominal pain/discomfort score was assumed. With a power of 80% and a significance level of 0.05, the difference between the treatment vs. placebo groups would be statistically significant with respectively 106 and 66 patients. In the present study, inclusion of 100 patients per group was considered realistic.

Randomisation schedules were generated using PROC PLAN SAS 9.1.3 Service Pack 4 software. Each subject included at the visit (V1) received in a random manner one of the two products (placebo or active). Block randomisation was performed by type of subject (with constipation (IBS-C), with diarrhoea (IBS-D), or mixed (IBS-M)) with dynamic allocation software using the block permutation technique. Product allocation remained blinded throughout the study.

Statistical analysis was performed by Biofortis using SAS 9.1.3 Service Pack 4 software. Analysis was performed on the per-protocol population as well as on the Intention To Treat (ITT)

population. This study presents the per-protocol analysis results taking into account the included subjects finishing the study without any major deviations.

3. Results

Patients

Baseline characteristics of the patients in the placebo and treatment groups showed no significant differences (Table 1). The flow of subjects through the protocol was presented in the figure 1. From the 262 screened subjects, 200 were randomized and equally distributed between the placebo (n=100) and treatment (n=100) groups. Six subjects were rapidly excluded (1 systemic disease, 5 voluntary withdrawal) and 15 discontinued the intervention (antibiotic treatment (n=12), bladder tumor (n=1), antidepressant treatment (n=1), colorectal cancer (n=1)) leaving respectively 86 and 93 subjects assigned to the treatment and placebo group giving a per protocol population of 179. Good compliances were recorded in the probiotic and placebo groups for the first and the second month of administration (respectively for V2+V3 99%±2.7 and 99%±3.2).

Primary outcome measures

Abdominal pain/discomfort scores expressed in arbitrary units (AU) on a scale from 0 (no symptoms) to 7 (severe symptoms) showed homogeneity at baseline for the placebo (3.23±1.12) and treatment group (3.16±1.12, $p>0.05$). Week by week analysis revealed a significant reduction of the abdominal pain/discomfort score in both groups throughout the 8 week treatment period (W1-8) compared with baseline (table 2). AUC calculated between W1 and W8, based on the score for abdominal pain/discomfort was not significantly different between placebo and treatment groups (17.46 ± 8.72 and 16.43 ± 7.27 respectively, $p=0.1314$) (Figure 2, table 3). However, analysis comparing the percentage of subjects with abdominal pain/discomfort improvement from W5 to W8 showed a higher percentage in the treatment group compared with the placebo group (respectively 62.79% vs. 47.31%, $p=0.0402$). The effect of the product was the

same whatever the type of IBS as "Type/Product" interaction was not significant for the weekly analyses or for AUCW1-W8 analyses.

Secondary outcome measures

Scores evaluating bloating/distension, movement difficulty, stool frequency and consistency during the study in the placebo and treatment groups are presented in the Figure 3. There was a good homogeneity for these 3 scores at baseline for both groups of patients. There was a significant reduction of scores evaluating bloating/distension and movement difficulty in both groups of patients. No significant variation of scores evaluating stool frequency and consistency was seen in the placebo and treatment groups during the time of the study. Results of the AUC analysis for bloating/distension, movement difficulty, stool frequency and stool consistency during the treatment period in the 2 groups of patients are given in the table 4, 5 , 6 and 7, showing no intergroup differences.

Adverse events

The adverse events and effects recorded during the study are listed in Table 9. No difference in adverse event frequency or severity was observed between the two groups. Two severe adverse events or effects were recorded during the study, a bladder neoplasm in the treatment group and a colorectal tumor in the placebo group.

Fecal calprotectin

The calprotectin parameter showed homogeneity at baseline for both groups. Intergroup analysis did not show a significant difference between the 2 groups, neither at W8 (end of the product administration period), nor at W11. On intragroup analysis, a significant increase in the mean

value for calprotectin was recorded in the placebo group, between W0 and W11 (0.517±0.974 log(µg/g), p=0.0069).

4. Discussion

The present placebo-controlled trial demonstrates that in a French population, *Saccharomyces cerevisiae* CNCM I-3856 is a probiotic strain able to relieve abdominal pain/discomfort in IBS patients fulfilling the Rome III criteria [242]. This 13 week clinical trial was performed according to the recommended designs of treatment trials for functional gastrointestinal disorders, in order to demonstrate statistical superiority of a treatment by *Saccharomyces cerevisiae* on the main symptom abdominal pain compared to placebo in a randomized double-blind placebo-controlled study.

It is the first clinical trial reporting an efficacy of yeast treatment on abdominal pain/discomfort in IBS patients. Abdominal pain was chosen as the primary end point since the selected strain of *Saccharomyces cerevisiae* CNCM I-3856 was able to induce a strong visceral analgesic effect allowing a 50% increased colorectal distension threshold in treated vs. untreated rats. Based on these data and expecting a 20% therapeutic gain over placebo for the score assessing abdominal pain/discomfort, 200 IBS patients were randomized and treated during 8 weeks by *Saccharomyces cerevisiae* CNCM I-3856 at a daily dose of 500 mg or a placebo. The 2 week prospective baseline observation period ensured that patients were currently symptomatic with comparable moderate abdominal pain score of 3.2 on the seven-point Likert scale in the active and placebo groups. Even if the optimal dose remains to be clearly established, the daily intake of $8x10^9$ CFU of *Saccharomyces cerevisiae* CNCM I-3856 was chosen based on preclinical studies performed in rats showing that escalating doses of this strain of yeast gave a linear analgesic dose-dependent effects beginning at 10^5 CFU/day and reaching a plateau at 10^9 CFU/day.

After 4 weeks of treatment, improvement of abdominal pain defined by a reduction in the abdominal pain/discomfort score of 1 for at least 50% of the time was significantly higher in

patients receiving *Saccharomyces cerevisiae* CNCM I-3856 compared to the placebo group (63% vs 47%, p=0.04). This improvement in the active group represented a mean 37.5% reduction in the initial visual analog Likert scale rating of abdominal pain severity. During the first month of treatment, changes in the intensity of abdominal pain/discomfort were similar in the groups of patients receiving the treatment or the placebo, suggesting a potential delayed action of *Saccharomyces cerevisiae* to induce analgesia. This hypothesis is consistent with previous findings obtained in rodents where the analgesic effect of *Saccharomyces cerevisiae* CNCM I-3856 appeared two weeks after the beginning of treatment. This delayed action of *Saccharomyces cerevisiae* may explain at least in part why the difference for the weekly scores evaluating abdominal pain/discomfort during the 8 week period of treatment was in the favor of *Saccharomyces cerevisiae* CNCM I-3856 therapy but without significant intergroup differences.

This trial was designed for a group of IBS patients of any subtype, complaining of moderate IBS symptoms and recruited by general practitioners. Several trials with probiotics have involved mainly IBS-D patients but microbiological studies have emphasized that qualitative changes of the microbiota exist in all IBS sub-types [258]. Therefore, we considered that any IBS patient, whatever the subtype, could be eligible to participate. Previous trials assessed the effect of *Saccharomyces boulardii* in patients with IBS [265, 272, 273]. These studies are not directly comparable because of the differences in the study design, selection of patients with diarrhea-predominant IBS and outcomes evaluation but also in the strains used.

In conclusion, this study provides evidence that oral administration of *Saccharomyces cerevisiae* CNCM I-3856 at a daily dose of $4X10^9$ CFU could be a safe and easy way of alleviating abdominal pain/discomfort, the major disabling symptom leading to the seeking of medical advice by IBS patients.

5. Tables and Figures :

Table 1: Patient baseline characteristics

	Placebo group (n=93)	CNCM-I3856 (n=86)	*p*
Age, y (mean±SD)	45.4 ± 14	42.5 ± 12.5	ns
Male, n (%)	11 (11.83)	14 (16.28)	ns
Female, n (%)	82 (88.17)	72 (83.72)	ns
Weight, kg (mean ±SD)	64.55 ± 22	65.23 ± 12.70	ns
Height, cm (mean±SD)	163.4 ± 7.5	165.9 ± 9.1	ns
Smokers, n (%)	18 (19.35)	26 (30.23)	ns
Type of IBS n (%)			ns
IBS-C	43 (46.24)	41 (47.67)	ns
IBS-D	27 (29.03)	24 (27.91)	ns
IBS-M	23 (24.73)	21 (24.42)	ns
Bowel Pain/discomfort , AU (mean±SD)	3.16 ± 1.12	3.23 ± 1.12	ns

Table 2: Abdominal/bowel pain and/or discomfort score analysis results (W0 to W11)

	Total population		
	Variations Wn-W0 (Mean ± SD)		**Intergroup comparison**
Week	**Placebo (N = 93)**	**CNCM I-3856 (N = 86)**	**Intergroup *p***
W1	-0.13 ± 0.87	-0.30 ± 0.90	0.1443
W2	-0.43 ± 1.12	-0.61 ± 1.09	0.2258
W3	-0.70 ± 1.26	-0.79 ± 1.01	0.3689
W4	-0.74 ± 1.33	-0.87 ± 1.23	0.3422
W5	-0.74 ± 1.31	-0.86 ± 1.27	0.5430
W6	-0.76 ± 1.33	-1.07 ± 1.18	0.1289
W7	-0.83 ± 1.30	-1.21 ± 1.31	0.0559
W8	-0.85 ± 1.44	-1.20 ± 1.31	0.0972
W9	-0.87 ± 1.35	-1.10 ± 1.24	0.2898
W10	-0.84 ± 1.40	-0.84 ± 1.16	0.9919
W11	-0.87 ± 1.42	-0.89 ± 1.25	0.9831
Intragroup comparison	**Intragroup *p***		
W2 - W0	0.0004 (***)	<0.0001 (***)	
W4 - W0	<0.0001 (***)	<0.0001 (***)	
W6 - W0	<0.0001 (***)	<0.0001 (***)	
W8 - W0	<0.0001 (***)	<0.0001 (***)	
W11 - W0	<0.0001 (***)	<0.0001 (***)	
W11 - W8	0.8913	0.0124 (*)	

Table 3: AUC_{W1-W8} analysis results for Abdominal/bowel pain and/or discomfort score

	Total population		Intergroup comparison
	AUC calculated on the score for abdominal pain/discomfort (W0-W6)		
Statistics	**Placebo (N = 93)**	**Active product (N = 86)**	**Intergroup p #**
Mean ± SD	17.46 ± 8.72	16.43 ± 7.27	0.1314
(Min; Max)	(1.5; 43.8)	(1.6; 39.1)	

Table 4: AUC_{W1-W8} analysis results for bloating and flatulence score

	Total population		Intergroup comparison
	AUC calculated on raw data		
Statistics	**Placebo (N = 93)**	**Active product (N = 86)**	**Intergroup p #**
Mean ± SD	18.32 ± 8.50	18.23 ± 7.72	0.6380
(Min; Max)	(0.0; 47.0)	(0.0; 40.9)	

Table 5: AUC_{W1-W8} analysis results for the difficulty with defecation score

	Total population		Intergroup comparison
	AUC calculated on raw data		
Statistics	**Placebo (N = 93)**	**Active product (N = 86)**	**Intergroup p #**
Mean ± SD	13.88 ± 9.95	12.83 ± 8.16	0.2152
(Min; Max)	(0.0; 48.6)	(0.0; 38.4)	

Table 6: AUC_{W1-W8} analysis results for number of stools per day

	Total population		Intergroup comparison
	AUC calculated on raw data		
Statistics	**Placebo (N = 93)**	**Active product (N = 86)**	**Intergroup p #**
Mean ± SD	8.36 ± 3.59	8.16 ± 3.58	0.7538
(Min; Max)	(1.6; 20.1)	(2.1; 19.9)	

Table 7: AUC_{W1-W8} analysis results for stool consistency score

	Total population		Intergroup comparison
	AUC calculated on raw data		
Statistics	**Placebo (N = 93)**	**Active product (N = 86)**	**Intergroup p #**
Mean ± SD	23.95 ± 6.67	25.96 ± 6.21	0.0203
(Min; Max)	(7.0; 35.4)	(10.0; 39.8)	

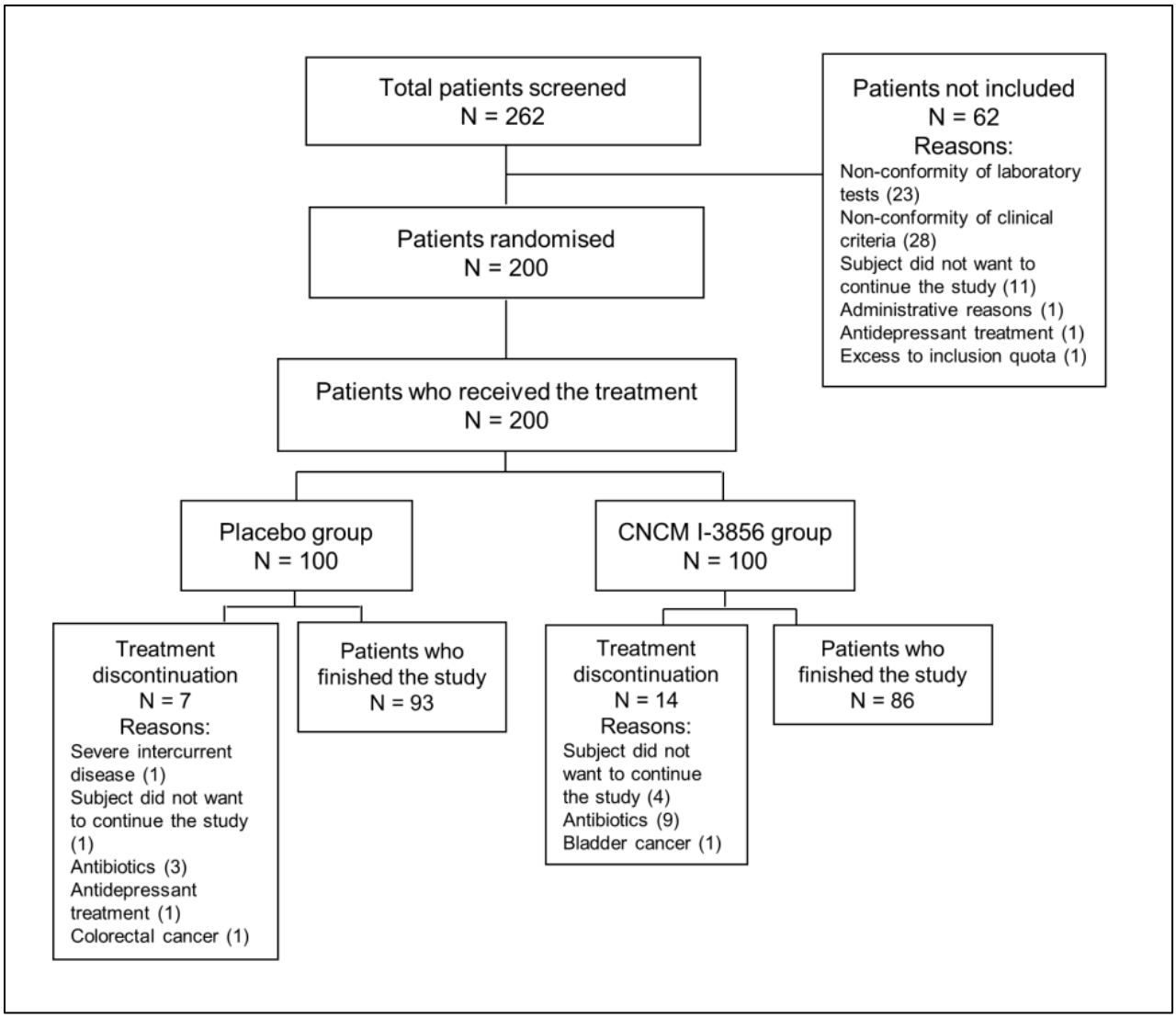

Figure 1 : flow chart.

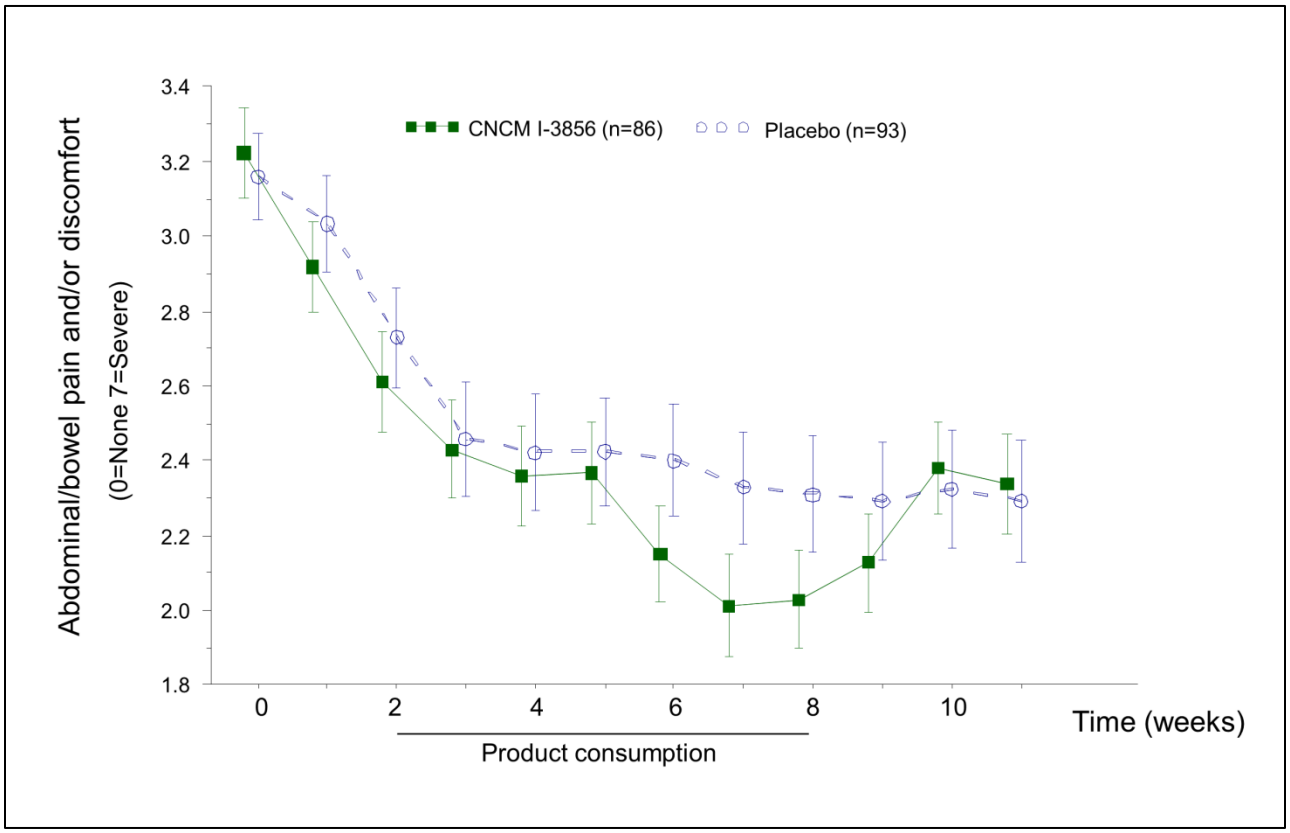

Figure 2: evolution of abdominal pain and discomfort in IBS patients with or without *Saccharomyces cerevisiae* (CNCM I-3856).

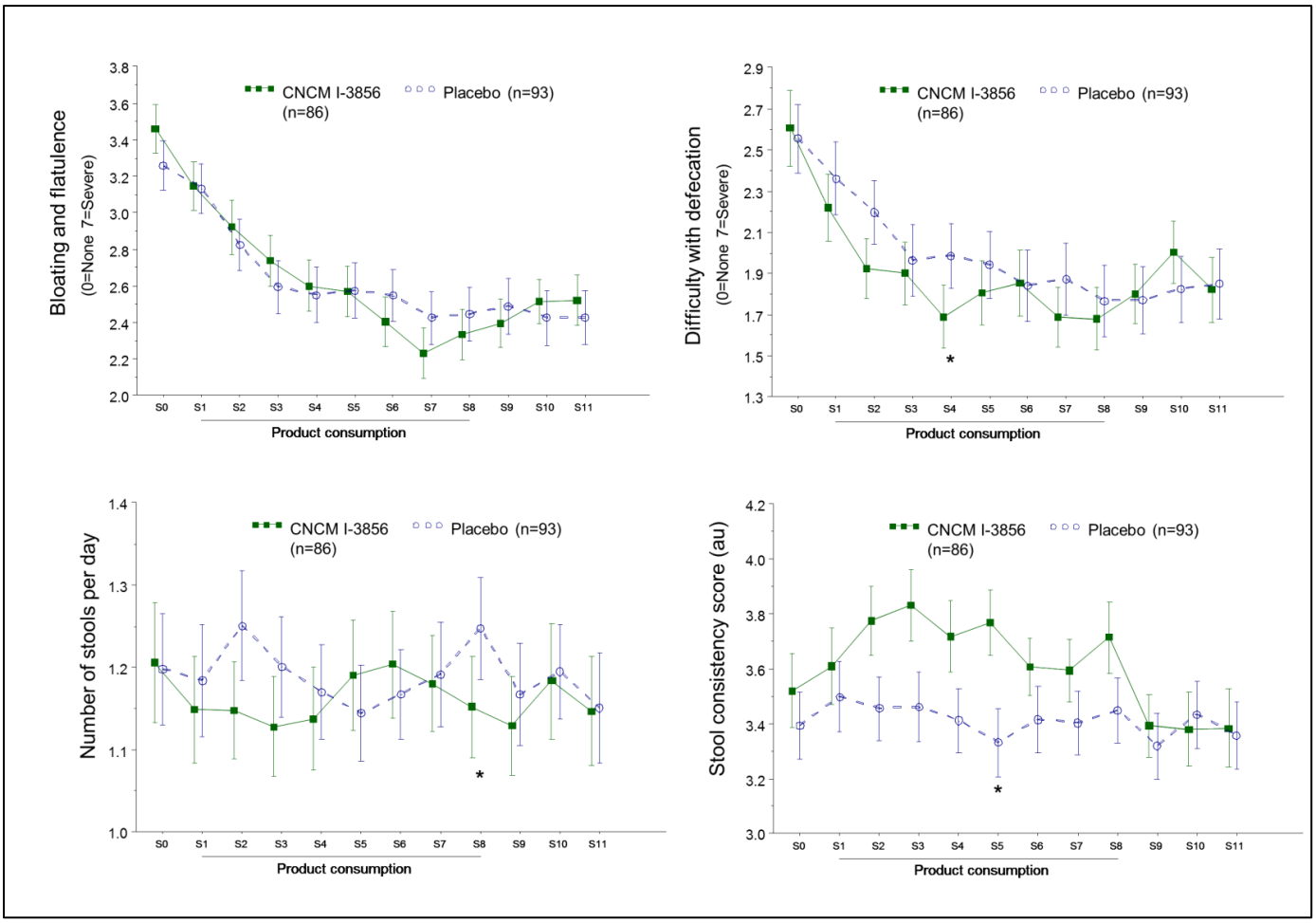

Figure 3: evolution of IBS symptoms in patients treated with *Saccharomyces cerevisiae* or placebo.

F. Conclusion :

La flore intestinale est actuellement reconnue comme un acteur majeur de certaines pathologies digestives ou systémiques. Elle est de plus en plus impliquée dans la régulation de l'inflammation intestinale et joue très probablement un rôle important dans les MICI et le SII. Dans ces deux pathologies il a été clairement démontré qu'il existait une dysbiose pouvant être à l'origine des anomalies organiques et fonctionnelles observées. Une des pistes thérapeutiques issue de ces constatations est la modulation de la flore intestinale par des agents probiotiques. Plusieurs bactéries et levures ont déjà été testées dans le traitement des MICI et du SSI.

Dans notre travail, nous avons choisi de tester l'effet d'une levure *Saccharomyces cerevisiae* qui n'avait jamais été testée auparavant dans ces pathologies chez l'homme. Dans le premier travail expérimental, nous avons montré que *Saccharomyces cerevisiae* CNCM I-3856 induisait l'expression de l'IL-10 et du récepteur nucléaire PPARα dans les cellules épithéliales intestinale *in vitro*. Nous avons ensuite montré que *Saccharomyces cerevisiae* CNCM I-3856 améliorait l'inflammation intestinale dans un modèle de colite chimique au TNBS induite chez la souris. De plus, *Saccharomyces cerevisiae* CNCM I-3856 réduisait le seuil de douleur abdominale dans un modèle de sensibilité viscérale chez le rat. Cet effet anti-nociceptif était médié au niveau intracellulaire par l'activation de PPARα. Ces données expérimentales suggéraient que *Saccharomyces cerevisiae* CNCM I-3856 pourrait avoir un effet bénéfique chez les patients atteints de MICI et de SII.

Nous avons ensuite choisi de tester *Saccharomyces cerevisiae* CNCM I-3856 comme traitement chez des patients atteints du SII. Dans une étude prospective randomisée en double aveugle contrôlée contre placébo nous avons montré que *Saccharomyces cerevisiae* CNCM I-

3856 améliorait l'inconfort intestinal et les douleurs abdominales chez les patients atteints de SII en comparaison au placébo.

V. Discussion

Environnement et rôle de l'aluminium

Dans ce travail de thèse nous avons étudié certains mécanismes pouvant être impliqués dans la régulation de l'inflammation intestinale chronique. Tout d'abord nous nous sommes intéressés aux facteurs environnementaux. Pourquoi s'intéresser aux facteurs environnementaux dans les MICI ? Parce que seuls ces facteurs permettent d'expliquer les principales caractéristiques épidémiologiques de ces maladies et qu'à la différence des gènes, ils peuvent être contrôlés pour réduire la fréquence et la morbidité de ces pathologies [6]. L'étude des facteurs environnementaux est complexe du fait de la multiplicité de ces facteurs, de leurs interactions et de la difficulté à affirmer leur imputabilité dans les pathologies. Comparativement à l'étude des facteurs génétiques, peu de travaux sont publiés concernant les facteurs environnementaux (FIGURE 19).

L'épidémiologie des MICI, montre qu'il existe un gradient Nord-Sud en France concernant la prévalence de la MC avec un nombre important de cas incident rapportés dans la région Nord Pas-de-Calais [282]. Cette région très industrialisée a été depuis les cinquante dernières années un lieu d'installation de nombreuses usines et avant cela le site de nombreuses entreprises minières participant à la pollution de l'air, de l'eau et des sols. Ces différentes constatations posent la question du rôle de la pollution dans le développement des MICI et plusieurs études épidémiologiques réalisées en Amérique du Nord suggèrent une implication de la pollution par les microparticules [40, 41]. De nombreuses études expérimentales ont testé l'effet de ces microparticules sur différentes maladies inflammatoire, respiratoire et cardiovasculaire en utilisant une collection de microparticules atmosphériques. L'avantage de

cette stratégie est de se rapprocher de l'exposition réelle des sujets, mais ne permet pas d'identifier les particules réellement responsables de l'effet toxique.

Nous avons choisi une autre approche en nous focalisant sur une seule particule après avoir choisi le meilleur candidat potentiellement impliqué dans le développement et l'entretien de l'inflammation intestinale : l'aluminium, en se basant sur des arguments épidémiologiques, expérimentaux et cliniques [67]. Notre travail expérimental montre que l'aluminium administré par voie orale pendant plusieurs semaines n'est pas toxique pour des souris saines. Par contre, l'aluminium aggrave l'inflammation intestinale dans des modèles de colites chimiques (TNBS et DSS) chez la souris et dans un modèle de colite chronique chez des souris déficientes pour le gène de l'IL-10. L'effet de l'aluminium implique plusieurs mécanismes avec une modification de la flore intestinale, une augmentation de la perméabilité intestinale et une augmentation de la réponse immunitaire intestinale et humorale vis-à-vis des bactéries entrainant en particulier la formation de granulomes. Ces résultats suggèrent que l'aluminium présente toutes les caractéristiques d'un facteur environnemental pouvant déclencher et aggraver l'inflammation intestinale chez des sujets génétiquement prédisposés.

Deux études précédant ce travail ont testées une alimentation pauvre en microparticule dans le traitement des patients atteints de MC [42, 47]. Les résultats de ces études sont contradictoires, mais l'étude la plus récente qui était multicentrique, randomisée contre placébo en simple aveugle ne montrait pas d'effet d'une alimentation pauvre en microparticule sur l'activité de la MC. Ces résultats ne sont donc pas en faveur d'un rôle des microparticules dans la physiopathologie des MICI. L'alimentation pauvre en microparticules utilisée dans ces études se focalisait sur l'élimination des aliments riches en titanium dioxyde (TiO_2) et en particules de silicate. Il n'est pas certains que ce régime ait éliminé un apport en aluminium et peu de données

sont disponibles sur la persistance de particules d'aluminium dans la muqueuse digestive même après l'arrêt de l'exposition. Aucune étude épidémiologique n'a à ce jour mis en évidence l'aluminium comme facteur de risque de développer une MICI, mais aucune de ces études n'a spécifiquement recherché par l'interrogatoire la consommation d'aluminium ou doser l'aluminium dans des liquides biologiques. Une étude épidémiologique de la pollution des sols dans le quart Nord-Ouest de la France met en évidence de large zone de pollution des eaux par l'aluminium et des travaux d'association entre ces données épidémiologiques et la répartition de cas de MICI dans la même région sont en cours. Des études épidémiologiques dédiées et des études cliniques chez l'homme sont nécessaires pour évaluer la contamination des sujets et des patients atteints de MICI par l'aluminium, la relation de cette contamination avec les anomalies génétiques présentées par les patients. L'effet de l'éviction de l'aluminium ou d'un traitement permettant son élimination devrait être évalué dans un essai thérapeutique contrôlé.

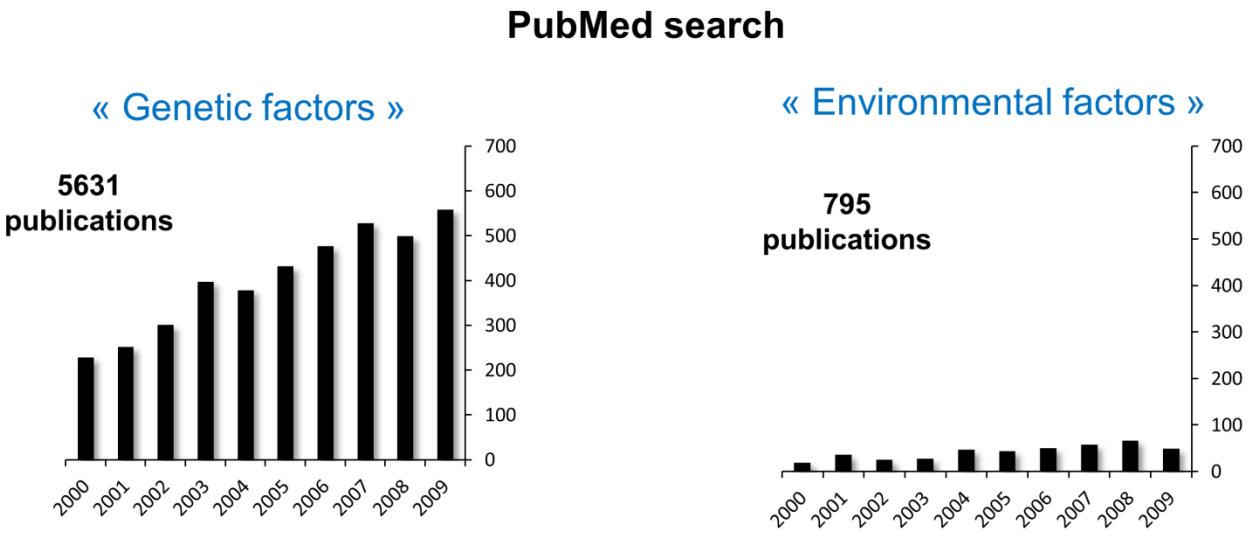

FIGURE 19 : Comparaison du nombre de publications concernant les facteurs génétiques et les facteurs environnementaux.

Facteurs moléculaires et rôle de la caspase-8

Les études génétiques concernant les MICI ont amélioré notre compréhension des altérations moléculaires impliquées dans l'inflammation intestinale chronique [25]. Les facteurs moléculaires identifiés à partir des études d'association pan génomique actuellement les plus étudiées sont NOD2, les gènes de l'autophagie, la voie de signalisation des lymphocytes Th17 et de l'IL-23 [2]. Par contre, les GWAS ont identifié de nombreux autres gènes de susceptibilité correspondant à des facteurs moléculaires et des voies de signalisation dont le rôle est encore méconnu [25]. Plusieurs gènes de susceptibilité retrouvés associés aux MICI nous indiquent que les voies de mort cellulaire (apoptose, nécroptose) jouent probablement un rôle dans le développement de l'inflammation intestinale. En effet, le gène CARD9 qui est une sous-unité des caspases impliquées dans la voie de l'apoptose est un gène de susceptibilité pour les MICI [106].

L'apoptose est un processus de mort cellulaire programmée qui joue un rôle majeur dans le maintien de l'architecture et de la différentiation de l'épithélium intestinal. Cette voie de signalisation est caractérisée par l'activation du récepteur transmembranaire au TNFα, qui active le complexe DISC puis une cascade de phosphorylation des caspases. La première caspase à interagir au niveau du complexe DISC est la caspase-8 qui est considérée comme une des protéines régulatrice majeure de l'apoptose.

Les résultats de notre travail montrent que la caspase-8 est indispensable au maintien de l'homéostasie intestinale et que son absence entraine une inflammation intestinale chronique. La caspase-8 agit en limitant l'endocytose de la membrane plasmique et des molécules d'adhésion au niveau de la membrane basale et en régulant l'autophagie dans les cellules épithéliales intestinales suit à un stimulus infectieux. Cet effet est dépendant de la voie de signalisation du TNFα et de son récepteur transmembranaire. Ces résultats ont été obtenus *in vivo* dans un modèle

de souris déficientes pour la caspase-8 spécifiquement au niveau des cellules épithéliales intestinales et répliqués dans un modèle d'organoïdes fait à partir de cryptes de ces même souris. Au long cours, les souris déficientes pour la caspase-8 développaient une inflammation intestinale chronique ressemblant sur le plan macroscopique et histologique à la MC. Ces résultats suggèrent fortement que la caspase-8 est un facteur moléculaire pouvant être impliqué dans la physiopathologie des MICI.

Si les études génétiques dans les MICI ont identifié CARD9 comme gène de susceptibilité, la caspase-8 elle-même n'a pas été identifié par les GWAS. Cette absence d'indentification de la caspase-8 comme gène de susceptibilité des MICI dans les GWAS pourrait s'expliquer par une fréquence trop rare de l'allèle en cause dans la population générale. Elle pourrait aussi s'expliquer par un rôle uniquement indirect de la caspase-8. Nous avons effectivement montré dans notre travail à l'aide d'une analyse bio-informatique que les interactions protéiques entre la caspase-8 et les gènes de susceptibilité pour les MICI étaient très importantes.

Dans notre travail nous montrons aussi que le déficit complet en caspase-8 dans les cellules épithéliales intestinales est compatible avec une embryogenèse normale et le développement normal des souris, mais que l'apparition de l'inflammation intestinale chez ces souris mène systématiquement au décès des animaux. Ce modèle est probablement trop complet au regard du déficit totale en caspase-8 et la présence d'un déficit uniquement partiel serait probablement plus compatible avec une inflammation intestinale chronique sans mortalité. Les données préliminaires que nous avons obtenues chez l'homme sont tout à fait compatibles avec cette hypothèse puisque les patients atteints de RCH et de MC présentent une diminution de l'expression de la caspase-8 sans disparition complète.

Le résultat original de notre travail est la mise en évidence d'une hyperactivation de l'autophagie dans les cellules épithéliales intestinales des souris déficientes pour la caspase-8, à l'origine de l'inflammation intestinale. ATG16L1 et IRGM deux gènes de l'autophagie ont été préalablement identifiés comme gène de susceptibilité pour les MICI [106]. L'hypothèse la plus répandue est un défaut de l'autophagie à l'origine d'une altération dans la reconnaissance et l'élimination des bactéries entrainant une réponse immunitaire dérégulée. Ce déficit de l'autophagie a surtout été testé expérimentalement au niveau des cellules du système immunitaire et non dans les cellules épithéliales intestinales [116]. De plus, il a été démontré que des souris déficientes pour l'autophagie dans les cellules épithéliales intestinales (par suppression du gène Atg7) ne présentaient pas d'anomalie particulière [283]. Finalement, plusieurs études ont montré qu'une hyperactivation de l'autophagie dans l'épithélium intestinale pouvait entrainer une inflammation intestinale comme dans notre travail [156]. Le rôle exact de l'autophagie dans la physiopathologie des MICI reste encore à explorer.

Ces résultats encourageant incitent à poursuivre l'exploration du rôle de la caspase-8 chez les patients atteints de MICI et à entreprendre un génotypage du gène caspase-8 chez ces patients pour rechercher une mutation éventuelle. Sur le plan expérimental, l'augmentation de l'expression de la caspase-8 pourrait être testée dans le traitement de l'inflammation intestinale dans des modèles animaux.

Saccharomyces cerevisiae, inflammation et sensibilité viscérale

La flore intestinale joue un rôle majeur dans l'initiation et l'entretien de l'inflammation intestinale chronique. Elle participe aussi au développement des symptômes chez les patients atteints du SII. La modulation de la flore intestinale est une piste thérapeutique prometteuse pour

le traitement des patients atteints de MICI et du SII. Plusieurs souches bactériennes ont déjà été testées dans le traitement du SII avec des résultats encourageant.

Dans un modèle expérimental nous avons testé *in vitro* et *in vivo* l'effet de *Saccharomyces cerevisiae* sur la régulation de l'inflammation intestinales et de la sensibilité viscérale. Les résultats de notre travail montrent que S. cerevisiae est capable d'améliorer l'inflammation intestinale et d'augmenter le seuil de sensibilité viscérale chez le rats. Chez l'homme nous avons ensuite montré que S. cerevisiae diminuait significativement les douleurs abdominales chez les patients atteints du SII.

Une autre levure *Saccharomyces boulardii* a été testée auparavant dans le traitement du SII sans véritable efficacité. Bien qu'issue de la même espèce ces deux souches de levure sont très différentes et *S. boulardii* semble plus agir sur la diarrhée que sur les douleurs abdominales. L'effet bénéfique observé chez l'animal de *S. cerevisiae* sur l'inflammation intestinale nous incite à tester cet effet chez les patients atteints de MICI. Par contre, la présence d'anticorps anti-*Saccharomyces cerevisiae* (ASCA) chez les patients atteints de MC plaide plutôt contre un effet bénéfique de cette levure. En fait, des données récentes ont montré que l'immunogène à l'origine de ces anticorps pourrait être *Candida albicans*, une levure pathogène.

VI. Conclusion

Les mécanismes physiopathologiques à l'origine de l'inflammation intestinale chronique responsable des MICI sont complexes et multiples. A partir d'une analyse bibliographique exhaustive, nous avons identifié trois axes de recherche concernant les facteurs régulant l'inflammation intestinale : l'environnement, la génétique et le microbiote. Pour chaque axe de recherche nous avons ensuite étudié une piste originale, novatrice pour tenter d'améliorer et d'élargir le champ de notre compréhension de la physiopathologie de l'inflammation intestinale. A l'aide de modèles expérimentaux validés et robustes nous avons testé nos hypothèses de travail.

En conclusion, ce travail de thèse montre que l'aluminium est un nouveau facteur environnemental aggravant l'inflammation intestinale *in vivo* chez la souris. La caspase-8 à un rôle majeur dans le maintien de l'homéostasie intestinale en limitant l'endocytose et l'autophagie et son déficit entraine le développement d'une inflammation intestinale *in vivo* chez la souris. *Saccharomyces cerevisiae* est capable d'induire une amélioration de l'inflammation intestinale et du seuil de douleur abdominale par l'intermédiaire de l'activation du récepteur nucléaire PPARα *in vivo* chez la souris.

Ces résultats nous apportent des éléments nouveaux concernant les mécanismes régulant l'inflammation intestinale et ouvre la voie à de nouvelles possibilités thérapeutiques dans les maladies inflammatoires chroniques digestives.

ABREVIATIONS

AIEC	adherent/invasive *Escherichia coli*
AP-1	adaptor protein 1
AP-2	adaptor protein 2
ATG7	autophagy-related protein 7
ATG16L1	autophagy-related protein 16L1
BAX	bcl-2 associated X protein
BCG	*Mycobacterium bovis* strain BCG
BrdU	bromodéoxyuridine
CARD9	caspase-associated recruitment domain 9
CARD15	caspase-associated recruitment domain 15
CFU	colony forming unit
DAI	disease Activity Index
DAPI	4',6-diamidino-2-phenylindole
DISC	death-inducing signaling complex
DC	dendritic cell
dsRNA	double-stranded RNA
DSS	dextran sodium sulfate
EDTA	ethylenediaminetetraacetic acid
FADD	Fas-Associated protein with Death Domain
FLIP	FLICE-like inhibitory protein
GWAS	genome-wide association study
H&E	hematoxylin and eosin
HRP	horseradish peroxidase
IEC	intestinal epithelial cells
IFN	interferon
IKK	IκB kinase
IL1R2	interleukin 1 receptor 2
$IL10^{-/-}$	B6-IL10tm1Cgn (interleukine 10-negative) mice
IL23R	interleukin 23 receptor
IRF	interferon regulatory factor

IRGM	immunity-related GTPase family M protein
LC3	light chain 3
LDH	lactate dehydrogenase
LPS	lipopolysaccharide
MAVS	mitochondrial antiviral-signaling protein
MEICS	murine endoscopic index of colitis severity
MGG	May-Grünwald-Giemsa
MLN	mesenteric lymph nodes
MPO	myeloperoxidase
NALP3	NACHT, LRR and PYD domains-containing protein 3
NOD2	nucleotide-binding oligomerization domain-containing protein 2
Ocln	occludin
PBMC	peripheral blood mononuclear cell
PCNA	proliferating cell nuclear antigen staining
pIC	polyinosinic:polycytidylic acid
PKR	double-stranded RNA-activated protein kinase
PPAR	peroxisome proliferator-activated receptor
PRR	pathogen pattern recognition receptor
RIPA	radioimmunoprecipitation assay buffer
RIPK	receptor-interacting protein kinase
RPMI	Roswell Park Memorial Institute medium
RT–qPCR	real-time quantitative polymerase chain reaction
SEM	standard error of the mean
SQSTM1	sequestosome-1
SMAD3	mothers against decapentaplegic homolog 3
SNPs	single nucleotide polymorphisms
TLR	Toll-like receptor
TNBS	2,4,6-trinitrobenzene sulfonic acid
TNF	tumor necrosis factor
TNFR1	tumor necrosis factor receptor 1

TRIF	TIR-domain-containing adapter-inducing interferon-β
TUNEL	terminal transferase dUTP nick end labeling

ANNEXES

1. Articles de l'auteur publiés ayant servis à élaborer le manuscrit :

- Pineton de Chambrun G, Cortot A, Cécile Vignal C, Neut C, Body-Malapel M, Colombel JF, Desreumaux P. Environnement : nouveaux facteurs environnementaux associés au développement des maladies inflammatoires chroniques intestinales. ***Progrès en hépato-gastroentérologie*** n°11, maladies Inflammatoires Chroniques Intestinales, janvier 2010.

- Cortot A, Pineton de Chambrun G, Vernier-Massouille G, Vigneron B, Gower Rousseau C. Inflammatory bowel diseases: Genetic or environmental diseases? ***Gastroenterol Clin Biol***. 2009 Aug-Sep;33(8-9):681-91.

- Pineton de Chambrun G, Body-Malapel M, Djouina M, Altare F, Arrieta MC, Zaki H, Kanneganti T, Cortot A, Colombel JF, Neut C, Desreumaux P, Vignal C. Aluminum enhances inflammation and decreases mucosal healing in experimental colitis in mice. ***Mucosal immunol***. Epub 2013 oct 16.

- McAllister CS, Lakhdari O, Pineton de Chambrun G, Gareau MG, Broquet A, Lee GH, Shenouda S, Eckmann L, Kagnoff MF. TLR3, TRIF, and Caspase 8 Determine Double-Stranded RNA-Induced Epithelial Cell Death and Survival In Vivo. ***J Immunol***. 2013 Jan 1;190(1):418-27.

- Pineton de Chambrun G, Colombel JF, Poulain D, Darfeuille-Michaud A. Pathogenic agents in Inflammatory Bowel Diseases. ***Curr Opin Gastroenterol***. 2008 24:440-447.

- Pineton de Chambrun G, Torres J, Darfeuille-Michaud A, Colombel JF. The Role of Anti(myco)bacterial Interventions in the Management of IBD: Is There Evidence at All?. ***Dig Dis***. 2012;30(4):358-67.

2. Présentations orales des résultats des travaux de thèse:

- Pineton de Chambrun G, Vignal C, Body-Malapel M, Djouina M, Altare F, Arrieta MC, Cortot A, Colombel JF, Neut C, Desreumaux P. Aluminum enhances inflammation and decreases healing in experimental models of colitis. (CO, JFHOD, Paris 2010)

- Pineton de Chambrun G, Vignal C, Body-Malapel M, Djouina M, Altare F, Arrieta MC, Cortot A, Colombel JF, Neut C, Desreumaux P. Aluminum enhances inflammation and decreases healing in experimental models of colitis. (CO, 5th international meeting on inflammatory bowel diseases, Capri, 2010, Paris 2010)

- Pineton de Chambrun G, Manthey C, McAllister C, Till A, Kagnoff M, Desreumaux P, Stupack D, Wang J, Eckmann L. Caspase 8 maintains epithelial cell adhesion and intestinal homeostasis *in vivo* through regulation of clathrin-dependent endocytosis and autophagy. ***Journal of Crohn's & Colitis.*** (CO, ECCO, Vienne 2013)

- Pineton de Chambrun G, Manthey C, McAllister C, Till A, Kagnoff M, Desreumaux P, Stupack D, Wang J, Eckmann L. Caspase 8 maintains epithelial cell adhesion and intestinal homeostasis *in vivo* through regulation of clathrin-dependent endocytosis and autophagy. ***Gastroenterology.*** (CO, DDW, Orlando 2013)

- Pineton de Chambrun G, Manthey C, McAllister C, Till A, Kagnoff M, Desreumaux P, Stupack D, Wang J, Eckmann L. Caspase 8 maintains epithelial cell adhesion and intestinal homeostasis *in vivo* through regulation of clathrin-dependent endocytosis and autophagy. (CO, UEGW, Berlin 2013)

3. Communications affichées des travaux de thèse:

- Pineton de Chambrun G, Vignal C, Body-Malapel M, Djouina M, Altare F, Arrieta MC, Cortot A, Colombel JF, Neut C, Desreumaux P. Aluminum enhances inflammation and decreases healing in experimental models of colitis. ***Journal of Crohn's & Colitis***. feb 2010; 4: S19. (CA, ECCO, Prague 2010)

- Pineton de Chambrun G, Vignal C, Body-Malapel M, Djouina M, Altare F, Arrieta MC, Cortot A, Colombel JF, Neut C, Desreumaux P. Aluminum enhances inflammation and decreases healing in experimental models of colitis. ***Gastroenterology***. 2011;138(5, suppl. 1):Su1773. (CA, DDW, Chicago 2011)

- Pineton de Chambrun G, Manthey C, McAllister C, Till A, Kagnoff M, Desreumaux P, Stupack D, Wang J, Eckmann L. Caspase 8 maintains epithelial cell adhesion and intestinal homeostasis *in vivo* through regulation of clathrin-dependent endocytosis and autophagy. (CA, JFHOD, Paris 2013)

BIBLIOGRAPHIE

1. Xavier RJ, Podolsky DK. Unravelling the pathogenesis of inflammatory bowel disease. Nature. 2007 Jul 26;448(7152):427-34.

2. Abraham C, Cho JH. Inflammatory bowel disease. N Engl J Med. 2009 Nov 19;361(21):2066-78.

3. Loftus EV, Jr. Clinical epidemiology of inflammatory bowel disease: Incidence, prevalence, and environmental influences. Gastroenterology. 2004 May;126(6):1504-17.

4. Baumgart DC, Carding SR. Inflammatory bowel disease: cause and immunobiology. Lancet. 2007 May 12;369(9573):1627-40.

5. Baumgart DC, Sandborn WJ. Inflammatory bowel disease: clinical aspects and established and evolving therapies. Lancet. 2007 May 12;369(9573):1641-57.

6. Pineton de Chambrun G, Cortot A, Vignal C *et al.* Environnement : nouveaux facteurs environnementaux associés au développement des maladies inflammatoires chroniques intestinales. 2010;Progrès en hépato-gastroentérologie n°11(Maladies Inflammatoires Chroniques Intestinales, chapitre 5):72-84.

7. Baumgart DC, Sandborn WJ. Crohn's disease. Lancet. 2012 Nov 3;380(9853):1590-605.

8. Podolsky DK. Inflammatory bowel disease. N Engl J Med. 2002 Aug 8;347(6):417-29.

9. Pineton de Chambrun G, Peyrin-Biroulet L, Lemann M *et al.* Clinical implications of mucosal healing for the management of IBD. Nat Rev Gastroenterol Hepatol. 2010 Jan;7(1):15-29.

10. Rutgeerts P, D'Haens G, Van Assche G *et al.* Adalimumab Induces and Maintains Mucosal Healing in Patients With Moderate to Severe Ileocolonic Crohn's Disease - First Results of the EXTEND Trial. DDW abstract. 2009.

11. Rutgeerts P, Sandborn WJ, Feagan BG *et al.* Infliximab for induction and maintenance therapy for ulcerative colitis. N Engl J Med. 2005 Dec 8;353(23):2462-76.

12. Sandborn WJ, Colombel JF, Reinisch W *et al.* Infliximab induces and maintains mucosal healing in ulcerative colitis patients: the ACT trials. Am J Gastroenterol. 2005;100:S310.

13. Colombel J, Rutgeerts P, Reinisch W *et al.* SONIC: a randomized, double-blind, controlled trial comparing infliximab and infliximab plus azathioprine to azathioprine in patients with Crohn's disease naive to immunomodulators and biological therapy. UEGW abstract. 2008:OP001.

14. Hanauer SB, Feagan BG, Lichtenstein GR *et al.* Maintenance infliximab for Crohn's disease: the ACCENT I randomised trial. Lancet. 2002 May 4;359(9317):1541-9.

15. Rutgeerts P, Feagan BG, Lichtenstein GR *et al.* Comparison of scheduled and episodic treatment strategies of infliximab in Crohn's disease. Gastroenterology. 2004 Feb;126(2):402-13.

16. Sands BE, Anderson FH, Bernstein CN *et al.* Infliximab maintenance therapy for fistulizing Crohn's disease. N Engl J Med. 2004 Feb 26;350(9):876-85.

17. Colombel JF, Peyrin-Biroulet L. Natalizumab: a promising treatment for Crohn's disease. Expert Review of Clinical Immunology. 2006 september;2(5):677-89.

18. Feagan BG, Rutgeerts P, Sands BE *et al.* Vedolizumab as induction and maintenance therapy for ulcerative colitis. N Engl J Med. 2013 Aug 22;369(8):699-710.

19. Sandborn WJ, Colombel JF, Enns R *et al.* Natalizumab induction and maintenance therapy for Crohn's disease. N Engl J Med. 2005 Nov 3;353(18):1912-25.

20. Sandborn WJ, Feagan BG, Rutgeerts P *et al.* Vedolizumab as induction and maintenance therapy for Crohn's disease. N Engl J Med. 2013 Aug 22;369(8):711-21.

21. Targan SR, Feagan BG, Fedorak RN *et al.* Natalizumab for the treatment of active Crohn's disease: results of the ENCORE Trial. Gastroenterology. 2007 May;132(5):1672-83.

22. Sandborn WJ, Gasink C, Gao LL *et al.* Ustekinumab induction and maintenance therapy in refractory Crohn's disease. N Engl J Med. 2012 Oct 18;367(16):1519-28.

23. Bernstein CN, Shanahan F. Disorders of a modern lifestyle: reconciling the epidemiology of inflammatory bowel diseases. Gut. 2008 Sep;57(9):1185-91.

24. Abraham C, Medzhitov R. Interactions between the host innate immune system and microbes in inflammatory bowel disease. Gastroenterology. 2011 May;140(6):1729-37.

25. Khor B, Gardet A, Xavier RJ. Genetics and pathogenesis of inflammatory bowel disease. Nature. 2011 Jun 16;474(7351):307-17.

26. Halfvarson J, Bodin L, Tysk C *et al.* Inflammatory bowel disease in a Swedish twin cohort: a long-term follow-up of concordance and clinical characteristics. Gastroenterology. 2003 Jun;124(7):1767-73.

27. Gower-Rousseau C, Vernier-Massouille G, Cortot A *et al. Données récentes sur l'épidémiologie mondiale des MICI* (Voir références associées à ce chapitre) Progrès en gastroentérologie2009.

28. Pinsk V, Lemberg DA, Grewal K *et al.* Inflammatory bowel disease in the South Asian pediatric population of British Columbia. Am J Gastroenterol. 2007 May;102(5):1077-83.

29. Bach JF. The effect of infections on susceptibility to autoimmune and allergic diseases. N Engl J Med. 2002 Sep 19;347(12):911-20.

30. Laharie D, Debeugny S, Peeters M *et al.* Inflammatory bowel disease in spouses and their offspring. Gastroenterology. 2001 Mar;120(4):816-9.

31. Soderholm JD, Olaison G, Lindberg E *et al.* Different intestinal permeability patterns in relatives and spouses of patients with Crohn's disease: an inherited defect in mucosal defence? Gut. 1999 Jan;44(1):96-100.

32. Teahon K, Smethurst P, Levi AJ *et al.* Intestinal permeability in patients with Crohn's disease and their first degree relatives. Gut. 1992 Mar;33(3):320-3.

33. Cosnes J. Tobacco and IBD: relevance in the understanding of disease mechanisms and clinical practice. Best Pract Res Clin Gastroenterol. 2004 Jun;18(3):481-96.

34. Cortot A, Pineton de Chambrun G, Vernier-Massouille G *et al.* [Inflammatory bowel disease: genetic or environmental diseases?]. Gastroenterologie clinique et biologique. 2009 Aug-Sep;33(8-9):681-91.

35. Rioux JD, Xavier RJ, Taylor KD *et al.* Genome-wide association study identifies new susceptibility loci for Crohn disease and implicates autophagy in disease pathogenesis. Nat Genet. 2007 May;39(5):596-604.

36. Larrieu S, Jusot JF, Blanchard M *et al.* Short term effects of air pollution on hospitalizations for cardiovascular diseases in eight French cities: the PSAS program. Sci Total Environ. 2007 Nov 15;387(1-3):105-12.

37. Powell JJ, Faria N, Thomas-McKay E *et al.* Origin and fate of dietary nanoparticles and microparticles in the gastrointestinal tract. Journal of autoimmunity. 2010 May;34(3):J226-33.

38. Bernstein JA, Alexis N, Barnes C *et al.* Health effects of air pollution. J Allergy Clin Immunol. 2004 Nov;114(5):1116-23.

39. Ananthakrishnan AN, McGinley EL, Binion DG *et al.* Ambient air pollution correlates with hospitalizations for inflammatory bowel disease: an ecologic analysis. Inflamm Bowel Dis. 2011 May;17(5):1138-45.

40. Kaplan G. Air pollution and the inflammatory bowel diseases. Inflamm Bowel Dis. 2011 May;17(5):1146-8.

41. Kaplan GG, Hubbard J, Korzenik J *et al.* The inflammatory bowel diseases and ambient air pollution: a novel association. Am J Gastroenterol. 2010 Nov;105(11):2412-9.

42. Lomer MC, Harvey RS, Evans SM *et al.* Efficacy and tolerability of a low microparticle diet in a double blind, randomized, pilot study in Crohn's disease. Eur J Gastroenterol Hepatol. 2001 Feb;13(2):101-6.

43. Mutlu EA, Engen PA, Soberanes S *et al.* Particulate matter air pollution causes oxidant-mediated increase in gut permeability in mice. Particle and fibre toxicology. 2011;8:19.

44. Powell JJ, Ainley CC, Harvey RS *et al.* Characterisation of inorganic microparticles in pigment cells of human gut associated lymphoid tissue. Gut. 1996 Mar;38(3):390-5.

45. Salim SY, Jovel J, Wine E *et al.* Exposure to ingested airborne pollutant particulate matter increases mucosal exposure to bacteria and induces early onset of inflammation in neonatal IL-10-deficient mice. Inflamm Bowel Dis. 2014 Jul;20(7):1129-38.

46. Shepherd NA, Crocker PR, Smith AP *et al.* Exogenous pigment in Peyer's patches. Hum Pathol. 1987 Jan;18(1):50-4.

47. Lomer MC, Grainger SL, Ede R *et al.* Lack of efficacy of a reduced microparticle diet in a multi-centred trial of patients with active Crohn's disease. Eur J Gastroenterol Hepatol. 2005 Mar;17(3):377-84.

48. Salim SY, Kaplan GG, Madsen KL. Air pollution effects on the gut microbiota: a link between exposure and inflammatory disease. Gut microbes. 2014 Mar-Apr;5(2):215-9.

49. Becaria A, Campbell A, Bondy SC. Aluminum as a toxicant. Toxicol Ind Health. 2002 Aug;18(7):309-20.

50. Gourier-Frery C, Frery N, Berr C *et al.* Aluminuim: Quels risques pour la santé? Synthèse des études épidémiologiques. Volet épidémiologiques de l'expertise collective InVS-Afssa-Afssaps. Institut de veille sanitaire, novembre. 2003:http://www.invs.sante.fr/publications/2003/aluminium_/.

51. Nayak P. Aluminum: impacts and disease. Environ Res. 2002 Jun;89(2):101-15.

52. Keith S. Toxicological profile: aluminum. US department of health and human services. Public health service. Agency for toxic substances and disease registry. September. 2008:http://www.atsdr.cdc.gov/toxprofiles/tp.asp?id=191&tid=34.

53. Exley C, Begum A, Woolley MP *et al.* Aluminum in tobacco and cannabis and smoking-related disease. Am J Med. 2006 Mar;119(3):276 e9-11.

54. Greger JL. Aluminum metabolism. Annu Rev Nutr. 1993;13:43-63.

55. Walton JR. A longitudinal study of rats chronically exposed to aluminum at human dietary levels. Neurosci Lett. 2007 Jan 22;412(1):29-33.

56. Lerner A. Aluminum is a potential environmental factor for Crohn's disease induction: extended hypothesis. Ann N Y Acad Sci. 2007 Jun;1107:329-45.

57. Osinska E, Kanoniuk D, Kusiak A. Aluminum hemotoxicity mechanisms. Ann Univ Mariae Curie Sklodowska [Med]. 2004;59(1):411-6.

58. Eisenbarth SC, Colegio OR, O'Connor W *et al.* Crucial role for the Nalp3 inflammasome in the immunostimulatory properties of aluminium adjuvants. Nature. 2008 Jun 19;453(7198):1122-6.

59. Hornung V, Bauernfeind F, Halle A *et al.* Silica crystals and aluminum salts activate the NALP3 inflammasome through phagosomal destabilization. Nat Immunol. 2008 Aug;9(8):847-56.

60. Kool M, Soullie T, van Nimwegen M *et al.* Alum adjuvant boosts adaptive immunity by inducing uric acid and activating inflammatory dendritic cells. J Exp Med. 2008 Apr 14;205(4):869-82.

61. Li H, Willingham SB, Ting JP *et al.* Cutting edge: inflammasome activation by alum and alum's adjuvant effect are mediated by NLRP3. J Immunol. 2008 Jul 1;181(1):17-21.

62. Armstrong RA, Winsper SJ, Blair JA. Hypothesis: is Alzheimer's disease a metal-induced immune disorder? Neurodegeneration. 1995 Mar;4(1):107-11.

63. Fogarty U, Perl D, Good P *et al.* A cluster of equine granulomatous enteritis cases: the link with aluminium. Vet Hum Toxicol. 1998 Oct;40(5):297-305.

64. Chen WJ, Monnat RJ, Jr., Chen M *et al.* Aluminum induced pulmonary granulomatosis. Hum Pathol. 1978 Nov;9(6):705-11.

65. Vogelbruch M, Nuss B, Korner M *et al.* Aluminium-induced granulomas after inaccurate intradermal hyposensitization injections of aluminium-adsorbed depot preparations. Allergy. 2000 Sep;55(9):883-7.

66. Schoultz I, Verma D, Halfvarsson J *et al.* Combined polymorphisms in genes encoding the inflammasome components NALP3 and CARD8 confer susceptibility to Crohn's disease in Swedish men. Am J Gastroenterol. 2009 May;104(5):1180-8.

67. Pineton de Chambrun G, Body-Malapel M, Frey-Wagner I *et al.* Aluminum enhances inflammation and decreases mucosal healing in experimental colitis in mice. Mucosal immunology. 2014 May;7(3):589-601.

68. Kabi A, Nickerson KP, Homer CR *et al.* Digesting the genetics of inflammatory bowel disease: insights from studies of autophagy risk genes. Inflamm Bowel Dis. 2012 Apr;18(4):782-92.

69. Kaser A, Zeissig S, Blumberg RS. Genes and environment: how will our concepts on the pathophysiology of IBD develop in the future? Dig Dis. 2010;28(3):395-405.

70. Molodecky NA, Soon IS, Rabi DM *et al.* Increasing incidence and prevalence of the inflammatory bowel diseases with time, based on systematic review. Gastroenterology. 2012 Jan;142(1):46-54 e42; quiz e30.

71. Cosnes J, Carbonnel F, Beaugerie L *et al.* Effects of appendicectomy on the course of ulcerative colitis. Gut. 2002 Dec;51(6):803-7.

72. De Vroey B, De Cassan C, Gower-Rousseau C *et al.* Editorial: Antibiotics earlier, IBD later? Am J Gastroenterol. Dec;105(12):2693-6.

73. Hviid A, Svanstrom H, Frisch M. Antibiotic use and inflammatory bowel diseases in childhood. Gut. 2011 Jan;60(1):49-54.

74. Greger JL, Sutherland JE. Aluminum exposure and metabolism. Crit Rev Clin Lab Sci. 1997 Oct;34(5):439-74.

75. Zaki MH, Boyd KL, Vogel P *et al.* The NLRP3 inflammasome protects against loss of epithelial integrity and mortality during experimental colitis. Immunity. 2010 Mar 26;32(3):379-91.

76. Puissegur MP, Botanch C, Duteyrat JL *et al.* An in vitro dual model of mycobacterial granulomas to investigate the molecular interactions between mycobacteria and human host cells. Cell Microbiol. 2004 May;6(5):423-33.

77. Meconi S, Vercellone A, Levillain F *et al.* Adherent-invasive Escherichia coli isolated from Crohn's disease patients induce granulomas in vitro. Cell Microbiol. 2007 May;9(5):1252-61.

78. Taylor GA, Moore PB, Ferrier IN *et al.* Gastrointestinal absorption of aluminium and citrate in man. J Inorg Biochem. 1998 Feb 15;69(3):165-9.

79. Meyer-Baron M, Schaper M, Knapp G *et al.* Occupational aluminum exposure: evidence in support of its neurobehavioral impact. Neurotoxicology. 2007 Nov;28(6):1068-78.

80. Malluche HH. Aluminium and bone disease in chronic renal failure. Nephrol Dial Transplant. 2002;17 Suppl 2:21-4.

81. Cunat L, Lanhers MC, Joyeux M *et al.* Bioavailability and intestinal absorption of aluminum in rats: effects of aluminum compounds and some dietary constituents. Biol Trace Elem Res. 2000 Jul;76(1):31-55.

82. Powell JJ, Ainley CC, Evans R *et al.* Intestinal perfusion of dietary levels of aluminium: association with the mucosa. Gut. 1994 Aug;35(8):1053-7.

83. Urbanski SJ, Arsenault AL, Green FH *et al.* Pigment resembling atmospheric dust in Peyer's patches. Mod Pathol. 1989 May;2(3):222-6.

84. Lerner A ES, Perl D, et al. The role of aluminum in bacterial-induced colitis in IL-10 deficient mice (abstract). Gastroenterology. 2006;130(4):362–3.

85. Burrell SA, Exley C. There is (still) too much aluminium in infant formulas. BMC Pediatr. 2010;10:63.

86. Sly PD, Flack F. Susceptibility of children to environmental pollutants. Ann N Y Acad Sci. 2008 Oct;1140:163-83.

87. Greger JL. Dietary and other sources of aluminium intake. Ciba Found Symp. 1992;169:26-35; discussion -49.

88. Aspenstrom-Fagerlund B, Sundstrom B, Tallkvist J *et al.* Fatty acids increase paracellular absorption of aluminium across Caco-2 cell monolayers. Chem Biol Interact. 2009 Oct 7;181(2):272-8.

89. Exley C, Siesjo P, Eriksson H. The immunobiology of aluminium adjuvants: how do they really work? Trends Immunol. 2010 Mar;31(3):103-9.

90. Perl DP, Fogarty U, Harpaz N *et al.* Bacterial-metal interactions: the potential role of aluminum and other trace elements in the etiology of Crohn's disease. Inflamm Bowel Dis. 2004 Nov;10(6):881-3.

91. Exley C, Swarbrick L, Gherardi RK *et al.* A role for the body burden of aluminium in vaccine-associated macrophagic myofasciitis and chronic fatigue syndrome. Med Hypotheses. 2009 Feb;72(2):135-9.

92. Sandstrom RE. Aluminum induced pulmonary granulomatosis. Hum Pathol. 1979 Jul;10(4):481.

93. van der Voet GB, Dijkmans BA, Frankfort C *et al.* Elevation of serum aluminium concentrations in patients with rheumatoid arthritis treated with drugs containing aluminium. British journal of rheumatology. 1989 Apr;28(2):144-6.

94. Roediger WE, Babidge W. Human colonocyte detoxification. Gut. 1997 Dec;41(6):731-4.

95. Kaminsky LS, Zhang QY. The small intestine as a xenobiotic-metabolizing organ. Drug Metab Dispos. 2003 Dec;31(12):1520-5.

96. Brant SR, Panhuysen CI, Nicolae D *et al.* MDR1 Ala893 polymorphism is associated with inflammatory bowel disease. Am J Hum Genet. 2003 Dec;73(6):1282-92.

97. Langmann T, Moehle C, Mauerer R *et al.* Loss of detoxification in inflammatory bowel disease: dysregulation of pregnane X receptor target genes. Gastroenterology. 2004 Jul;127(1):26-40.

98. Wirtz S, Neufert C, Weigmann B *et al.* Chemically induced mouse models of intestinal inflammation. Nat Protoc. 2007;2(3):541-6.

99. Ameho CK, Adjei AA, Harrison EK *et al.* Prophylactic effect of dietary glutamine supplementation on interleukin 8 and tumour necrosis factor alpha production in trinitrobenzene sulphonic acid induced colitis. Gut. 1997 Oct;41(4):487-93.

100. Yan Y, Kolachala V, Dalmasso G *et al.* Temporal and spatial analysis of clinical and molecular parameters in dextran sodium sulfate induced colitis. PLoS One. 2009;4(6):e6073.

101. Obermeier F, Kojouharoff G, Hans W *et al.* Interferon-gamma (IFN-gamma)- and tumour necrosis factor (TNF)-induced nitric oxide as toxic effector molecule in chronic dextran sulphate sodium (DSS)-induced colitis in mice. Clin Exp Immunol. 1999 May;116(2):238-45.

102. Becker C, Fantini MC, Neurath MF. High resolution colonoscopy in live mice. Nat Protoc. 2006;1(6):2900-4.

103. Anton PM, Gay J, Mykoniatis A *et al.* Corticotropin-releasing hormone (CRH) requirement in Clostridium difficile toxin A-mediated intestinal inflammation. Proceedings of the National Academy of Sciences of the United States of America. 2004 Jun 1;101(22):8503-8.

104. Aamodt G, Bukholm G, Jahnsen J *et al.* The association between water supply and inflammatory bowel disease based on a 1990-1993 cohort study in southeastern Norway. Am J Epidemiol. 2008 Nov 1;168(9):1065-72.

105. Zhang YZ, Li YY. Inflammatory bowel disease: pathogenesis. World J Gastroenterol. 2014 Jan 7;20(1):91-9.

106. Jostins L, Ripke S, Weersma RK *et al.* Host-microbe interactions have shaped the genetic architecture of inflammatory bowel disease. Nature. 2012 Nov 1;491(7422):119-24.

107. Ogura Y, Bonen DK, Inohara N *et al.* A frameshift mutation in NOD2 associated with susceptibility to Crohn's disease. Nature. 2001 May 31;411(6837):603-6.

108. Travassos LH, Carneiro LA, Ramjeet M *et al.* Nod1 and Nod2 direct autophagy by recruiting ATG16L1 to the plasma membrane at the site of bacterial entry. Nat Immunol. 2010 Jan;11(1):55-62.

109. Shaw MH, Kamada N, Warner N *et al.* The ever-expanding function of NOD2: autophagy, viral recognition, and T cell activation. Trends Immunol. 2011 Feb;32(2):73-9.

110. Hampe J, Franke A, Rosenstiel P *et al.* A genome-wide association scan of nonsynonymous SNPs identifies a susceptibility variant for Crohn disease in ATG16L1. Nat Genet. 2007 Feb;39(2):207-11.

111. McCarroll SA, Huett A, Kuballa P *et al.* Deletion polymorphism upstream of IRGM associated with altered IRGM expression and Crohn's disease. Nat Genet. 2008 Sep;40(9):1107-12.

112. Gunther C, Martini E, Wittkopf N *et al.* Caspase-8 regulates TNF-alpha-induced epithelial necroptosis and terminal ileitis. Nature. 2011 Sep 15;477(7364):335-9.

113. Hall PA, Coates PJ, Goodlad RA *et al.* Proliferating cell nuclear antigen expression in non-cycling cells may be induced by growth factors in vivo. British journal of cancer. 1994 Aug;70(2):244-7.

114. Goto Y, Ivanov, II. Intestinal epithelial cells as mediators of the commensal-host immune crosstalk. Immunology and cell biology. 2013 Mar;91(3):204-14.

115. Nenci A, Becker C, Wullaert A *et al.* Epithelial NEMO links innate immunity to chronic intestinal inflammation. Nature. 2007 Mar 29;446(7135):557-61.

116. Nunes T, Bernardazzi C, de Souza HS. Cell Death and Inflammatory Bowel Diseases: Apoptosis, Necrosis, and Autophagy in the Intestinal Epithelium. BioMed research international. 2014;2014:218493.

117. Sanders DS. Mucosal integrity and barrier function in the pathogenesis of early lesions in Crohn's disease. Journal of clinical pathology. 2005 Jun;58(6):568-72.

118. Becker C, Watson AJ, Neurath MF. Complex roles of caspases in the pathogenesis of inflammatory bowel disease. Gastroenterology. 2013 Feb;144(2):283-93.

119. Gunther C, Neumann H, Neurath MF *et al.* Apoptosis, necrosis and necroptosis: cell death regulation in the intestinal epithelium. Gut. 2013 Jul;62(7):1062-71.

120. Piao X, Komazawa-Sakon S, Nishina T *et al.* c-FLIP maintains tissue homeostasis by preventing apoptosis and programmed necrosis. Science signaling. 2012 Dec 18;5(255):ra93.

121. Welz PS, Wullaert A, Vlantis K *et al.* FADD prevents RIP3-mediated epithelial cell necrosis and chronic intestinal inflammation. Nature. 2011 Sep 15;477(7364):330-4.

122. Fuchs Y, Steller H. Programmed cell death in animal development and disease. Cell. 2011 Nov 11;147(4):742-58.

123. Taylor RC, Cullen SP, Martin SJ. Apoptosis: controlled demolition at the cellular level. Nature reviews Molecular cell biology. 2008 Mar;9(3):231-41.

124. Fulda S. Caspase-8 in cancer biology and therapy. Cancer letters. 2009 Aug 28;281(2):128-33.

125. Stupack DG. Caspase-8 as a therapeutic target in cancer. Cancer letters. 2010 Sep 1.

126. Kaiser WJ, Upton JW, Long AB *et al.* RIP3 mediates the embryonic lethality of caspase-8-deficient mice. Nature. 2011 Mar 17;471(7338):368-72.

127. Austin CD, Lawrence DA, Peden AA *et al.* Death-receptor activation halts clathrin-dependent endocytosis. Proceedings of the National Academy of Sciences of the United States of America. 2006 Jul 5;103(27):10283-8.

128. Barbero S, Mielgo A, Torres V *et al.* Caspase-8 association with the focal adhesion complex promotes tumor cell migration and metastasis. Cancer Res. 2009 May 1;69(9):3755-63.

129. Finlay D, Vuori K. Novel noncatalytic role for caspase-8 in promoting SRC-mediated adhesion and Erk signaling in neuroblastoma cells. Cancer Res. 2007 Dec 15;67(24):11704-11.

130. Bell BD, Leverrier S, Weist BM *et al.* FADD and caspase-8 control the outcome of autophagic signaling in proliferating T cells. Proceedings of the National Academy of Sciences of the United States of America. 2008 Oct 28;105(43):16677-82.

131. Dupaul-Chicoine J, Dagenais M, Saleh M. Crosstalk between the intestinal microbiota and the innate immune system in intestinal homeostasis and inflammatory bowel disease. Inflamm Bowel Dis. 2013 Sep;19(10):2227-37.

132. Glocker EO, Kotlarz D, Boztug K *et al.* Inflammatory bowel disease and mutations affecting the interleukin-10 receptor. N Engl J Med. 2009 Nov 19;361(21):2033-45.

133. Beisner DR, Ch'en IL, Kolla RV *et al.* Cutting edge: innate immunity conferred by B cells is regulated by caspase-8. J Immunol. 2005 Sep 15;175(6):3469-73.

134. Madison BB, Dunbar L, Qiao XT *et al.* Cis elements of the villin gene control expression in restricted domains of the vertical (crypt) and horizontal (duodenum, cecum) axes of the intestine. The Journal of biological chemistry. 2002 Sep 6;277(36):33275-83.

135. Maaser C, Housley MP, Iimura M *et al.* Clearance of Citrobacter rodentium requires B cells but not secretory immunoglobulin A (IgA) or IgM antibodies. Infection and immunity. 2004 Jun;72(6):3315-24.

136. Feil R, Wagner J, Metzger D *et al.* Regulation of Cre recombinase activity by mutated estrogen receptor ligand-binding domains. Biochemical and biophysical research communications. 1997 Aug 28;237(3):752-7.

137. Goretsky T, Dirisina R, Sinh P *et al.* p53 mediates TNF-induced epithelial cell apoptosis in IBD. The American journal of pathology. 2012 Oct;181(4):1306-15.

138. White LE, Santora RJ, Cui Y *et al.* TNFR1-dependent pulmonary apoptosis during ischemic acute kidney injury. American journal of physiology Lung cellular and molecular physiology. 2012 Sep;303(5):L449-59.

139. Takahashi N, Duprez L, Grootjans S *et al.* Necrostatin-1 analogues: critical issues on the specificity, activity and in vivo use in experimental disease models. Cell death & disease. 2012;3:e437.

140. Stutzmann J, Bellissent-Waydelich A, Fontao L *et al.* Adhesion complexes implicated in intestinal epithelial cell-matrix interactions. Microscopy research and technique. 2000 Oct 15;51(2):179-90.

141. Robinson MS. Adaptable adaptors for coated vesicles. Trends in cell biology. 2004 Apr;14(4):167-74.

142. Ares GR, Ortiz PA. Dynamin2, clathrin, and lipid rafts mediate endocytosis of the apical Na/K/2Cl cotransporter NKCC2 in thick ascending limbs. The Journal of biological chemistry. 2012 Nov 2;287(45):37824-34.

143. Ravikumar B, Moreau K, Jahreiss L *et al.* Plasma membrane contributes to the formation of pre-autophagosomal structures. Nature cell biology. 2010 Aug;12(8):747-57.

144. Tanida I, Ueno T, Kominami E. LC3 conjugation system in mammalian autophagy. The international journal of biochemistry & cell biology. 2004 Dec;36(12):2503-18.

145. Komatsu M, Waguri S, Ueno T *et al.* Impairment of starvation-induced and constitutive autophagy in Atg7-deficient mice. The Journal of cell biology. 2005 May 9;169(3):425-34.

146. Goto Y, Kiyono H. Epithelial barrier: an interface for the cross-communication between gut flora and immune system. Immunological reviews. 2012 Jan;245(1):147-63.

147. Camilleri M, Madsen K, Spiller R *et al.* Intestinal barrier function in health and gastrointestinal disease. Neurogastroenterology and motility : the official journal of the European Gastrointestinal Motility Society. 2012 Jun;24(6):503-12.

148. Deuring JJ, de Haar C, Kuipers EJ *et al.* The cell biology of the intestinal epithelium and its relation to inflammatory bowel disease. The international journal of biochemistry & cell biology. 2013 Apr;45(4):798-806.

149. Hall PA, Coates PJ, Ansari B *et al.* Regulation of cell number in the mammalian gastrointestinal tract: the importance of apoptosis. Journal of cell science. 1994 Dec;107 (Pt 12):3569-77.

150. Watson AJ, Hughes KR. TNF-alpha-induced intestinal epithelial cell shedding: implications for intestinal barrier function. Ann N Y Acad Sci. 2012 Jul;1258:1-8.

151. Rubinstein AD, Kimchi A. Life in the balance - a mechanistic view of the crosstalk between autophagy and apoptosis. Journal of cell science. 2012 Nov 15;125(Pt 22):5259-68.

152. Yu L, Alva A, Su H *et al.* Regulation of an ATG7-beclin 1 program of autophagic cell death by caspase-8. Science. 2004 Jun 4;304(5676):1500-2.

153. Buchler G, Wos-Oxley ML, Smoczek A *et al.* Strain-specific colitis susceptibility in IL10-deficient mice depends on complex gut microbiota-host interactions. Inflamm Bowel Dis. 2012 May;18(5):943-54.

154. Colombel JF, Sandborn WJ, Reinisch W *et al.* Infliximab, azathioprine, or combination therapy for Crohn's disease. N Engl J Med. 2010 Apr 15;362(15):1383-95.

155. Marchiando AM, Ramanan D, Ding Y *et al.* A Deficiency in the Autophagy Gene Atg16L1 Enhances Resistance to Enteric Bacterial Infection. Cell host & microbe. 2013 Aug 14;14(2):216-24.

156. Thachil E, Hugot JP, Arbeille B *et al.* Abnormal activation of autophagy-induced crinophagy in Paneth cells from patients with Crohn's disease. Gastroenterology. 2012 May;142(5):1097-9 e4.

157. Chiu CJ, McArdle AH, Brown R *et al.* Intestinal mucosal lesion in low-flow states. I. A morphological, hemodynamic, and metabolic reappraisal. Archives of surgery. 1970 Oct;101(4):478-83.

158. Abreu MT. Toll-like receptor signalling in the intestinal epithelium: how bacterial recognition shapes intestinal function. Nat Rev Immunol. 2010 Feb;10(2):131-44.

159. Kawai T, Akira S. Toll-like receptor and RIG-I-like receptor signaling. Ann N Y Acad Sci. 2008 Nov;1143:1-20.

160. Thompson AJV, Locarnini SA. Toll-like receptors, RIG-I-like RNA helicases and the antiviral innate immune response. Immunology and cell biology. 2007;85(6):435-45.

161. Zhou R, Wei H, Sun R *et al.* Recognition of double-stranded RNA by TLR3 induces severe small intestinal injury in mice. J Immunol. 2007 Apr 1;178(7):4548-56.

162. Clarke P, Tyler KL. Apoptosis in animal models of virus-induced disease. Nat Rev Micro. 2009;7(2):144-55.

163. Chattopadhyay S, Marques JT, Yamashita M *et al.* Viral apoptosis is induced by IRF-3-mediated activation of Bax. EMBO J. 2010 May 19;29(10):1762-73.

164. Kalai M, Van Loo G, Vanden Berghe T *et al.* Tipping the balance between necrosis and apoptosis in human and murine cells treated with interferon and dsRNA. Cell Death Differ. 2002 Sep;9(9):981-94.

165. Kaiser WJ, Offermann MK. Apoptosis induced by the toll-like receptor adaptor TRIF is dependent on its receptor interacting protein homotypic interaction motif. J Immunol. 2005 Apr 15;174(8):4942-52.

166. Feoktistova M, Geserick P, Kellert B *et al.* cIAPs block Ripoptosome formation, a RIP1/caspase-8 containing intracellular cell death complex differentially regulated by cFLIP isoforms. Mol Cell. 2011 Aug 5;43(3):449-63.

167. Estornes Y, Toscano F, Virard F *et al.* dsRNA induces apoptosis through an atypical death complex associating TLR3 to caspase-8. Cell Death Differ. 2012 Mar 16;Epub.

168. Van Herreweghe F, Festjens N, Declercq W *et al.* Tumor necrosis factor-mediated cell death: to break or to burst, that's the question. Cell Mol Life Sci. 2010 May;67(10):1567-79.

169. Piguet PF, Vesin C, Guo J *et al.* TNF-induced enterocyte apoptosis in mice is mediated by the TNF receptor 1 and does not require p53. Eur J Immunol. 1998 Nov;28(11):3499-505.

170. Lau KS, Juchheim AM, Cavaliere KR *et al.* In vivo systems analysis identifies spatial and temporal aspects of the modulation of TNF-alpha-induced apoptosis and proliferation by MAPKs. Science signaling. 2011;4(165):ra16.

171. Fan Y, Bergmann A. The cleaved-Caspase-3 antibody is a marker of Caspase-9-like DRONC activity in Drosophila. Cell Death Differ. 2009;17(3):534-9.

172. Balachandran S, Roberts PC, Kipperman T *et al.* Alpha/beta interferons potentiate virus-induced apoptosis through activation of the FADD/Caspase-8 death signaling pathway. J Virol. 2000 Feb;74(3):1513-23.

173. Jiang Z, Mak TW, Sen G *et al.* Toll-like receptor 3-mediated activation of NF-kappaB and IRF3 diverges at Toll-IL-1 receptor domain-containing adapter inducing IFN-beta. Proceedings of the National Academy of Sciences of the United States of America. 2004 Mar 9;101(10):3533-8.

174. Egan LJ, Eckmann L, Greten FR *et al.* IkappaB-kinasebeta-dependent NF-kappaB activation provides radioprotection to the intestinal epithelium. Proceedings of the National Academy of Sciences of the United States of America. 2004 Feb 24;101(8):2452-7.

175. Eckmann L, Nebelsiek T, Fingerle AA *et al.* Opposing functions of IKKbeta during acute and chronic intestinal inflammation. Proceedings of the National Academy of Sciences of the United States of America. 2008 Sep 30;105(39):15058-63.

176. Page ST, van Oers NS, Perlmutter RM *et al.* Differential contribution of Lck and Fyn protein tyrosine kinases to intraepithelial lymphocyte development. Eur J Immunol. 1997 Feb;27(2):554-62.

177. Abe K, Nguyen KP, Fine SD *et al.* Conventional dendritic cells regulate the outcome of colonic inflammation independently of T cells. Proceedings of the National Academy of Sciences. 2007 October 23, 2007;104(43):17022-7.

178. Mocarski ES, Upton JW, Kaiser WJ. Viral infection and the evolution of caspase 8-regulated apoptotic and necrotic death pathways. Nat Rev Immunol. 2011 Feb;12(2):79-88.

179. Broquet AH, Hirata Y, McAllister CS *et al.* RIG-I/MDA5/MAVS are required to signal a protective IFN response in rotavirus-infected intestinal epithelium. J Immunol. 2011 Feb 1;186(3):1618-26.

180. Hirata Y, Broquet AH, Menchen L *et al.* Activation of innate immune defense mechanisms by signaling through RIG-I/IPS-1 in intestinal epithelial cells. J Immunol. 2007 Oct 15;179(8):5425-32.

181. Elewaut D, DiDonato JA, Kim JM *et al.* NF-kappa B is a central regulator of the intestinal epithelial cell innate immune response induced by infection with enteroinvasive bacteria. J Immunol. 1999 Aug 1;163(3):1457-66.

182. Chae S, Eckmann L, Miyamoto Y *et al.* Epithelial cell I kappa B-kinase beta has an important protective role in Clostridium difficile toxin A-induced mucosal injury. J Immunol. 2006 Jul 15;177(2):1214-20.

183. Linkermann A, Brasen JH, De Zen F *et al.* Dichotomy between RIP1- and RIP3-mediated Necroptosis in Tumor Necrosis Factor alpha-induced Shock. Mol Med. 2012 Feb 24.

184. Cho YS, Challa S, Moquin D *et al.* Phosphorylation-driven assembly of the RIP1-RIP3 complex regulates programmed necrosis and virus-induced inflammation. Cell. 2009 Jun 12;137(6):1112-23.

185. Leist M, Gantner F, Bohlinger I *et al.* Tumor necrosis factor-induced hepatocyte apoptosis precedes liver failure in experimental murine shock models. The American journal of pathology. 1995 May;146(5):1220-34.

186. Jiang Q, Wei H, Tian Z. Poly I:C enhances cycloheximide-induced apoptosis of tumor cells through TLR3 pathway. BMC Cancer. 2008;8:12.

187. Plumpe J, Malek NP, Bock CT *et al.* NF-kappaB determines between apoptosis and proliferation in hepatocytes during liver regeneration. Am J Physiol Gastrointest Liver Physiol. 2000 Jan;278(1):G173-83.

188. Inan MS, Tolmacheva V, Wang QS *et al.* Transcription factor NF-kappaB participates in regulation of epithelial cell turnover in the colon. Am J Physiol Gastrointest Liver Physiol. 2000 Dec;279(6):G1282-91.

189. Tong X, Yin L, Washington R *et al.* The p50-p50 NF-kappaB complex as a stimulus-specific repressor of gene activation. Mol Cell Biochem. 2004 Oct;265(1-2):171-83.

190. Toruner M, Fernandez-Zapico M, Sha JJ *et al.* Antianoikis effect of nuclear factor-kappaB through up-regulated expression of osteoprotegerin, BCL-2, and IAP-1. The Journal of biological chemistry. 2006 Mar 31;281(13):8686-96.

191. Davidson GP, Barnes GL. Structural and functional abnormalities of the small intestine in infants and young children with rotavirus enteritis. Acta Paediatr Scand. 1979 Mar;68(2):181-6.
192. Salim AF, Phillips AD, Walker-Smith JA *et al.* Sequential changes in small intestinal structure and function during rotavirus infection in neonatal rats. Gut. 1995 Feb;36(2):231-8.
193. Otto PH, Clarke IN, Lambden PR *et al.* Infection of calves with bovine norovirus GIII.1 strain Jena virus: an experimental model to study the pathogenesis of norovirus infection. Journal of Virology. 2011 November 15, 2011;85(22):12013-21.
194. Ahlquist P. Parallels among positive-strand RNA viruses, reverse-transcribing viruses and double-stranded RNA viruses. Nat Rev Microbiol. 2006 May;4(5):371-82.
195. McCartney SA, Thackray LB, Gitlin L *et al.* MDA-5 recognition of a murine norovirus. PLoS Pathog. 2008 Jul;4(7):e1000108.
196. Pott J, Stockinger S, Torow N *et al.* Age-Dependent TLR3 Expression of the Intestinal Epithelium Contributes to Rotavirus Susceptibility. PLoS Pathog. 2012 May;8(5):e1002670.
197. Zhou R, Wei H, Sun R *et al.* NKG2D recognition mediates Toll-like receptor 3 signaling-induced breakdown of epithelial homeostasis in the small intestines of mice. Proceedings of the National Academy of Sciences of the United States of America. 2007 May 1;104(18):7512-5.
198. Lodolce JP, Burkett PR, Boone DL *et al.* T cell-independent interleukin 15Ralpha signals are required for bystander proliferation. J Exp Med. 2001 Oct 15;194(8):1187-94.
199. Kariko K, Ni H, Capodici J *et al.* mRNA is an endogenous ligand for Toll-like receptor 3. The Journal of biological chemistry. 2004 Mar 26;279(13):12542-50.
200. Brentano F, Schorr O, Gay RE *et al.* RNA released from necrotic synovial fluid cells activates rheumatoid arthritis synovial fibroblasts via Toll-like receptor 3. Arthritis Rheum. 2005 Sep;52(9):2656-65.
201. Murray LA, Knight DA, McAlonan L *et al.* Deleterious role of TLR3 during hyperoxia-induced acute lung injury. Am J Respir Crit Care Med. 2008 Dec 15;178(12):1227-37.
202. Cavassani KA, Ishii M, Wen H *et al.* TLR3 is an endogenous sensor of tissue necrosis during acute inflammatory events. J Exp Med. 2008 Oct 27;205(11):2609-21.
203. Hoebe K, Du X, Georgel P *et al.* Identification of Lps2 as a key transducer of MyD88-independent TIR signalling. Nature. 2003 Aug 14;424(6950):743-8.
204. Knudson CM, Tung KS, Tourtellotte WG *et al.* Bax-deficient mice with lymphoid hyperplasia and male germ cell death. Science. 1995 Oct 6;270(5233):96-9.

205. Mombaerts P, Iacomini J, Johnson RS *et al.* RAG-1-deficient mice have no mature B and T lymphocytes. Cell. 1992 Mar 6;68(5):869-77.

206. Kopf M, Baumann H, Freer G *et al.* Impaired immune and acute-phase responses in interleukin-6-deficient mice. Nature. 1994 Mar 24;368(6469):339-42.

207. Glaccum MB, Stocking KL, Charrier K *et al.* Phenotypic and functional characterization of mice that lack the type I receptor for IL-1. J Immunol. 1997 Oct 1;159(7):3364-71.

208. Kennedy MK, Glaccum M, Brown SN *et al.* Reversible defects in natural killer and memory CD8 T cell lineages in interleukin 15-deficient mice. J Exp Med. 2000 Mar 6;191(5):771-80.

209. Van Uden JH, Tran CH, Carson DA *et al.* Type I interferon is required to mount an adaptive response to immunostimulatory DNA. Eur J Immunol. 2001 Nov;31(11):3281-90.

210. Yang YL, Reis LF, Pavlovic J *et al.* Deficient signaling in mice devoid of double-stranded RNA-dependent protein kinase. EMBO J. 1995 Dec 15;14(24):6095-106.

211. Adachi O, Kawai T, Takeda K *et al.* Targeted disruption of the MyD88 gene results in loss of IL-1- and IL-18-mediated function. Immunity. 1998 Jul;9(1):143-50.

212. Honda K, Sakaguchi S, Nakajima C *et al.* Selective contribution of IFN-alpha/beta signaling to the maturation of dendritic cells induced by double-stranded RNA or viral infection. Proceedings of the National Academy of Sciences of the United States of America. 2003 Sep 16;100(19):10872-7.

213. Nenci A, Becker C, Wullaert A *et al.* Epithelial NEMO links innate immunity to chronic intestinal inflammation. Nature. 2007;446(7135):557-61.

214. Hoshino K, Takeuchi O, Kawai T *et al.* Cutting edge: Toll-like receptor 4 (TLR4)-deficient mice are hyporesponsive to lipopolysaccharide: evidence for TLR4 as the Lps gene product. J Immunol. 1999 Apr 1;162(7):3749-52.

215. Sato M, Suemori H, Hata N *et al.* Distinct and essential roles of transcription factors IRF-3 and IRF-7 in response to viruses for IFN-alpha/beta gene induction. Immunity. 2000 Oct;13(4):539-48.

216. Sun Q, Sun L, Liu HH *et al.* The specific and essential role of MAVS in antiviral innate immune responses. Immunity. 2006 May;24(5):633-42.

217. Gareau MG, Jury J, MacQueen G *et al.* Probiotic treatment of rat pups normalises corticosterone release and ameliorates colonic dysfunction induced by maternal separation. Gut. 2007 Nov;56(11):1522-8.

218. Pierdomenico M, Negroni A, Stronati L *et al.* Necroptosis is active in children with inflammatory bowel disease and contributes to heighten intestinal inflammation. Am J Gastroenterol. 2014 Feb;109(2):279-87.

219. Round JL, Mazmanian SK. The gut microbiota shapes intestinal immune responses during health and disease. Nat Rev Immunol. 2009 May;9(5):313-23.

220. Gionchetti P, Rizzello F, Lammers KM *et al.* Antimicrobials in the management of inflammatory bowel disease. Digestion. 2006;73 Suppl 1:77-85.

221. Isaacs KL, Sartor RB. Treatment of inflammatory bowel disease with antibiotics. Gastroenterol Clin North Am. 2004 Jun;33(2):335-45, x.

222. Perencevich M, Burakoff R. Use of antibiotics in the treatment of inflammatory bowel disease. Inflamm Bowel Dis. 2006 Jul;12(7):651-64.

223. Sartor RB. Therapeutic manipulation of the enteric microflora in inflammatory bowel diseases: antibiotics, probiotics, and prebiotics. Gastroenterology. 2004 May;126(6):1620-33.

224. D'Haens GR, Geboes K, Peeters M *et al.* Early lesions of recurrent Crohn's disease caused by infusion of intestinal contents in excluded ileum. Gastroenterology. 1998 Feb;114(2):262-7.

225. Rutgeerts P, Goboes K, Peeters M *et al.* Effect of faecal stream diversion on recurrence of Crohn's disease in the neoterminal ileum. Lancet. 1991 Sep 28;338(8770):771-4.

226. Baumgart M, Dogan B, Rishniw M *et al.* Culture independent analysis of ileal mucosa reveals a selective increase in invasive Escherichia coli of novel phylogeny relative to depletion of Clostridiales in Crohn's disease involving the ileum. ISME J. 2007 Sep;1(5):403-18.

227. Darfeuille-Michaud A, Boudeau J, Bulois P *et al.* High prevalence of adherent-invasive Escherichia coli associated with ileal mucosa in Crohn's disease. Gastroenterology. 2004 Aug;127(2):412-21.

228. Frank DN, St Amand AL, Feldman RA *et al.* Molecular-phylogenetic characterization of microbial community imbalances in human inflammatory bowel diseases. Proceedings of the National Academy of Sciences of the United States of America. 2007 Aug 21;104(34):13780-5.

229. Neut C, Bulois P, Desreumaux P *et al.* Changes in the bacterial flora of the neoterminal ileum after ileocolonic resection for Crohn's disease. Am J Gastroenterol. 2002 Apr;97(4):939-46.

230. Swidsinski A, Ladhoff A, Pernthaler A *et al.* Mucosal flora in inflammatory bowel disease. Gastroenterology. 2002 Jan;122(1):44-54.

231. Tamboli CP, Neut C, Desreumaux P *et al.* Dysbiosis in inflammatory bowel disease. Gut. 2004 Jan;53(1):1-4.

232. Pineton de Chambrun G, Colombel JF, Poulain D *et al.* Pathogenic agents in inflammatory bowel diseases. Curr Opin Gastroenterol. 2008 Jul;24(4):440-7.

233. Duchmann R, Kaiser I, Hermann E *et al.* Tolerance exists towards resident intestinal flora but is broken in active inflammatory bowel disease (IBD). Clin Exp Immunol. 1995 Dec;102(3):448-55.

234. Macpherson A, Khoo UY, Forgacs I *et al.* Mucosal antibodies in inflammatory bowel disease are directed against intestinal bacteria. Gut. 1996 Mar;38(3):365-75.

235. Kobayashi KS, Chamaillard M, Ogura Y *et al.* Nod2-dependent regulation of innate and adaptive immunity in the intestinal tract. Science. 2005 Feb 4;307(5710):731-4.

236. Thompson AI, Lees CW. Genetics of ulcerative colitis. Inflamm Bowel Dis. 2011 Mar;17(3):831-48.

237. Wehkamp J, Harder J, Weichenthal M *et al.* NOD2 (CARD15) mutations in Crohn's disease are associated with diminished mucosal alpha-defensin expression. Gut. 2004 Nov;53(11):1658-64.

238. Sartor RB. Targeting enteric bacteria in treatment of inflammatory bowel diseases: why, how, and when. Curr Opin Gastroenterol. 2003 Jul;19(4):358-65.

239. Manichanh C, Rigottier-Gois L, Bonnaud E *et al.* Reduced diversity of faecal microbiota in Crohn's disease revealed by a metagenomic approach. Gut. 2006 Feb;55(2):205-11.

240. Camilleri M. Peripheral mechanisms in irritable bowel syndrome. N Engl J Med. 2012 Oct 25;367(17):1626-35.

241. Camilleri M, Lasch K, Zhou W. Irritable bowel syndrome: methods, mechanisms, and pathophysiology. The confluence of increased permeability, inflammation, and pain in irritable bowel syndrome. Am J Physiol Gastrointest Liver Physiol. 2012 Oct;303(7):G775-85.

242. Longstreth GF, Thompson WG, Chey WD *et al.* Functional bowel disorders. Gastroenterology. 2006 Apr;130(5):1480-91.

243. Lee YJ, Park KS. Irritable bowel syndrome: emerging paradigm in pathophysiology. World J Gastroenterol. 2014 Mar 14;20(10):2456-69.

244. Barrett JS, Gibson PR. Fermentable oligosaccharides, disaccharides, monosaccharides and polyols (FODMAPs) and nonallergic food intolerance: FODMAPs or food chemicals? Therapeutic advances in gastroenterology. 2012 Jul;5(4):261-8.

245. Guilarte M, Santos J, de Torres I *et al.* Diarrhoea-predominant IBS patients show mast cell activation and hyperplasia in the jejunum. Gut. 2007 Feb;56(2):203-9.

246. Mearin F, Perez-Oliveras M, Perello A *et al.* Dyspepsia and irritable bowel syndrome after a Salmonella gastroenteritis outbreak: one-year follow-up cohort study. Gastroenterology. 2005 Jul;129(1):98-104.

247. Simren M, Barbara G, Flint HJ *et al.* Intestinal microbiota in functional bowel disorders: a Rome foundation report. Gut. 2013 Jan;62(1):159-76.

248. van der Veek PP, van den Berg M, de Kroon YE *et al.* Role of tumor necrosis factor-alpha and interleukin-10 gene polymorphisms in irritable bowel syndrome. Am J Gastroenterol. 2005 Nov;100(11):2510-6.

249. Martinez C, Lobo B, Pigrau M *et al.* Diarrhoea-predominant irritable bowel syndrome: an organic disorder with structural abnormalities in the jejunal epithelial barrier. Gut. 2013 Aug;62(8):1160-8.

250. Talley NJ, Spiller R. Irritable bowel syndrome: a little understood organic bowel disease? Lancet. 2002 Aug 17;360(9332):555-64.

251. Chadwick VS, Chen W, Shu D *et al.* Activation of the mucosal immune system in irritable bowel syndrome. Gastroenterology. 2002 Jun;122(7):1778-83.

252. Balsari A, Ceccarelli A, Dubini F *et al.* The fecal microbial population in the irritable bowel syndrome. Microbiologica. 1982 Jul;5(3):185-94.

253. Bonfrate L, Tack J, Grattagliano I *et al.* Microbiota in health and irritable bowel syndrome: current knowledge, perspectives and therapeutic options. Scand J Gastroenterol. 2013 Sep;48(9):995-1009.

254. Si JM, Yu YC, Fan YJ *et al.* Intestinal microecology and quality of life in irritable bowel syndrome patients. World J Gastroenterol. 2004 Jun 15;10(12):1802-5.

255. Carroll IM, Ringel-Kulka T, Keku TO *et al.* Molecular analysis of the luminal- and mucosal-associated intestinal microbiota in diarrhea-predominant irritable bowel syndrome. Am J Physiol Gastrointest Liver Physiol. 2011 Nov;301(5):G799-807.

256. Rajilic-Stojanovic M, Biagi E, Heilig HG *et al.* Global and deep molecular analysis of microbiota signatures in fecal samples from patients with irritable bowel syndrome. Gastroenterology. 2011 Nov;141(5):1792-801.

257. Horvath A, Szajewska H. Probiotics, prebiotics, and dietary fiber in the management of functional gastrointestinal disorders. World review of nutrition and dietetics. 2013;108:40-8.

258. Sanders ME, Guarner F, Guerrant R *et al.* An update on the use and investigation of probiotics in health and disease. Gut. 2013 May;62(5):787-96.

259. Bron PA, Tomita S, van S, II *et al.* Lactobacillus plantarum possesses the capability for wall teichoic acid backbone alditol switching. Microbial cell factories. 2012;11:123.

260. Neish AS. Microbes in gastrointestinal health and disease. Gastroenterology. 2009 Jan;136(1):65-80.

261. Rousseaux C, Thuru X, Gelot A *et al.* Lactobacillus acidophilus modulates intestinal pain and induces opioid and cannabinoid receptors. Nature medicine. 2007 Jan;13(1):35-7.

262. Moayyedi P, Ford AC, Talley NJ *et al.* The efficacy of probiotics in the treatment of irritable bowel syndrome: a systematic review. Gut. 2010 Mar;59(3):325-32.

263. Clarke G, Cryan JF, Dinan TG *et al.* Review article: probiotics for the treatment of irritable bowel syndrome--focus on lactic acid bacteria. Aliment Pharmacol Ther. 2012 Feb;35(4):403-13.

264. Quinton JF, Sendid B, Reumaux D *et al.* Anti-Saccharomyces cerevisiae mannan antibodies combined with antineutrophil cytoplasmic autoantibodies in inflammatory bowel disease: prevalence and diagnostic role. Gut. 1998 Jun;42(6):788-91.

265. McFarland LV. Systematic review and meta-analysis of Saccharomyces boulardii in adult patients. World J Gastroenterol. 2010 May 14;16(18):2202-22.

266. Pothoulakis C. Review article: anti-inflammatory mechanisms of action of Saccharomyces boulardii. Aliment Pharmacol Ther. 2009 Oct 15;30(8):826-33.

267. Dubuquoy L, Jansson EA, Deeb S *et al.* Impaired expression of peroxisome proliferator-activated receptor gamma in ulcerative colitis. Gastroenterology. 2003 May;124(5):1265-76.

268. Calignano A, La Rana G, Giuffrida A *et al.* Control of pain initiation by endogenous cannabinoids. Nature. 1998 Jul 16;394(6690):277-81.

269. D'Agostino G, La Rana G, Russo R *et al.* Acute intracerebroventricular administration of palmitoylethanolamide, an endogenous peroxisome proliferator-activated receptor-alpha agonist, modulates carrageenan-induced paw edema in mice. The Journal of pharmacology and experimental therapeutics. 2007 Sep;322(3):1137-43.

270. LoVerme J, La Rana G, Russo R *et al.* The search for the palmitoylethanolamide receptor. Life sciences. 2005 Aug 19;77(14):1685-98.

271. LoVerme J, Russo R, La Rana G *et al.* Rapid broad-spectrum analgesia through activation of peroxisome proliferator-activated receptor-alpha. The Journal of pharmacology and experimental therapeutics. 2006 Dec;319(3):1051-61.

272. Abbas Z, Yakoob J, Jafri W *et al.* Cytokine and clinical response to Saccharomyces boulardii therapy in diarrhea-dominant irritable bowel syndrome: a randomized trial. Eur J Gastroenterol Hepatol. 2014 Jun;26(6):630-9.

273. Choi CH, Jo SY, Park HJ *et al.* A randomized, double-blind, placebo-controlled multicenter trial of saccharomyces boulardii in irritable bowel syndrome: effect on quality of life. J Clin Gastroenterol. 2011 Sep;45(8):679-83.

274. Edwards-Ingram L, Gitsham P, Burton N *et al.* Genotypic and physiological characterization of Saccharomyces boulardii, the probiotic strain of Saccharomyces cerevisiae. Applied and environmental microbiology. 2007 Apr;73(8):2458-67.

275. Fietto JL, Araujo RS, Valadao FN *et al.* Molecular and physiological comparisons between Saccharomyces cerevisiae and Saccharomyces boulardii. Canadian journal of microbiology. 2004 Aug;50(8):615-21.

276. Hennequin C, Thierry A, Richard GF *et al.* Microsatellite typing as a new tool for identification of Saccharomyces cerevisiae strains. Journal of clinical microbiology. 2001 Feb;39(2):551-9.

277. Al-Chaer ED, Kawasaki M, Pasricha PJ. A new model of chronic visceral hypersensitivity in adult rats induced by colon irritation during postnatal development. Gastroenterology. 2000 Nov;119(5):1276-85.

278. Bourdu S, Dapoigny M, Chapuy E *et al.* Rectal instillation of butyrate provides a novel clinically relevant model of noninflammatory colonic hypersensitivity in rats. Gastroenterology. 2005 Jun;128(7):1996-2008.

279. Tarrerias AL, Millecamps M, Alloui A *et al.* Short-chain fatty acid enemas fail to decrease colonic hypersensitivity and inflammation in TNBS-induced colonic inflammation in rats. Pain. 2002 Nov;100(1-2):91-7.

280. Whorwell PJ. Effective management of irritable bowel syndrome--the Manchester Model. The International journal of clinical and experimental hypnosis. 2006 Jan;54(1):21-6.

281. Heaton KW, Radvan J, Cripps H *et al.* Defecation frequency and timing, and stool form in the general population: a prospective study. Gut. 1992 Jun;33(6):818-24.

282. Molinie F, Gower-Rousseau C, Yzet T *et al.* Opposite evolution in incidence of Crohn's disease and ulcerative colitis in Northern France (1988-1999). Gut. 2004 Jun;53(6):843-8.

283. Wittkopf N, Gunther C, Martini E *et al.* Lack of intestinal epithelial atg7 affects paneth cell granule formation but does not compromise immune homeostasis in the gut. Clinical & developmental immunology. 2012;2012:278059.